

**Characterization of molecular mechanisms
involved in intrinsic and extrinsic skin aging
of *in situ* aged normal human dermal
fibroblasts**

Inaugural-Dissertation

Zur Erlangung des Doktorgrades
der Mathematisch-Naturwissenschaftlichen Fakultät
der Heinrich-Heine-Universität Düsseldorf

vorgelegt von

Sabine Schneider

aus Haan, Deutschland

Düsseldorf, Mai 2021

aus dem IUF – Leibniz-Institut für Umweltmedizinische Forschung gGmbH
an der Heinrich-Heine-Universität Düsseldorf

Gedruckt mit der Genehmigung der
Mathematisch-Naturwissenschaftlichen Fakultät der
Heinrich-Heine-Universität Düsseldorf

Referent: Prof. Dr. med. Jean Krutmann

Korreferent: Prof. Dr. rer. nat. William F. Martin

Tag der mündlichen Prüfung: 06.09.2021

Summary

Aging is principally driven by the combination of intrinsic and extrinsic factors. Whereas intrinsic factors (genetic constitution, somatic capacity, composition) define the scope of possibilities, extrinsic factors such as the individual's behavior and the resulting exposure to environmental factors determine to what extent this is exploited. The skin is particularly suited for comparing intrinsic *versus* extrinsic aging, since the entire skin ages intrinsically, but only certain areas (e.g. face, neck) are subjected to environmental influences and thus to extrinsic aging. Textbook knowledge generally assumes that extrinsic skin aging superimposes intrinsic skin aging, but corresponding studies and thus scientific evidence to show that this is indeed the case are scarce. To assess this relationship more closely, we have focused on dermal fibroblasts (NHDF), because aging of this non-proliferating, skin-resident cell population is thought to be of key importance to both intrinsic and extrinsic skin aging. Specifically, we have compared NHDF isolated from buttocks skin, as an example of intrinsically aged skin (NHDF^{INT}), *versus* neck skin, as a skin area representative for extrinsically aged skin (NHDF^{EXT}). These cells aged *in situ* in human skin, i.e. they were obtained from human volunteers of three different age groups [young (Y), 20-25 yr.; middle-aged (M), 36-49 yr.; old (O), 60-64 yr.]. Performing proteome analysis via quantitative, label-free mass spectrometry, we found that NHDF^{INT} *versus* NHDF^{EXT} fundamentally differed in age-dependent trajectories of protein levels. Accordingly, quantitative assessments demonstrated that NHDF^{INT} exhibited gradual, almost linear changes in protein abundances over all three age groups (Y<M<O and Y>M>O). This was in sharp contrast to NHDF^{EXT}, in which alterations of protein quantities showed a non-linear kinetic. Specifically, almost no changes could be detected in cells isolated from Y *versus* M probands (Y=M), whereas a marked difference was observed between cells derived from M *versus* O donors (M<<O and M>>O). These changes were very pronounced and outreached the ones found in NHDF^{INT}. At a qualitative level, it appeared that in NHDF^{EXT} proteins involved in cellular respiration were among the most strongly affected. For example, tricarboxylic acid (TCA) cycle-related proteins were upregulated in NHDF^{EXT} *versus* NHDF^{INT} of M donors and at the same time, NAD⁺ levels were reduced and ADP/ATP ratios elevated. These observations indicate for Y and M donors, that NHDF^{EXT}, in contrast to NHDF^{INT}, show a compensatory behavior to cope with a situation characterized by enhanced energy demands and an energy deficit. However, when NHDF^{EXT} of M *versus* O donors were compared, NHDF^{EXT} of O donors seemed to have passed a "tipping point", at which compensatory mechanisms failed. Accordingly, we observed a dramatic decline of TCA cycle-associated proteins accompanied by a severe reduction of protein diversity and protein biosynthesis, i.e. two biological processes known to consume vast amounts of ATP. Taken together these findings suggest an energy crisis in NHDF^{EXT} of O donors that seems to cause a collapse of compensatory metabolic processes and protein production. In NHDF^{EXT} *versus*

NHDF^{INT} of M donors, this energy deficit was associated with decreased sirtuin-1 (SIRT1) protein levels and compromised deacetylation of lysine 56 of histone 3 (H3K56) and lysine 16 of histone 4 (H4K16). Also, mitochondrial superoxide levels and ROS-related gene expression were elevated in NHDF^{EXT} *versus* NHDF^{INT} of M probands. Of note, the mitochondrial phenotype present in NHDF^{EXT} of M donors could be rescued upon treatment of these cells with the NAD⁺ precursor β -nicotinamide mononucleotide (NMN). Specifically, NAD⁺ concentration, ADP/ATP ratio, levels of TCA cycle-related proteins, SIRT1 abundance and deacetylation of H3K56 and H4K16 were normalized to levels observed in age group-matched NHDF^{INT}. These studies demonstrate that the relationship between intrinsic and extrinsic skin aging might be more complex than originally thought and different from a simple superimposition, because age-dependent proteomic/metabolic changes in NHDF^{EXT} follow a substantially different kinetic compared to NHDF^{INT}. They identify restricted availability of NAD⁺ as a factor driving metabolic/epigenetic alterations contributing to extrinsic skin aging. It is thus tempting to speculate that treatment of NHDF^{EXT} with NMN might be efficient to switch NHDF^{EXT} into NHDF^{INT} and thereby protect these cells from reaching the “tipping point”.

Zusammenfassung

Der Alterungsprozess wird durch die Kombination von intrinsischen und extrinsischen Einflüssen vorangetrieben. Während die intrinsischen Faktoren (genetische Konstitution, somatische Kapazität, Zusammensetzung) den Rahmen des Möglichen bestimmen, wird das Ausmaß, mit dem dieser ausgeschöpft wird, durch das individuelle Verhalten und die damit einhergehende Exposition gegenüber Umweltfaktoren festgelegt. Die Haut ist für einen Vergleich intrinsischer und extrinsischer Organalterung besonders geeignet, da die gesamte Haut intrinsisch altert, aber nur bestimmte Hautbereiche (z.B. Gesichts-, Nackenhaut) extrinsischen Einflussfaktoren und damit extrinsischen Alterungsprozessen ausgesetzt sind. Es wird allgemein angenommen, dass die extrinsische Hautalterung sich auf die intrinsische Hautalterung aufsetzt. Allerdings gibt es nur wenige wissenschaftliche Nachweise für diese Annahme. Um diese Interaktion näher zu untersuchen, haben wir uns auf dermale Fibroblasten (NHDF) fokussiert, da diese nichtproliferierende Population hautresidenter Zellen sowohl für intrinsische als auch extrinsische Hautalterung wichtig zu sein scheint. Verglichen wurden NHDF von Gesäß- *versus* Nackenhaut, als repräsentative Hautareale für intrinsisches (NHDF^{INT}) *versus* extrinsisches Hautaltern (NHDF^{EXT}). Die Fibroblasten alterten *in situ* in der menschlichen Haut, da sie von Spendern aus drei verschiedenen Altersgruppen [jung (Y), 20-25 Jahre; mittelalt (M), 36-49 Jahre; alt (O), 60-64 Jahre] stammten. Durch eine Proteom-Analyse mittels markierungsfreier Massenspektrometrie haben wir herausgefunden, dass sich NHDF^{INT} *versus* NHDF^{EXT} grundlegend in ihren altersabhängigen Verläufen der Proteinkonzentrationen unterschieden. Dementsprechend zeigten die quantitativen Auswertungen, dass sich die Proteinmengen über die drei Altersgruppen in NHDF^{INT} graduell und fast linear veränderten ($Y < M < O$ und $Y > M > O$). Das war im deutlichen Kontrast zu NHDF^{EXT}, in denen Änderungen der Proteinmengen eine nicht-lineare Kinetik aufwiesen. Konkret wurden nahezu keine Unterschiede in Y *versus* M Probanden ($Y = M$) detektiert, während drastische Verschiebungen zwischen M *versus* O Spendern ($M \ll O$ und $M \gg O$) stattfanden, die sogar die in NHDF^{INT} beobachteten Veränderungen übertrafen. Auf qualitativer Ebene wurde gezeigt, dass an der Zellatmung beteiligte Proteine von diesem Phänomen besonders betroffen waren. Beispielsweise waren Citratzyklus-Proteine in NHDF^{EXT} *versus* NHDF^{INT} von M Probanden hochreguliert, wobei gleichzeitig das NAD⁺-Level reduziert und das ADP/ATP-Verhältnis erhöht waren. Diese Beobachtungen weisen darauf hin, dass NHDF^{EXT} von Y und M Spendern im Gegensatz zu NHDF^{INT} ein kompensatorisches Verhalten zeigen, um eine Situation zu bewältigen, die von einem erhöhten Energiebedarf und einem Energiedefizit geprägt ist. Beim Vergleich von NHDF^{EXT} von M *versus* O Probanden scheinen NHDF^{EXT} von O Spendern allerdings einen "Wendepunkt" überschritten zu haben, an dem die o.g. kompensatorischen Mechanismen versagen. Demnach wurde eine erhebliche Reduktion von Citratzyklus-assoziierten Proteinen beobachtet. Diese ging einher mit einer

deutlichen Verringerung der Protein-Diversität und Proteinsynthese, zwei biologische Prozesse, die enorme Mengen an ATP konsumieren. Zusammengefasst deuten diese Befunde auf eine Energiekrise in NHDF^{EXT} von O Probanden hin, die einen Zusammenbruch von kompensatorischen metabolischen Prozessen und der Proteinproduktion verursacht. Dieses Energiedefizit war in NHDF^{EXT} versus NHDF^{INT} von M Spendern von einer verringerten Proteinkonzentration von Sirtuin-1 (SIRT1) und einer beeinträchtigten Deacetylierung von Lysin 56 von Histon 3 (H3K56) und von Lysin 16 von Histon 4 (H4K16) begleitet. Zudem waren die mitochondriale Superoxid-Menge und die ROS-bezogene Genexpression in NHDF^{EXT} versus NHDF^{INT} von M Probanden erhöht. Interessanterweise konnte der in NHDF^{EXT} von M Spendern vorhandene Phänotyp durch eine Behandlung mit der NAD⁺-Vorstufe β -Nikotinamid-Mononucleotid (NMN) verbessert werden. Konkret wurden die NAD⁺-Konzentration, das ADP/ATP-Verhältnis, die Mengen der Citratzyklus-assoziierten Proteine und von SIRT1 sowie die Deacetylierung von H3K56 und H4K16 auf die in entsprechenden NHDF^{INT} beobachteten Levels normalisiert. Diese Ergebnisse weisen darauf hin, dass die Beziehung zwischen intrinsischer und extrinsischer Hautalterung bei Weitem komplexer ist als ursprünglich gedacht. So setzt sich die extrinsische Alterung nicht einfach auf die intrinsische auf, da die altersabhängigen Proteom- und Metabolismus-Veränderungen in NHDF^{EXT} einer grundsätzlich anderen Kinetik folgen als in NHDF^{INT}. Zusätzlich haben diese Ergebnisse aufgezeigt, dass limitierte NAD⁺-Verfügbarkeit eine potentiell entscheidende Triebkraft für metabolische und epigenetische Veränderungen darstellt, die zur extrinsischen Hautalterung beitragen. Insofern vermuten wir, dass NHDF^{EXT} durch NMN-Behandlung in NHDF^{INT} transformiert und dadurch vor dem Erreichen des Wendepunkts geschützt werden könnten.

Table of contents

Summary	I
Zusammenfassung	III
1. Introduction.....	1
1.1 The human skin	1
1.1.1 Epidermis	2
1.1.2 Dermis.....	2
1.1.3 Subcutis.....	3
1.2 Skin aging.....	3
1.2.1 Intrinsic skin aging.....	3
1.2.2 Extrinsic skin aging	5
1.3 Pathomechanisms of skin aging	6
1.3.1 Mitochondrial dysfunction and oxidative stress	7
1.3.2 ECM alterations.....	9
1.3.3 Cellular senescence.....	9
1.4 Aims of the thesis	11
2. Materials and Methods.....	12
2.1 Materials.....	12
2.1.1 Chemicals	12
2.1.2 Kits	13
2.1.3 Consumables.....	14
2.1.4 Devices	15
2.1.5 Software.....	16
2.2 Cell culture technique	18
2.2.1 Isolation and culture of dermal fibroblasts.....	18
2.2.2 Treatment with substances intervening in nicotinamide adenine dinucleotide (NAD ⁺) metabolism	19
2.3 Secretome and proteome analysis	20
2.3.1 Secretome and proteome preparation	20
2.3.2 Mass spectrometric analysis	20
2.3.3 Protein identification and quantification.....	21
2.3.4 Bioinformatics analysis	22
2.4 Western blot analysis	23
2.4.1 Protein isolation and quantification	23
2.4.2 Histone extraction.....	24
2.4.3 SDS-PAGE	24
2.4.4 Western blot and immunodetection of proteins	25
2.5 Measurement of pyruvate consumption.....	27
2.6 Messenger ribonucleic acid (mRNA) analytics.....	27
2.6.1 RNA isolation and quantification	27
2.6.2 Complementary DNA (cDNA) synthesis	28
2.6.3 Real-Time quantitative PCR (RT-qPCR)	29
2.7 Determination of mitochondrial superoxide levels	30
2.8 mtDNA analytics.....	30
2.8.1 DNA isolation and quantification	30
2.8.2 Measurement of mtDNA content	30

2.9	Determination of ADP/ATP ratios	31
2.10	Measurement of NAD⁺ levels	32
2.11	Statistics.....	32
3.	Results.....	33
3.1	Age-related change of protein diversity differed between NHDF^{EXT} and NHDF^{INT} ...	33
3.1.1	Protein diversity of secretomes was increased in aged NHDF ^{INT} but remained unchanged in NHDF ^{EXT}	33
3.1.2	Protein diversity of proteomes declined linearly in aged NHDF ^{INT} but non-linearly in NHDF ^{EXT}	35
3.2	Age-dependent change of protein abundance patterns followed a non-linear course in NHDF^{EXT}, but in a linear course in NHDF^{INT}	37
3.3	Comparison of NHDF^{EXT} vs NHDF^{INT} within each age group revealed differences in changes of metabolism-associated proteins	41
3.3.1	Examination of significantly altered proteins in NHDF ^{EXT} vs NHDF ^{INT} revealed clusters of metabolic proteins in the Y and M group	41
3.3.2	Levels of metabolism-associated proteins were increased in NHDF ^{EXT} vs NHDF ^{INT} of Y and M donors.....	45
3.4	NHDF^{EXT} vs NHDF^{INT} of M donors showed mitochondrial dysfunction.....	46
3.4.1	TCA cycle was dysregulated in NHDF ^{EXT} vs NHDF ^{INT} of M donors	46
3.4.2	Evidence for oxidative stress in NHDF ^{EXT} vs NHDF ^{INT} of M donors.....	49
3.4.3	ATP and NAD ⁺ metabolisms were compromised in NHDF ^{EXT} vs NHDF ^{INT} of M donors	51
3.5	Sirtuin (SIRT) abundances and related histone deacetylation were dysregulated in NHDF^{EXT} vs NHDF^{INT} of M donors.....	52
3.5.1	SIRT levels were altered in NHDF ^{EXT} vs NHDF ^{INT} of M donors	52
3.5.2	Reduced SIRT1 abundance in NHDF ^{EXT} of M donors correlated with histone hyperacetylation	53
3.6	Chemical intervention in NAD⁺ metabolism rescued decreased NAD⁺ level in NHDF^{EXT} of M donors.....	55
3.6.1	Treatment with olaparib and compound 78c rescued decreased NAD ⁺ levels in NHDF ^{EXT} of M donors.....	56
3.6.2	β -nicotinamide mononucleotide (NMN) treatment retrieved NAD ⁺ level and ADP/ATP ratio in NHDF ^{EXT} of M donors	58
3.7	NMN treatment rescued SIRT1 abundance and related histone deacetylation in NHDF^{EXT} of M donors.....	59
3.7.1	SIRT1 level in NHDF ^{EXT} of M donors was retrieved by NMN treatment.....	59
3.7.2	NMN treatment of NHDF ^{EXT} of M donors resulted in selective rescue of deacetylation of H3K56 and H4K16	60
3.8	NMN treatment rescued parts of the mitochondrial phenotype of NHDF^{EXT} of M donors.....	62
3.8.1	NMN treatment of NHDF ^{EXT} of M donors attenuated dysregulation of TCA cycle	62
3.8.2	Increased mitochondrial ROS levels in NHDF ^{EXT} of M donors were not reduced through treatment with NMN	64
4.	Discussion.....	66
4.1	NHDF^{EXT} showed non-linear, age-dependent changes in protein abundance patterns, which were different from the linearly developing patterns in NHDF^{INT} .	67
4.2	Failure of NHDF^{EXT} to compensate for their energy deficit resulted in a crisis situation.....	68
4.2.1	Evidence for an enhanced metabolic flux in NHDF ^{EXT} of Y and M donors as an attempt to compensate for their energy deficit	69

4.2.2	NHDF ^{EXT} of O donors plunged into an energy crisis upon collapse of compensatory mechanisms	72
4.3	Metabolic dysregulation in NHDF^{EXT} contributed to disrupted proteostasis	72
4.3.1	Age-dependent decline of mitochondrial respiration in NHDF ^{INT} and NHDF ^{EXT} correlated with disturbance of proteostasis	73
4.3.2	Metabolic dysregulation strictly correlated with attenuated protein diversity and protein biosynthesis	73
4.4	The energy deficit induced epigenetic dysregulation in NHDF^{EXT} of M donors	75
4.4.1	Histone hyperacetylation was both result and source of metabolic dysregulation in NHDF ^{EXT}	76
4.5	Restricted NAD⁺ availability was the major force driving metabolic and epigenetic changes in NHDF^{EXT}	77
4.5.1	Overactivation of NAD ⁺ -consuming enzymes contributed to metabolic dysregulation in NHDF ^{EXT}	78
4.5.2	Restricted NAD ⁺ availability was the primary cause for metabolic dysregulation in NHDF ^{EXT}	78
4.5.3	Limited NAD ⁺ availability was the major driver for epigenetic changes in NHDF ^{EXT}	80
4.6	Reassessment of the generally accepted superimposition theory of intrinsic and extrinsic aging is crucial	81
5.	References	84
	Appendix	97
	Eidesstattliche Erklärung	146
	Danksagung	147

1. Introduction

1.1 The human skin

The human skin is the body's first line of defense against environmental influences. Accounting for a surface area of 1.5-1.8 m² and approximately 1/5 of the overall body weight, the skin is not only the largest organ of the body but fulfills a wide range of functions.

Acting as a natural barrier and thus separating the interior of the body from the surrounding environment, the skin provides protection against biological (e.g. invasion of pathogens and microorganisms), chemical (e.g. penetration of toxic substances such as pollutants) and physical impacts (e.g. radiation, mechanical stresses). Pigmentation, hair and the stratum corneum play an important role in prevention of damaging effects of ultraviolet radiation (UVR). For sensory perception the skin is equipped with different types of receptors: thermoreceptors (temperature), mechanoreceptors (touch, pressure, stretch, vibration) and nociceptors (pain). The temperature balance of the body is controlled through vasoconstriction/vasodilation and a variety of exocrine glands residing in the skin, hair and subcutaneous fat. Other important functions of the skin include regulation of water and electrolyte balance as well as vitamin D synthesis.

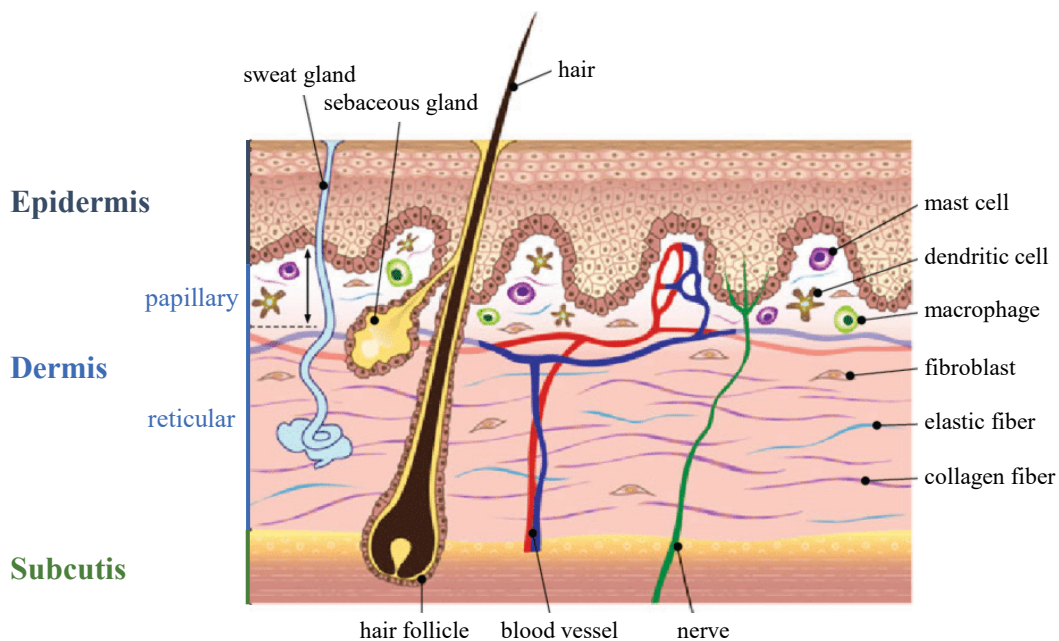


Figure 1: Structure of the human skin. The skin consists of three layers: the epidermis, the outermost layer, the dermis, and the subcutis, the innermost layer. Adapted from [1].

The human skin is composed of three distinct layers: epidermis, dermis and subcutis, and contains various adnexa including glands, hair follicles and nails (**Figure 1**).

1.1.1 Epidermis

The epidermis, a stratified squamous epithelium, is the outermost skin layer directly exposed to the environment and most important for the barrier function of the skin. The epidermis comprises five layers from the inside out: stratum basale, stratum spinosum, stratum granulosum, stratum lucidum and stratum corneum.

Keratinocytes, the major epidermal cell type, differentiate from stem cells located in the stratum basale. During their migration through the epidermal strata, they undergo keratinization. They arrive in the stratum corneum as dead, flattened corneocytes without organelles and nuclei and are ultimately lost by desquamation. This process leads to a constant renewal of the epidermis every four weeks. Less frequent though important epidermal cells are melanocytes. They produce the pigment melanin which plays a key role in photoprotection of the skin due to its ability for absorption of UVR. Melanocytes transfer melanin to surrounding keratinocytes that gather the pigment in the perinuclear region to protect their deoxyribonucleic acid (DNA) from UVR-induced lesions [2]. Another cell type occurring in the epidermis are dendritic cells which are termed as Langerhans cells. In the presence of antigens, they are activated and migrate into nearby lymph nodes to present antigens to naïve T cells.

1.1.2 Dermis

The dermis is composed of connective tissue of mesenchymal origin enclosing a variety of accessory structures like hair follicles, blood and lymphatic vessels, nerve endings, thermo- and mechanoreceptors as well as different types of glands. Important functions of the dermis include support and protection of the skin and its subjacent structures, nourishment of the epidermis, thermoregulation and sensory perception. The dermis can be subdivided into two layers: papillary and reticular dermis. The upper papillary layer is connected to the overlying epidermis via the dermal-epidermal junction. Its finger-like extensions, called dermal papillae, contain blood vessels to supply hair follicles and epidermis with nutrients and oxygen. The papillary dermis is characterized by densely residing fibroblasts embedded in a network of loosely arranged, fine fibers. In contrast, the subjacent reticular dermis is less densely populated by fibroblasts, but is much thicker due to a more pronounced and tighter arranged fiber network.

Fibroblasts, the main cell type of the dermis, produce the extracellular matrix (ECM) which is composed of fibers such as collagen, elastic and reticular fibers surrounded by a gel-like substance, the ground substance. The latter contains proteoglycans, glycosaminoglycans (e.g. hyaluronic acid), adhesion proteins (e.g. laminins, fibronectins), water and electrolytes. The homeostasis of the ECM is regulated by fibroblasts via secretion of matrix-degrading enzymes like matrix metalloproteinases (MMPs) and tissue inhibitors of metalloproteinases (TIMPs). MMPs particularly degrade collagens but also other proteins of the ECM and TIMPs counteract this degrading activity. Fibroblasts play a prominent role in skin aging, wound healing, inflammation and tumorigenesis [3-6]. Aside from fibroblasts, the dermis contains mast cells, macrophages, dendritic cells, neutrophils, other immune cells and adipocytes [7, 8].

1.1.3 Subcutis

The subcutis consists of adipose tissue that is surrounded by connective tissue and septa, which attach the dermis to subjacent structures, such as fasciae and bones. Cell types occurring in the subcutis include adipocytes, fibroblasts and macrophages. Functions of the subcutis comprise energy storage, thermal insulation and mechanical protection.

1.2 Skin aging

Aging is principally driven by the combination of intrinsic and extrinsic influences. Whereas intrinsic factors define the scope of possibilities, the individual's behavior and thus the exposure to extrinsic factors determine to what extent these are exhausted. The skin is of particular importance in terms of aging studies because of its unique feature that though the entire organ ages chronologically, only certain areas (e.g. face, neck) are subjected to environmental impacts [9]. Therefore, in contrast to other organs, the skin allows for a comparative analysis of exclusively intrinsically aged tissue *vs* extrinsically and intrinsically aged tissue (for simplicity referred to as extrinsic aging).

1.2.1 Intrinsic skin aging

Chronologically aged skin is clinically characterized by formation of fine wrinkles and expression lines, laxity, xerosis and development of benign neoplasms like cherry angiomas and seborrheic

keratoses [10]. Factors driving intrinsic skin aging comprise genetic constitution, ethnicity, somatic capacity, hormonal changes and composition (**Figure 2**) [9].



Figure 2: Intrinsic and extrinsic factors driving skin aging. Adapted from [11].

Genetic makeup as an intrinsic driver of skin aging is exemplified by the existence of several inheritable gene mutations leading to progeroid syndromes. Well-known diseases include cockayne syndrome [12, 13] and xeroderma pigmentosum [14]. Moreover, also genetic variants in healthy individuals can influence a person's susceptibility for certain age-related processes. A cohort study of 697 elderly women revealed that carriers of specific genetic polymorphisms in the ECM degrading enzymes MMP-1 or MMP-3 were more prone to wrinkle formation [15].

Ethnicity considerably affects chronological skin aging since certain symptoms vary concerning their severity and time of onset. Comparative analysis of East Asians and Caucasians showed that wrinkles occurred earlier and more pronounced in Caucasians, whereas pigment spots were prevalent in East Asians [16-18]. Another study reported varying severity of age-related increase of dryness across different ethnic groups [19].

Regarding alterations of the endocrine environment, levels of several hormones decrease with age, including melatonin [20] and testosterone [21]. In females, estrogen concentrations strongly decline with the onset of menopause. In postmenopausal women, a rapid increase in wrinkle formation and skin dryness as well as a reduction in elasticity of the skin were observed and estrogen replacement therapy led to an amelioration of these symptoms [22, 23].

1.2.2 Extrinsic skin aging

Characteristic clinical symptoms of extrinsically aged skin include coarse wrinkles, solar lentigines, irregular pigmentation and elastosis. Other features comprise a typical leathery and yellowish appearance of the skin as well as vascular changes like telangiectasia. In addition to benign neoplasms, premalignancies e.g. actinic keratoses and malignant tumors, such as basal cell carcinoma or squamous cell carcinoma, may occur [10, 24]. Apart from intrinsic impacts, skin aging is promoted through environmental influences and lifestyle. According to the skin aging exposome described by Krutmann, Bouloc et al., these factors can be assigned to six categories: solar radiation, cigarette smoking, air pollution, nutrition, cosmetics and other factors (stress, lack of sleep, temperature effects) (**Figure 2**) [11].

A link between sun exposure and skin aging was first proposed by Kligman [25] and subsequently reinforced by several epidemiological studies [26-28]. Nowadays, solar radiation is generally considered to be the most relevant driver of extrinsic skin aging, which is therefore often referred to as photoaging [29]. The solar spectrum consists of UVR ($\lambda=100-400$ nm), visible light (VL; $\lambda=400-740$ nm) and infrared radiation (IRR; $\lambda=740$ nm-1 mm). The subtypes of UVR reaching the earth's surface are defined as UVB ($\lambda=280-315$ nm) and UVA ($\lambda=315-400$ nm) which can be divided into UVA1 ($\lambda=340-400$ nm) and UVA2 ($\lambda=315-340$ nm). Short-wave UVB is absorbed by the epidermis for the most part, whereas UVA, particularly UVA1, penetrates deeply into the dermis. IRR can be subdivided into IRA ($\lambda=740-1,400$ nm), IRB ($\lambda=1,400-3,000$ nm) and IRC ($\lambda=3,000$ nm-1 mm). Long-wave IRA and VL both penetrate the dermis and even reach the subcutis to some extent (**Figure 3**).

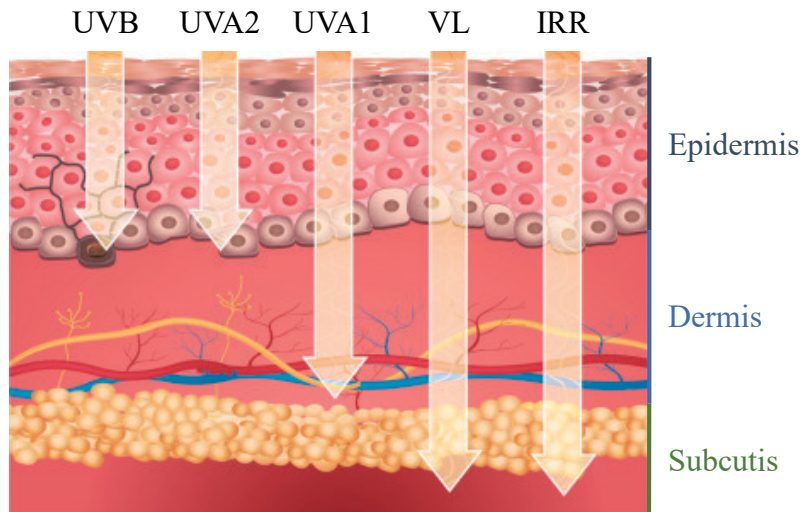


Figure 3: Penetration depth of different radiation types of the solar spectrum into the human skin. Adapted from [11].

Several studies emphasized a link between cigarette smoking and skin aging. Daniell found that the severity of wrinkle formation correlated with smoking habits in both genders [30]. Accordingly, an investigation of identical twins showed that the twin with a smoking history exhibited more pronounced skin aging symptoms as compared to the other, who was a non-smoker [31].

Epidemiological evidence for an association between air pollution and skin aging was first provided by the SALIA cohort study (study on the influence of air pollution on lung function, inflammation and aging) involving 400 female Caucasians aged between 70 and 80 years. The study demonstrated that exposure to traffic-caused airborne particles correlated with pigmentation and wrinkle formation [32]. In line with this, Li, Vierkötter et al. showed that air pollution due to fossil fuels was associated with increased severity of wrinkling in Chinese women [33].

1.3 Pathomechanisms of skin aging

In the epidermis, accumulation of cellular damage in keratinocytes is prevented through constant renewal and shedding of corneocytes. In contrast, the dermal, long-living fibroblasts, which only rarely divide, are a target for continuous age-dependent accumulation of macromolecular damage and require adaptive responses. The dermis is considered to be the major driving force of skin aging and expands the aging process onto the other skin layers via paracrine interactions [4, 9].

Fibroblast aging is characterized by mitochondrial dysfunction, modified gene expression patterns and disturbed proteostasis including ECM alterations, cellular senescence, genomic

instability, telomere attrition and epigenetic changes [34]. The following sections elaborate on the role of mitochondrial dysfunction, ECM alterations and senescence in aging.

1.3.1 Mitochondrial dysfunction and oxidative stress

Mitochondria are the most important location for cellular energy production. Under normal conditions, more than 90% of cellular adenosine triphosphate (ATP) is generated via oxidative phosphorylation (OXPHOS), comprising five protein complexes. OXPHOS involves the establishment of a proton gradient across the inner mitochondrial membrane that is used by the ATP synthase (complex V) to produce ATP through phosphorylation of adenosine diphosphate (ADP). Apart from their role in energy supply, mitochondria are a major site of formation of reactive oxygen species (ROS), particularly superoxide (O_2^-) and hydrogen peroxide (H_2O_2). These are produced as byproducts of OXPHOS at complex I and III due to occasional errors. Normally, low ROS levels are maintained through antioxidant systems consisting of enzymatic (e.g. superoxide dismutase (SOD), catalase (CAT), glutathione peroxidase, thioredoxin) and nonenzymatic scavenger (e.g. vitamin A, C, E, glutathione, melatonin). However, excessive ROS production may overwhelm the antioxidative defense resulting in oxidative stress. ROS damage nearby macromolecules, especially mitochondrial DNA (mtDNA), potentially inducing mtDNA mutations [35]. Mitochondria own repair systems for removal of oxidative damage [36]. However, according to the current state of knowledge, they lack mechanisms to eliminate bulky mtDNA photo adducts [37, 38]. In addition, mitochondria do not possess any mtDNA protecting histone proteins, in contrast to nuclear DNA (nDNA) [39]. The oxidative environment as well as the absence of nucleotide excision repair (NER) and histones make the mitochondrial genome more susceptible to damage. In fact, a higher abundance of mutations in mtDNA compared to nDNA has been observed [40-42].

The mitochondrial free radical theory of aging assumes that during both intrinsic and extrinsic skin aging, excessive generation of ROS induces an accumulation of damaged mitochondrial macromolecules including mtDNA mutations. This leads to dysfunction of the respiratory chain and thereby to even more enhanced ROS production, resulting in a vicious cycle (**Figure 4**) [43-45]. Studies of various species and tissues suggested an age-related increase of mtDNA mutations [46-50]. Trifunovic, Wredenberg et al. and Kujoth, Hiona et al. created a mouse model with a proof-reading-deficient mitochondrial DNA polymerase γ , consequently exhibiting elevated amounts of mtDNA mutations. These mtDNA mutator mice developed many characteristics of premature aging as well as a reduced lifespan [51, 52]. Although the abundance of mtDNA mutations enhances with chronological aging, they especially accumulate during photoaging. The most frequent mutation within the mitochondrial genome is a 4,977-bp deletion, which is referred

to as the common deletion. Berneburg, Gattermann et al. showed that the amount of the common deletion was 10-fold higher in sun-exposed than in sun-protected human skin of the same individual [53]. Accordingly, repeatedly UVA-irradiated normal human dermal fibroblasts (NHDF) exhibited an increase of the common deletion mediated via singlet oxygen [54].

Importantly, elevation of the common deletion as well as mtDNA mutations in general correlated with mitochondrial dysfunction [46-50, 55]. mtDNA encodes for genes whose protein products are involved in OXPHOS. Mutations in these genes can lead to defects in respiratory chain, increased ROS generation and inadequate energy production. Mitochondrial dysfunction and age-related decline of antioxidative capacity in the dermis both contribute to chronic oxidative stress [45, 56].

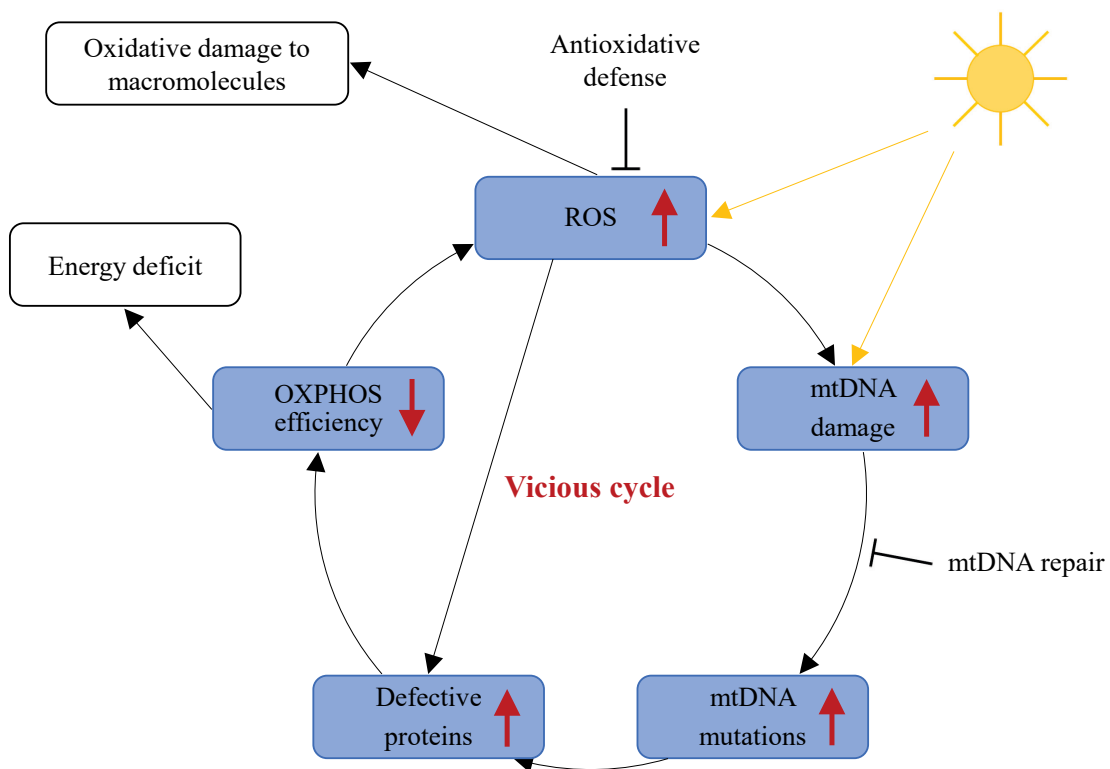


Figure 4: Vicious cycle of mitochondrial dysfunction and ROS production.

Aside from mtDNA lesions, ROS also cause oxidative damage to other macromolecules such as lipids, proteins and nDNA. ROS-induced lipid peroxidation results in membrane damage, activates autophagy and may lead to cell death [57]. Furthermore, ROS can react with proteins in which the amino acids methionine and cysteine are particularly prone to oxidative damage. Oxidation of proteins may alter their biochemical and physical properties and thereby affect their functionality [58]. Moreover, ROS can induce oxidative DNA damage, like 8-oxoguanine (8-oxoG) and single-strand breaks (SSBs). These are repaired by base excision repair (BER) and SSB repair (SSBR) [59-61].

1.3.2 ECM alterations

A hallmark of skin aging, particularly photoaging, is wrinkle formation which relies on alterations of the dermal ECM. Aging is associated with a progressive loss of mature collagen and elastin [62, 63], whereas disorganized, fragmented collagen and elastic fibers accumulate in the dermis. In photoaged human skin, the amount of collagen precursors decreases even more, which especially applies to the predominant collagen subtypes I and III [64]. UVR exposure causes a reduction of procollagen synthesis [65, 66] and disturbs the balance between ECM-degrading MMPs and TIMPs. Levels and activities of MMPs, e.g. MMP-1, MMP-3 and MMP-9, are elevated in human skin in response to UVR. Induction of these MMPs is mediated by activation of the transcription factors activator protein 1 (AP-1) and nuclear factor kappa light chain enhancer of activated B cells (NF κ B) [67, 68]. Moreover, UVR-induced mtDNA mutations are involved in the upregulation of MMP-1 [69].

MMPs degrade dermal matrix proteins like collagen and elastin and vary regarding their substrate specificity. MMP-1 degrades type I and III collagen, whereas MMP-3 only cleaves type I collagen. Less abundant type IV collagen is a substrate of MMP-2 and MMP-9 and elastin is degraded by MMP-7 and MMP-12 [70].

1.3.3 Cellular senescence

Cellular senescence is a state in which cells undergo an irreversible, persistent growth arrest while still remaining metabolically active. Entry into senescence can be triggered by several stimuli like replicative telomere shortening [71], DNA damage [72], activation of oncogenes [73], inactivation of tumor suppressor genes [74] and oxidative stress [75].

Many studies suggested an accumulation of senescent cells in aged tissues which contributes to disturbance of their functions [76-79]. Apart from aging, cellular senescence is implicated in further physiological processes including development [80, 81], wound healing [82] and tumor suppression [83]. Also, cellular senescence plays a role in pathological processes i.e. age-related diseases [84] such as type 2 diabetes [85], neurodegenerative disorders like Alzheimer's disease [86, 87], cardiovascular diseases e.g. atherosclerosis [88] and various cancers [89-91].

Senescent cells feature resistance to apoptosis [92] as well as a flattened and enlarged morphology [93]. Moreover, cellular senescence is characterized by nuclear alterations comprising increased formation of heterochromatin [94] and persistence of foci containing proteins involved in DNA damage response. The latter is termed as DNA segments with chromatin alterations reinforcing

senescence (DNA-SCARS) [95]. Another typical feature of cellular senescence is the induction of a senescence-associated secretory phenotype (SASP). Specifically, senescent cells secrete pro-inflammatory cytokines (e.g. interleukin 6 (IL-6), IL-8), chemokines (e.g. monocyte chemoattractant proteins (MCPs)), proteases (e.g. MMPs), and growth factors (e.g. transforming growth factor- β (TGF- β)) into the extracellular space [96]. Importantly, Waldera-Lupa, Kalfalah et al. demonstrated that the SASP of NHDF driven into senescence *in vitro* only partly corresponded to the skin aging-associated secreted proteins (SAASP) of *in situ* aged NHDF [97].

Senescent cells affect the ECM, surrounding cells and tissues through their SASP. Specifically, the release of proteolytic factors such as MMPs promotes modification of ECM. Secretion of cytokines and chemokines attracts and activates immune cells (e.g. macrophages, natural killer cells, T cells) which eliminate senescent cells [98]. Nevertheless, senescent cells accumulate during aging. This might be based on age-dependent impairment of immune function [99]. Senescent cells can propagate senescence to neighboring cells via SASP-mediated paracrine signaling [100]. Through generation of a pro-inflammatory environment, the SASP also contributes to chronic inflammation which is considered a hallmark of aging [101].

1.4 Aims of the thesis

There is strong scientific evidence demonstrating that intrinsic and extrinsic factors drive skin aging. Yet little is known about the interaction between intrinsic (=chronological) and extrinsic (=environmentally induced) skin aging. It is generally assumed that extrinsic skin aging superimposes intrinsic skin aging, even though this hypothesis has never been proven. Specifically, scientific studies comparing intrinsic with extrinsic skin aging via a systematic high-throughput analysis are scarce. Thus, the aim of this thesis was a structured and comprehensive characterization of intrinsic and extrinsic skin aging as well as their interactions through an unbiased proteomic approach. To this end, NHDF isolated from intrinsically (buttocks; NHDF^{INT}) or extrinsically aged skin (neck; NHDF^{EXT}) of young (Y; 20-25 yr.), middle-aged (M; 36-49 yr.) and old (O; 60-64 yr.) donors were compared.

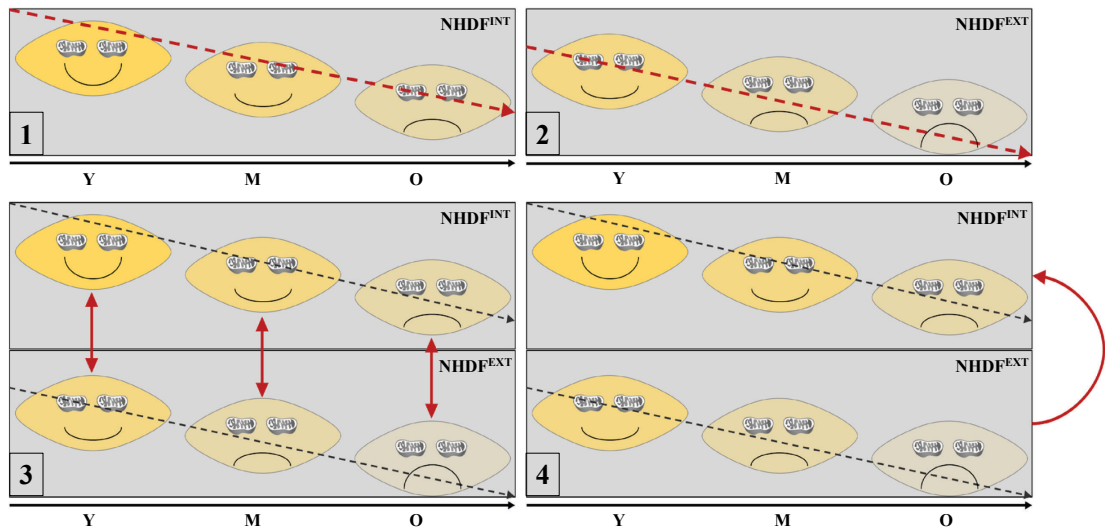


Figure 5: Structured approach for the investigation of intrinsic and extrinsic skin aging and their interactions.

In particular, the following questions have been addressed in this thesis (**Figure 5**):

1. What age-dependent changes do secretomes and proteomes of NHDF^{INT} reveal?
2. What age-dependent changes do secretomes and proteomes of NHDF^{EXT} reveal?
3. How do NHDF^{INT} and NHDF^{EXT} differ from each other within the different age groups?
What is the relationship between intrinsic and extrinsic skin aging?
4. Can treatment with appropriate substances convert NHDF^{EXT} into NHDF^{INT} ?

2. Materials and Methods

2.1 Materials

In the following sections, the chemicals, kits, consumables, devices and software utilized throughout this thesis are listed.

2.1.1 Chemicals

Chemicals which have been used for the experiments of this project are specified in **Table 1**.

Table 1: Chemicals.

Chemical	Supplier	Catalog no.
Alanyl-Glutamine 200 mM	Sigma-Aldrich / St. Louis, MO, USA	G8541
Albumin Bovine Fraction V, pH 7.0	Serva / Heidelberg, Germany	11930.03
Antibiotic-Antimycotic (100x)	Thermo Fisher Scientific / Waltham, MA, USA	15240062
APS	Sigma-Aldrich	A3678
Bromophenol blue	Merck / Darmstadt, Deutschland	108122
CD38 inhibitor 1 (compound 78c)	MedChemExpress / Princeton, NJ, USA	HY-123999
cOmplete, Mini, EDTA-free Protease Inhibitor Cocktail	Sigma-Aldrich	11836170001
DAPI	Sigma-Aldrich	D9542
DEPC-H ₂ O	Carl Roth / Karlsruhe, Germany	T143.4
DMEM, high glucose	Thermo Fisher Scientific	11965092
DMEM, high glucose, no glutamine, no phenol red	Thermo Fisher Scientific	31053028
DMSO	Sigma-Aldrich	D2650
DPBS, no calcium, no magnesium	Thermo Fisher Scientific	14190094
DTT	Carl Roth	6908
Ethanol	Carl Roth	9065.4
FBS Superior	Sigma-Aldrich	S0615
Glycerol	Carl Roth	3783.1
Glycine	Carl Roth	3790.3
HCl	Carl Roth	0992.1
iTaq Universal SYBR Green Supermix	BioRad / Hercules, CA, USA	172-5124
Methanol	Carl Roth	P717.1

2. Materials and Methods

MitoSOX Red Mitochondrial Superoxide Indicator	Thermo Fisher Scientific	M36008
M-MLV RT (200u/μl)	Promega / Madison, WI, USA	M1705
M-MLV RT 5x Buffer	Promega	M5313
NaCl	Carl Roth	3957.2
NMN	Cayman Chemical Company / Ann Arbor, MI, USA	16411
Olaparib	MedChemExpress	HY-10162
PCR Nucleotide Mix (10 mM)	Promega	C1145
PFA	Carl Roth	0335.3
PMSF	AppliChem / Darmstadt, Germany	A0999
Precision Plus Protein Dual Color Standard	BioRad	1610394
Primer	Eurofins Genomics / Ebersberg, Germany	
Random Primer (500 μg/ml)	Promega	C1181
RNasin Ribonuclease Inhibitor (40u/μl)	Promega	N2515
RIPA buffer	Cell Signaling / Danvers, MA, USA	9806
Roti-Quant	Carl Roth	K015.1
SDS	Carl Roth	CN30.1
Sodium pyruvate	Merck	L0473
TEMED	Carl Roth	2367.2
TG buffer	BioRad	1610734
TGS buffer	BioRad	1610772
Thiazovivin	PeproTech / Rocky Hill, NJ, USA	1227180
Tris	Carl Roth	AE15.3
Trypsin-EDTA (0.05%), phenol red	Thermo Fisher Scientific	25300054
Tween-20	Carl Roth	9127.2
WesternBright ECL HRP substrate	Advansta / San Jose, CA, USA	K-12045-D50

2.1.2 Kits

Kits that were utilized for the experiments of this thesis are listed in **Table 2**.

Table 2: Kits.

Label	Supplier	Catalog no.
ADP/ATP Ratio Bioluminescence Assay Kit, ApoSENSOR	BioVision / Milpitas, CA, USA	K255-200
DNase I Digest Kit peqGOLD	VWR Peqlab / Radnor, PA, USA	13-1091
EpiQuik Total Histone Extraction Kit	EpiGentek / Farmingdale, NY, USA	OP-0006-100
NAD/NADH Quantitation Colorimetric Kit	BioVision	K337-100
Pyruvate Assay Kit	Abcam / Cambridge, UK	ab65342
QIAamp DNA Mini Kit	Qiagen / Hilden, Germany	51306
TGX Stain-Free FastCast Acrylamide Kit, 12%	BioRad	1610185
Total RNA Kit peqGOLD	VWR Peqlab	13-6834
Trans-Blot Turbo RTA Mini 0.2 µm PVDF Transfer Kit	BioRad	1704272

2.1.3 Consumables

Consumables which have been used for the experiments of this project are specified in **Table 3**.

Table 3: Consumables.

Article	Size	Supplier
96-Well Black/Clear Bottom Plate, TC Surface		Thermo Fisher Scientific
96-Well White/Clear Bottom Plate, TC Surface		Thermo Fisher Scientific
96-well, pureGrade, PS, white, F-bottom		Brand / Wertheim, Germany
Acrodisc Syringe Filters with Supor Membrane, Sterile	0.2 µM; 32 mm	Pall Corporation / Port Washington, NY, USA
Amicon Ultra Centrifugal Filters	0.5 ml	Merck
BD Microlance Hypodermic Needle 27G x ¾		BD / Franklin Lakes, NJ, USA
C-Chip / Neubauer Improved		NanoEnTek / Pleasanton, CA, USA

2. Materials and Methods

Cell culture flask	T175	Greiner Bio-One / Frickenhausen, Germany
Cell scraper		Corning / Schiphol-Rijk, the Netherlands
Centrifuge tube	15 ml, 50 ml	TPP / Trasadingen, Switzerland
Filter tips, Biosphere	20 μ l, 100 μ l, 1,000 μ l	Sarstedt / Nümbrecht, Germany
Glass bottle	250 ml, 1,000 ml	Schott / Mainz, Germany
Glass pipette	2 ml, 5 ml, 10 ml, 25 ml, 50 ml	Sarstedt
Hard-Shell 96-Well PCR Plates, low profile, thin wall, skirted, white/clear		BioRad
Microseal 'B' PCR Plate Sealing Film, adhesive, optical		BioRad
Mini-PROTEAN Casting Stand		BioRad
Mini-PROTEAN Comb	10-well, 15-well	BioRad
Mini-PROTEAN Short Plates		BioRad
Mini-PROTEAN Spacer Plates with 1.0 mm Integrated Spacers		BioRad
Omnifix Luer Lock Solo	20 ml	Braun / Melsungen, Germany
Parafilm		Merck
Pipette tips without filter	10 μ l, 100 μ l, 1,000 μ l	Sarstedt
Pipette	2 μ l, 10 μ l, 100 μ l, 1,000 μ l	Eppendorf / Hamburg, Germany
Pipettor Pipetus		Hirschmann / Eberstadt, Germany
Reaction tube	0.5 ml, 1 ml, 2 ml, 5 ml	Eppendorf
Single-use cuvettes ROTILABO Polystyrene, Semi-micro	1.6 ml	Carl Roth
Tissue culture dish	\varnothing 100 mm	TPP
Tissue culture dish	\varnothing 150 mm	Sarstedt
Tissue culture plate, 96-well, flat bottom, with lid, sterile		Greiner Bio-One
UV-Cuvette micro	70 μ l	Brand

2.1.4 Devices

Devices that were utilized for measurements in experiments relevant for this thesis are listed in **Table 4**.

Table 4: Devices.

Device	Supplier
Analytical balance	Sartorius / Göttingen, Germany
Axio Imager 2	Carl Zeiss / Jena, Germany
Axiovert 25	Carl Zeiss
BioSpectrometer fluorescence	Eppendorf
Centrifuge 5417R	Eppendorf
Centrifuge 5424	Eppendorf
Clean Bench Hera Safe	Thermo Fisher Scientific
CFX Connect Real-time-PCR Detection System	BioRad
Freezer -20°C	Liebherr / Bulle, Switzerland
Freezer -80°C	Thermo Fisher Scientific
Fridge +4°C	Liebherr
Incubator Hera Cell 240	Thermo Fisher Scientific
Megafuge 1.0R	Thermo Fisher Scientific
Mini-PROTEAN Tetra Vertical Electrophoresis Cell for Mini Precast Gels	BioRad
MS1 Minishaker	IKA / Staufen, Germany
Odyssey Fc Imaging System	LI-COR Biosciences / Lincoln, NE, USA
Standard Power Pack P25	Biometra / Göttingen, Germany
Tecan Infinite 200 PRO	Tecan Group / Männedorf, Switzerland
Thermocycler T-Gradient	Biometra
Thermomixer comfort	Eppendorf
Trans-Blot Turbo Transfer System	BioRad
Water bath	Memmert / Schwabach, Germany

2.1.5 Software

Software which has been applied for data analysis during this project is specified in **Table 5**.

Table 5: Software.

Software / Supplier / URL	Version	Application
Cell Counter Plugin https://imagej.nih.gov/ij/plugins/cell-counter.html		Nuclei counting
CFX Manager Software BioRad	3.1	Gene expression analysis

2. Materials and Methods

DAVID https://david.ncifcrf.gov/	6.8	Functional analysis of proteome data
i-control Microplate Reader Software Tecan Group	1.11.1.0	Detection of absorbance, fluorescence and bioluminescence
ImageJ https://imagej.net/	1.46r	Nuclei counting
GraphPad Prism Graphpad	8.3.0	Statistical analysis, preparation of figures
LI-COR Image Studio Software LI-COR Biosciences	5.2.5	Chemiluminescence detection and quantification
MaxQuant https://www.maxquant.org/	1.6.2.6	Protein identification and quantification
Perseus https://maxquant.net/perseus/	1.6.2.2	Processing of proteome and secretome data, statistical analysis
R https://www.r-project.org/	4.0.3	Statistical analysis, preparation of figures
R package: corrplot https://cran.r-project.org/web/packages/corrplot/	0.84	Statistical analysis, correlograms
R package: ggplot2 https://cran.r-project.org/web/packages/ggplot2/	3.3.2	PCA, protein profile plots
R package: ggpubr https://cran.r-project.org/web/packages/ggpubr/	0.4.0	Statistical analysis
R package: Hmisc https://cran.r-project.org/web/packages/Hmisc/	4.4.2	Statistical analysis, correlograms
R package: pheatmap https://cran.r-project.org/web/packages/pheatmap/	1.0.12	Heatmaps
R package: plyr https://cran.r-project.org/web/packages/plyr/	1.8.6	Statistical analysis
R package: tidyverse https://cran.r-project.org/web/packages/tidyverse/	1.3.0	Statistical analysis, heatmaps, protein profile plots
R package: VennDiagram https://cran.r-project.org/web/packages/VennDiagram/	1.6.20	Venn diagrams
RStudio https://rstudio.com/	1.3.1093	Statistical analysis, preparation of figures
STRING https://string-db.org/	11.0	PPIN construction, clustering
UniProt/Swiss-Prot database https://www.uniprot.org/	July 17, 2018	Download of reference proteome for protein identification
Zen 2012 Imaging Software / Carl Zeiss	Blue edition	Microscopic image analysis

2.2 Cell culture technique

2.2.1 Isolation and culture of dermal fibroblasts

In this project, female volunteers from three age groups were included: Y (20, 23, 25, 25, 25 yr.), M (36, 36, 37, 37, 42, 46, 47, 48, 49 yr.) and O (60, 60, 61, 61, 64 yr.). Only probands without tanning bed and smoking history were selected. From each donor, 4 mm punch biopsies were obtained from buttocks and neck skin. The study conforms to the principles of the Declaration of Helsinki and was approved by the Ethics Committee of the Medical Faculty of the University of Düsseldorf (# 3361) in 2010. All donors have given their informed written consent.

NHDF were isolated as described previously [102] and subsequently stored in liquid nitrogen. Cells were thawed in a water bath at 37°C and immediately transferred into cell culture medium containing 5 µM thiazovivin (**Table 6**). After 24 h, this was replaced by cell culture medium as specified in **Table 7**, which was exchanged every three days. NHDF were cultivated under standard conditions of 37°C and 5% CO₂.

Table 6: Composition of cell culture medium for thawed cells.

Cell culture medium for thawed cells	
Dulbecco's Modified Eagle's medium (DMEM), high glucose	500 ml
Fetal calf serum (FCS)	15%
Antibiotics / antimycotics (100x)	1%
Thiazovivin	5 µM

Table 7: Composition of cell culture medium.

Cell culture medium	
DMEM, high glucose	500 ml
FCS	10%
Antibiotics / antimycotics (100x)	1%

After reaching a confluency of 90%, NHDF were washed with Dulbecco's Phosphate Buffered Saline (DPBS, **Table 8**) and detached through incubation with 0.05% Trypsin-ethylenediamine tetraacetic acid (EDTA) for 5 min at 37°C. Then, cell culture medium was added to stop the trypsin reaction. After centrifugation (1,200 rpm, 5 min), NHDF were resuspended in cell culture medium and cell number was determined using a Neubauer counting chamber. Cells were further

cultivated in T175 flasks and plated on 96-well plates or petri dishes (Ø 100 mm, 150 mm) for experiments which were conducted with cells in passages 5-10.

Table 8: Composition of DPBS.

1x DPBS pH 7.0-7.3	
KCl	2.7 mM
KH ₂ PO ₄	1.5 mM
NaCl	137.9 mM
Na ₂ HPO ₄ -7H ₂ O	8.1 mM

2.2.2 Treatment with substances intervening in nicotinamide adenine dinucleotide (NAD⁺) metabolism

During experiments, cells were cultured in starvation medium as stated in **Table 9** for 48 h. NHDF were treated with the following substances: poly(ADP-ribose) polymerases (PARP) inhibitor olaparib, cluster of differentiation 38 (CD38) inhibitor 78c and NAD⁺ precursor β-nicotinamide mononucleotide (NMN). The substances were resolved either in starvation medium or dimethyl sulfoxide (DMSO) and diluted with starvation medium (**Table 10**).

Table 9: Composition of starvation medium.

Starvation medium	
DMEM, high glucose, no glutamine, no phenol red	500 ml
FCS	1%
Alanyl-Glutamine	1%
Antibiotics / antimycotics (100x)	1%

Table 10: Substances intervening in NAD⁺ metabolism.

Substance	Solvent	Final concentration
Olaparib	DMSO	2 μM, 3 μM
78c	DMSO	50 nM, 500 nM
NMN	Starvation medium	2 mM, 3 mM

2.3 Secretome and proteome analysis

2.3.1 Secretome and proteome preparation

NHDF were plated in T175 cell culture flasks. At a confluency of 90%, the cells were washed three times with DPBS and incubated with serum-free medium (**Table 11**) for 48 h. Samples for secretome and proteome analysis were prepared each from the same flask.

Table 11: Composition of serum-free cell culture medium.

Serum-free cell culture medium	
DMEM, high glucose	500 ml
Antibiotics / antimycotics (100x)	1%

For secretome analysis, the supernatants were collected, centrifuged (1,000 g, 5 min, 4°C) and filtered with a 0.2 µm Acrodisc Syringe Filter. Thereafter, 1.5 protease inhibitor cocktail tablets were dissolved in the supernatants through mixing for 2-5 min. The samples were stored temporarily at -80°C. Further secretome preparation for subsequent mass spectrometric analysis was performed as described elsewhere [97].

For proteome analysis, cells were washed three times with cold DPBS. NHDF were detached with a cell scraper in DPBS under constant cooling and centrifuged (2,000 rcf, 3 min, 4°C). The cell pellets were resuspended in 1 ml DPBS and transferred into reaction tubes. After centrifugation (14,000 rpm, 3 min, 4°C), the cell pellets were stored temporarily at -80°C. Proteins were extracted from frozen cell pellets as described elsewhere [103]. Protein concentration was determined through Pierce 660 nm Protein Assay (Thermo Fischer Scientific). For sodium dodecyl sulfate polyacrylamide gel electrophoresis (SDS-PAGE), 10 µg protein per sample were loaded on the gel. For in-gel-digestion, the isolated gel pieces were reduced (10 mM dithiothreitol (DTT)), alkylated (50 mM iodoacetamide) and underwent tryptic digestion (200 ng trypsin/100 mM ammonium bicarbonate). The peptides were resolved in 0.1% trifluoroacetic acid and subjected to liquid chromatography.

2.3.2 Mass spectrometric analysis

Mass spectrometric analysis of secretomes and proteomes was performed by the Molecular Proteomics Laboratory of the Biological-Medical Research Centre (BMFZ) of the Heinrich Heine

University Düsseldorf (HHU). For label-free liquid chromatography-mass spectrometry (LC-MS), a Q Exactive Plus (Thermo Fisher Scientific) connected with an Ultimate 3000 Rapid Separation liquid chromatography system (Dionex / Thermo Fisher Scientific, Idstein, Germany) equipped with an Acclaim PepMap 100 C18 column (75 μm inner diameter, 25 cm length, 2 mm particle size from Thermo Fisher Scientific) was applied. The LC gradient time was 120 min. The mass spectrometer was operating in positive mode and coupled with a nano-electrospray ionization source. Capillary temperature was set to 250°C and source voltage to 1.5 kV. In the Q Exactive Plus mass spectrometer, for the survey scans, a mass range from 350 to 2000 m/z at a resolution of 140,000 was used. The automatic gain control was set to 3,000,000 and the maximum fill time was 80 ms. The ten most intensive peptide ions were isolated and fragmented by high-energy collision dissociation.

2.3.3 Protein identification and quantification

Protein identification was conducted with MaxQuant v1.6.2.6 [104] applying Andromeda search engine [105] with default settings. All proteins of *Homo sapiens* extracted from the UniProt/Swiss-Prot database (July 17, 2018) served as reference data set. For peptide and protein identification, the false discovery rate was set to 1% ($p \leq 0.01$). In the case that an identified peptide was mapped to more than one protein, these proteins were presented as one protein group. Further parameter settings are listed in **Table 12**. Label-free quantification (LFQ) of proteins was performed by MaxLFQ algorithm that is integrated in the MaxQuant software [106]. For quantification, ≥ 2 unique or razor peptides were required.

Table 12: Parameter settings in MaxQuant.

Item	Value
Enzyme specificity	Trypsin
Max. missed cleavages	2
First search peptide tolerance	20 ppm
Main search peptide tolerance	4.5 ppm
Variable modifications	Oxidation (M), Acetyl (Protein N-term)
Fixed modifications	Carbamidomethyl (C)

The protein groups file from MaxQuant was imported into Perseus v1.6.2.2 [107] to conduct further data analysis. LFQ intensities were pre-processed and $\log_2(x)$ transformed. The samples were classified into six groups according to the age group of the donor and the aging type of the tissue: Y-NHDF^{INT}, M-NHDF^{INT}, O-NHDF^{INT}, Y-NHDF^{EXT}, M-NHDF^{EXT} and O-NHDF^{EXT}. For

determination of protein diversity, proteins were defined as 'identified', if they were present in ≥ 3 samples of ≥ 1 group.

For the statistical evaluation, only proteins were included which occurred in ≥ 3 samples in each group considered for the respective analysis. To investigate age-dependent alterations, statistical analysis was performed separately for NHDF^{INT} and NHDF^{EXT}. The correlation between donor age and protein levels was assessed via Spearman's correlation using R v3.5.2 and the R packages corrplot v0.84, ggpubr v0.4.0, Hmisc v4.4.2, plyr v1.8.6 and tidyverse v1.3.0. The fold change (FC) cut-off was set to $|1.5|$ and a significance threshold of $p < 0.05$ was applied. To examine differences between NHDF^{EXT} vs NHDF^{INT} within each age group, Student's t-test was conducted using Perseus v1.6.2.2. Proteins with $FC > |1.5|$ and $p < 0.05$ were defined as significant.

2.3.4 Bioinformatics analysis

Functional enrichment analysis (FEA) was performed using the Database for Annotation, Visualization and Integrated Discovery (DAVID) v6.8 tool [108, 109]. As input lists, significantly increased or decreased proteins showing an age-dependent change or a difference between NHDF^{EXT} vs NHDF^{INT} were uploaded. The DAVID default whole human genome was applied as background list and enrichment was assessed for gene ontology (GO) biological process terms. Fisher's exact test was performed and a significance threshold of $p < 0.05$ was applied. Terms with at least three (age-dependent changes) or two (NHDF^{EXT} vs NHDF^{INT}) assigned proteins per term were considered. Representative GO terms are depicted in the figures.

Protein-protein interaction networks (PPIN) were constructed from significantly regulated proteins in NHDF^{EXT} vs NHDF^{INT} of Y, M or O donors, applying the Search Tool for the Retrieval of Interacting Genes/Proteins (STRING) v11.0 [110, 111]. The network edges represent functional and physical protein associations and line thickness displays the strength of data support. Interaction search was performed with a medium confidence score of 0.4. Seven interaction sources were included: experiments, gene fusion, co-expression, co-occurrence, databases, neighborhood, text mining. Disconnected nodes in the PPIN were hidden and neglected. To identify clusters within every PPIN, Markov cluster (MCL) algorithm was used with an inflation parameter of three. To determine the most important functions of the four largest clusters of the PPIN, FEA was performed, as described before.

Principal component analysis (PCA) was performed using the R package ggplot2 v3.3.2. The analysis was based on $\log_2(x)$ transformed LFQ values of proteins of secretomes or proteomes from NHDF^{INT} and NHDF^{EXT} of the individual Y and O donors.

Correlograms were generated with R packages Hmisc v4.4.2 and corrplot v0.84 and were based on Spearman's correlation. Group mean or individual $\log_2(x)$ transformed LFQ values of proteins of secretomes or proteomes from NHDF^{INT} and NHDF^{EXT} of Y, M and O probands were utilized.

Hierarchical clustering and preparation of heatmap were conducted applying the R packages pheatmap v1.0.12 and tidyverse v1.3.0. Initially, group means of $\log_2(x)$ transformed LFQ values of proteins of proteomes from NHDF^{INT} or/and NHDF^{EXT} of Y, M and O donors were calculated. Z-score normalization was performed over all group means and hierarchical clustering of proteins was carried out with Euclidean distance as the similarity measure.

For generation of protein profile plots, the R packages ggplot2 v3.3.2 and tidyverse v1.3.0 were used. Group means of $\log_2(x)$ transformed LFQ values of proteins of proteomes from NHDF^{INT} and NHDF^{EXT} of Y, M and O probands were calculated. Then, Z-score normalization was conducted over all group means. For the smoothing function, a linear model was utilized as smoothing method and a second order polynomial formula ($y \sim \text{poly}(x, 2)$) was applied.

Venn diagrams were created with VennDiagram v1.6.20. Only proteins which were quantified or identified in ≥ 3 samples of ≥ 1 group were considered.

2.4 Western blot analysis

2.4.1 Protein isolation and quantification

For protein isolation, NHDF were detached in DPBS with a cell scraper under constant cooling and centrifuged (1,400 rpm, 5 min, 4°C). Then, cell pellets were resuspended in radio immunoprecipitation assay (RIPA) buffer containing 0.1% phenylmethylsulfonyl fluoride (PMSF) (**Table 13**). During the following incubation for 30 min at 4°C, the samples were mixed several times. After subsequent centrifugation (14,000 rpm, 15 min, 4°C), the supernatants, containing the dissolved proteins, were collected and stored at -80 °C.

Protein quantification was conducted via Bradford protein assay. For this, 1 μl protein lysate was diluted with 799 μl dH₂O and incubated with 200 μl Roti-Quant for 5 min at room temperature (RT). The absorbance was measured at the wavelength $\lambda=595$ nm with a BioSpectrometer fluorescence. Standardization was performed with a bovine serum albumin (BSA) standard curve.

Table 13: Composition of RIPA buffer.

1x RIPA buffer (0.1% PMSF)	
Tris/HCl pH 7.5	20 mM
NaCl	150 mM
Na ₂ EDTA	1 mM
EGTA	1 mM
NP-40	1%
Sodium deoxycholate	1%
Sodium pyrophosphate	2.5 mM
β-glycerophosphate	1 mM
Na ₃ VO ₄	1 mM
Leupeptin	1 µg/ml
PMSF	0.1%

2.4.2 Histone extraction

Histone extraction was performed with an EpiQuik Total Histone Extraction Kit according to the manufacturer's instructions.

2.4.3 SDS-PAGE

For protein denaturation, 15 µg protein lysate or 5 µl histone extract was mixed with 5x sodium dodecyl sulfate (SDS) loading buffer (**Table 14**) and incubated at 95°C for 5 min. 12% SDS polyacrylamide gels were prepared using a TGX Stain-Free FastCast Acrylamide Kit, 12% as well as tetramethyl ethylenediamine (TEMED) and ammonium persulfate (APS). Proteins were separated via a Mini-PROTEAN Tetra Vertical Electrophoresis Cell for Mini Precast Gels applying a voltage of 80 V and 120 V for the stacking and separating gel, respectively [112]. 10x Tris/Glycine/SDS (TGS) buffer (**Table 15**) was utilized and protein sizes were determined with a Precision Plus Protein Dual Color Standard.

Table 14: Composition of SDS loading buffer.

5x SDS loading buffer	
Tris/HCl	312.5 mM
SDS	10%
Glycerol	50%
DTT	250 mM
Bromophenol blue	10%

Table 15: Composition of TGS buffer.

10x TGS buffer pH 8.3	
Tris	25 mM
Glycine	192 mM
SDS	0.1%

2.4.4 Western blot and immunodetection of proteins

Proteins were transferred from the polyacrylamide gel to a polyvinylidene difluoride (PVDF) membrane via semi-dry blotting technique. For assembly of the blotting sandwich, the Trans-Blot Turbo RTA Mini 0.2 μ m PVDF Transfer Kit was utilized. The PVDF membrane was activated in methanol for 10 s. Membrane, polyacrylamide gel and filter paper were incubated for several minutes in 10x Tris/Glycine (TG) buffer (**Table 16**). For the transfer, a Trans-Blot Turbo Transfer System was used and the STANDARD SD transfer protocol was applied (30 min, 25 V, \leq 1.0 A).

Table 16: Composition of transfer buffer.

10x TG buffer pH 8.3	
Tris	25 mM
Glycine	192 mM

After blotting, the PVDF membrane was blocked with 5% BSA/Tris-buffered saline with Tween-20 (TBS-T) (**Table 17**) for 1 h at RT to prevent subsequent unspecific antibody binding.

Table 17: Composition of TBS-T buffer.

1x TBS-T buffer pH 7.6	
Tris	50 mM
NaCl	150 mM
Tween-20	0.1%

Incubation of the membrane with primary antibody (**Table 18**) was conducted at 4°C overnight and with secondary antibody (**Table 19**) at RT for 2 h. After each antibody incubation the membrane was washed in TBS-T (3x 10 min at RT).

Table 18: Primary antibodies.

Antigen	Size (kDa)	Species	Dilution	Supplier
β-Actin	42	Mouse	1:10,000	Sigma-Aldrich
CAT	60	Rabbit	1:1,000	Cell Signaling
CS	45	Rabbit	1:1,000	Cell Signaling
Histone H3	15	Rabbit	1:1,000	GeneTex / Irvine, CA, USA
H3K9ac	15	Mouse	1:1,000	GeneTex
H3K9me3	15	Rabbit	1:1,000	GeneTex
H3K14ac	17	Rabbit	1:1,000	Cell Signaling
H3K56ac	15	Rabbit	1:1,000	GeneTex
Histone H4	11	Rabbit	1:2,000	Cell Signaling
H4K8ac	11	Mouse	1:10,000	Abcam
H4K12ac	11	Rabbit	1:500	Cell Signaling
H4K16ac	11	Rabbit	1:1,000	Cell Signaling
IDH2	43	Rabbit	1:1,000	Cell Signaling
Lamin A/C	63, 74	Mouse	1:1,000	Cell Signaling
ME2	65	Rabbit	1:1,000	Cell Signaling
PDHA1	43	Rabbit	1:1,000	GeneTex
SDHA	73	Rabbit	1:1,000	Cell Signaling
SIRT1	110-120	Mouse	1:1,000	Abcam
SIRT3	28	Rabbit	1:1,000	Cell Signaling
SOD2	25	Rabbit	1:1,000	GeneTex
SOD2K68ac	25	Rabbit	1:500	Abcam

Table 19: Secondary antibodies.

Antigen	Species	Labeling	Dilution	Supplier
Anti-Mouse	Goat	HRP	1:5,000	LI-COR Biosciences
Anti-Rabbit	Goat	HRP	1:5,000	LI-COR Biosciences

For protein detection, the membrane was incubated with WesternBright ECL horseradish peroxidase (HRP) substrate for 3 min. Afterwards, the chemiluminescence signal was captured via an Odyssey Fc Imaging System. For protein lysates or histone extracts, β -actin or Lamin A/C was utilized as loading control. Detection of chemiluminescence and quantification of protein amounts were conducted via the LI-COR Image Studio Software v5.2.5.

2.5 Measurement of pyruvate consumption

NHDF were incubated with 1 mM sodium pyruvate/DMEM for 48 h. The pyruvate concentrations of the supernatants (48 h), the initial solution (0 h) and the control (DMEM) were determined with a Pyruvate Assay Kit according to the manufacturer's instructions. Fluorescence (Fl) at Ex/Em=535/587 nm of triplicates of each sample was measured in a black-walled 96-well plate with clear bottom via a Tecan Infinite 200 PRO and processed with the i-control Microplate Reader Software v1.11.1.0. For determination of pyruvate consumption, $Fl_{48\text{ h}}$ was subtracted from $Fl_{0\text{ h}}$. Pyruvate consumption concentrations were normalized to the protein content to enable comparison among different samples.

2.6 Messenger ribonucleic acid (mRNA) analytics

2.6.1 RNA isolation and quantification

RNA isolation and enzymatic DNA digestion were performed with a Total RNA Kit peqGOLD and DNase I Digest Kit peqGOLD according to the manufacturer's instructions. For quantification and purity assessment, RNA was diluted 1:100 in DEPC-H₂O and the absorbances at $\lambda=260$ nm and $\lambda=280$ nm were measured via a BioSpectrometer fluorescence.

2.6.2 Complementary DNA (cDNA) synthesis

For cDNA synthesis, 1 µg RNA in a volume of 20 µl DEPC-H₂O and a Thermocycler T-Gradient were utilized. Primer annealing was conducted through incubation of RNA with Random Primers and polymerase chain reaction (PCR) Nucleotide Mix for 5 min at 65°C (**Table 20**).

Table 20: Reaction mixture for primer annealing.

Primer annealing	
1 µg RNA diluted in DEPC-H ₂ O	20 µl
Random Primer (100 ng/µl)	2 µl
PCR Nucleotide Mix (10 mM)	2 µl
5 min	65°C

In the next step, the samples were preincubated with RNasin Ribonuclease Inhibitor, Moloney Murine Leukemia Virus Reverse Transcriptase (M-MLV RT) 5x Buffer and DEPC-H₂O for 2 min at 37°C (**Table 21**).

Table 21: Reaction mixture for preincubation for reverse transcription.

Preincubation for reverse transcription	
RNasin Ribonuclease Inhibitor (40u/µl)	2 µl
M-MLV RT 5x Buffer	8 µl
DEPC-H ₂ O	4 µl
2 min	37°C

For cDNA synthesis, M-MLV RT was added and the samples were incubated for 10 min at 25°C and for 50 min at 37°C. Subsequent heat inactivation of M-MLV RT at 70°C was performed for 15 min (**Table 22**).

Table 22: Reaction mixture for reverse transcription.

Reverse transcription	
M-MLV RT (200u/µl)	2 µl
10 min	25°C
50 min	37°C
15 min	70°C

2.6.3 Real-Time quantitative PCR (RT-qPCR)

For RT-qPCR, a mix of cDNA with iTaq Universal SYBR Green Supermix, forward (FW) primer, reverse (RV) primer (Table 23) and DEPC-H₂O was prepared as specified in Table 24. According to the presented protocol (Table 24), 40 PCR cycles were conducted applying a CFX Connect Real-time-PCR Detection System. The quantification cycle (C_q) values were calculated by the CFX Manager Software v3.1. Expression of target genes was normalized to *β-actin* and the calculation of relative gene expression was based on the 2^{-ΔΔC_t} (threshold cycle) method [113].

Table 23: Primer sequences.

Target gene	Sequences
<i>β-Actin</i>	FW: 5'-CCC CAG GCA CCA GGG CGT GAT-3' RV: 5'-GGT CAT CTT CTC GCG GTT GGC CTT GGG GT-3'
<i>HMOX1</i>	FW: 5'-GCC ATG AAC TTT GTC CGG TG-3' RV: 5'-GGA TGT GCT TTT CGT TGG GG-3'
<i>CAT</i>	FW: 5'-GAC CGA GAG AGA ATT CCT GAG A-3' RV: 5'-TCA AAT ACC TTT GCC TTG GAG T-3'
<i>SOD2</i>	FW: 5'-AGC ACG CTT ACT ACC TTC AG-3' RV: 5'-ACT TTT TGC AAG CCA TGT AT-3'
<i>SIRT3</i>	FW: 5'-TCT TTT TCT GTG GGT GCT TC-3' RV: 5'-GTA CTG CTG GAG GTT GCT GT-3'

Table 24: Reaction mixture and protocol for RT-qPCR.

RT-qPCR mix per reaction		
cDNA	1.5 μl	
iTaq Universal SYBR Green Supermix	12.5 μl	
FW primer	1.25 μl	
RV primer	1.25 μl	
DEPC-H ₂ O	8.5 μl	
Protocol (40 PCR cycles)		
Denaturation	20 s	94°C
Annealing	20 s	56°C
Elongation	30 s	72°C

2.7 Determination of mitochondrial superoxide levels

MitoSOX is a fluorogenic dye applied for the detection of mitochondrial superoxide, which oxidizes MitoSOX, thereby producing a red fluorescence signal. Initially, NHDF were plated in a black-walled 96-well plate with clear bottom. For staining, the cells were washed with DPBS and incubated with 5 μ M MitoSOX/DPBS for 30 min at 37°C protected from light. The dye solution was removed and NHDF were washed twice with DPBS. Fluorescence at Ex/Em=510/580 nm of triplicates of each sample was measured via a Tecan Infinite 200 PRO and processed with the i-control Microplate Reader Software v1.11.1.0. Relative superoxide levels were calculated as FC referring to NHDF^{INT}.

To enable comparison between different samples, the superoxide concentration was normalized to the cell number. For this purpose, after fluorescence measurement, DPBS was removed and NHDF were incubated with 2% paraformaldehyde (PFA)/DPBS for 15 min at RT. Then, cells were washed with DPBS and nuclei were stained with 5.72 mM 4',6-diamidino-2-phenylindole (DAPI)/DPBS for 5 min at RT protected from light. NHDF were washed with DPBS and image capturing of stained nuclei was performed via an Axio Imager 2 and the Zen 2012 Imaging Software. Nuclei were counted with the Cell Counter Plugin from ImageJ 1.46r.

2.8 mtDNA analytics

2.8.1 DNA isolation and quantification

DNA isolation was performed via a QIAamp DNA Mini Kit according to the manufacturer's instructions. For DNA quantification and purity assessment, the absorbances at $\lambda=260$ nm and $\lambda=280$ nm were measured with a Tecan Infinite 200 PRO and processed through the i-control Microplate Reader Software v1.11.1.0.

2.8.2 Measurement of mtDNA content

For measurement of mtDNA content via RT-qPCR, a mix of DNA with iTaq Universal SYBR Green Supermix, FW primer and RV primer (**Table 25**) was prepared as specified in **Table 26**.

Table 25: Primer sequences for measurement of mtDNA content.

Target gene	Sequences
<i>β-Globin</i>	FW: 5'-AGA AGT CTG CCG TTA CTG CC-3' RV: 5'-CTG TCT CCA CAT GCC CAG TT-3'
<i>IS</i>	FW: 5'-GAT TTG GGT ACC ACC CAA GTA TTG-3' RV: 5'-AAT ATT CAT GGT GGC TGG CAG TA-3'

According to the presented protocol (**Table 26**), 40 PCR cycles were conducted applying a CFX Connect Real-time-PCR Detection System. The quantification cycle (C_q) values were calculated by the CFX Manager Software v3.1. The internal standard (IS), an 83-bp sequence unique to mtDNA, is used as a measure for the total mtDNA amount [114]. The expression of the IS fragment was normalized to *β-globin* [115] and the calculation of the relative mtDNA concentration was based on the $2^{-\Delta\Delta C_t}$ method [113].

Table 26: Reaction mixture and protocol for RT-qPCR for determination of mtDNA content.

RT-qPCR mix per reaction			
DNA	50 ng		
iTaq Universal SYBR Green Supermix	12.5 μ l		
FW primer	1.25 μ l		
RV primer	1.25 μ l		
Protocol			
	3 min	95°C	
Denaturation	20 s	94°C	40 PCR cycles
Annealing	20 s	56°C	
Elongation	30 s	72°C	
	7 min	72°C	
Melting curve	5 s	65°C-95°C (0.5°C steps)	

2.9 Determination of ADP/ATP ratios

ADP/ATP ratios were determined with the ADP/ATP Ratio Bioluminescence Assay Kit, ApoSENSOR according to the manufacturer's instructions. Bioluminescence signals of triplicates of each sample were captured in a white-walled 96-well plate with white bottom via a Tecan Infinite 200 PRO and processed with the i-control Microplate Reader Software v1.11.1.0.

2.10 Measurement of NAD⁺ levels

For determination of NAD⁺ concentration, the NAD/NADH Quantitation Colorimetric Kit was used according to the manufacturer's instructions. Absorbances of triplicates of each sample were measured in a white-walled 96-well plate with clear bottom via a Tecan Infinite 200 PRO and processed with the i-control Microplate Reader Software v1.11.1.0. NAD⁺ concentrations were normalized to the protein content to enable comparison among different samples.

2.11 Statistics

All experiments were performed with NHDF of ≥ 3 distinct donors (biological replicates). Unless otherwise stated, data are represented as mean \pm standard error of the mean (SEM) and as FC referring to NHDF^{INT}. Statistical analysis was performed with GraphPad Prism v8.3.0. For comparison of two data sets, Student's t-test was applied and for comparison of three data sets, one-way analysis of variance (ANOVA) and a follow-up Holm-Sidak's multiple comparisons test were conducted. A p-value below 0.05 ($p < 0.05$) was considered significant.

3. Results

It is generally assumed that extrinsic skin aging superimposes intrinsic skin aging. This means that both processes overlap to a certain degree and that further mechanisms are introduced through extrinsic aging. This hypothesis, however, has never been proven and interactions might be far more complex.

3.1 Age-related change of protein diversity differed between NHDF^{EXT} and NHDF^{INT}

To investigate the relationship between intrinsic and extrinsic skin aging, the proteomes and corresponding secretomes of *in situ* aged primary normal human dermal fibroblasts (NHDF) were analyzed. NHDF were isolated from buttocks (=intrinsically aged; NHDF^{INT}) vs neck (=extrinsically aged; NHDF^{EXT}) skin of female volunteers from three different age groups: young (Y; 20-25 yr.), middle-aged (M; 36-49 yr.) and old (O; 60-64 yr.).

3.1.1 Protein diversity of secretomes was increased in aged NHDF^{INT} but remained unchanged in NHDF^{EXT}

Applying label-free liquid chromatography-mass spectrometry (LC-MS), a total of 659 proteins were identified in the secretomes of NHDF of Y, M and O donors. Interestingly, the protein diversity of secretomes of NHDF^{INT} increased with age (**Figure 6A**). Whereas NHDF^{INT} of Y probands contained 224 diverse proteins (100%), those of M donors exhibited 251 different ones (112%) (**Table 27**). In NHDF^{INT} of the O group the protein number was even 292 (130%). In contrast to NHDF^{INT}, protein diversity in secretomes of NHDF^{EXT} remained unaltered with age showing 240-248 (98-101%) diverse proteins within the different age groups.

Label-free quantification (LFQ) of proteins in secretomes was conducted based on precursors signal intensities. Principal component analysis (PCA) of all \log_2 (protein quantities) of NHDF^{INT} vs NHDF^{EXT} of Y vs O donors was performed (**Figure 6B**). The PCA plot revealed no clustering of samples neither according to the age nor to the aging type. This suggested an absence of substantial quantitative differences between the considered groups, a high interindividual variability within the groups or both.

3. Results

Table 27: Protein diversity in secretomes of NHDF^{INT} and NHDF^{EXT} of Y, M and O probands.

NHDF ^{INT}	Y	M	O
Number of diverse proteins	224	251	292
Percentage of diverse proteins referred to Y donors	100%	112%	130%
NHDF ^{EXT}	Y	M	O
Number of diverse proteins	245	248	240
Percentage of diverse proteins referred to Y donors	100%	101%	98%

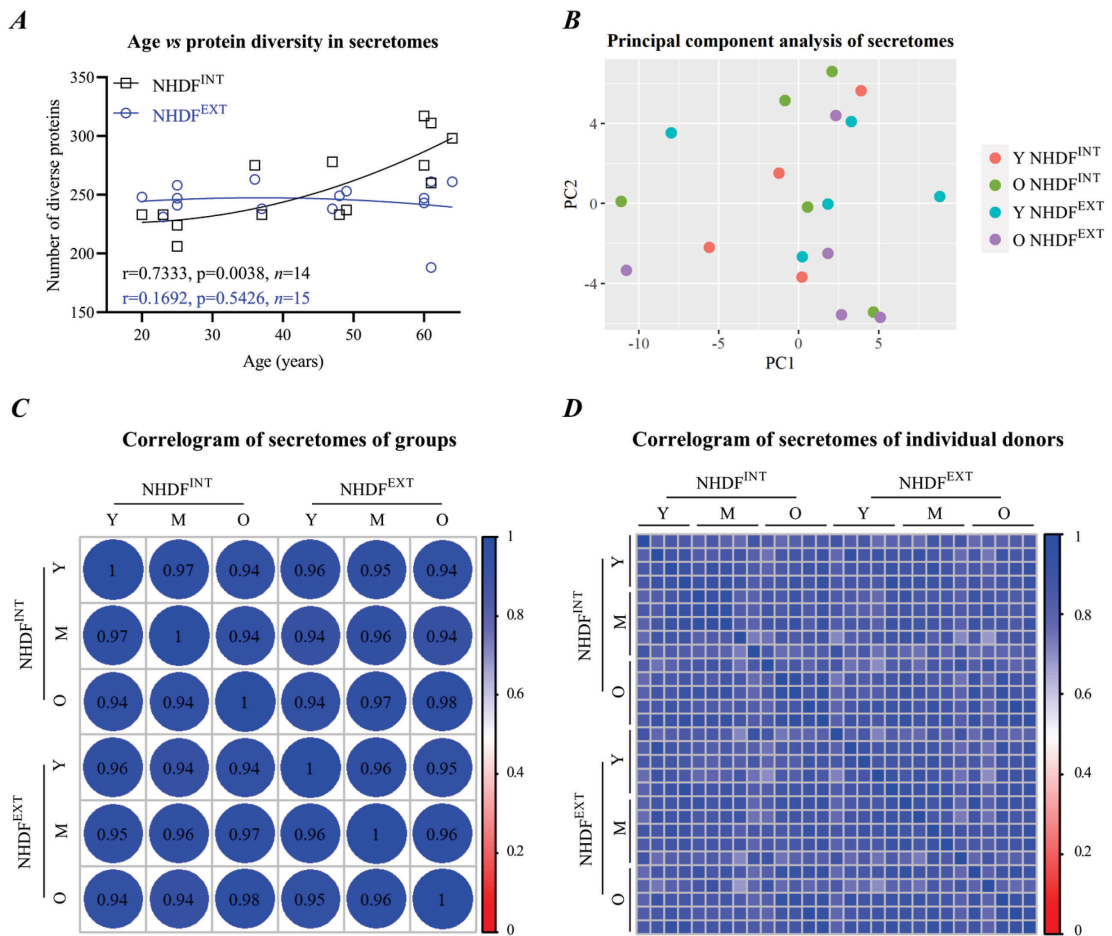


Figure 6: Age-related increase of protein diversity of secretomes was observed in intrinsically (NHDF^{INT}) but not in extrinsically aged normal human dermal fibroblasts (NHDF^{EXT}). Secretomes of NHDF^{INT} and NHDF^{EXT} of young (Y), middle-aged (M) and old (O) donors were analyzed via LC-MS (n=4-5). (A) Correlation of proband age vs number of diverse proteins with second order polynomial regression. Spearman's correlation coefficient (r) and p-value are shown. (B) Principal component analysis (PCA) of NHDF^{INT} vs NHDF^{EXT} of Y vs O donors based on log₂(protein quantities). Correlogram of mean (C) or individual donor's log₂(protein quantities) (D) of NHDF^{INT} vs NHDF^{EXT} of Y vs M vs O donors. Color and size of circles or squares indicate the strength of correlation. Spearman's correlation coefficient is depicted within the circles.

The presumption of absent quantitative differences between groups was reinforced by investigating the correlation of NHDF^{INT} vs NHDF^{EXT} of Y vs M vs O probands based on mean log₂(protein quantities). The correlogram demonstrated a high concordance between the compared groups with correlation coefficients $r \geq 0.94$ (**Figure 6C**). To evaluate interindividual variability within the groups, the correlation of log₂(protein quantities) of secretomes of individual donors was examined. Biological replicates of the same group were very similar pointing to a low interindividual variability (**Figure 6D**).

In summary, secretomes of aged NHDF^{INT} and NHDF^{EXT} demonstrated a qualitative difference regarding their protein diversity. However, first quantitative assessments of secretomes indicated that differences between the groups were rather minor.

3.1.2 Protein diversity of proteomes declined linearly in aged NHDF^{INT} but non-linearly in NHDF^{EXT}

LC-MS revealed 3,563 proteins in proteomes of NHDF of Y, M and O donors. The protein diversity showed a significant age-dependent decline in both NHDF^{INT} and NHDF^{EXT} (**Figure 7A**). It was striking that the average number of different proteins in NHDF^{INT} declined rather continuously, i.e. in a linear fashion, during aging: 1,999 proteins (100%) were identified in Y donors vs 1,518 proteins (76%) in M donors vs 1,217 proteins (61%) in O donors (**Table 28**). In contrast, in NHDF^{EXT} a non-linear and non-uniform reduction of protein diversity was observed. NHDF^{EXT} of Y vs M probands exhibited only a minor difference containing 2,070 (100%) vs 1,801 (87%) diverse proteins. However, the loss of protein diversity was far more pronounced in NHDF^{EXT} of M vs O donors with the latter showing only 894 various proteins. This corresponded to only 43% of the number originally identified in NHDF^{EXT} of Y donors. Thereby, the protein number in NHDF^{EXT} of O donors even dropped below the protein number detected in NHDF^{INT} of the same age group.

Table 28: Protein diversity in proteomes of NHDF^{INT} and NHDF^{EXT} of Y, M and O probands.

NHDF ^{INT}	Y	M	O
Number of diverse proteins	1999	1518	1217
Percentage of diverse proteins referred to Y donors	100%	76%	61%
NHDF ^{EXT}	Y	M	O
Number of diverse proteins	2070	1801	894
Percentage of diverse proteins referred to Y donors	100%	87%	43%

NHDF^{EXT} of Y vs O donors were more dissimilar than NHDF^{INT} of both groups. Correlation of log₂(protein quantities) of proteomes of individual probands revealed that interindividual variability increased with age (**Figure 7D**). Interestingly, the variability of biological replicates was higher in NHDF^{INT} than in NHDF^{EXT}.

In conclusion, these findings suggested that aging of NHDF was associated with a loss of protein diversity and an alteration of protein quantities in the proteomes. Both observations were more pronounced in NHDF^{EXT} than in NHDF^{INT}. It was particularly noticeable that protein diversity of proteomes declined non-linearly in NHDF^{EXT} but rather continuously in NHDF^{INT}.

3.2 Age-dependent change of protein abundance patterns followed a non-linear course in NHDF^{EXT}, but in a linear course in NHDF^{INT}

Statistical analysis of proteomes was performed over all three age groups separately for NHDF^{INT} and NHDF^{EXT} to investigate age-associated changes of protein quantities more closely. NHDF^{INT} and NHDF^{EXT} contained 601 and 444 significantly regulated proteins (Spearman's correlation: age vs protein quantity, $p < 0.05$; $FC > |1.5|$). Interestingly, NHDF^{INT} and NHDF^{EXT} exhibited a fundamentally different pattern of alterations of protein levels. NHDF^{INT} showed gradually, almost linearly developing changes in protein quantities over all three age groups (**Cluster 1**: Y<M<O; **Cluster 3**: Y>M>O) (**Figure 8A, B**). In contrast, in NHDF^{EXT}, age-dependent alterations of protein concentrations did not develop gradually but rather non-linearly. Protein levels were almost identical between Y and M donors (Y=M). However, NHDF^{EXT} of M vs O donors demonstrated a dramatic alteration of protein abundances that even outreached changes observed in NHDF^{INT} (**Cluster 2**: M<<O; **Cluster 4**: M>>O).

Comparison of age-dependently regulated proteins of NHDF^{INT} and NHDF^{EXT} (**Figure 8C**) revealed 297 proteins (139 upregulated, 158 downregulated) changed in both aging types (**Table S1**). Interestingly, 304 proteins (106 upregulated, 198 downregulated) exclusively altered in NHDF^{INT} were detected (**Table S2**) and 147 proteins (56 upregulated, 91 downregulated) only regulated in NHDF^{EXT} (**Table S3**).

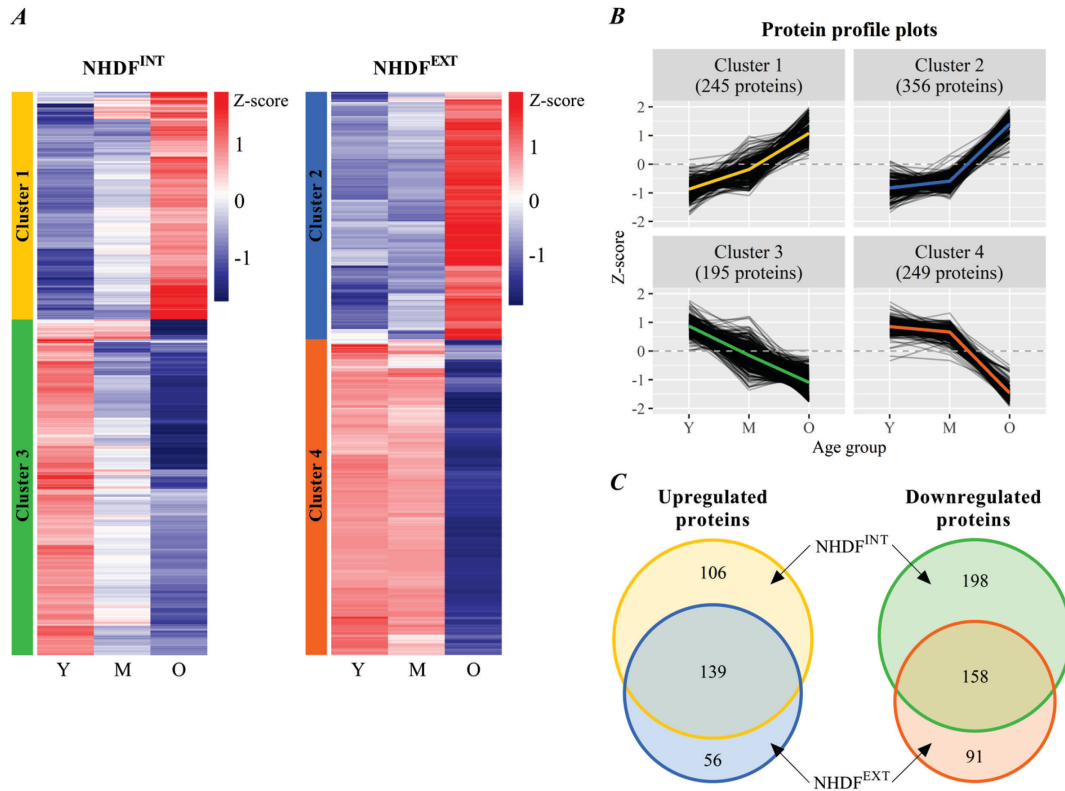


Figure 8: Age-associated changes of protein abundances in NHDF^{EXT} unlike NHDF^{INT} were characterized by a non-linear course. Proteomes of NHDF^{INT} and NHDF^{EXT} of Y, M and O donors were analyzed via LC-MS. (A) Heatmaps of age-dependently, significantly regulated proteins in NHDF^{INT} and NHDF^{EXT} revealed two clusters each. Z-score of mean $\log_2(x)$ label-free quantification (LFQ) intensities of proteins is plotted; Spearman's correlation, $p < 0.05$; $FC > |1.5|$; $n = 5$. (B) Protein profile plots of upregulated and downregulated proteins over the three age groups of previously identified clusters in NHDF^{INT} and NHDF^{EXT}. (C) Venn diagrams showing the intersection of clusters of age-dependently increased or decreased proteins in NHDF^{INT} vs NHDF^{EXT}.

To examine biological processes which were either relevant for both NHDF^{INT} and NHDF^{EXT} or unique to only one of the aging types, functional enrichment analysis (FEA) was performed applying the Database for Annotation, Visualization and Integrated Discovery (DAVID) v6.8. The whole human genome was used as background list and enrichment was assessed for gene ontology (GO) biological process terms.

FEA of jointly age-dependently, increased proteins in NHDF^{INT} and NHDF^{EXT} revealed the biological processes 'integrin-mediated signaling pathway' ($p = 1.6 \times 10^{-5}$), 'extracellular matrix organization' ($p = 2.1 \times 10^{-4}$) and 'wound healing' ($p = 4.2 \times 10^{-3}$) among the enriched GO terms (Figure 9A). Exclusively in NHDF^{INT} elevated proteins were involved in 'endoplasmic reticulum (ER) unfolded protein response' ($p = 2.7 \times 10^{-3}$) and 'DNA repair' ($p = 1.5 \times 10^{-2}$) (Figure 9B). Proteins only enhanced in NHDF^{EXT} were significantly enriched in 'collagen degradation' ($p = 1.6 \times 10^{-6}$), 'protein N-linked glycosylation' ($p = 6.2 \times 10^{-6}$) and 'ER unfolded protein response; inositol-requiring enzyme 1 (IRE1) signaling' ($p = 8.1 \times 10^{-4}$) (Figure 9C).

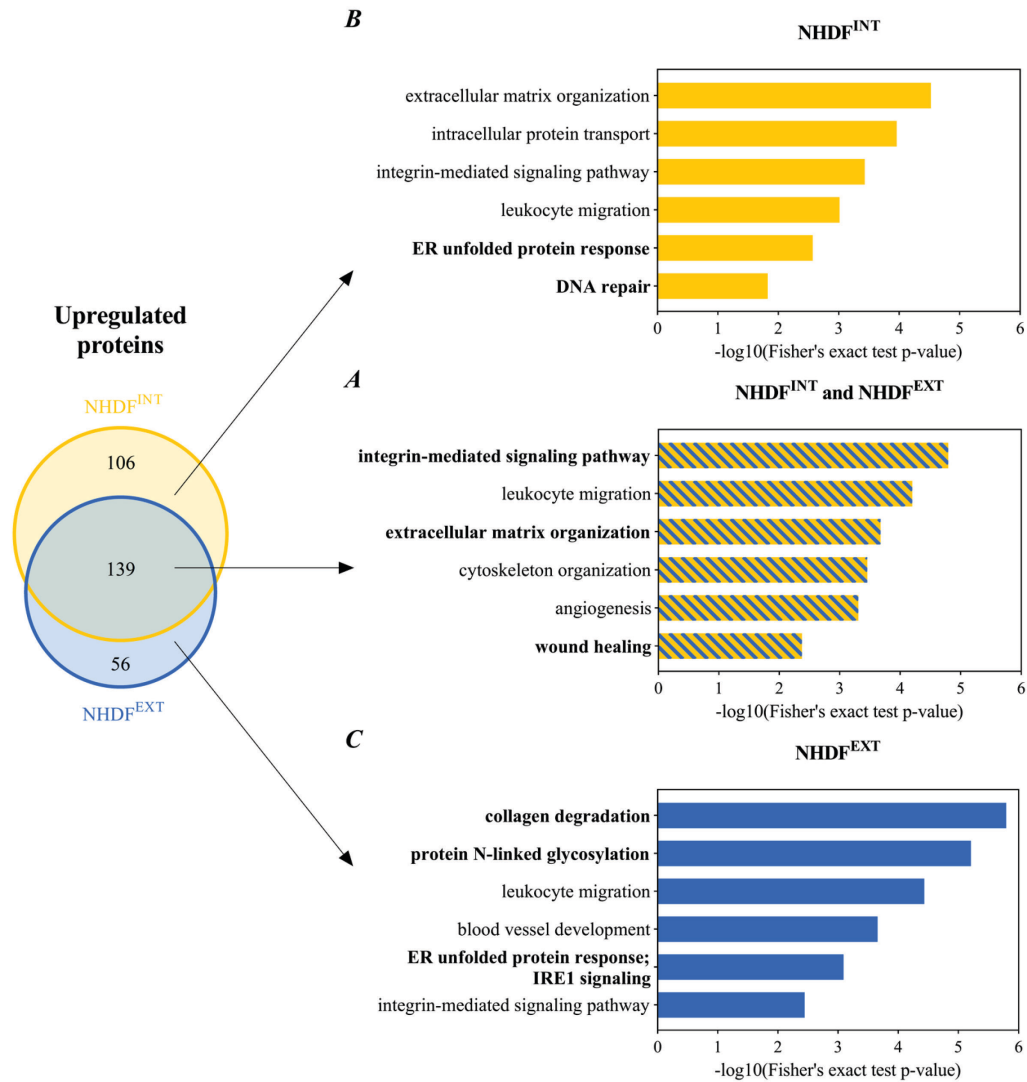


Figure 9: *In situ* aging of NHDF was accompanied by an increase of proteins involved in extracellular matrix organization and wound healing. Gene ontology (GO) enrichment analysis of age-dependently increased proteins in NHDF^{INT} and NHDF^{EXT} was conducted using the Database for Annotation, Visualization and Integrated Discovery (DAVID). Analysis was performed separately for proteins changed in both NHDF^{INT} and NHDF^{EXT} (A) or exclusively altered in NHDF^{INT} (B) or NHDF^{EXT} (C). Six representative GO biological process terms are presented. Fisher's exact test, $p < 0.05$.

The shared age-dependently decreased proteins in NHDF^{INT} and NHDF^{EXT} were enriched in 'tricarboxylic acid cycle' ($p = 6.2 \times 10^{-6}$) as well as 'translation' ($p = 6.5 \times 10^{-7}$) and 'mRNA splicing, via spliceosome' ($p = 4.1 \times 10^{-5}$) (Figure 10A). The solely in NHDF^{INT} reduced proteins were associated with 'cell redox homeostasis' ($p = 2.7 \times 10^{-4}$) and 'proteasomal ubiquitin-dependent protein degradation' ($p = 2.6 \times 10^{-3}$) (Figure 10B). Exclusively in NHDF^{EXT} downregulated proteins were involved in 'ATP biosynthesis' ($p = 1.7 \times 10^{-5}$) and 'glycolytic process' ($p = 8.2 \times 10^{-4}$) (Figure 10C).

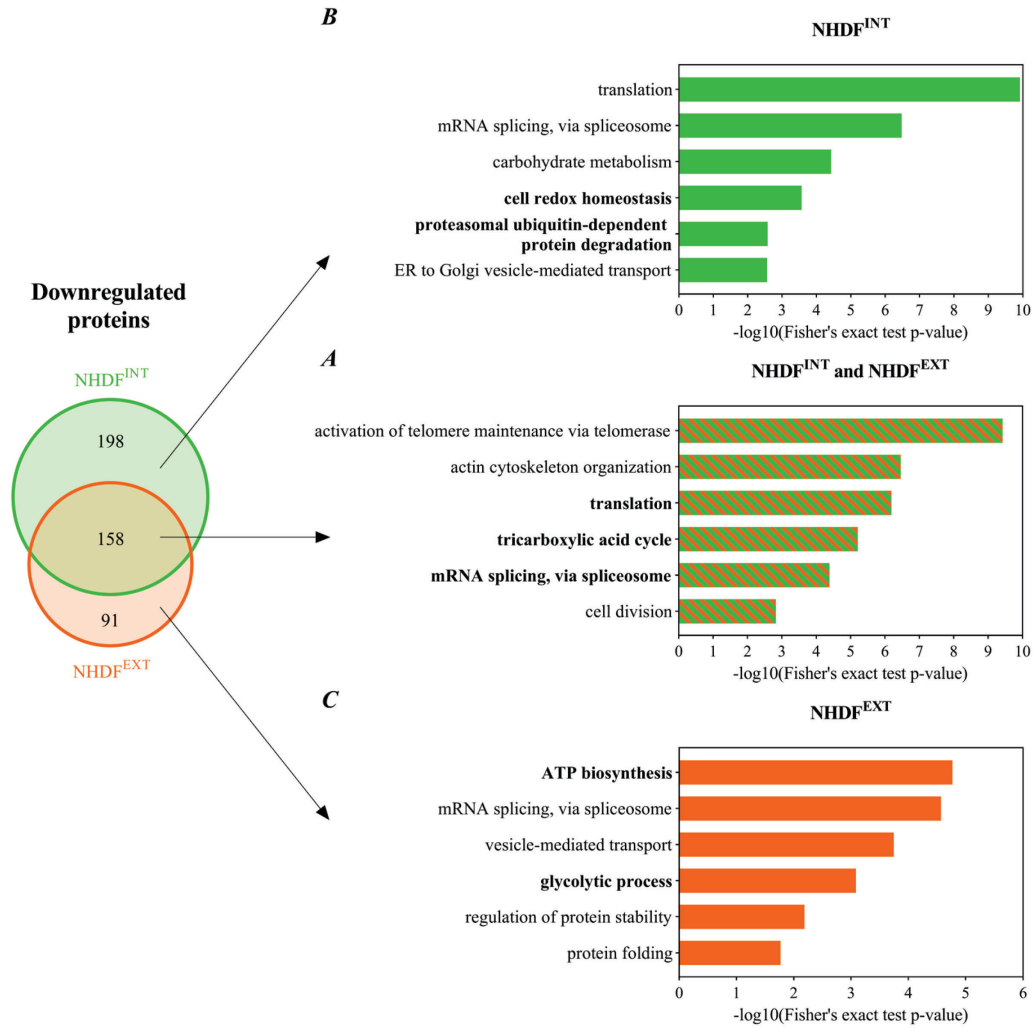


Figure 10: *In situ* aging of NHDF was characterized by a decline of proteins involved in tricarboxylic acid cycle and translation. GO enrichment analysis of age-dependently decreased proteins in NHDF^{INT} and NHDF^{EXT} was conducted using the DAVID functional annotation tool. Analysis was performed separately for proteins changed in both NHDF^{INT} and NHDF^{EXT} (A) or exclusively altered in NHDF^{INT} (B) or NHDF^{EXT} (C). Six representative GO biological process terms are presented. Fisher's exact test, $p < 0.05$.

In summary, aging of NHDF^{EXT}, unlike NHDF^{INT}, was not only characterized by a non-linear course of alterations of protein diversity, but also of protein abundances involving a pronounced acceleration of these changes between NHDF^{EXT} of M and O donors. On top of that, there were proteins showing age-related changes exclusively in NHDF^{INT}. Collectively, these findings suggested that extrinsic skin aging did not simply superimpose intrinsic skin aging, but rather indicated that interactions between both processes were more complex.

3.3 Comparison of NHDF^{EXT} vs NHDF^{INT} within each age group revealed differences in changes of metabolism-associated proteins

Age-dependent shifts of diversity and abundance patterns of proteins fundamentally differed between NHDF^{INT} and NHDF^{EXT}. These changes occurred linearly in NHDF^{INT} but non-linearly in NHDF^{EXT}. To further elucidate the relationship between intrinsic and extrinsic aging of NHDF, the differences of NHDF^{EXT} vs NHDF^{INT} within each age group were assessed more closely.

3.3.1 Examination of significantly altered proteins in NHDF^{EXT} vs NHDF^{INT} revealed clusters of metabolic proteins in the Y and M group

A comparison of the overlap of proteins identified in NHDF^{EXT} vs NHDF^{INT} within each age group revealed that the number and percentage of shared proteins dropped with advancing age (**Figure 11**). Whereas in Y and M donors NHDF^{INT} and NHDF^{EXT} shared 89% and 85% of their proteins, this intersection was considerably reduced to 67% in O probands. Apart from that, NHDF^{EXT} of the Y and M group exhibited a larger amount of uniquely identified proteins compared to NHDF^{INT} of the same age group each. However, this phenomenon was drastically reversed in O probands in which NHDF^{EXT} showed only 35 unique proteins (2%). This was in marked contrast to NHDF^{INT} of the same age group containing even 434 uniquely identified proteins (30%). These observations are in line with the aforementioned age-related loss of protein diversity in NHDF and the more pronounced decline of protein diversity in NHDF^{EXT} of M vs O donors.

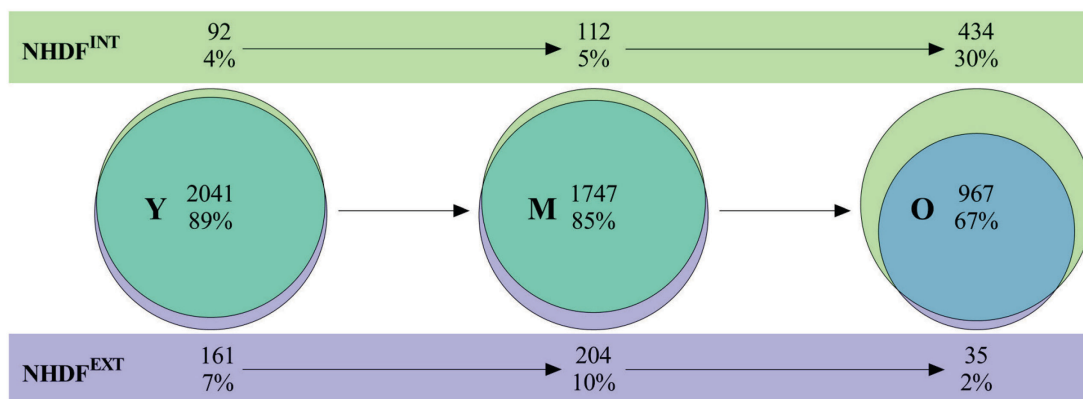


Figure 11: The intersection of shared proteins between NHDF^{INT} and NHDF^{EXT} decreased with age. Venn diagrams of proteins present in NHDF^{INT} and NHDF^{EXT} of Y, M and O donors. Total numbers and percentage of shared and unique proteins are depicted.

3. Results

Statistical analysis of LC-MS data of the shared proteins of NHDF^{EXT} vs NHDF^{INT} within each age group was performed (Student's t-test, $p < 0.05$; $FC > 1.5$). Protein-protein interaction networks (PPIN) were constructed with significantly regulated proteins applying the Search Tool for the Retrieval of Interacting Genes/Proteins (STRING) v11.0. To identify clusters within every PPIN, Markov cluster (MCL) algorithm was used. To determine the most important functions of the four largest clusters of the PPIN, FEA was performed, as described before.

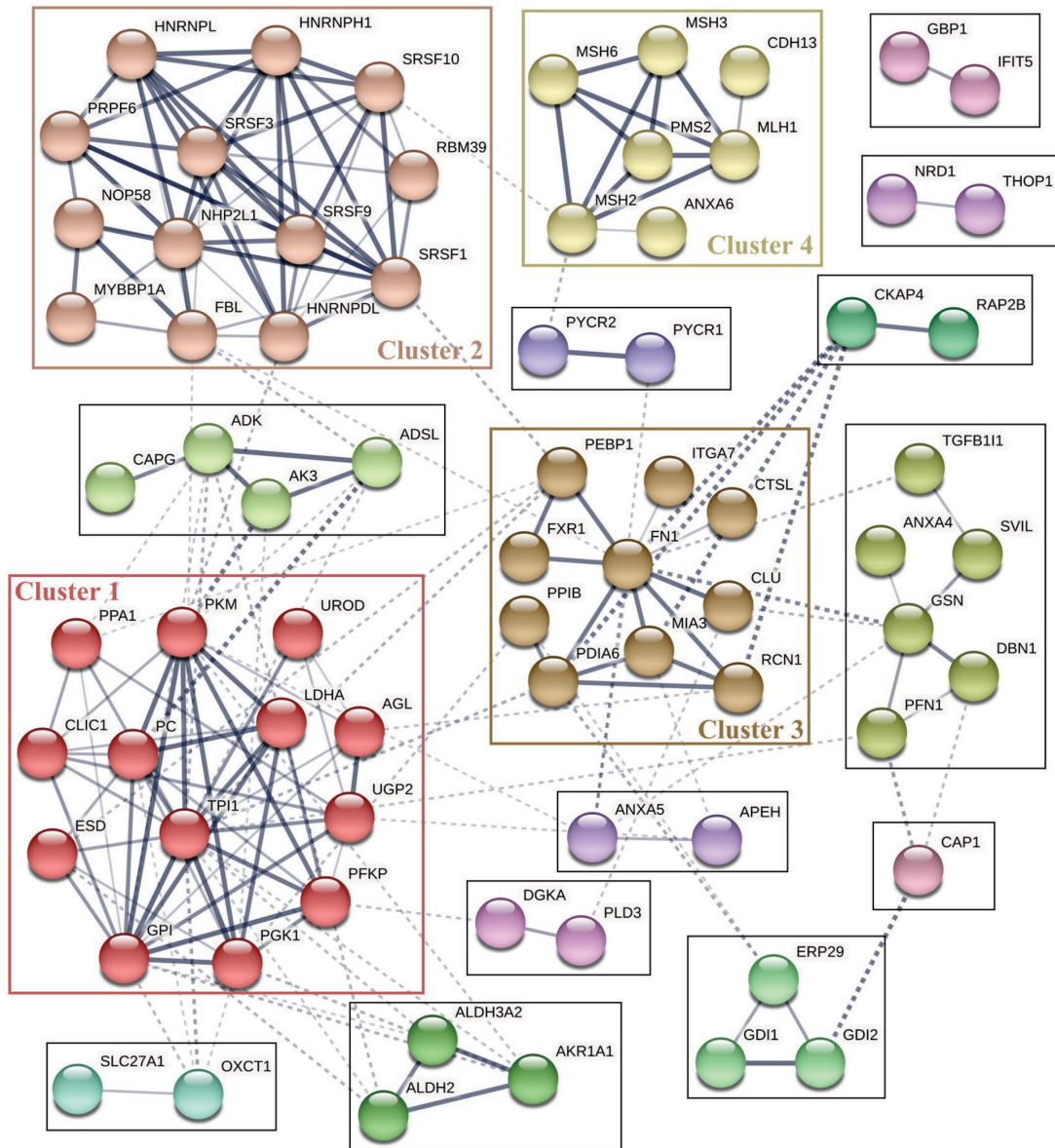


Figure 12: Network analysis of 82 significantly regulated proteins in NHDF^{EXT} vs NHDF^{INT} of Y donors performed with the Search Tool for the Retrieval of Interacting Genes/Proteins (STRING). Application of Markov cluster (MCL) algorithm with an inflation parameter of 3.0 revealed 16 clusters. The color of the nodes indicates the belonging to a certain cluster. The thickness of the edges is based on the strength of data support for the interaction. The minimum required interaction score was medium confidence (0.4). Disconnected nodes were removed from the network.

proteins) included proteins involved in ‘proteolysis’ ($p=5.1 \times 10^{-3}$) and ‘mRNA splicing, via spliceosome’ ($p=9.0 \times 10^{-6}$).

In the O group, 54 proteins were significantly regulated in NHDF^{EXT} vs NHDF^{INT} and application of MCL algorithm on their PPIN resulted in twelve clusters (**Figure 14**). Proteins of **cluster 1** (8 proteins) functioned in ‘protein N-linked glycosylation via asparagine’ ($p=7.0 \times 10^{-7}$). **Cluster 2** (6 proteins) contained proteins involved in ‘endocytosis’ ($p=1.0 \times 10^{-3}$). Proteins of **cluster 3** (4 proteins) and **cluster 4** (4 proteins) played roles in ‘extracellular matrix organization’ ($p=8.0 \times 10^{-4}$) and ‘transcription, DNA-templated’ ($p=5.8 \times 10^{-3}$).

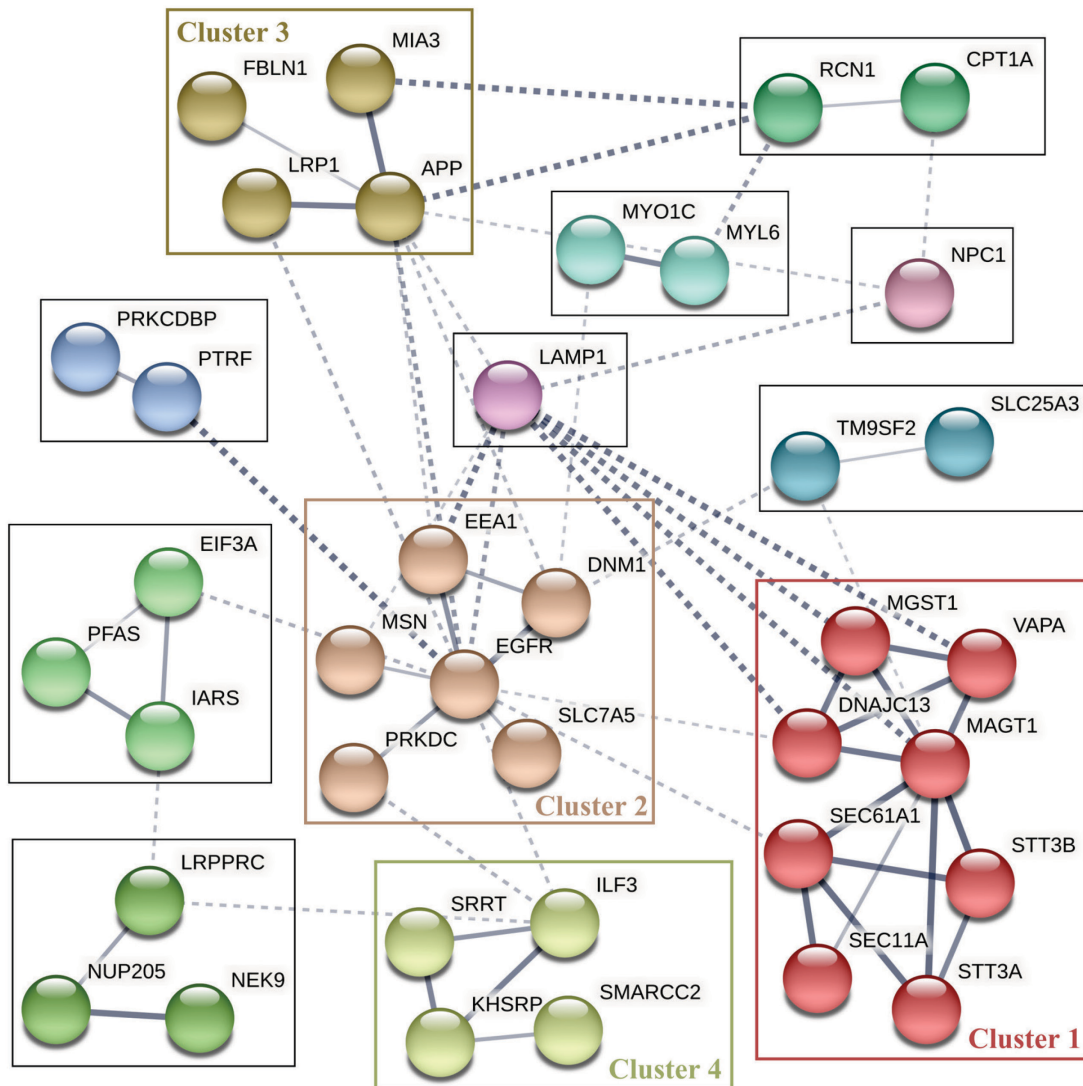


Figure 14: STRING network analysis of 54 significantly regulated proteins in NHDF^{EXT} vs NHDF^{INT} of O donors. Application of MCL algorithm with 3.0 as an inflation parameter revealed twelve clusters. The color of the nodes indicates the belonging to a certain cluster. The thickness of the edges is based on the strength of data support for the interaction. The minimum required interaction score was medium confidence (0.4). Disconnected nodes were removed from the network.

The investigation of significantly altered proteins in NHDF^{EXT} vs NHDF^{INT} of each age group via PPIN and clustering analysis showed that there were considerable functional differences. It was particularly interesting that proteins of the largest clusters identified in NHDF of Y and M probands were involved in glycolysis and tricarboxylic acid (TCA) cycle. These detected differences between NHDF^{EXT} vs NHDF^{INT} might contribute to or be causative for the non-linear course of protein abundance changes in NHDF^{EXT}.

3.3.2 Levels of metabolism-associated proteins were increased in NHDF^{EXT} vs NHDF^{INT} of Y and M donors

To further unravel differences and regulation of detected mechanisms in NHDF^{EXT} vs NHDF^{INT}, significantly changed proteins were separated into two groups: upregulated (NHDF^{EXT} > NHDF^{INT}) and downregulated proteins (NHDF^{EXT} < NHDF^{INT}). FEA was conducted for increased or decreased proteins in NHDF^{EXT} vs NHDF^{INT} of every age group.

The 82 significantly altered proteins in NHDF^{EXT} vs NHDF^{INT} of Y probands were classified into 47 upregulated and 35 downregulated proteins (**Table S4**). FEA of increased proteins revealed ‘canonical glycolysis’ ($p=7.0 \times 10^{-7}$) as the top enriched GO term (**Figure 15A**). Decreased proteins were involved in ‘mRNA splicing, via spliceosome’ ($p=1.0 \times 10^{-3}$) (**Figure 15B**).

The 61 differentially regulated proteins in NHDF^{EXT} vs NHDF^{INT} of M donors were classified into 34 increased and 27 decreased proteins (**Table S5**). Increased proteins were mainly enriched in metabolic processes like ‘tricarboxylic acid cycle’ ($p=2.5 \times 10^{-9}$) and ‘pyruvate metabolism’ ($p=8.4 \times 10^{-4}$) (**Figure 15C**). Decreased proteins functioned in ‘translation’ ($p=1.1 \times 10^{-7}$) and ‘ribosomal small subunit biogenesis’ ($p=2.0 \times 10^{-6}$) (**Figure 15D**).

The 54 significantly changed proteins in NHDF^{EXT} vs NHDF^{INT} of O probands were classified into 35 increased and 19 decreased proteins (**Table S6**). Increased proteins had functions in ‘protein N-linked glycosylation via asparagine’ ($p=5.9 \times 10^{-5}$) (**Figure 15E**), whereas decreased proteins were involved in ‘mRNA transport’ ($p=1.1 \times 10^{-3}$) (**Figure 15F**).

It was striking that in Y and particularly in M donors, increased proteins in NHDF^{EXT} vs NHDF^{INT} were enriched in different steps of aerobic respiration: glycolysis (Y), TCA cycle (M) and pyruvate metabolism (M).

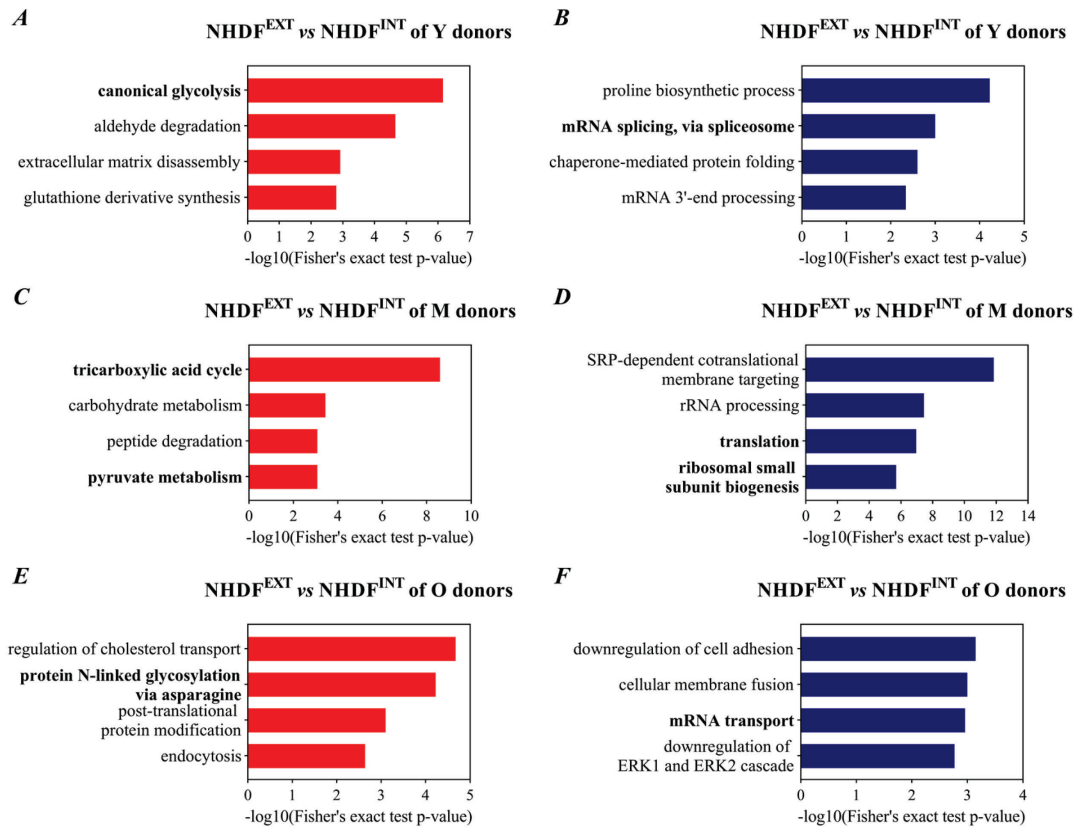


Figure 15: Metabolism-associated proteins were increased in NHDF^{EXT} vs NHDF^{INT} of Y and M donors. GO enrichment analysis of increased (red; *A*, *C*, *E*) and decreased (blue; *B*, *D*, *F*) proteins in NHDF^{EXT} vs NHDF^{INT} of Y (*A*, *B*), M (*C*, *D*) and O (*E*, *F*) donors was conducted using the DAVID functional annotation tool. Four representative GO biological process terms are presented. Fisher's exact test, $p < 0.05$.

3.4 NHDF^{EXT} vs NHDF^{INT} of M donors showed mitochondrial dysfunction

3.4.1 TCA cycle was dysregulated in NHDF^{EXT} vs NHDF^{INT} of M donors

14 of 61 differentially regulated proteins in NHDF^{EXT} vs NHDF^{INT} of M donors were involved in metabolic processes. Interestingly, when comparing the levels of these metabolic proteins in NHDF^{INT} and NHDF^{EXT} over all age groups, the aforementioned difference in protein abundance patterns was reflected (**Figure 16A**). In NHDF^{INT}, the decline of quantities of metabolism-associated proteins was rather continuously and less pronounced. However, in NHDF^{EXT}, the abundances of these proteins were similar between Y and M donors, but drastically decreased between M and O donors. Importantly, the levels of metabolic proteins were considerably lower in NHDF^{EXT} vs NHDF^{INT} of O donors. To examine possible mechanisms responsible for these

3. Results

striking differences between NHDF^{EXT} from M vs. O donors, we asked if NHDF^{EXT} vs NHDF^{INT} of M donors differed metabolically.

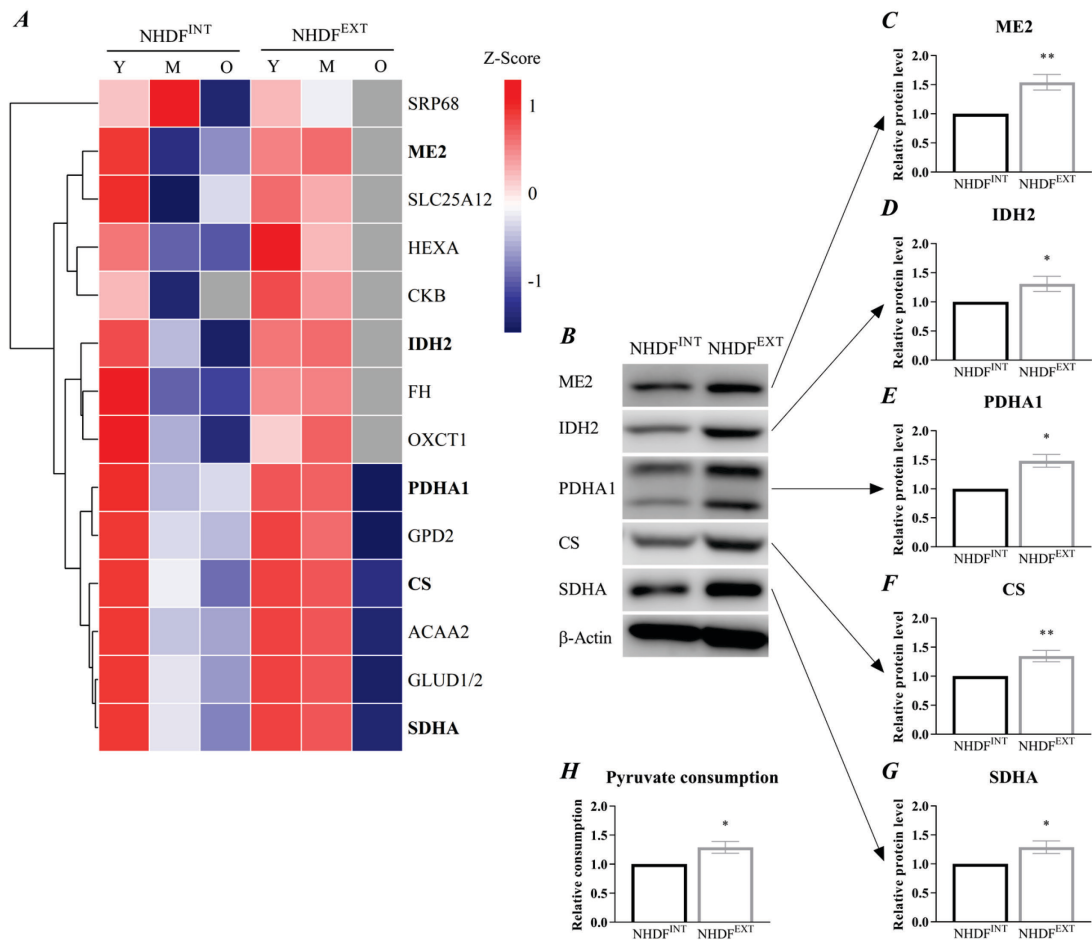


Figure 16: NHDF^{EXT} vs NHDF^{INT} of M donors exhibited elevated tricarboxylic acid (TCA) cycle-related protein levels. (A) Hierarchically clustered heatmap of metabolism-associated proteins in NHDF^{INT} and NHDF^{EXT} of Y, M and O donors. Z-score of log₂(x) LFQ intensities is plotted (grey: missing values); n=5. Representative western blots (B) and densitometric analysis of chemiluminescent signals of NAD-dependent malic enzyme (ME2) (C), isocitrate dehydrogenase [NADP] (IDH2) (D), pyruvate dehydrogenase E1 component subunit alpha (PDHA1) (E), citrate synthase (CS) (F) and succinate dehydrogenase [ubiquinone] flavoprotein subunit (SDHA) (G) of NHDF^{INT} and NHDF^{EXT} of M donors. Protein levels were normalized to β-actin. Normalized protein levels were related to NHDF^{INT}. Mean ± SEM; Student's t-test, *p<0.05, **p<0.01; n=7, PDHA1: n=3. (H) Pyruvate consumption of NHDF^{INT} and NHDF^{EXT} of M donors after incubation with 1 mM pyruvate for 48 h. Fold change (FC) relative to NHDF^{INT} is reported. Mean ± SEM; Student's t-test, *p<0.05; n=3.

Out of the 14 metabolism-associated proteins significantly changed in NHDF^{EXT} vs NHDF^{INT}, 13 proteins were increased and only one protein was decreased. Most of these enhanced metabolic proteins were associated with TCA cycle, others played roles e.g. in pyruvate metabolism, glucose metabolism or different types of lipid metabolism (Table 29).

Table 29: Metabolism-associated proteins altered in NHDF^{EXT} vs NHDF^{INT} of M donors. Functional analysis via Reactome database was performed on the 61 significantly changed proteins. Among these, 14 proteins associated with metabolic processes are listed.

Gene name	Uniprot ID	Protein description	FC	p-value	Regulation	Metabolic process
ACAA2	P42765	3-ketoacyl-CoA thiolase, mitochondrial	5.5	4.87E-02	↑	Fatty acid metabolism
CKB	P12277	Creatine kinase B-type	2.3	2.05E-02	↑	Creatine metabolism
CS	O75390	Citrate synthase, mitochondrial	3.1	2.75E-02	↑	TCA cycle
FH	P07954	Fumarate hydratase, mitochondrial	1.8	2.50E-02	↑	TCA cycle
GLUD1	P00367	Glutamate dehydrogenase 1, mitochondrial	3.1	3.71E-02	↑	Glutamate and glutamine metabolism
GLUD2	P49448	Glutamate dehydrogenase 2, mitochondrial				
GPD2	P43304	Glycerol-3-phosphate dehydrogenase, mitochondrial	2.5	3.51E-02	↑	Phospholipid metabolism, triglyceride metabolism
HEXA	P06865	Beta-hexosaminidase subunit alpha	1.6	4.05E-02	↑	Sphingolipid metabolism
IDH2	P48735	Isocitrate dehydrogenase [NADP], mitochondrial	2.9	4.06E-02	↑	TCA cycle
ME2	P23368	NAD-dependent malic enzyme, mitochondrial	1.9	1.66E-03	↑	TCA cycle
OXCT1	P55809	Succinyl-CoA:3-ketoacid coenzyme A transferase 1, mitochondrial	1.6	4.05E-02	↑	Ketone body metabolism
PDHA1	P08559	Pyruvate dehydrogenase E1 component subunit alpha, somatic form, mitochondrial	2.6	2.87E-02	↑	Pyruvate metabolism
SDHA	P31040	Succinate dehydrogenase [ubiquinone] flavoprotein subunit, mitochondrial	1.9	4.42E-02	↑	TCA cycle
SLC25A12	O75746	Calcium-binding mitochondrial carrier protein Aralar1	1.6	1.52E-02	↑	Glucose metabolism
SRP68	Q9UHB9	Signal recognition particle subunit SRP68	1.9	2.15E-02	↓	Phospholipid metabolism, triglyceride metabolism

Regarding the pyruvate metabolism, the abundance of mitochondrial pyruvate dehydrogenase E1 component subunit alpha (PDHA1) was elevated by a factor of 2.6. The enhanced TCA cycle-related proteins included mitochondrial NAD-dependent malic enzyme (ME2), isocitrate dehydrogenase [NADP] (IDH2), fumarate hydratase (FH), citrate synthase (CS) and succinate dehydrogenase [ubiquinone] flavoprotein subunit (SDHA). Among these, IDH2 and CS showing fold changes (FC) of 2.9 and 3.1 were particularly increased in NHDF^{EXT}.

Importantly, the results from mass spectrometric analysis were validated by a second independent method. Accordingly, the increased expression of ME2 (**Figure 16C**), IDH2 (**Figure 16D**), PDHA1 (**Figure 16E**), CS (**Figure 16F**) and SDHA (**Figure 16G**) in NHDF^{EXT} vs NHDF^{INT} of M donors could be confirmed via western blot analysis (**Figure 16B**).

In mitochondria, pyruvate, the end product of glycolysis, is converted by the pyruvate dehydrogenase complex to acetyl coenzyme A (acetyl-CoA), which then enters the TCA cycle. The observed dysregulation of TCA cycle-associated proteins in NHDF^{EXT} of M donors raised the question whether pyruvate turnover might be affected. Indeed, NHDF^{EXT} vs NHDF^{INT} exhibited a significantly elevated pyruvate consumption by a factor of 1.3 (**Figure 16H**), which was in line with increased levels of TCA cycle-related proteins. These observations indicated an enhanced respirational turnover in NHDF^{EXT} vs NHDF^{INT} of M donors, which might help the cells to compensate for elevated energy demands to cope with UVR-induced damage.

3.4.2 Evidence for oxidative stress in NHDF^{EXT} vs NHDF^{INT} of M donors

Mitochondrial respiration, particularly the electron transport chain (ETC), localized at the inner mitochondrial membrane, is the primary source of endogenous ROS formation. In addition, oxidative stress can be caused by environmental factors, such as UVR, and is thought to contribute to cellular damage and aging. Since NHDF^{EXT} were obtained from UVR-exposed tissue and NHDF^{EXT} vs NHDF^{INT} of M donors showed a dysregulation of mitochondrial energy production, we wondered whether these alterations were associated with the presence of oxidative stress.

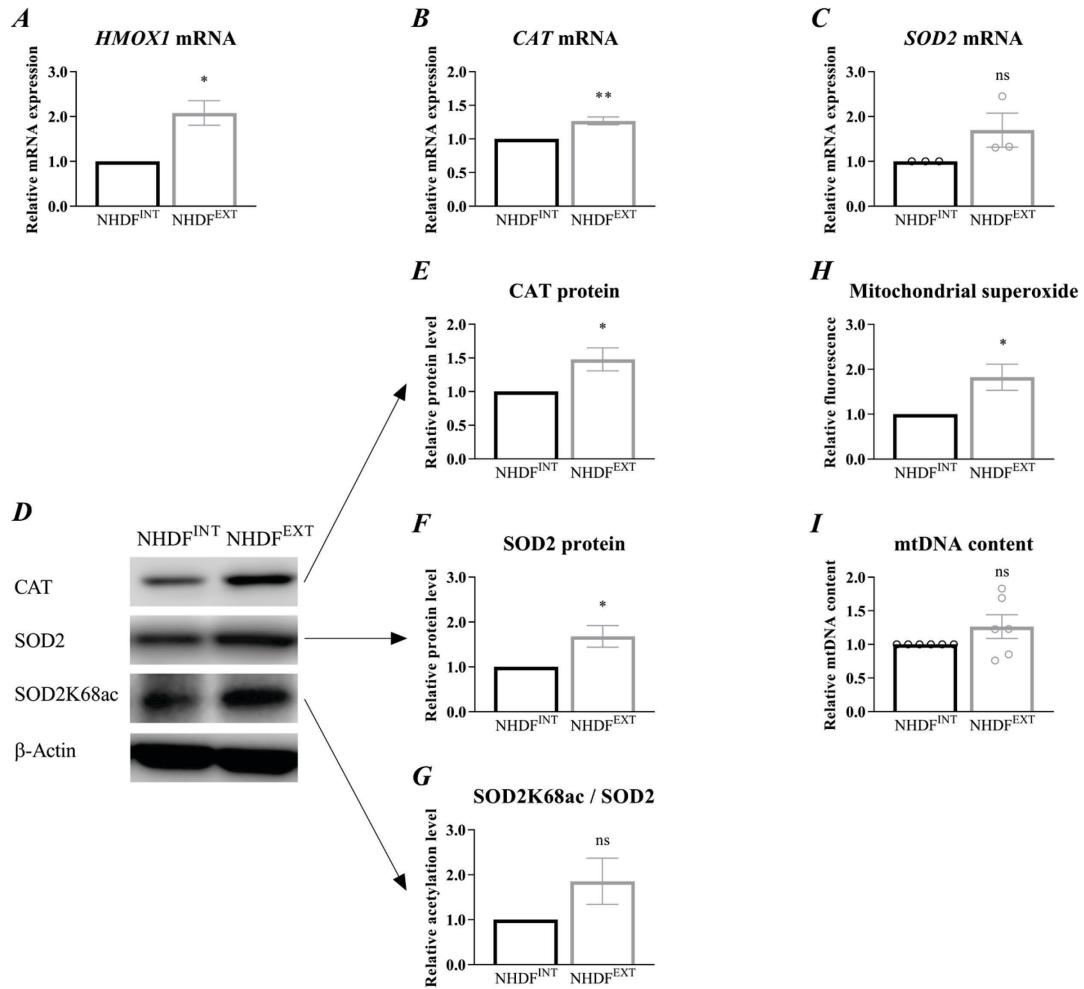


Figure 17: Evidence for the presence of oxidative stress in NHDF^{EXT} compared to NHDF^{INT} of M donors. RT-qPCR analysis of heme oxygenase 1 (*HMOX1*) (A), catalase (*CAT*) (B) and superoxide dismutase 2 (*SOD2*) (C) mRNA level. Expression was normalized to β-actin and referred to NHDF^{INT}. Mean ± SEM and for *SOD2* additionally FC of NHDF^{EXT} of individual donors are shown; Student's t-test, *p<0.05, **p<0.01; n=3. Representative western blots (D) and densitometric analysis of chemiluminescent signals of *CAT* (E), *SOD2* (F) and acetylated *SOD2* at lysine 68 (*SOD2K68ac*) (G). *CAT* and *SOD2* were normalized to β-actin, *SOD2K68ac* was normalized to *SOD2*. Normalized protein levels were referred to NHDF^{INT}. Mean ± SEM; Student's t-test, *p<0.05; n=3. (H) Mitochondrial superoxide content was defined using MitoSOX Red mitochondrial superoxide indicator. Fluorescence intensity is shown as FC related to NHDF^{INT}. Mean ± SEM; Student's t-test, *p<0.05; n=3. (I) Mitochondrial DNA (mtDNA) content was analyzed via RT-qPCR. Signals were normalized to nuclear β-globin and referred to NHDF^{INT}. Mean ± SEM and FC of NHDF^{EXT} of individual donors are shown; Student's t-test, p>0.05; n=6.

There were indeed several hints that oxidative stress was present in NHDF^{EXT}. In NHDF^{EXT} vs NHDF^{INT} of M donors, an enhanced expression of ROS-related genes was observed. An important oxidative stress marker is heme oxygenase (HMOX) [116]. HMOX is part of the heme metabolism and mediates the degradation of heme to biliverdin that is subsequently converted to bilirubin. It is assumed that bilirubin plays an antioxidant role [117]. HMOX exists in two isoforms: the stress-inducible HMOX1 and the constitutively expressed HMOX2. In NHDF^{EXT}, the mRNA expression of the oxidative stress marker *HMOX1* was increased by a factor of 2 (Figure 17A). Another relevant antioxidant enzyme is catalase (*CAT*) which detoxifies H₂O₂

through its conversion to H₂O and O₂. A significant 1.3- and 1.5-fold increase of *CAT* mRNA expression (**Figure 17B**) and CAT protein levels (**Figure 17D, E**) was detected in NHDF^{EXT} compared to NHDF^{INT}. H₂O₂ can be generated during oxidation of fatty acids, degradation of purines and detoxification of O₂⁻. The latter reaction is catalyzed by the superoxide dismutase 2 (SOD2). NHDF^{EXT} exhibited elevated SOD2 expression on mRNA (**Figure 17C**) and protein level by a factor of 1.7 (**Figure 17D, F**). Interestingly, a hyperacetylation of SOD2 at lysine 68 (SOD2K68ac) was observed in NHDF^{EXT} vs NHDF^{INT} suggesting a reduced antioxidative activity of this enzyme in these cells (**Figure 17D, G**).

Since an induction of mRNA and protein expression of common ROS-related genes was detected in NHDF^{EXT}, we next investigated superoxide levels. Fluorescence intensity after incubation with the superoxide indicator MitoSOX was 1.8-fold higher in NHDF^{EXT} than in NHDF^{INT} (**Figure 17H**).

The mtDNA content of a cell is an important marker for mitochondrial dysfunction in connection with oxidative stress. Oxidative stress can lead to an increased mitochondrial biogenesis and thus to a higher mtDNA content as an adaptive response to oxidative stress [118]. In line with the evidence for oxidative stress, NHDF^{EXT} vs NHDF^{INT} from four of six donors exhibited an increased mtDNA content (**Figure 17I**). To summarize, NHDF^{EXT} vs NHDF^{INT} of M donors showed a mitochondrial phenotype, which was not only characterized by a dysregulation of mitochondrial energy metabolism, but also by increased oxidative stress levels and elevated ROS-related gene expression.

3.4.3 ATP and NAD⁺ metabolisms were compromised in NHDF^{EXT} vs NHDF^{INT} of M donors

TCA cycle and downstream ETC are the primary source of energy production within cells. Energy is generated during the TCA cycle directly as guanosine-5'-triphosphate (GTP) and indirectly through transfer of electrons to the coenzymes NAD⁺ and flavin adenine dinucleotide (FAD). These in turn provide electrons to the ETC which ultimately produces ATP.

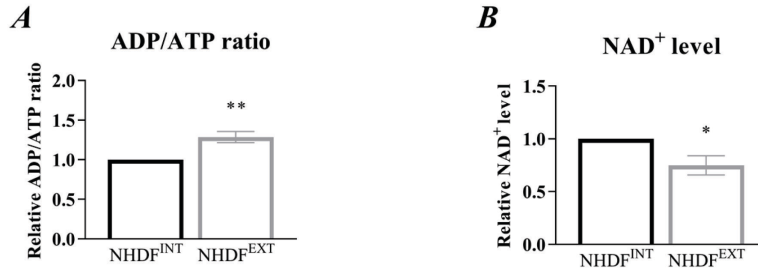


Figure 18: NHDF^{EXT} vs NHDF^{INT} of M donors showed increased ADP/ATP ratio and NAD⁺ depletion. (A) Relative ADP/ATP ratio of NHDF^{EXT} referred to NHDF^{INT}. Mean \pm SEM; Student's t-test, ** $p < 0.01$, $n = 5$. (B) NAD⁺ level in NHDF^{EXT} are depicted. NAD⁺ levels were normalized to protein content and reported as FC relative to NHDF^{INT}. Mean \pm SEM; Student's t-test, * $p < 0.05$; $n = 5$.

The dysregulation of TCA cycle-related proteins in NHDF^{EXT} vs NHDF^{INT} of M donors raised the question if ATP and NAD⁺ level might be dysbalanced. We observed that NHDF^{EXT} have a 1.3-fold increase of ADP/ATP ratio (**Figure 18A**) which could be the result of a higher ADP concentration, a reduced ATP level or both. In addition, intracellular NAD⁺ concentration was decreased by 25% in NHDF^{EXT} compared to NHDF^{INT} (**Figure 18B**). These results suggested a higher ATP and NAD⁺ consumption, which might be due to enhanced energy demands to cope with UVR-induced damage.

3.5 Sirtuin (SIRT) abundances and related histone deacetylation were dysregulated in NHDF^{EXT} vs NHDF^{INT} of M donors

An important protein family that fundamentally depends on intracellular NAD⁺ as a co-substrate are SIRT^s acting as deacetylases [119, 120], mono-ADP-ribosyl transferases [121, 122] or both. In mammals, seven SIRT^s (SIRT1-7) have been discovered, which differ in their cellular localization and substrate specificity [123]. Due to their wide range of substrates, SIRT^s are involved in various cellular processes including direct and indirect regulation of epigenetic mechanisms [119, 124], DNA damage repair [125, 126], oxidative stress response [127] and metabolic regulation [128]. Moreover, SIRT^s are implicated in cell survival [129], tumorigenesis [130] and longevity [131].

3.5.1 SIRT levels were altered in NHDF^{EXT} vs NHDF^{INT} of M donors

Due to the observed reduction of NAD⁺ concentration in NHDF^{EXT} vs NHDF^{INT} of M donors, we assessed in the following experiments, if the abundance of SIRT^s was affected. NHDF^{EXT} indeed

exhibited significantly decreased protein levels of SIRT1 to 0.7-fold of NHDF^{INT} (**Figure 19A, B**).

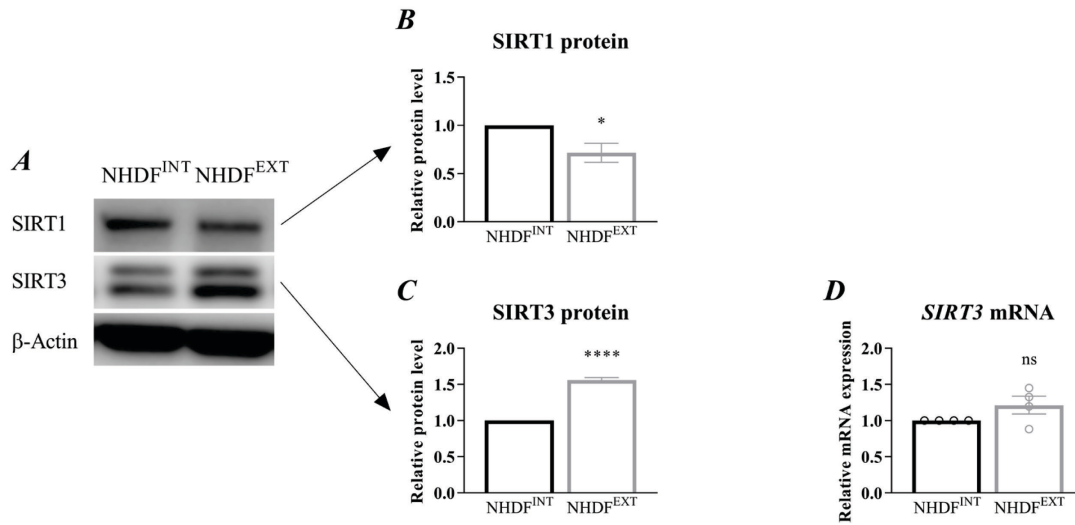


Figure 19: Abundance of sirtuins (SIRT) was dysregulated in NHDF^{EXT} vs NHDF^{INT} of M donors. Representative western blots (**A**) and densitometric analysis of chemiluminescent signals of SIRT1 (**B**) and SIRT3 (**C**). Protein levels were normalized to β -actin and related to protein level of NHDF^{INT}. Mean \pm SEM; Student's t-test, * $p < 0.05$, **** $p < 0.0001$; $n = 3$. (**D**) RT-qPCR analysis of *SIRT3* mRNA level. Expression was normalized to β -actin and referred to NHDF^{INT}. Mean \pm SEM and FC of NHDF^{EXT} of individual donors are shown; Student's t-test, $p > 0.05$; $n = 4$.

While SIRT1 is located either in the nucleus or the cytoplasm, SIRT3 is primarily found in the mitochondria, where it acts as a central regulator controlling acetylation and activity of numerous proteins including SOD2 [132]. In contrast to SIRT1, SIRT3 protein was 1.6-times more abundant in NHDF^{EXT} vs NHDF^{INT} (**Figure 19A, C**). This observation was reinforced by RT-qPCR results showing that mRNA expression of *SIRT3* was enhanced in NHDF^{EXT} from three of four donors (**Figure 19D**). Thus, alteration of NAD⁺ level in NHDF^{EXT} of M donors was accompanied by abundance changes of NAD⁺-dependent SIRTs.

3.5.2 Reduced SIRT1 abundance in NHDF^{EXT} of M donors correlated with histone hyperacetylation

Although occurring in the cytoplasm, SIRT1 is predominantly located in the nucleus [123], where it deacetylates a variety of proteins including histones. Histone targets of SIRT1 encompass several lysine residues of histone 3 (H3) and histone 4 (H4) [119, 133-136]. The acetylation status of histones is involved in the regulation of all major cellular functions related to DNA including activation/repression of gene expression, repair and replication.

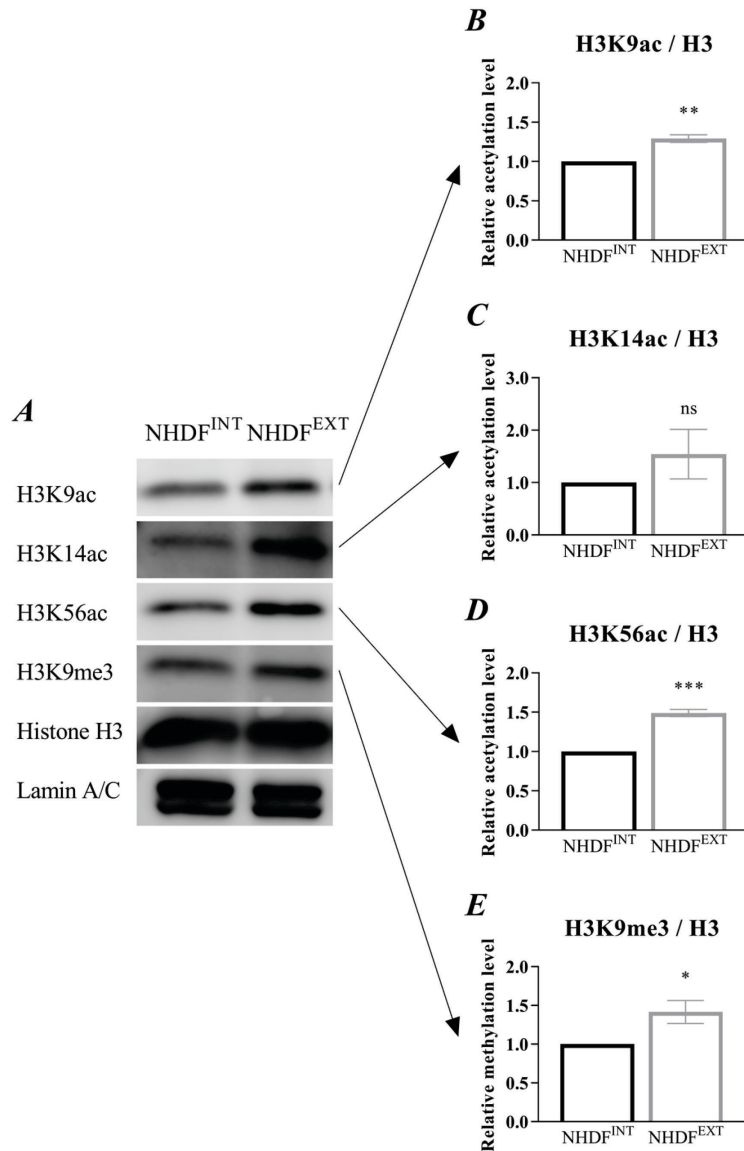


Figure 20: Deacetylation of histone 3 (H3) target sites of NAD⁺-dependent SIRT1 is impaired in NHDF^{EXT} vs NHDF^{INT} of M donors. Representative western blots (A) and densitometric analysis of chemiluminescent signals of acetylated H3 at lysine 9 (H3K9ac) (B), lysine 14 (H3K14ac) (C), lysine 56 (H3K56ac) (D), methylated H3 at lysine 9 (H3K9me3) (E) and H3. Lamin A/C served as loading control. Acetylation or methylation levels were normalized to H3 and reported as FC relative to NHDF^{INT}. Mean \pm SEM; Student's t-test, * p <0.05, ** p <0.01, *** p <0.001; n =3.

In accordance with decreased NAD⁺ concentrations and SIRT1 protein abundance in NHDF^{EXT} vs NHDF^{INT} of M donors, hyperacetylation of H3 at lysine 9 (H3K9ac) (Figure 20A, B) and lysine 14 (H3K14ac) (Figure 20A, C) was observed. In addition, acetylation of H3 at lysine 56 (H3K56ac) was increased by 1.5-fold in NHDF^{EXT} (Figure 20A, D). SIRT1 has been shown to indirectly facilitate methylation of H3 at lysine 9 (H3K9me3) by deacetylating and thereby activating the histone methyltransferase suppressor of variegation 3-9 homologue 1 (SUV39H1) [124]. Although SIRT1 abundance was reduced in NHDF^{EXT}, H3K9 was hypermethylated (Figure 20A, E).

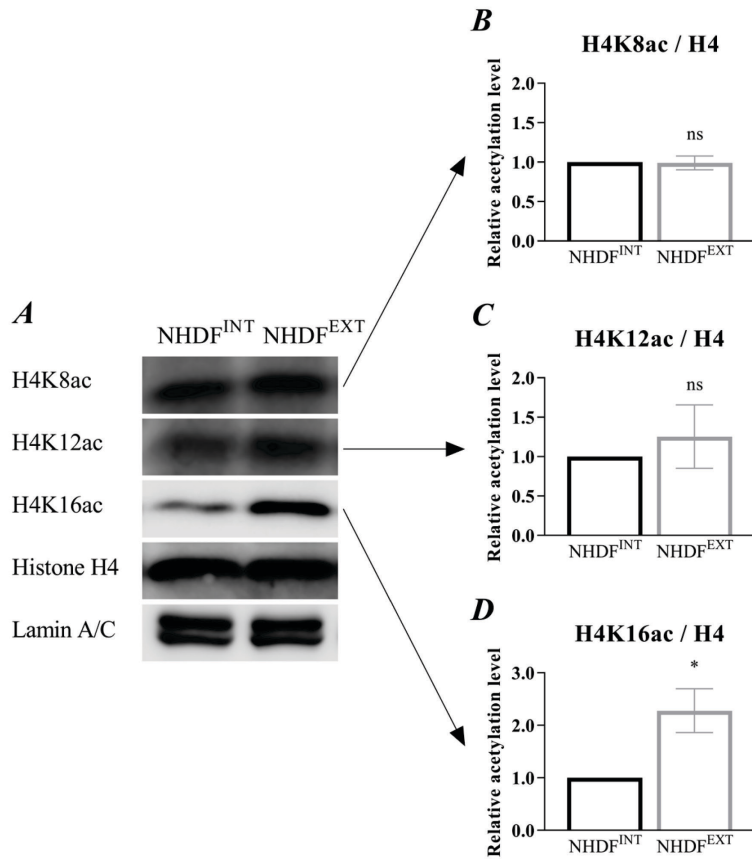


Figure 21: Deacetylation of histone 4 (H4) target sites of NAD⁺-dependent SIRT1 is impaired in NHDF^{EXT} vs NHDF^{INT} of M donors. Representative western blots (A) and densitometric analysis of chemiluminescent signals of acetylated H4 at lysine 8 (H4K8ac) (B), lysine 12 (H4K12ac) (C), lysine 16 (H4K16ac) (D) and H4. Lamin A/C served as loading control. Acetylation levels were normalized to H4 and reported as FC relative to NHDF^{INT}. Mean \pm SEM; Student's t-test, * $p < 0.05$; $n = 3$.

Regarding H4, acetylation at lysine 8 (H4K8ac) (Figure 21A, B) and lysine 12 (H4K12ac) (Figure 21A, C) was comparable in NHDF^{EXT} and NHDF^{INT} of M donors. In contrast, acetylation level of lysine 16 (H4K16ac) was even 2.3-fold enhanced in NHDF^{EXT} (Figure 21A, D).

In conclusion, NHDF^{EXT} vs NHDF^{INT} of M donors showed a decline of NAD⁺ concentrations which was accompanied by SIRT1 reduction and impaired deacetylation of certain lysine residues of H3 and H4.

3.6 Chemical intervention in NAD⁺ metabolism rescued decreased NAD⁺ level in NHDF^{EXT} of M donors

There is compelling evidence showing that NAD⁺ concentration decreases with aging in different tissue types of several species including humans [137-144]. Moreover, several studies suggested

an association of NAD^+ depletion with a variety of age-related diseases e.g. type 2 diabetes [139], Alzheimer's disease [145] or obesity [146]. In addition, Gary and Rochette demonstrated that UVB irradiation of NHDF led to a strong decrease of NAD^+ level [147].

Reduced NAD^+ concentrations were observed in NHDF^{EXT} vs NHDF^{INT} of M donors. This might be the result of an excessive consumption through NAD^+ -dependent enzymes and/or a compromised biosynthesis of NAD^+ . In the following experiments, NHDF^{EXT} were treated with substances which intervene in NAD^+ metabolism with the aim of retrieving NAD^+ level and reversing further metabolic alterations.

3.6.1 Treatment with olaparib and compound 78c rescued decreased NAD^+ levels in NHDF^{EXT} of M donors

Besides SIRT6, important NAD^+ -consuming enzymes include poly(ADP-ribose) polymerases (PARP) and cluster of differentiation 38 (CD38). PARPs are responsible for poly(ADP-ribosyl)ation of target proteins and thereby contribute to a variety of cellular processes like DNA damage repair or cell survival [148]. Jacobson, Antol et al. demonstrated that UVB irradiation of NHDF caused elevation of poly(ADP ribose) as well as a depletion of NAD^+ [149]. Inhibition of PARP has been shown to rescue NAD^+ levels in NHDF and HaCaT cells [149, 150]. A well-known selective inhibitor for PARP1 and PARP2 is olaparib which is clinically used as a drug in the treatment of breast cancer gene (BRCA) related cancers [151-153].

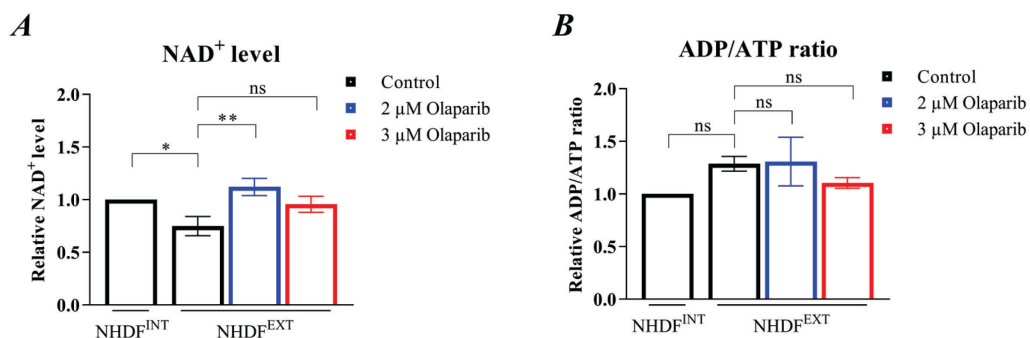


Figure 22: Treatment of NHDF^{EXT} of M donors with olaparib improved NAD^+ level. NHDF^{EXT} were treated with 2 and 3 μM olaparib for 48 h. DMEM-incubated NHDF^{INT} and NHDF^{EXT} of the same donors served as a control. (A) NAD^+ levels were defined, normalized to protein content and reported as FC relative to NHDF^{INT} . Mean \pm SEM; Holm-Sidak's multiple comparisons test, * $p < 0.05$, ** $p < 0.01$; $n = 3-5$. (B) Relative ADP/ATP ratios referred to NHDF^{INT} . Mean \pm SEM; Holm-Sidak's multiple comparisons test, $p > 0.05$; $n = 3-5$.

To examine if an excessive NAD^+ consumption through PARP was causative for NAD^+ decline and if PARP inhibition might restore decreased NAD^+ level, NHDF^{EXT} of M donors were treated

with 2 and 3 μM olaparib for 48 h. Incubation with 2 μM olaparib led to a significant increase of NAD^+ concentrations (**Figure 22A**). In the following experiments, the effect of olaparib on ADP/ATP ratio was examined, since NAD^+ and ATP metabolism are strongly interconnected. NHDF^{EXT} vs NHDF^{INT} of M donors demonstrated a significant elevation of ADP/ATP ratio. While treatment with 2 μM olaparib did not show any effect on the ADP/ATP ratio, application of 3 μM reduced the ADP/ATP ratio by trend, although the effect failed to reach significance (**Figure 22B**).

Another important NAD^+ -degrading enzyme is CD38, a cyclic ADP ribose hydrolase. CD38 functions in different processes e.g. immune response, calcium signaling and energy metabolism [154-157]. Camacho-Pereira, Tarrago et al. showed that CD38 age-dependently increased in various murine tissues and caused a reduction of NAD^+ concentrations and mitochondrial dysfunction [158]. Application of compound 78c, a specific CD38 inhibitor, reversed the age-associated decline of NAD^+ levels in aged mice [159].

To investigate if NAD^+ levels decreased due to excessive NAD^+ consumption by CD38 and if its concentration could be retrieved through CD38 inhibition, NHDF^{EXT} of M donors were treated with 50 and 500 nM 78c. Incubation with both concentrations for 48 h normalized NAD^+ concentration (**Figure 23A**) and ADP/ATP ratio (**Figure 23B**) in NHDF^{EXT} by trend, although the effect did not reach significance.

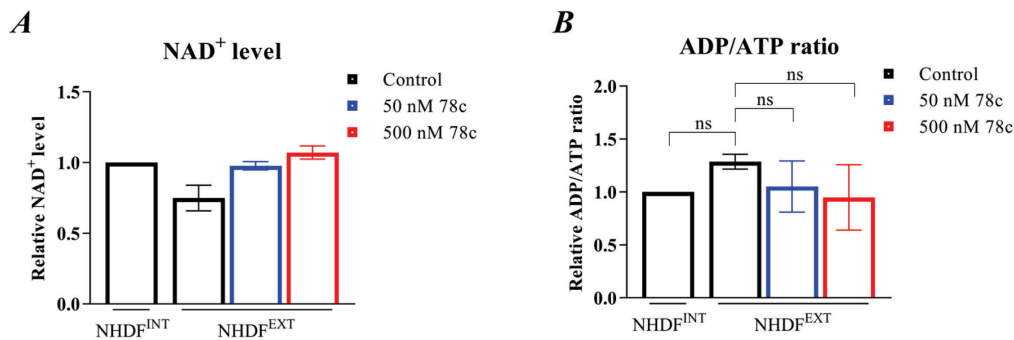


Figure 23: Treatment of NHDF^{EXT} of M donors with compound 78c tended to enhance NAD^+ level. NHDF^{EXT} were treated with 50 and 500 nM 78c for 48 h. DMEM-incubated NHDF^{INT} and NHDF^{EXT} of the same donors served as a control. (A) NAD^+ levels were defined, normalized to protein content and reported as FC relative to NHDF^{INT} . Mean \pm SEM; control: $n=5$, 78c: $n=2$. (B) Relative ADP/ATP ratios referred to NHDF^{INT} . Mean \pm SEM; Holm-Sidak's multiple comparisons test, $p>0.05$; $n=3-5$.

These observations indicated that treatment of NHDF^{EXT} of M probands with the PARP inhibitor olaparib or the CD38 inhibitor 78c retrieved NAD^+ level and normalized the ADP/ATP ratio by trend. This suggested that excessive NAD^+ consumption through the NAD^+ -dependent enzymes PARP and CD38 contributed to a decline of NAD^+ concentrations and an increase of ADP/ATP ratios in NHDF^{EXT} .

3.6.2 β -nicotinamide mononucleotide (NMN) treatment retrieved NAD^+ level and ADP/ATP ratio in NHDF^{EXT} of M donors

Besides reduction of NAD^+ levels through enhanced consumption by NAD^+ -dependent enzymes, the observed decline may also result from a compromised biosynthesis of NAD^+ . There are three pathways to synthesize NAD^+ in mammals: the *de novo* pathway, the Preiss-Handler pathway and the salvage pathway, of which the latter constitutes the major source for NAD^+ . The salvage pathway recycles nicotinamide (NAM) or utilizes nicotinamide riboside (NR) to generate NAD^+ . NAD^+ -consuming enzymes such as SIRT6 or PARPs produce NAM as a by-product. Nicotinamide phosphoribosyl transferase (NAMPT) converts NAM to NMN which is then transformed to NAD^+ by nicotinamide/nicotinic acid mononucleotide adenylyl transferase (NMNAT). NAD^+ can also be produced from the precursor NR, which is initially converted to NMN and then to NAD^+ [160].

Several studies in different murine tissues showed that supplementation of the NAD^+ precursor NMN enhances NAD^+ levels under normal and under pathological conditions [138, 139, 161, 162]. In line with that, treatment of NHDF^{EXT} of M donors with 2 and 3 mM NMN for 48 h resulted in a significant increase of NAD^+ concentrations even exceeding the levels measured in NHDF^{INT} (**Figure 24A**). This indicated the existence of an imbalance between NAD^+ consumption and precursor availability in NHDF^{EXT} , which would limit the sufficient supply of NAD^+ . Incubation of NHDF^{EXT} with NMN could not only enhance NAD^+ concentration, but also rescued ADP/ATP ratios to the same ratios as detected in NHDF^{INT} (**Figure 24B**).

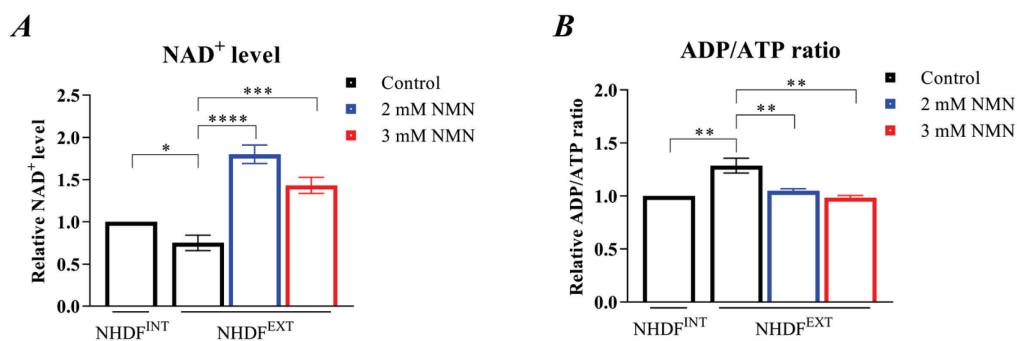


Figure 24: Treatment of NHDF^{EXT} of M donors with β -nicotinamide mononucleotide (NMN) improved NAD^+ level and ADP/ATP ratio. NHDF^{EXT} were treated with 2 and 3 mM NMN for 48 h. DMEM-incubated NHDF^{INT} and NHDF^{EXT} of the same donors served as a control. (A) NAD^+ levels were defined, normalized to protein content and reported as FC relative to NHDF^{INT} . Mean \pm SEM; Holm-Sidak's multiple comparisons test, * $p < 0.05$, *** $p < 0.001$, **** $p < 0.0001$; $n = 3-5$. (B) Relative ADP/ATP ratios referred to NHDF^{INT} . Mean \pm SEM; Holm-Sidak's multiple comparisons test, ** $p < 0.01$; $n = 3-5$.

These findings indicated that the decreased NAD^+ levels in NHDF^{EXT} of M donors were caused by excessive consumption of NAD^+ through PARP and CD38 as well as insufficient NAD^+

precursor availability. Interestingly, incubation of NHDF^{EXT} with NMN, olaparib or 78c also rescued ADP/ATP ratios. However, the effect was only statistically significant for NMN. For this reason, further investigations focused on treatment of NHDF^{EXT} of M donors with 3 mM NMN.

3.7 NMN treatment rescued SIRT1 abundance and related histone deacetylation in NHDF^{EXT} of M donors

3.7.1 SIRT1 level in NHDF^{EXT} of M donors was retrieved by NMN treatment

Decreased NAD⁺ concentrations in NHDF^{EXT} vs NHDF^{INT} of M donors were associated with aberrant abundance of SIRT1 and SIRT3. In the following, the impact of NMN on protein levels of SIRT1 and SIRT3 in NHDF^{EXT} of M donors was examined via western blot analysis.

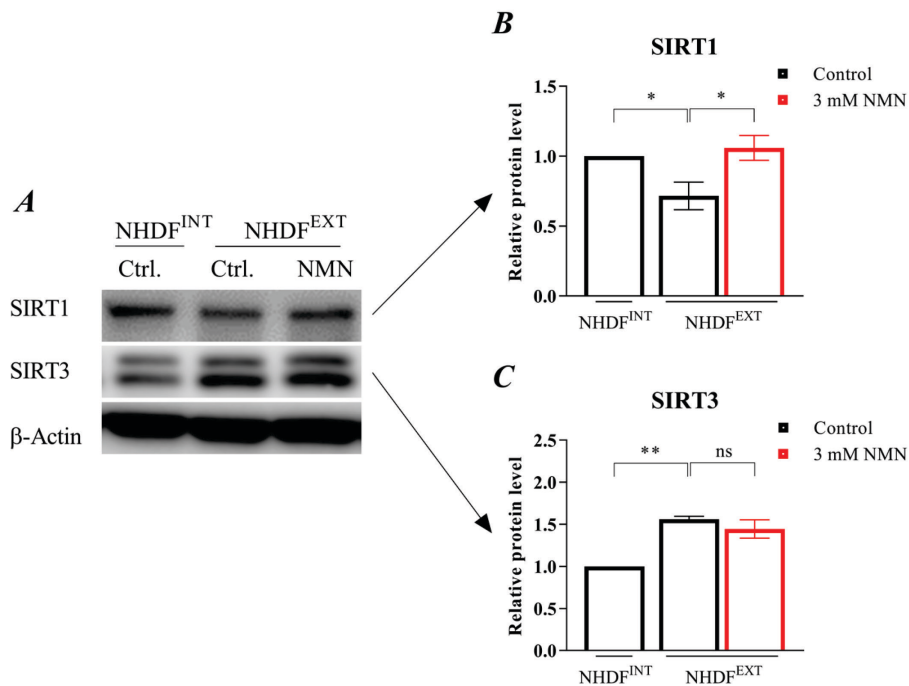


Figure 25: Incubation of NHDF^{EXT} of M donors with NMN rescued SIRT1 protein level. NHDF^{EXT} were treated with 3 mM NMN for 48 h. DMEM-incubated NHDF^{INT} and NHDF^{EXT} of the same donors served as a control. Representative western blots (**A**) and densitometric analysis of chemiluminescent signals of SIRT1 (**B**) and SIRT3 (**C**). Protein levels were normalized to β -actin and related to protein level of NHDF^{INT}. Mean \pm SEM; Holm-Sidak's multiple comparisons test, * $p < 0.05$, ** $p < 0.01$; $n = 3$.

Protein levels of SIRT1 were diminished to 0.7-fold in NHDF^{EXT} vs NHDF^{INT} and incubation of NHDF^{EXT} with 3 mM NMN for 48 h rescued SIRT1 protein abundance (**Figure 25A, B**). In contrast to SIRT1, SIRT3 protein abundance was 1.6-times elevated in NHDF^{EXT} and was not

altered through NMN treatment (**Figure 25A, C**). These observations indicated that NAD^+ deficiency caused a decrease of SIRT1 in NHDF^{EXT} vs NHDF^{INT} which was reversible, because NMN treatment could retrieve SIRT1 levels in NHDF^{EXT} .

3.7.2 NMN treatment of NHDF^{EXT} of M donors resulted in selective rescue of deacetylation of H3K56 and H4K16

As a consequence of reduced NAD^+ concentrations and SIRT1 abundance, lysine residues of H3 and H4, substrates of SIRT1, were hyperacetylated in NHDF^{EXT} vs NHDF^{INT} of M donors. Therefore, the effect of NMN exposure on histone deacetylation was examined.

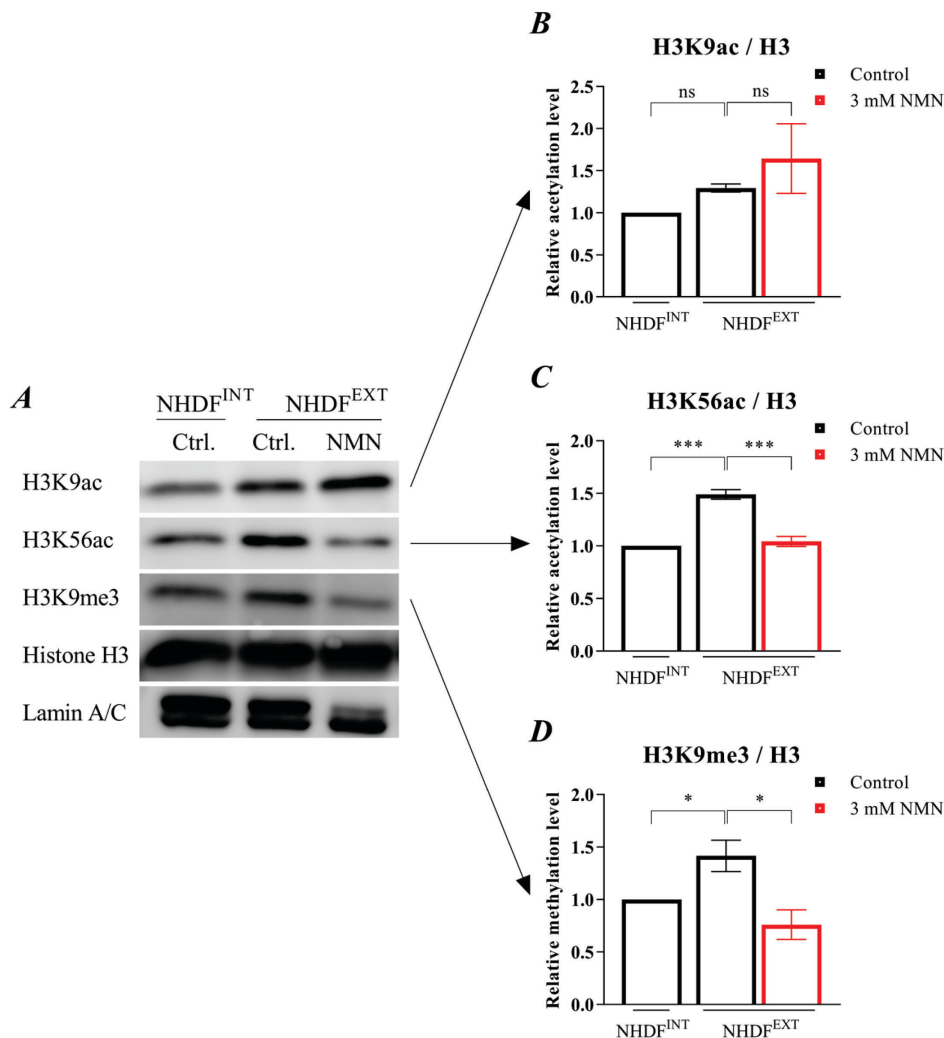


Figure 26: NMN treatment led to a selective alleviation of hyperacetylation of specific H3 lysine residues in NHDF^{EXT} of M donors. NHDF^{EXT} were treated with 3 mM NMN for 48 h. DMEM-incubated NHDF^{INT} and NHDF^{EXT} of the same donors served as a control. Representative western blots (**A**) and densitometric analysis of chemiluminescent signals of H3K9ac (**B**), H3K56ac (**C**), H3K9me3 (**D**) and H3. Lamin A/C served as a loading

3. Results

control. Acetylation or methylation levels were normalized to H3 and are shown as FC relative to NHDF^{INT}. Mean \pm SEM; Holm-Sidak's multiple comparisons test, * $p < 0.05$, *** $p < 0.001$; $n = 3$.

Acetylation levels of H3K9 and H3K56 were significantly increased in NHDF^{EXT} by a factor of 1.3 and 1.5. Interestingly, after treatment of NHDF^{EXT} with NMN, H3K9 remained hyperacetylated (**Figure 26A, B**). In contrast, deacetylation of H3K56 was rescued and its acetylation level was reduced to the same level as observed in NHDF^{INT} (**Figure 26A, C**). NHDF^{EXT} previously showed a 1.4-fold enhancement of H3K9 methylation compared to NHDF^{INT}. NMN incubation of NHDF^{EXT} even induced a hypomethylation of this lysine residue reducing methylation level to 0.8-fold of that detected in NHDF^{INT} (**Figure 26A, D**).

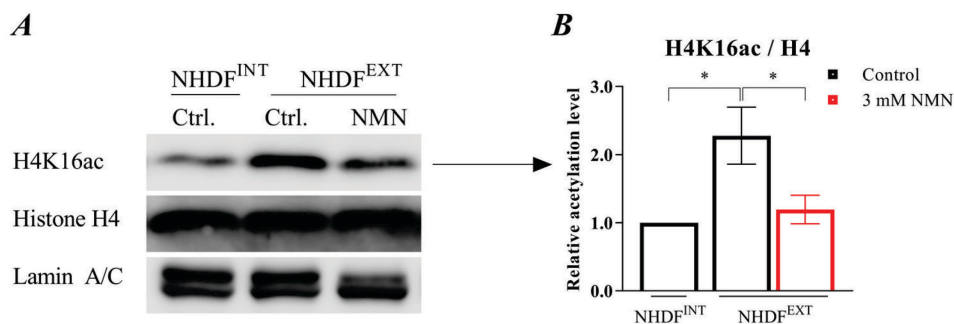


Figure 27: NMN treatment led to an alleviation of hyperacetylation of H4K16 in NHDF^{EXT} of M donors. NHDF^{EXT} were treated with 3 mM NMN for 48 h. DMEM-incubated NHDF^{INT} and NHDF^{EXT} of the same donors served as a control. Representative western blots (**A**) and densitometric analysis of chemiluminescent signals of H4K16ac (**B**) and H4. Lamin A/C served as a loading control. H4K16 acetylation level was normalized to H4. Acetylation level is shown as FC relative to NHDF^{INT}. Mean \pm SEM; Holm-Sidak's multiple comparisons test, * $p < 0.05$; $n = 3$.

Regarding H4, acetylation of H4K16 was 2.3-times higher in NHDF^{EXT} vs NHDF^{INT}. NMN treatment of NHDF^{EXT} attenuated hyperacetylation of this histone lysine residue mitigating acetylation level to 1.2-fold of NHDF^{INT} (**Figure 27A, B**). The selective approximation of acetylation levels of H3K56 and H4K16 in NMN-treated NHDF^{EXT} to those found in NHDF^{INT} suggested a major role of SIRT1 for the deacetylation of these lysine residues, in contrast to H3K9.

3.8 NMN treatment rescued parts of the mitochondrial phenotype of NHDF^{EXT} of M donors

3.8.1 NMN treatment of NHDF^{EXT} of M donors attenuated dysregulation of TCA cycle

An elevation of TCA cycle-associated protein levels was observed in NHDF^{EXT} vs NHDF^{INT} of M donors. Treatment of NHDF^{EXT} with NMN improved NAD⁺ level and normalized ADP/ATP ratio. In the following experiments, the effect of NMN on expression levels of proteins involved in TCA cycle was investigated.

Western blot analysis revealed that treatment of NHDF^{EXT} of seven different M donors with 3 mM NMN for 48 h diminished the quantities of TCA cycle-associated proteins (**Figure 28A**). NMN incubation of NHDF^{EXT} alleviated protein levels of ME2 (**Figure 28B**) and IDH2 abundance was even reduced to a level similar to that observed in NHDF^{INT} (**Figure 28C**). A 1.5-fold elevation of protein level of PDHA1 was shown in NHDF^{EXT} vs NHDF^{INT} of M donors which was significantly decreased in NMN-treated NHDF^{EXT} (**Figure 28D**). Furthermore, NMN treatment slightly lowered protein abundances of CS (**Figure 28E**) and SDHA (**Figure 28F**).

Since NMN treatment ameliorated dysregulation of TCA cycle-related protein abundances in NHDF^{EXT}, we next asked if their increased pyruvate consumption will be attenuated as well. In NHDF^{EXT} vs NHDF^{INT} of M donors, the pyruvate consumption was significantly elevated by a factor of 1.3. Incubation of NHDF^{EXT} with NMN indeed diminished pyruvate consumption to the same level as detected in NHDF^{INT} (**Figure 28G**). These results demonstrated that NMN treatment of NHDF^{EXT} of M donors did not only improve NAD⁺ level and ADP/ATP ratio, but also normalized the regulation of the TCA cycle in NHDF^{EXT}.

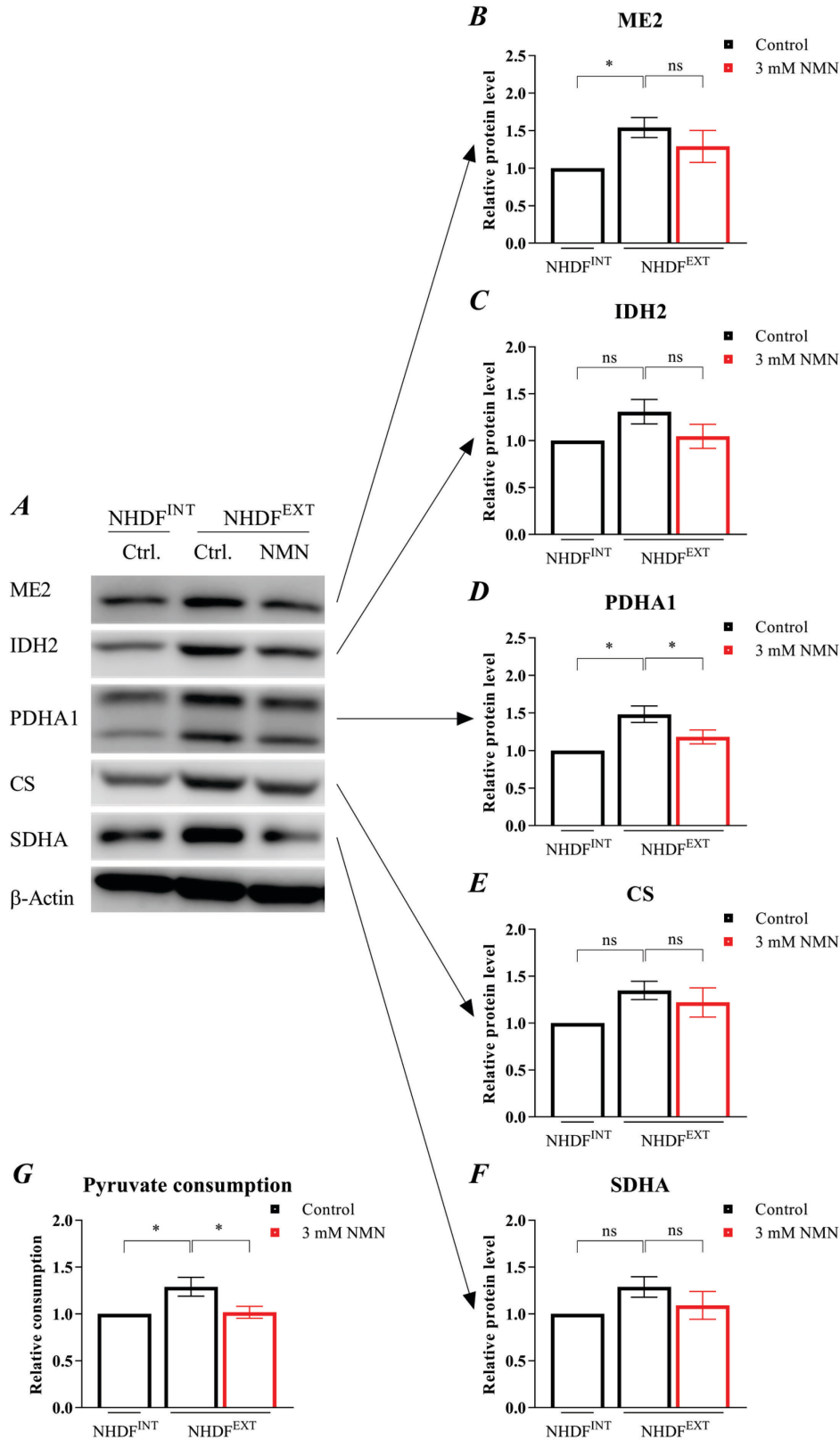


Figure 28: Treatment of NHDF^{EXT} of M donors with NMN mitigated dysregulation of TCA cycle-related proteins. NHDF^{EXT} were treated with 3 mM NMN for 48 h. DMEM-incubated NHDF^{INT} and NHDF^{EXT} of the same donors served as a control. Representative western blots (**A**) and densitometric analysis of chemiluminescent signals of ME2 (**B**), IDH2 (**C**), PDHA1 (**D**), CS (**E**) and SDHA (**F**). Protein levels were normalized to β -actin. Normalized protein levels were related to NHDF^{INT}. Mean \pm SEM; Holm-Sidak's multiple

comparisons test, * $p < 0.05$; $n = 7$, PDHA1: $n = 3$. (G) Pyruvate consumption after incubation of NHDF with 1 mM pyruvate for 48 h. FC relative to NHDF^{INT} is reported. Mean \pm SEM; Holm-Sidak's multiple comparisons test, * $p < 0.05$; $n = 3$.

3.8.2 Increased mitochondrial ROS levels in NHDF^{EXT} of M donors were not reduced through treatment with NMN

In NHDF^{EXT} vs NHDF^{INT} of M donors, dysregulated mitochondrial energy production was accompanied by an elevated ROS level and alterations of abundances of antioxidative enzymes. In the following, the effect of NMN on oxidative stress homeostasis was therefore examined.

NHDF^{EXT} of M donors exhibited a significant increase of mRNA and protein levels of genes important for detoxification of ROS. Incubation of NHDF^{EXT} with 3 mM NMN for 48 h did not result in an alteration of CAT protein abundance (**Figure 29A, B**). Moreover, NMN treatment of NHDF^{EXT} of M donors did neither affect SOD2 protein level (**Figure 29A, C**) nor its acetylation status at lysine 68 (**Figure 29A, D**).

The superoxide anion content was determined via the superoxide indicator MitoSOX. NHDF^{EXT} of M donors demonstrated a 1.8-fold increase in superoxide level compared to NHDF^{INT}. In NHDF^{EXT}, mitigation of elevated superoxide concentration was not achieved through NMN treatment (**Figure 29E**). This was in line with the observation that levels of ROS detoxifying proteins also remained unchanged.

In conclusion, NMN treatment reduced the increase of TCA cycle-related proteins and pyruvate consumption in NHDF^{EXT} of M donors. However, an amelioration of oxidative stress was not observed in NMN-treated NHDF^{EXT}.

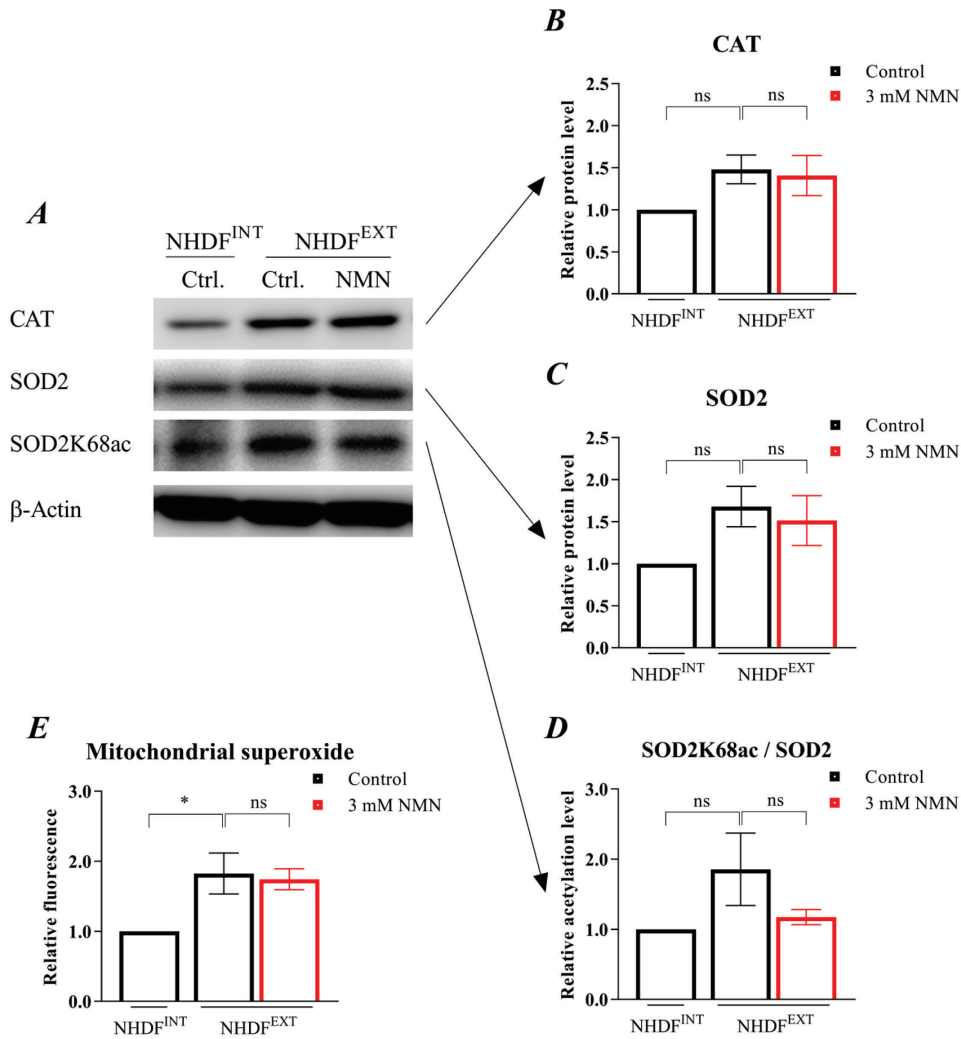


Figure 29: Treatment of NHDF^{EXT} of M donors with NMN did not attenuate oxidative stress levels. NHDF^{EXT} were treated with 3 mM NMN for 48 h. DMEM-incubated NHDF^{INT} and NHDF^{EXT} of the same donors served as a control. Representative western blots (A) and densitometric analysis of chemiluminescent signals of CAT (B), SOD2 (C) and SOD2K68ac (D). CAT and SOD2 were normalized to β-actin, SOD2K68ac was normalized to SOD2. Normalized protein levels were referred to NHDF^{INT}. Mean ± SEM; Holm-Sidak's multiple comparisons test, $p > 0.05$; $n = 3$. (E) Mitochondrial superoxide content was defined using MitoSOX Red mitochondrial superoxide indicator. Fluorescence intensity is shown as FC related to NHDF^{INT}. Mean ± SEM; Holm-Sidak's multiple comparisons test, $*p < 0.05$; $n = 3$.

4. Discussion

Aging is a time-dependent process characterized by the continuous functional decline of cells, tissues, organs and ultimately the whole organism causing a characteristic pattern of diseases and death. Although several theories of aging have been proposed so far, our understanding of this process still remains far from being complete. In general, it is assumed that genetical (intrinsic) as well as environmental (extrinsic) factors contribute to organismal aging. The skin is an ideal model to prove the validity of this concept as it is subjected to intrinsic aging like other organs, but some areas are additionally exposed to environmental factors causing extrinsic skin aging, including UVR as the most important example. Accordingly, numerous studies have analyzed the features of extrinsic *vs* intrinsic aging by comparing UVR-exposed and UVR-protected skin areas in rodents and humans [163-168]. Many of these studies support the concept that skin aging is primarily driven by changes occurring in the dermis rather than the epidermis and in particular concern dermal fibroblasts. Fibroblasts are thought to promote skin aging by an altered secretion of factors shifting the otherwise precisely regulated equilibrium of extracellular matrix synthesis and degradation to the latter one. Ultimately, these alterations may give rise to the formation of wrinkles, a hallmark of intrinsic and extrinsic skin aging. Even though the phenotypic outcome of intrinsic and extrinsic skin aging shares some similarities, marked differences have been documented as well. Clinically, e.g. intrinsically aged skin shows a pattern of fine wrinkles while extrinsically aged skin is characterized by coarse wrinkles. Another clinical feature of extrinsically, but not of intrinsically aged skin, is the appearance of small dilated blood vessels, a condition called telangiectasia. Moreover, histopathological analysis shows that extrinsically aged skin is characterized by the presence of infiltrates of immune cells, a phenomenon for which the term “heliodermatitis” was coined, whereas in intrinsically aged skin, these changes are lacking. These differences suggest a qualitative difference between extrinsic and intrinsic skin aging rather than a simple addition of the same mechanisms. Although, it is assumed that extrinsic aging superimposes intrinsic aging, supporting scientific data for this hypothesis remain rare.

Dermal fibroblasts are thought to be of critical importance for both, intrinsic and extrinsic skin aging. In particular, senescent fibroblasts are thought to play a major role in promoting skin aging as they secrete a distinct pattern of soluble factors capable of perturbing the function of adjacent cells and the surrounding tissue. Even though the pattern of secreted factors, which has also been described in other senescent cell types and tissues, shows some degree of variation, it can be considered as a fingerprint of senescent dysfunctional cells and is referred to as senescence-associated secretory phenotype (SASP). Hallmarks of aging of dermal fibroblasts have been mostly investigated in cells having become senescent *in vitro*, despite of the fact that it has meanwhile become accepted that senescent cells also exist *in vivo* and appear to contribute

to tissue aging and dysfunction. Various mechanisms are capable of inducing senescence in cultured cells including telomere shortening, genomic damage, oncogene activation and oxidative stress [95, 169-171]. *In vitro* aged NHDF manifested telomere attrition [172], genomic instability [71], epigenetic alterations [173], mitochondrial dysfunction [45, 174], impaired proteostasis [175] and developed a SASP [176], amongst others [34]. Yet only little is known about the relevance of these features for *in vivo* aged NHDF [34]. Recent studies demonstrated that characteristics of cells aged in the skin partly deviated from those aged *in vitro* [34, 97, 177]. Accordingly, Waldera-Lupa, Kalfalah et al. showed that also *in situ* aged NHDF developed a secretory phenotype with 70 skin aging-associated secreted proteins (SAASP). However, the SAASP differed from the classical SASP and contained 27 uniquely secreted proteins involved in metabolism and adherens junction interactions [97]. Another feature of cultured, replicative senescent NHDF was telomere shortening [172]. Again, this did not apply to *in situ* aged NHDF of donors aged between 20 and 67 exhibiting comparable telomere lengths [97].

To overcome disadvantages of *in vitro* models and to more closely reflect *in vivo* aging, an *ex vivo* model of *in situ* aged NHDF was applied in this study. Skin biopsies were acquired from 15 healthy, female donors from three different age groups (five donors/age group): Y (20-25 yr.), M (36-49 yr.) and O (60-64 yr.). From each donor, NHDF were isolated from buttocks (=intrinsically aged; NHDF^{INT}) and neck skin (=extrinsically aged; NHDF^{EXT}). Since studies employing high-throughput technologies to examine *in vivo* aging have been scarce [34], this thesis incorporated a secretome and a proteome analysis. Most previous studies focused on either intrinsically or extrinsically aged cells [97, 178, 179], whereas here we aimed at a combined analysis of both conditions from the same donors. This approach allowed us to compare intrinsic vs. extrinsic skin aging intra-individually, i.e. for the same donor. Analysis of NHDF was performed at low passage numbers (PN \leq 10), but potential selection effects or phenotypical alterations through the brief cultivation period could not be excluded.

4.1 NHDF^{EXT} showed non-linear, age-dependent changes in protein abundance patterns, which were different from the linearly developing patterns in NHDF^{INT}

As part of this project, it has been demonstrated that the dynamics of age-associated trajectories of protein abundances fundamentally differed between proteomes of NHDF^{INT} and NHDF^{EXT}. In particular, NHDF^{INT} showed linear, steady shifts of protein levels across the three age groups. In contrast, protein quantities in NHDF^{EXT} changed non-linearly with age. At the early stage (M vs Y), protein abundances remained almost at the same level, but at the late stage (O vs M), shifts of

protein quantities in NHDF^{EXT} were particularly severe and exceeded those detected in NHDF^{INT} (**Figure 8A, B**).

This unusual trajectory of protein levels in NHDF^{EXT} suggests the existence of a tipping point in fibroblasts from aged donors reflecting the sudden breakdown of compensatory mechanisms due to chronic environmental impact. Although respective studies are scarce, proteome-wide, non-linear alterations in protein levels with age have been reported previously [180, 181]. Lehallier, Gate et al. examined human plasma proteomes of 4,263 individuals aged between 18 and 95 years. They observed that the levels of most plasma proteins changed non-linearly with age, i.e. they followed exponential, logarithmic or stepwise trajectories. In addition, Lehallier, Gate et al. found that the alterations of the proteome occurred in three waves in the fourth, seventh and eighth decade of life [181]. These findings were substantiated through a further study by Tanaka, Basisty et al. who also analyzed human plasma proteomes of individuals aged between 21 and 102 years and confirmed the existence of a wave of differential expression at the eighth decade of life [180]. In comparison to these two studies, our study did not only reveal age-dependent, non-linear trajectories of protein levels, but also allowed for a comparison of these in intrinsically *vs* extrinsically aged cells. The direct comparison of NHDF^{EXT} *vs* NHDF^{INT} demonstrated that age-dependent, non-linear changes of protein levels were principally driven by environmental influences rather than intrinsic factors. Moreover, our study is the first to describe proteome-wide, non-linear protein abundance patterns for extrinsic aging in human skin cells.

4.2 Failure of NHDF^{EXT} to compensate for their energy deficit resulted in a crisis situation

A central mechanism following the previously described dynamics of protein abundance changes was cellular respiration. TCA cycle-associated proteins were age-dependently downregulated in NHDF^{INT} or NHDF^{EXT} (**Figure 10A**) suggesting a lowering of energy production. This was in line with studies in various human tissues, providing evidence for age-related reduction of mitochondrial respiratory capacity, ATP production as well as decrease of abundance and activity of mitochondrial proteins [182-187].

It is postulated that age-dependent deterioration of mitochondrial function is accompanied by increased ROS generation [49, 188]. The ETC is the primary source of endogenous ROS formation due to the mechanism of electron leakage [189, 190]. Mitochondrial ROS damage adjacent macromolecules, especially mtDNA. Many genes of mtDNA code for proteins involved in OXPHOS. Therefore, age-related elevation of mtDNA damage is associated with impaired

efficiency and accuracy of OXPHOS [47-49]. This in turn leads to enhanced ROS formation, hypothetically resulting in a vicious cycle [188].

4.2.1 Evidence for an enhanced metabolic flux in NHDF^{EXT} of Y and M donors as an attempt to compensate for their energy deficit

Importantly, metabolic and proteomic data indicate the presence of an enhanced metabolic flux in NHDF^{EXT} vs NHDF^{INT} of Y and M donors. This was substantiated by the following observations:

- (i) Comparing M vs Y probands, TCA cycle-associated proteins were decreased in NHDF^{INT}, but remained unchanged in NHDF^{EXT} (**Figure 16A**).
- (ii) Proteins involved in glycolysis and TCA cycle were upregulated in NHDF^{EXT} vs NHDF^{INT} of Y (**Figure 15A**) and M donors (**Table 29, Figure 15C, Figure 16A-G**).
- (iii) Pyruvate consumption was higher in NHDF^{EXT} vs NHDF^{INT} of M probands (**Figure 16H**).

Despite this evidence for an enhanced metabolic flux, NHDF^{EXT} vs NHDF^{INT} of M donors revealed a raised ADP/ATP ratio (**Figure 18A**) and diminished NAD⁺ levels (**Figure 18B**). Correspondingly, an elevation of ADP/ATP ratio was observed in the skin of hairless mice in response to chronic UVB irradiation [191]. In addition, Gary and Rochette reported a decrease of NAD⁺ levels in primary NHDF after UVB exposure [147]. Thus, the increase of TCA cycle-related proteins in NHDF^{EXT} vs NHDF^{INT} could be considered as an attempt to compensate for an energy deficit. This might be caused by lower efficiency of energy production in NHDF^{EXT} and at the same time higher energy demands.

Lower efficiency of energy production and elevated protein levels as a compensational attempt might be a consequence of hyperacetylation of TCA cycle-associated proteins due to decreased NAD⁺ levels and consequent dysfunction of SIRT3, which is the major mitochondrial NAD⁺-dependent deacetylase. Accordingly, loss of SIRT3 in cancer cells has been reported to result in increased acetylation of the TCA cycle-related protein IDH2 at lysine 413, which leads to its decreased enzymatic activity, elevated ROS levels and stimulation of glycolysis [192]. Interestingly, IDH2 was one of the TCA cycle-associated proteins found to be upregulated in NHDF^{EXT}. In liver mitochondria of SIRT3^{-/-} (KO) mice, 43% of TCA cycle-related proteins displayed enhanced acetylation [193]. Similar effects have also been observed in the brain of mice fed on a western diet [194]. In general, hyperacetylation of mitochondrial proteins due to limited SIRT3 function is often associated with a decrease of their enzymatical activity causing mitochondrial dysfunction and affecting cellular energy homeostasis [195]. As UVR has been

shown to decrease enzymatical activity of SIRT3 in human keratinocytes [196], it appears to be likely that the energetic/metabolic alterations found in NHDF^{EXT} are based on UVR-induced damage and possibly at least partially by dysfunction of mitochondrial SIRT3.

Solar radiation is the most important and best studied contributor to environmentally induced skin aging. Whereas UVB radiation is absorbed through the epidermis to a great extent, UVA rays penetrate the dermis [45, 197, 198]. UVA radiation primarily exerts its detrimental effects on cells indirectly via photosensitization which triggers generation of ROS [55]. In accordance with this finding, mitochondrial superoxide levels (**Figure 17H**) and ROS-related gene expression (**Figure 17A-F**) were elevated in NHDF^{EXT} vs NHDF^{INT} of M donors. More specifically, an increase of HMOX1, CAT and SOD2 was detected on mRNA and protein level. Sundaresan, Gupta et al. demonstrated that gene expression of *CAT* and *SOD2* was induced by SIRT3 via activation of Forkhead box O3 (FOXO3a) [199]. Correspondingly, SIRT3 protein level was upregulated in NHDF^{EXT} vs NHDF^{INT} of M probands (**Figure 19A, C**). Presumably, elevated SIRT3 level enhanced gene transcription and protein translation of CAT and SOD2 to counteract oxidative stress in NHDF^{EXT} (**Figure 30**). Moreover, SIRT3 has also been shown to directly modulate SOD2 activity through deacetylation of lysine 68 [200]. In line with this, a hypoacetylation of SOD2 due to increased SIRT3 levels would be expected in NHDF^{EXT} vs NHDF^{INT} of M probands. However, the opposite occurred: SOD2K68ac was elevated supporting the hypothesis that the function of SIRT3 is impaired in NHDF^{EXT}. Importantly, Qiu, Brown et al. reported that SIRT3-mediated deacetylation of further sites of SOD2 at lysine 53 and 89 were necessary for its activation [201]. These data suggest that decreased SIRT3 function in NHDF^{EXT} causes hyperacetylation and functional impairment of SOD2 resulting in increased mitochondrial superoxide levels.

High ROS levels can be detrimental for the cell as they can perturb cellular signaling and inflict damage on macromolecules. In particular, increased mitochondrial ROS levels – as well as UVR – can cause damage of the mtDNA, which is linked to manifestation of metabolic and aging-associated disorders [202]. Therefore, chronic exposure to UVR and elevated mitochondrial ROS levels could provoke an increase of mtDNA damage in NHDF^{EXT} vs NHDF^{INT}. Although the load of mtDNA damage was not investigated as part of this thesis, this presumption was supported by the study of Berneburg, Gattermann et al. They showed that the rate of the common deletion, the most frequent mtDNA mutation, was 10-times higher in sun-exposed than in sun-protected human skin [53]. A follow-up study revealed that generation of the common deletion in repeatedly UVA-exposed NHDF was mediated by oxidative stress [54]. In NHDF^{EXT}, UVR-caused oxidative stress and presumably mtDNA damage may have accelerated and aggravated the decline of mitochondrial function which was already progressing due to chronological aging. As a consequence, the efficiency of energy production was

compromised. Mitochondrial deterioration was not only manifested by dysregulation of metabolic proteins and pyruvate consumption, but also by enhanced mtDNA content in NHDF^{EXT} vs NHDF^{INT} of M donors (**Figure 17J**). According to this, copy number of mtDNA was increased in the skin of chronically UVR-irradiated hairless mice [191]. The mtDNA content is considered as a biomarker for mitochondrial dysfunction [203]. Patients with mitochondrial genetic disorders exhibited higher copy numbers of mtDNA which was thought to be a strategy to compensate for diminished respiratory capacity [204-206].

Apart from damaging mtDNA, UVR also triggers oxidative modifications of nuclear DNA and other macromolecules like proteins, RNA and lipids [207, 208]. Oxidative DNA damage is generally removed by BER [209]. During BER, ATP and NAD⁺ are required at various steps including e.g. for enzymatic activity of DNA damage sensor PARP1 [210], chromatin remodeling [211] and DNA ligation [212]. Oxidized proteins are eliminated via ubiquitin-proteasome system (UPS) or autophagy-lysosome system [213] whose proteolytic activity depends on ATP [214, 215]. These examples demonstrate that repair or removal of UVR-induced macromolecular damage require energy-intensive processes. Consequently, it can be hypothesized that NHDF^{EXT} had higher energy demands than NHDF^{INT} to mitigate UVR-caused macromolecular damage.

Due to the interplay of both lower energy production and raised energy demands, NHDF^{EXT} faced an extensive energy deficit. Even though they appeared to enhance metabolic flux, NAD⁺ concentration and ADP/ATP ratio were compromised (**Figure 30**). Therefore, it can be concluded that NHDF^{EXT} were not capable to counterbalance their substantial energy lack.

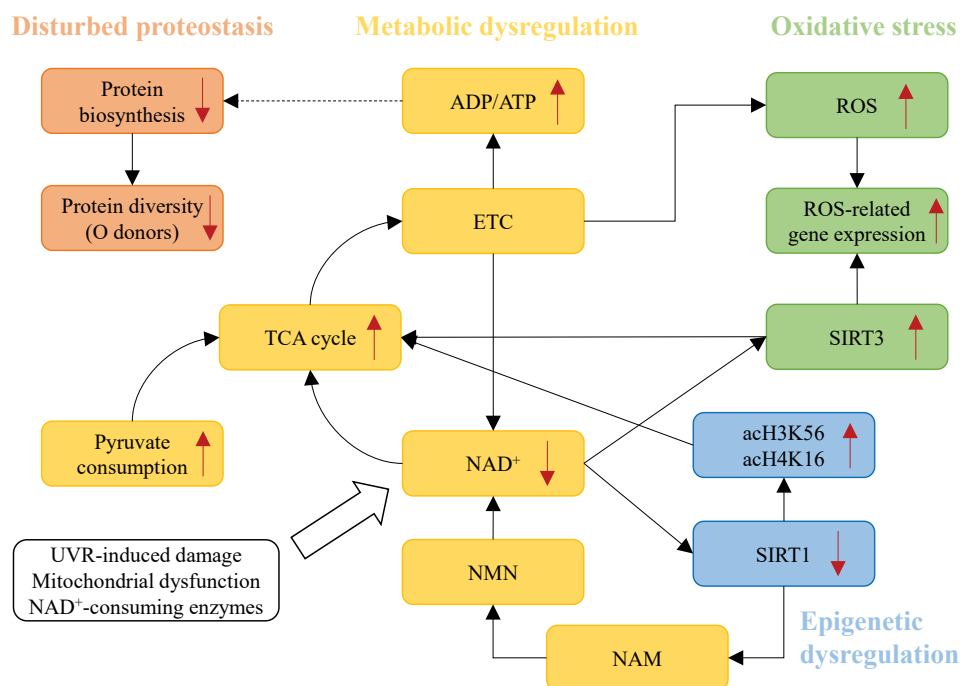


Figure 30: Overview of dysregulated processes and their potential interrelations in NHDF^{EXT} vs NHDF^{INT} of M probands.

4.2.2 NHDF^{EXT} of O donors plunged into an energy crisis upon collapse of compensatory mechanisms

Comparing O vs M probands, TCA cycle-associated proteins were moderately reduced in NHDF^{INT}, but drastically declined in NHDF^{EXT}. Consequently, in O donors, the levels of these proteins were considerably lower in NHDF^{EXT} vs NHDF^{INT} (**Figure 16A**). It may be assumed that metabolic overexploitation and failure of sufficient compensation aggravate the energy deficit so that NHDF^{EXT} of O donors eventually plunged into an energy crisis. This was manifested by a collapse of the initial compensatory increase in mitochondrial respiration. Probably, the sudden and sharp deterioration of NHDF^{EXT} might be the result of a threshold effect potentially of mtDNA mutation load.

An important characteristic of most patients of mitochondrial genetic disorders is heteroplasmy, meaning that their mitochondria do not only contain mutant but also wild-type mtDNA [216]. The proportion between these is pivotal for the severity of their symptoms and the existence of a threshold effect has been shown. The phenotypic threshold effect implies that if the proportion of mutated mtDNA crosses a critical value, defects of respiratory chain will emerge [216, 217]. This threshold varies between individuals and depends on the type of tissue and mutation [216-218]. It is proposed that the threshold value for the proportion of mtDNA mutations ranges from 60% to 80% [216, 217, 219, 220]. After exceeding the threshold value, detrimental effects of mutated mtDNA cannot be counterbalanced anymore by intact proteins and RNA derived from wild-type mtDNA [217].

It can be speculated that such a threshold also exists in NHDF. Besides intrinsic factors, the additional impact of UVR on NHDF^{EXT} led to an increase of ROS level and most likely to an accumulation of mtDNA mutations. Probably, this contributed to an exceedance of the critical threshold of mtDNA mutations in NHDF^{EXT} as opposed to NHDF^{INT}. As a result, the mitochondrial phenotype vastly exacerbated in NHDF^{EXT} of O probands which became apparent by the sudden and drastic decline of metabolic proteins.

4.3 Metabolic dysregulation in NHDF^{EXT} contributed to disrupted proteostasis

The crisis situation of NHDF^{EXT} was not only restricted to a deterioration of metabolic processes. Rather, it was accompanied by a progressive disruption of proteostasis.

4.3.1 Age-dependent decline of mitochondrial respiration in NHDF^{INT} and NHDF^{EXT} correlated with disturbance of proteostasis

Proteostasis regulates protein biosynthesis, folding, quality control and degradation, thereby ensuring the maintenance of functional proteins. Aging is related to impairment of the proteostasis network and accumulation of damaged and misfolded proteins [221, 222]. Studies in various species including humans demonstrated that the rate of global protein biosynthesis diminished in an age-dependent manner [223]. Zou, Long et al. found a downregulation of ribosomal proteins in *in situ* aged dermal fibroblasts isolated from the eyelid [178]. Accordingly, NHDF^{INT} and NHDF^{EXT} exhibited an age-associated decline of proteins involved in mRNA splicing and protein translation (**Figure 10A**), suggesting that this phenomenon could contribute to an attenuated protein synthesis. Additional mechanisms possibly involved in the loss of proteins observed in NHDF^{EXT} are activation of UPR and energy depletion.

An important part of the proteostasis network is the ER that controls folding, assembly and modification of proteins. Diverse stimuli can trigger ER stress overwhelming its functional capacity. ER stress is characterized by an accumulation of unfolded and misfolded proteins as well as initiation of UPR [224-226]. In both NHDF^{INT} and NHDF^{EXT}, proteins implicated in UPR were age-dependently upregulated (**Figure 9B, C**), which might be caused by an age-related accumulation of unfolded and misfolded proteins. Activated UPR attenuates protein biosynthesis, induces chaperones and degradation of misfolded proteins [224-226]. Thus, initiation of UPR in NHDF^{INT} and NHDF^{EXT} might have contributed to the observed decline of protein synthesis.

Several steps of transcription, mRNA splicing and translation require ATP [227-229]. For example, charging of transfer RNA (tRNA) with amino acids or recycling of nucleotides for mRNA transcripts are ATP-dependent processes [230]. Protein synthesis expends by far the largest amounts of ATP amongst the cellular biosynthetic processes of macromolecules [231]. Therefore, in NHDF^{INT} and NHDF^{EXT}, age-related reduction of mitochondrial respiration, hence presumably lower ATP availability can be regarded as a restraining factor for protein synthesis. Inversely, it is conceivable that attenuation of protein synthesis was an attempt to compensate for decreased energy levels.

4.3.2 Metabolic dysregulation strictly correlated with attenuated protein diversity and protein biosynthesis

Comparison within the age groups revealed a downregulation of proteins involved in mRNA splicing, protein translation, ribosomal small subunit biogenesis and mRNA transport in

NHDF^{EXT} vs NHDF^{INT} (**Figure 15B, D, F**). Studies demonstrated that exposure to UVR resulted in a decline of global protein production [232-234]. Thus, it can be concluded that age-associated reduction of protein biosynthesis was intensified in NHDF^{EXT} due to additional suppressive impact of UVR. This may be explained by direct interference of UVR with the protein biosynthesis pathway and by the energy problem in NHDF^{EXT}.

UVR affects both transcription [235-239] and translation [235, 240]. UVR-caused repression of transcription initiation is based on decreased availability of unphosphorylated RNA polymerase II (RNAP II) which is required for the transcription initiation complex [238]. Transcription elongation can be interrupted at sites of UVR-induced bulky DNA damage leading to a stall of RNAP II and initiation of transcription coupled NER (TC-NER) before mRNA synthesis is resumed [236, 237]. UVR influences protein translation via phosphorylation of eukaryotic translation initiation factor 2 subunit 1 ($eIF2\alpha$), thereby suppressing protein translation [240, 241]. It is likely that UVR-induced inhibition of these processes contributed to a reduction of protein biosynthesis in NHDF^{EXT} vs NHDF^{INT}.

As discussed before, transcription, mRNA splicing and translation involve many ATP-consuming steps. A potential interrelation between energy metabolism and protein biosynthesis in NHDF^{INT} and NHDF^{EXT} is reinforced by the finding that abundance shifts of metabolic proteins strictly correlated with protein diversity changes (**Table 28, Figure 7A**). In specific terms, the following observations were made:

- (i) In NHDF^{EXT}, metabolic protein quantities and overall protein diversity remained on equal levels in M vs Y donors, but were drastically decreased in O vs M probands.
- (ii) In NHDF^{INT}, both were reduced continuously across the three age groups.
- (iii) In Y and M donors, metabolic protein levels and global protein diversity were enhanced in NHDF^{EXT} vs NHDF^{INT}.
- (iv) In O probands, both were diminished in NHDF^{EXT} vs NHDF^{INT}.

These findings strongly hint at a connection of energy crisis in NHDF^{EXT} with the decline of protein diversity and protein production (**Figure 30**). Correspondingly, the dependence of protein synthesis rate on ATP concentration has been demonstrated in cell-free systems [230, 242].

The exact mechanism of the correlation of both processes in NHDF, however, remained elusive. On the one hand, proteins synthesis might be decreased in NHDF^{EXT} as a consequence of the strong energy deficit, hence insufficient ATP availability. On the other hand, attenuation of protein production may have been an attempt to countervail the energy lack. To clarify the interrelation between metabolism and protein synthesis, further examinations are necessary. For

example, it could be investigated if treatment of aged NHDF with energy precursors might retrieve protein synthesis and diversity.

4.4 The energy deficit induced epigenetic dysregulation in NHDF^{EXT} of M donors

The energy deficit in NHDF^{EXT} of M probands was manifested by diminished NAD⁺ concentration compared to NHDF^{INT}. As a consequence, protein level of NAD⁺-dependent SIRT1 was decreased in NHDF^{EXT} (**Figure 19A, B**). This was in accordance with findings of Cao, Lu et al. showing a downregulation of SIRT1 in cultured human keratinocytes in response to UVR [243]. SIRT1s are important regulators in a wide range of cellular processes including DNA repair, aging and particularly metabolism [244]. SIRT1 activation mitigated insulin resistance and ameliorated glucose homeostasis, therefore playing an important role in metabolic diseases such as diabetes [245-247]. Furthermore, SIRT1 is a central regulator of epigenetic mechanisms through histone deacetylation [119, 124]. Correspondingly, reduction of SIRT1 and NAD⁺ levels resulted in hyperacetylation of certain histone lysine residues in NHDF^{EXT} vs NHDF^{INT} of M donors (**Figure 20, Figure 21**). Acetylation levels of H3K9, H3K56 and H4K16 were increased in NHDF^{EXT}. This was in line with many studies proving the influence of UVR on acetylation of these lysine residues of histones [248-250]. In contrast to hyperacetylation of those histone sites, acetylation levels of H3K14, H4K8 and H4K12 remained the same in NHDF^{EXT} vs NHDF^{INT} of M probands. These results proved that hyperacetylation was specific to certain histone residues rather than part of a global increase of histone acetylation in NHDF^{EXT}.

Histone acetylation/deacetylation plays an important role in DNA damage repair, DNA replication and transcription due to modification of chromatin structure. Transfer of acetyl groups to lysine residues of histones neutralizes their positive charge and mitigates electrostatic interactions of histones with negatively charged phosphate groups of the DNA backbone. This leads to an opening of chromatin structure which improves accessibility for DNA-binding factors to specific genomic sites, thereby facilitating DNA repair, replication and transcription [251-254].

Several studies reported that histone acetylation was involved in removal of photo-adducts via NER. Acetylation of H3 and H4 induced chromatin opening and facilitated recruitment of xeroderma pigmentosum complementation group A (XPA) protein [249, 255-257]. In double-strand breaks (DSB) repair, H3K56ac was necessary for sister chromatid recombination in HR [258] and for chromatin reassembly after DSB repair [259]. Besides, H3K56ac interacted with phosphorylated histone H2AX (γ -H2AX) and colocalized with biomarkers for DSBs [260]. An implication in DSB repair was also reported for H4K16ac which was required for recruitment

of mediator of DNA damage checkpoint protein 1 (MDC1) [261-263]. MDC1 interacts with γ -H2AX and thereby recruits further proteins acting in DNA damage response [264]. Moreover, a role of H3K56ac in BER has been reported where it induced an increase of apurinic/apyrimidinic endonuclease 1 (APE1) [265].

Possibly, UVR-caused DNA damage including bulky photo-adducts, oxidative DNA damage, SSBs and DSBs have accumulated in NHDF^{EXT} of M donors. Therefore, hyperacetylation of H3K9, H3K56 and H4K16 may have facilitated initiation of DNA damage repair apart from just being a consequence of decreased SIRT1 and NAD⁺ levels. However, neither the existence of any DNA damage nor the activation of factors implicated in repair pathways have been investigated as part of this thesis. Thus, further examinations are necessary to allow for concrete conclusions.

4.4.1 Histone hyperacetylation was both result and source of metabolic dysregulation in NHDF^{EXT}

Several studies suggested a mutual link between metabolism and epigenetics [266-268]. On the one hand, metabolic state affects histone modifications and on the other hand, histone modifications modulate transcription of genes whose proteins play a role in metabolism.

Many enzymes require metabolites for their histone-modifying activities. Histone methylation is regulated through histone methyltransferases (HMTs) and histone demethylases (HDMs). HMTs depend on S-adenosylmethionine which is generated from ATP and methionine and serves as methyl donor for diverse substrates. HDMs need α -ketoglutarate, an intermediate of the TCA cycle [269]. Acetylation state of histones is controlled by the interplay of histone deacetylases (HDACs) and histone acetyltransferases (HATs). Whereas SIRTs, class III HDACs, require NAD⁺, HATs utilize acetyl-CoA as a cofactor [270, 271]. Acetyl-CoA is the starting molecule for the TCA cycle and a substrate for synthesis of macromolecules like amino acids, cholesterol and lipids [266]. A correlation of metabolic state and acetyl-CoA level with histone acetylation and gene expression has been reported in yeast, *Drosophila* and mammalian cells [272-275]. Thus, it is very likely that hyperacetylation of histones was the consequence of the energy deficit in NHDF^{EXT} of M donors.

Conversely, some studies showed that histone acetylation/deacetylation also regulated transcription of metabolism-associated genes. Zhong, D'Urso et al. observed that H3K9 acetylation was associated with elevated expression of glycolytic genes [276]. In sun-exposed epidermis of the forearm, enriched H3 acetylation was found at genes whose proteins act in energy metabolism including TCA cycle, e.g. *CS* and *dihydrolipoamide S-succinyltransferase (DLST)* [134]. Moreover, overexpression of H4K16 in yeast was associated with transcriptional activation

of metabolic genes like *pyruvate dehydrogenase E1 component subunit alpha, mitochondrial (PDA1)* which is very similar to human *PDHA1* [277]. In NHDF^{EXT} vs NHDF^{INT} of M probands, levels of H3K9ac, H3K56ac and H4K16ac as well as concentrations of PDHA1, CS and other TCA cycle-related proteins were enhanced. Therefore, histone hyperacetylation may have facilitated transcriptional activation and thereby contributed to the increase of metabolic proteins in NHDF^{EXT} (Figure 30).

4.5 Restricted NAD⁺ availability was the major force driving metabolic and epigenetic changes in NHDF^{EXT}

A central finding of the dysregulated metabolism in NHDF^{EXT} vs NHDF^{INT} of M probands was the decrease of NAD⁺ concentration. This might be caused by excessive NAD⁺ consumption, compromised NAD⁺ synthesis or both. To examine the underlying reasons and to figure out if NAD⁺ decline was a causative factor for metabolic dysregulation, NHDF^{EXT} were treated with substances intervening in NAD⁺ metabolism at different steps (Figure 31).

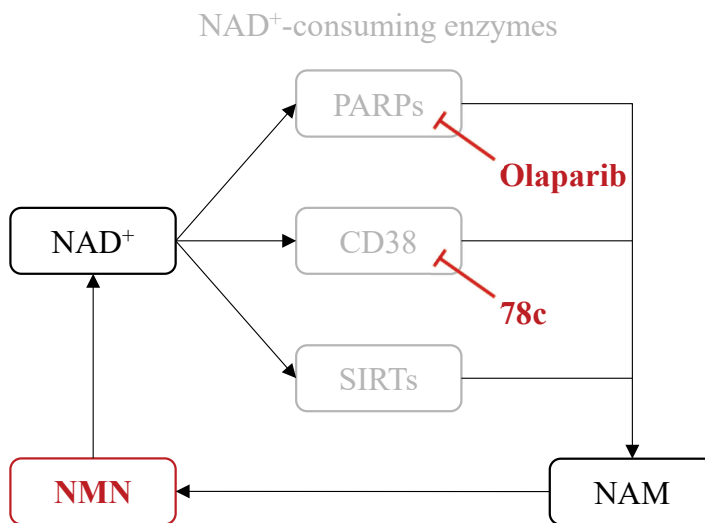


Figure 31: Applied substances for intervention in NAD⁺ metabolism. NAD⁺-consuming enzymes PARP and CD38 were inhibited with olaparib and compound 78c. NAD⁺ precursor availability was modulated through treatment with NMN.

4.5.1 Overactivation of NAD⁺-consuming enzymes contributed to metabolic dysregulation in NHDF^{EXT}

An important NAD⁺-degrading enzyme is PARP which is activated in response to DNA damage and is known to play a role in DSB repair, BER and NER [278-281]. A study of mouse embryonic fibroblasts showed that UVB irradiation entailed a two-phase activation of PARP1. Whereas the immediate induction was caused through direct DNA photo-adducts, oxidative DNA damage was responsible for the late response [282]. In UVR-exposed HaCaT cells and NHDF, inhibition of PARP rescued decline of NAD⁺ level and led to an accumulation of DNA damage [149, 150]. In NHDF^{EXT} of M probands, treatment with the PARP inhibitor olaparib enhanced NAD⁺ level (**Figure 22A**) and reduced ADP/ATP ratio (**Figure 22B**). These results demonstrated that PARP was activated in NHDF^{EXT} and contributed to the energy depletion due to excessive consumption of NAD⁺ and ATP. Since NHDF^{EXT} were exposed to environmental factors, a probable reason for PARP induction might have been the accumulation of directly and indirectly UVR-caused DNA damage.

It is well known that UVR triggers inflammatory processes including induction of pro-inflammatory cytokines and activation of NF-κB signaling pathway [283-285]. The NAD⁺-dependent enzyme CD38 is involved in inflammatory processes, immune response, but also in metabolic disorders and cancer [159, 286, 287]. It was shown that CD38 increased with aging which was accompanied by a decline of NAD⁺ and ATP concentration as well as mitochondrial dysfunction [158, 288]. Correspondingly, in NHDF^{EXT} of M donors, exposure to CD38 inhibitor 78c increased NAD⁺ concentration (**Figure 23A**) and normalized ADP/ATP ratio (**Figure 23B**). These observations proved that CD38 activity was also causative for NAD⁺ depletion and disbalanced ADP/ATP ratio in NHDF^{EXT}.

4.5.2 Restricted NAD⁺ availability was the primary cause for metabolic dysregulation in NHDF^{EXT}

NMN, a precursor of NAD⁺, is a promising substance that is known to elevate cellular NAD⁺ levels in human cells. In mouse models, NMN improved age-associated diseases like diabetes, Alzheimer's disease and ischemia-reperfusion injury [289]. Treatment of NHDF^{EXT} of M probands with NMN significantly elevated the NAD⁺ level (**Figure 24A**) and rescued the ADP/ATP ratio (**Figure 24B**). In line, an enhancement of NAD⁺ level following NMN incubation has been shown in various tissues [138, 139, 161, 162]. NAD⁺, an important electron transport molecule, accepts electrons during several steps of TCA cycle and delivers them to complex I of

ETC. Presumably, increased NAD^+ availability in NMN-treated NHDF^{EXT} facilitated this electron transfer and thereby ATP synthesis through OXPHOS, which resulted in lowering of ADP/ATP ratio.

Apart from retrieval of NAD^+ level and ADP/ATP ratio, NMN treatment of NHDF^{EXT} also normalized levels of TCA cycle-associated proteins (**Figure 28A-F**) and pyruvate consumption (**Figure 28G**). These findings reinforced the assumption that enhancement of metabolic flux was a compensatory effect to combat the extensive energy deficit. NMN treatment of NHDF^{EXT} led to sufficient NAD^+ availability to overcome the energy problem. As a result, compensatory mechanisms were not required anymore and disabled. These results demonstrated that limited NAD^+ availability was the primary cause for metabolic dysregulation in NHDF^{EXT} since restoration of NAD^+ level through NMN treatment rescued all observed metabolic alterations (**Figure 32**).

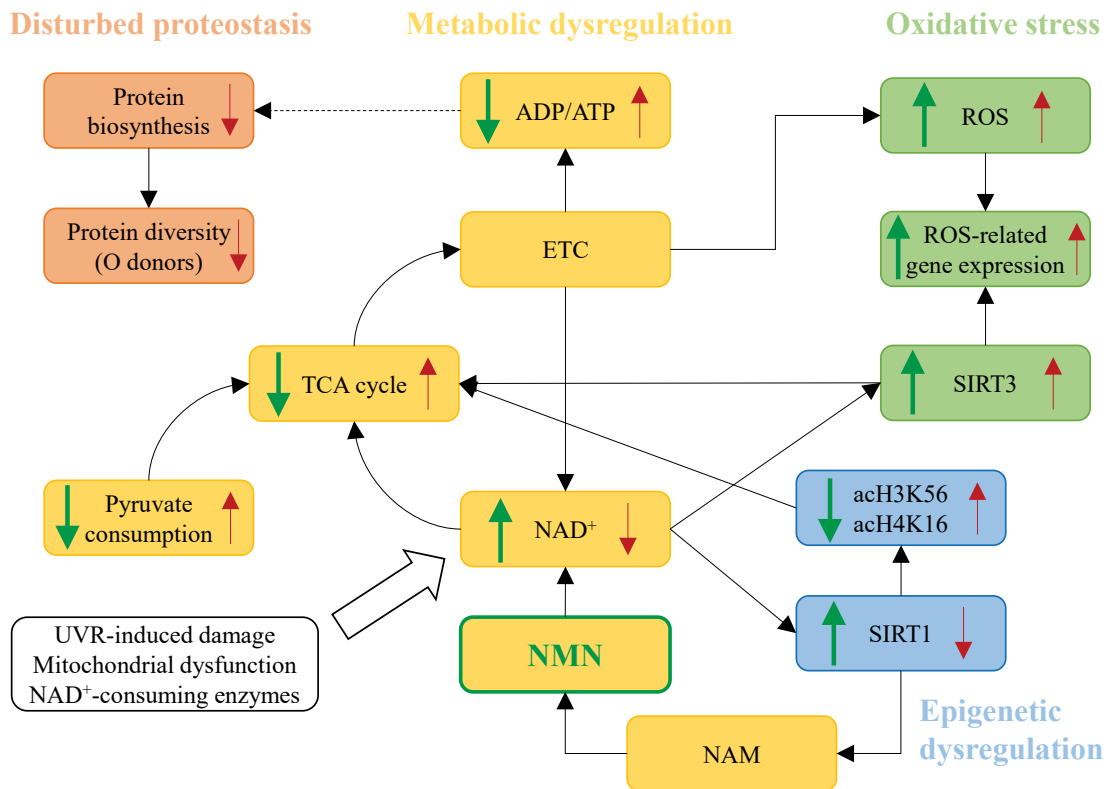


Figure 32: Overview of the impact of NMN treatment on dysregulated processes in NHDF^{EXT} of M probands.

In NHDF^{EXT} of M donors, UVR-induced ROS and consequent oxidative damage of macromolecules, particularly in mitochondria, caused enhanced superoxide concentration and expression of antioxidant genes. Even though dysregulation of metabolic mechanisms was alleviated through NMN treatment, neither elevation of mitochondrial superoxide levels (**Figure 29E**) nor ROS-related gene expression were ameliorated (**Figure 29A-D**). These findings

suggested that the integrity or function of the ETC may be compromised in NHDF^{EXT} giving rise to a decreased oxidation capacity of NADH but enhanced ROS generation. In accordance with these observations, SIRT3 level was also unaffected in NMN-incubated NHDF^{EXT} (**Figure 25A, C**). As discussed in section 4.2.1, SIRT3 was presumably involved in regulation of ROS-related gene expression. These results demonstrated that NAD⁺ decline and associated metabolic dysregulation did not primarily contribute to the formation of oxidative stress in NHDF^{EXT} (**Figure 32**).

4.5.3 Limited NAD⁺ availability was the major driver for epigenetic changes in NHDF^{EXT}

Several studies reported that NMN exposure did not only lead to restoration of NAD⁺ levels, but also to an upregulation of SIRT1 [290-292]. Accordingly, SIRT1 protein level was recovered in NHDF^{EXT} upon NMN treatment (**Figure 25A, B**). Moreover, hyperacetylation of H3K56 (**Figure 26A, C**) and H4K16 (**Figure 27**) was reversed. These findings demonstrated that SIRT1 played a major role in deacetylation of these histone sites in NHDF^{EXT}. In addition, the results showed that restricted NAD⁺ availability in NHDF^{EXT} was the major cause for the observed epigenetic dysregulation (**Figure 32**). As discussed in section 4.4.1, H3K56ac and H4K16ac may be involved in transcriptional regulation of metabolic genes. Since NMN-treated NHDF^{EXT} exhibited normalization of H3K56ac, H4K16ac and TCA cycle-related protein concentrations, a link between these findings may be assumed. It might be conceivable that alleviation of hyperacetylation of H3K56 and H4K16, potentially at promoters of metabolic genes, mediated normalization of TCA cycle-associated protein levels.

Interestingly, hyperacetylation of H3K9 was not rescued through NMN incubation (**Figure 26A, B**). Presumably, other enzymes than SIRT1, which were not affected by the applied NMN concentration, were more important in regulation of acetylation state of H3K9. Studies reported that H3K9 is also deacetylated by SIRT6 and NAD⁺-independent enzymes such as HDAC1 or HDAC3 [293, 294]. Additionally, H3K9ac may have been influenced by the activity of HATs [295]. A potential dysregulation of HATs and HDACs, besides SIRTs, has not been examined by this work. However, as NMN treatment did not affect acetylation state of H3K9, it can be assumed that H3K9ac was regulated by NAD⁺-independent mechanisms.

4.6 Reassessment of the generally accepted superimposition theory of intrinsic and extrinsic aging is crucial

There is general consensus in textbooks that environmentally induced skin aging superimposes chronological skin aging, which in the following is referred to as ‘superimposition theory’. On the one hand, this assumes that extrinsic skin aging accelerates and exacerbates mechanisms of intrinsic skin aging. On the other hand, new mechanisms might be introduced through environmentally induced skin aging. However, this hypothesis has not been proven and interactions between both aging types might be more complex than a simple superimposition. Therefore, one aim of this thesis was to assess the interaction between intrinsic and extrinsic skin aging in terms of the superimposition theory.

Some findings within this thesis are consistent with the superimposition theory. mRNA splicing and protein translation were age-dependently reduced in both NHDF^{INT} and NHDF^{EXT} (**Figure 10A**). In NHDF^{EXT} vs NHDF^{INT} of Y donors, proteins involved in mRNA splicing and mRNA 3'-end processing were decreased (**Figure 15B**). In NHDF^{EXT} vs NHDF^{INT} of M probands, translation and ribosomal small subunit biogenesis were attenuated (**Figure 15D**). In NHDF^{EXT} vs NHDF^{INT} of O donors, proteins implicated in mRNA transport were diminished (**Figure 15F**). Thus, age-dependent decline of mRNA splicing and protein translation was accelerated and more pronounced in NHDF^{EXT} which would support the superimposition theory. Importantly, only NHDF^{EXT} exhibited age-associated increase of proteins involved in N-linked glycosylation (**Figure 9C**). This would be in accordance with the superimposition theory as it displayed a new, age-associated mechanism that was introduced through the impact of environmental factors.

Although some observations might support the superimposition theory, there are several hints within this thesis pointing to a more complex interaction between intrinsic and extrinsic skin aging than a superimposition.

The first observation challenging the superimposition theory is the discrepancy of age-associated alterations of protein diversity in secretomes of NHDF^{INT} and NHDF^{EXT}. Protein diversity was elevated in NHDF^{INT} with age, but remained unchanged in NHDF^{EXT} (**Table 27, Figure 6A**). This is surprising, because in accordance with the superimposition theory, one would expect an age-dependent increase of protein diversity in secretomes of NHDF^{EXT} as well.

The second hint contradicting the superimposition theory is the different dynamic of age-related decline of protein diversity in proteomes of NHDF^{INT} and NHDF^{EXT} of M vs Y donors. Whereas NHDF^{INT} showed a decrease in protein diversity, no alteration occurred in NHDF^{EXT} (**Table 28, Figure 7A**). This is in conflict with the superimposition theory anticipating an at least likewise

decline of protein diversity in NHDF^{EXT} of M vs Y probands. However, when comparing O vs M donors, observations were in accordance with the superimposition theory: protein diversity in NHDF^{INT} was reduced and a more pronounced decline was found in NHDF^{EXT}.

The third indication arguing against the superimposition theory was the difference in the dynamic of age-related trajectories of protein abundances in proteomes of NHDF^{INT} and NHDF^{EXT} of M vs Y donors. NHDF^{INT} already showed noticeable alterations, as opposed to NHDF^{EXT} revealing almost steady protein quantities (**Figure 8A, B**). Pursuant to the superimposition theory, in NHDF^{EXT} protein quantities would have shifted at least to the same extent as observed in NHDF^{INT}. Again, the comparison of O vs M donors was consistent with the superimposition theory. NHDF^{EXT} exhibited alterations which were more severe than the changes of protein abundances found in NHDF^{INT} of O vs M probands.

The fourth hint challenging the superimposition theory is the unexpected large amount of age-regulated proteins unique to proteomes of NHDF^{INT} (**Figure 8C**). Specifically, 106 or 198 proteins were up- or downregulated only in NHDF^{INT}. Corresponding to the superimposition theory, age-associated alterations occurring in NHDF^{INT} would have been anticipated to appear also in NHDF^{EXT}.

These four outlined points indicate that some age-related processes present in NHDF^{INT} were absent in NHDF^{EXT} due to the impact of environmental factors. This clearly contradicts the superimposition theory which would expect mechanisms observed in NHDF^{INT} to occur in NHDF^{EXT}, possibly aggravated. A relationship involving an elimination of parts of the chronological aging process through extrinsic aging mechanisms has not yet been described for skin aging or aging in general. By this work, it was shown for the first time that the interaction between intrinsic and extrinsic skin aging does not only include superimposition of mechanisms, but also elimination effects. This thesis provides clear evidence that the relationship of chronologically and environmentally induced skin aging is far more complex than previously assumed (**Figure 33**). Therefore, it is crucial to critically reconsider the general assumption of a superimposition of intrinsic and extrinsic skin aging.

Despite of the relevance of the obtained results, possible limitations of this study have to be considered. Accordingly, an important point is the cultivation period of fibroblasts between biopsy isolation and sample preparation for experiments. This cultivation period was unavoidable since the experiments of this study either required large amounts of biological material (e.g. western blot analysis, measurement of NAD⁺ levels) or could not be conducted directly on the biopsies (e.g. measurement of pyruvate consumption, collection of secretomes). Perhaps, the cultivation might result in a negative selection eliminating the most damaged and senescent

fibroblasts particularly of O donors, since they are less likely to divide. However, the findings of this study demonstrate that these cells still exhibit a clear phenotype arguing against this objection.

Another limitation of this study is that it cannot be excluded that apart from extrinsic factors, also the different anatomical locations, from which NHDF^{INT} and NHDF^{EXT} were isolated, might contribute to differences between these cells. However, a study of Kimball, Alora-Palli et al. supports the notion that the different kinetics of age-related changes of protein abundances as well as the existence of a mitochondrial phenotype in NHDF^{EXT} is driven by extrinsic factors, independent of the anatomical location. Kimball, Alora-Palli et al. investigated the transcriptome of full-thickness dorsal forearm skin, a skin area representative for extrinsic skin aging, from women aged between 20 and 74 years. They found an age-dependent downregulation of mitochondrial genes, which proceeded rather non-linearly. Whereas mitochondrial gene levels in the skin of probands between the 20s and 50s differed only slightly, a strong decline was detected between donors in the 50s and 60s [296]. These findings in forearm skin do not only resemble the “tipping point” observed in NHDF^{EXT} of neck skin of M vs O donors within our study, but also confirm the age-related, accelerated decrease of mitochondrial gene expression in another UVR-exposed skin area beside neck skin.

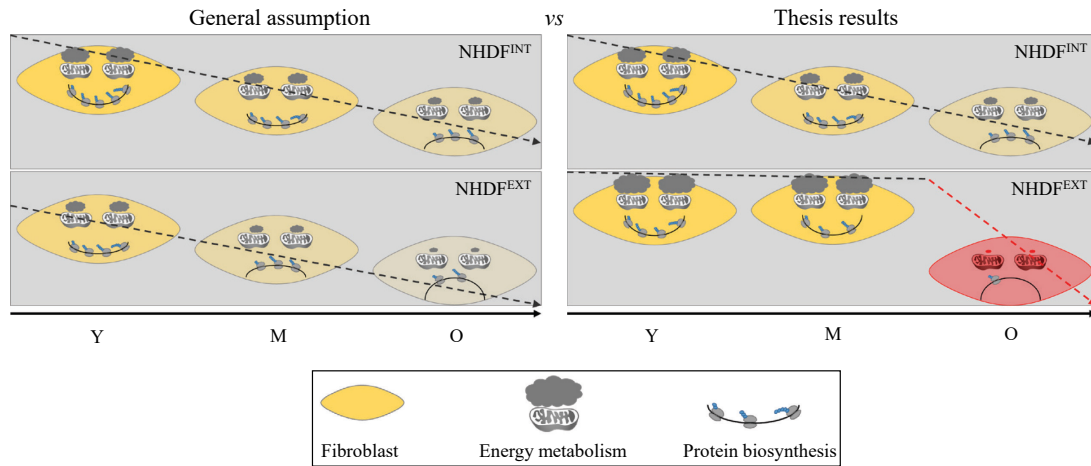


Figure 33: Interaction between intrinsic and extrinsic skin aging is more complex than a superimposition. NHDF^{INT} exhibited an age-dependent, linear decline of mitochondrial function, protein biosynthesis and diversity. According to the general assumption of a superimposition of intrinsic and extrinsic skin aging, an accelerated and more pronounced reduction of these processes was expected in NHDF^{EXT}. However, NHDF^{EXT} demonstrated a non-linear progress of mitochondrial deterioration and protein diversity decrease. This was manifested by an initial compensation and suppression of changes of these processes and a subsequent crisis which was characterized by collapse of compensatory metabolic mechanisms and substantial loss of protein diversity.

5. References

1. Kawasumi, A., et al., *Wound healing in mammals and amphibians: toward limb regeneration in mammals*. *Curr Top Microbiol Immunol*, 2013. 367: p. 33-49.
2. Kaidbey, K.H., et al., *Photoprotection by melanin--a comparison of black and Caucasian skin*. *J Am Acad Dermatol*, 1979. 1(3): p. 249-60.
3. Kalluri, R. and M. Zeisberg, *Fibroblasts in cancer*. *Nat Rev Cancer*, 2006. 6(5): p. 392-401.
4. Krutmann, J., *[How the sun ages our skin. The dermis as the driving force]*. *Hautarzt*, 2011. 62(8): p. 588-90.
5. Bainbridge, P., *Wound healing and the role of fibroblasts*. *J Wound Care*, 2013. 22(8): p. 407-8, 410-12.
6. Buckley, C.D., et al., *Fibroblasts regulate the switch from acute resolving to chronic persistent inflammation*. *Trends in Immunology*, 2001. 22(4): p. 199-204.
7. Driskell, R.R., et al., *Defining dermal adipose tissue*. *Exp Dermatol*, 2014. 23(9): p. 629-31.
8. Guillems, M., et al., *Dendritic cells, monocytes and macrophages: a unified nomenclature based on ontogeny*. *Nat Rev Immunol*, 2014. 14(8): p. 571-8.
9. Krutmann, J., et al., *Environmentally-Induced (Extrinsic) Skin Aging: Exposomal Factors and Underlying Mechanisms*. *Journal of Investigative Dermatology*, 2021.
10. Yaar, M. *Clinical and Histological Features of Intrinsic versus Extrinsic Skin Aging*. 2006.
11. Krutmann, J., et al., *The skin aging exposome*. *J Dermatol Sci*, 2017. 85(3): p. 152-161.
12. Cockayne, E.A., *Dwarfism with retinal atrophy and deafness*. *Arch Dis Child*, 1936. 11(61): p. 1-8.
13. Neill, C.A. and M.M. Dingwall, *A syndrome resembling progeria: A review of two cases*. *Arch Dis Child*, 1950. 25(123): p. 213-23.
14. Hebra, F. and M. Kaposi, *On Diseases of the skin including exanthemata*. New Sydenham Soc, 1874. 61: p. 252-258.
15. Vierkotter, A., et al., *MMP-1 and -3 promoter variants are indicative of a common susceptibility for skin and lung aging: results from a cohort of elderly women (SALIA)*. *J Invest Dermatol*, 2015. 135(5): p. 1268-1274.
16. Nouveau-Richard, S., et al., *Skin ageing: a comparison between Chinese and European populations. A pilot study*. *J Dermatol Sci*, 2005. 40(3): p. 187-93.
17. Tsukahara, K., et al., *Comparison of age-related changes in wrinkling and sagging of the skin in Caucasian females and in Japanese females*. *International Journal of Cosmetic Science*, 2004. 26(6): p. 314-314.
18. Vierkötter, A., et al., *Extrinsic skin ageing in German, Chinese and Japanese women manifests differently in all three groups depending on ethnic background, age and anatomical site*. *Journal of Dermatological Science*, 2016. 83(3): p. 219-225.
19. Diridollou, S., et al., *Comparative study of the hydration of the stratum corneum between four ethnic groups: influence of age*. *Int J Dermatol*, 2007. 46 Suppl 1: p. 11-4.
20. Sack, R.L., et al., *Human melatonin production decreases with age*. *J Pineal Res*, 1986. 3(4): p. 379-88.
21. Harman, S.M., et al., *Longitudinal effects of aging on serum total and free testosterone levels in healthy men. Baltimore Longitudinal Study of Aging*. *J Clin Endocrinol Metab*, 2001. 86(2): p. 724-31.
22. Thornton, M.J., *Estrogens and aging skin*. *Dermatoendocrinol*, 2013. 5(2): p. 264-70.
23. Dunn, L.B., et al., *Does estrogen prevent skin aging? Results from the First National Health and Nutrition Examination Survey (NHANES I)*. *Arch Dermatol*, 1997. 133(3): p. 339-42.
24. Kaddurah, H., et al., *The Impact of Sunlight on Skin Aging*. *Current Geriatrics Reports*, 2018. 7.

25. Kligman, A.M., *Early destructive effect of sunlight on human skin*. *Jama*, 1969. 210(13): p. 2377-80.
26. Akiba, S., et al., *Influence of chronic UV exposure and lifestyle on facial skin photoaging--results from a pilot study*. *J Epidemiol*, 1999. 9(6 Suppl): p. S136-42.
27. Flament, F., et al., *Solar exposure(s) and facial clinical signs of aging in Chinese women: impacts upon age perception*. *Clin Cosmet Investig Dermatol*, 2015. 8: p. 75-84.
28. Flament, F., et al., *Effect of the sun on visible clinical signs of aging in Caucasian skin*. *Clin Cosmet Investig Dermatol*, 2013. 6: p. 221-32.
29. Kligman, L.H. and A.M. Kligman, *The nature of photoaging: its prevention and repair*. *Photodermatol*, 1986. 3(4): p. 215-27.
30. Daniell, H.W., *Smoker's wrinkles. A study in the epidemiology of "crow's feet"*. *Ann Intern Med*, 1971. 75(6): p. 873-80.
31. Doshi, D.N., K.K. Hanneman, and K.D. Cooper, *Smoking and skin aging in identical twins*. *Arch Dermatol*, 2007. 143(12): p. 1543-6.
32. Vierkötter, A., et al., *Airborne Particle Exposure and Extrinsic Skin Aging*. *Journal of Investigative Dermatology*, 2010. 130(12): p. 2719-2726.
33. Li, M., et al., *Epidemiological evidence that indoor air pollution from cooking with solid fuels accelerates skin aging in Chinese women*. *Journal of Dermatological Science*, 2015. 79(2): p. 148-154.
34. Tigges, J., et al., *The hallmarks of fibroblast ageing*. *Mech Ageing Dev*, 2014. 138: p. 26-44.
35. Krutmann, J., *Pathomechanisms of Photoaged Skin*, in *Textbook of Aging Skin*, M.A. Farage, K.W. Miller, and H.I. Maibach, Editors. 2017, Springer Berlin Heidelberg: Berlin, Heidelberg. p. 121-129.
36. Wisnovsky, S., S.R. Jean, and S.O. Kelley, *Mitochondrial DNA repair and replication proteins revealed by targeted chemical probes*. *Nat Chem Biol*, 2016. 12(7): p. 567-73.
37. Clayton, D.A., J.N. Doda, and E.C. Friedberg, *The absence of a pyrimidine dimer repair mechanism in mammalian mitochondria*. *Proc Natl Acad Sci U S A*, 1974. 71(7): p. 2777-81.
38. Clayton, D.A., J.N. Doda, and E.C. Friedberg, *Absence of a pyrimidine dimer repair mechanism for mitochondrial DNA in mouse and human cells*. *Basic Life Sci*, 1975. 5b: p. 589-91.
39. Alexeyev, M., et al., *The maintenance of mitochondrial DNA integrity--critical analysis and update*. *Cold Spring Harbor perspectives in biology*, 2013. 5(5): p. a012641-a012641.
40. Brown, W.M., M. George, Jr., and A.C. Wilson, *Rapid evolution of animal mitochondrial DNA*. *Proc Natl Acad Sci U S A*, 1979. 76(4): p. 1967-71.
41. Richter, C., J.W. Park, and B.N. Ames, *Normal oxidative damage to mitochondrial and nuclear DNA is extensive*. *Proc Natl Acad Sci U S A*, 1988. 85(17): p. 6465-7.
42. Ballard, J.W. and M.C. Whitlock, *The incomplete natural history of mitochondria*. *Mol Ecol*, 2004. 13(4): p. 729-44.
43. Miquel, J., et al., *Mitochondrial role in cell aging*. *Exp Gerontol*, 1980. 15(6): p. 575-91.
44. Harman, D., *Aging: a theory based on free radical and radiation chemistry*. *J Gerontol*, 1956. 11(3): p. 298-300.
45. Krutmann, J. and P. Schroeder, *Role of mitochondria in photoaging of human skin: the defective powerhouse model*. *J Investig Dermatol Symp Proc*, 2009. 14(1): p. 44-9.
46. Corral-Debrinski, M., et al., *Mitochondrial DNA deletions in human brain: regional variability and increase with advanced age*. *Nat Genet*, 1992. 2(4): p. 324-9.
47. Wallace, D.C., *Mitochondrial genetics: a paradigm for aging and degenerative diseases?* *Science*, 1992. 256(5057): p. 628-32.
48. Ames, B.N., M.K. Shigenaga, and T.M. Hagen, *Mitochondrial decay in aging*. *Biochim Biophys Acta*, 1995. 1271(1): p. 165-70.
49. Richter, C., *Oxidative damage to mitochondrial DNA and its relationship to ageing*. *Int J Biochem Cell Biol*, 1995. 27(7): p. 647-53.
50. Khaidakov, M., et al., *Accumulation of point mutations in mitochondrial DNA of aging mice*. *Mutat Res*, 2003. 526(1-2): p. 1-7.

51. Trifunovic, A., et al., *Premature ageing in mice expressing defective mitochondrial DNA polymerase*. *Nature*, 2004. 429(6990): p. 417-23.
52. Kujoth, G.C., et al., *Mitochondrial DNA mutations, oxidative stress, and apoptosis in mammalian aging*. *Science*, 2005. 309(5733): p. 481-4.
53. Berneburg, M., et al., *Chronically ultraviolet-exposed human skin shows a higher mutation frequency of mitochondrial DNA as compared to unexposed skin and the hematopoietic system*. *Photochem Photobiol*, 1997. 66(2): p. 271-5.
54. Berneburg, M., et al., *Singlet oxygen mediates the UVA-induced generation of the photoaging-associated mitochondrial common deletion*. *J Biol Chem*, 1999. 274(22): p. 15345-9.
55. Berneburg, M., H. Plettenberg, and J. Krutmann, *Photoaging of human skin*. *Photodermatol Photoimmunol Photomed*, 2000. 16(6): p. 239-44.
56. Rhie, G., et al., *Aging- and photoaging-dependent changes of enzymic and nonenzymic antioxidants in the epidermis and dermis of human skin in vivo*. *J Invest Dermatol*, 2001. 117(5): p. 1212-7.
57. Su, L.-J., et al., *Reactive Oxygen Species-Induced Lipid Peroxidation in Apoptosis, Autophagy, and Ferroptosis*. *Oxidative Medicine and Cellular Longevity*, 2019. 2019: p. 5080843.
58. Zhang, W., S. Xiao, and D.U. Ahn, *Protein oxidation: basic principles and implications for meat quality*. *Crit Rev Food Sci Nutr*, 2013. 53(11): p. 1191-201.
59. David, S.S., V.L. O'Shea, and S. Kundu, *Base-excision repair of oxidative DNA damage*. *Nature*, 2007. 447(7147): p. 941-950.
60. Hegde, M.L., T.K. Hazra, and S. Mitra, *Early steps in the DNA base excision/single-strand interruption repair pathway in mammalian cells*. *Cell research*, 2008. 18(1): p. 27-47.
61. Caldecott, K.W., *Single-strand break repair and genetic disease*. *Nature Reviews Genetics*, 2008. 9(8): p. 619-631.
62. Duncan, K.O. and D.J. Leffell, *Preoperative assessment of the elderly patient*. *Dermatol Clin*, 1997. 15(4): p. 583-93.
63. Brincat, M., et al., *A study of the decrease of skin collagen content, skin thickness, and bone mass in the postmenopausal woman*. *Obstet Gynecol*, 1987. 70(6): p. 840-5.
64. Talwar, H.S., et al., *Reduced type I and type III procollagens in photodamaged adult human skin*. *J Invest Dermatol*, 1995. 105(2): p. 285-90.
65. Varani, J., et al., *Inhibition of type I procollagen synthesis by damaged collagen in photoaged skin and by collagenase-degraded collagen in vitro*. *Am J Pathol*, 2001. 158(3): p. 931-42.
66. Varani, J., et al., *Decreased collagen production in chronologically aged skin: roles of age-dependent alteration in fibroblast function and defective mechanical stimulation*. *Am J Pathol*, 2006. 168(6): p. 1861-8.
67. Fisher, G.J., et al., *Retinoic acid inhibits induction of c-Jun protein by ultraviolet radiation that occurs subsequent to activation of mitogen-activated protein kinase pathways in human skin in vivo*. *J Clin Invest*, 1998. 101(6): p. 1432-40.
68. Fisher, G.J., et al., *Molecular basis of sun-induced premature skin ageing and retinoid antagonism*. *Nature*, 1996. 379(6563): p. 335-9.
69. Berneburg, M., et al., *Creatine supplementation normalizes mutagenesis of mitochondrial DNA as well as functional consequences*. *J Invest Dermatol*, 2005. 125(2): p. 213-20.
70. Pittayapruek, P., et al., *Role of Matrix Metalloproteinases in Photoaging and Photocarcinogenesis*. *International journal of molecular sciences*, 2016. 17(6): p. 868.
71. d'Adda di Fagagna, F., et al., *A DNA damage checkpoint response in telomere-initiated senescence*. *Nature*, 2003. 426(6963): p. 194-8.
72. Di Leonardo, A., et al., *DNA damage triggers a prolonged p53-dependent G1 arrest and long-term induction of Cip1 in normal human fibroblasts*. *Genes Dev*, 1994. 8(21): p. 2540-51.
73. Serrano, M., et al., *Oncogenic ras provokes premature cell senescence associated with accumulation of p53 and p16INK4a*. *Cell*, 1997. 88(5): p. 593-602.

74. Young, A.P., et al., *VHL loss actuates a HIF-independent senescence programme mediated by Rb and p400*. Nat Cell Biol, 2008. 10(3): p. 361-9.
75. Dasari, A., et al., *Oxidative stress induces premature senescence by stimulating caveolin-1 gene transcription through p38 mitogen-activated protein kinase/Sp1-mediated activation of two GC-rich promoter elements*. Cancer research, 2006. 66(22): p. 10805-10814.
76. Dimri, G.P., et al., *A biomarker that identifies senescent human cells in culture and in aging skin in vivo*. Proc Natl Acad Sci U S A, 1995. 92(20): p. 9363-7.
77. Jeyapalan, J.C., et al., *Accumulation of senescent cells in mitotic tissue of aging primates*. Mechanisms of Ageing and Development, 2007. 128(1): p. 36-44.
78. Krishnamurthy, J., et al., *Ink4a/Arf expression is a biomarker of aging*. The Journal of Clinical Investigation, 2004. 114(9): p. 1299-1307.
79. Baker, D.J., et al., *Opposing roles for p16Ink4a and p19Arf in senescence and ageing caused by BubR1 insufficiency*. Nat Cell Biol, 2008. 10(7): p. 825-36.
80. Storer, M., et al., *Senescence is a developmental mechanism that contributes to embryonic growth and patterning*. Cell, 2013. 155(5): p. 1119-30.
81. Muñoz-Espín, D., et al., *Programmed cell senescence during mammalian embryonic development*. Cell, 2013. 155(5): p. 1104-18.
82. Jun, J.I. and L.F. Lau, *The matricellular protein CCN1 induces fibroblast senescence and restricts fibrosis in cutaneous wound healing*. Nat Cell Biol, 2010. 12(7): p. 676-85.
83. Campisi, J., *Cellular senescence as a tumor-suppressor mechanism*. Trends Cell Biol, 2001. 11(11): p. S27-31.
84. Baker, D.J., et al., *Clearance of p16Ink4a-positive senescent cells delays ageing-associated disorders*. Nature, 2011. 479(7372): p. 232-6.
85. Minamino, T., et al., *A crucial role for adipose tissue p53 in the regulation of insulin resistance*. Nat Med, 2009. 15(9): p. 1082-7.
86. Musi, N., et al., *Tau protein aggregation is associated with cellular senescence in the brain*. Aging Cell, 2018. 17(6): p. e12840.
87. Bussian, T.J., et al., *Clearance of senescent glial cells prevents tau-dependent pathology and cognitive decline*. Nature, 2018. 562(7728): p. 578-582.
88. Minamino, T., et al., *Endothelial cell senescence in human atherosclerosis: role of telomere in endothelial dysfunction*. Circulation, 2002. 105(13): p. 1541-4.
89. Yoshimoto, S., et al., *Obesity-induced gut microbial metabolite promotes liver cancer through senescence secretome*. Nature, 2013. 499(7456): p. 97-101.
90. Gonzalez-Meljem, J.M., et al., *Stem cell senescence drives age-attenuated induction of pituitary tumours in mouse models of paediatric craniopharyngioma*. Nature Communications, 2017. 8(1): p. 1819.
91. Lau, L., et al., *Uncoupling the Senescence-Associated Secretory Phenotype from Cell Cycle Exit via Interleukin-1 Inactivation Unveils Its Protumorigenic Role*. Mol Cell Biol, 2019. 39(12).
92. Rochette, P.J. and D.E. Brash, *Progressive apoptosis resistance prior to senescence and control by the anti-apoptotic protein BCL-xL*. Mechanisms of ageing and development, 2008. 129(4): p. 207-214.
93. Chen, Q.M., et al., *Involvement of Rb family proteins, focal adhesion proteins and protein synthesis in senescent morphogenesis induced by hydrogen peroxide*. Journal of Cell Science, 2000. 113(22): p. 4087-4097.
94. Narita, M., et al., *Rb-mediated heterochromatin formation and silencing of E2F target genes during cellular senescence*. Cell, 2003. 113(6): p. 703-16.
95. Rodier, F., et al., *DNA-SCARS: distinct nuclear structures that sustain damage-induced senescence growth arrest and inflammatory cytokine secretion*. J Cell Sci, 2011. 124(Pt 1): p. 68-81.
96. Coppé, J.P., et al., *The senescence-associated secretory phenotype: the dark side of tumor suppression*. Annu Rev Pathol, 2010. 5: p. 99-118.
97. Waldera-Lupa, D.M., et al., *Characterization of Skin Aging-Associated Secreted Proteins (SAASP) Produced by Dermal Fibroblasts Isolated from Intrinsically Aged Human Skin*. J Invest Dermatol, 2015. 135(8): p. 1954-1968.

98. Prata, L.G.P.L., et al., *Senescent cell clearance by the immune system: Emerging therapeutic opportunities*. *Seminars in immunology*, 2018. 40: p. 101275-101275.
99. Schroth, J., C. Thiemermann, and S.M. Henson, *Senescence and the Aging Immune System as Major Drivers of Chronic Kidney Disease*. *Frontiers in Cell and Developmental Biology*, 2020. 8(1084).
100. Xu, M., et al., *Senolytics improve physical function and increase lifespan in old age*. *Nat Med*, 2018. 24(8): p. 1246-1256.
101. Sikora, E., A. Bielak-Zmijewska, and G. Mosieniak, *Cellular senescence in ageing, age-related disease and longevity*. *Curr Vasc Pharmacol*, 2014. 12(5): p. 698-706.
102. Tigges, J., et al., *Aryl Hydrocarbon Receptor Repressor (AhRR) Function Revisited: Repression of CYP1 Activity in Human Skin Fibroblasts Is Not Related to AhRR Expression*. *Journal of Investigative Dermatology*, 2013. 133(1): p. 87-96.
103. Poschmann, G., et al., *High-Fat Diet Induced Isoform Changes of the Parkinson's Disease Protein DJ-1*. *Journal of Proteome Research*, 2014. 13(5): p. 2339-2351.
104. Cox, J. and M. Mann, *MaxQuant enables high peptide identification rates, individualized p.p.b.-range mass accuracies and proteome-wide protein quantification*. *Nat Biotechnol*, 2008. 26(12): p. 1367-72.
105. Cox, J., et al., *Andromeda: a peptide search engine integrated into the MaxQuant environment*. *J Proteome Res*, 2011. 10(4): p. 1794-805.
106. Cox, J., et al., *Accurate proteome-wide label-free quantification by delayed normalization and maximal peptide ratio extraction, termed MaxLFQ*. *Mol Cell Proteomics*, 2014. 13(9): p. 2513-26.
107. Tyanova, S., et al., *The Perseus computational platform for comprehensive analysis of (prote)omics data*. *Nat Methods*, 2016. 13(9): p. 731-40.
108. Huang da, W., B.T. Sherman, and R.A. Lempicki, *Bioinformatics enrichment tools: paths toward the comprehensive functional analysis of large gene lists*. *Nucleic Acids Res*, 2009. 37(1): p. 1-13.
109. Huang da, W., B.T. Sherman, and R.A. Lempicki, *Systematic and integrative analysis of large gene lists using DAVID bioinformatics resources*. *Nat Protoc*, 2009. 4(1): p. 44-57.
110. Szklarczyk, D., et al., *STRING v11: protein-protein association networks with increased coverage, supporting functional discovery in genome-wide experimental datasets*. *Nucleic Acids Res*, 2019. 47(D1): p. D607-d613.
111. von Mering, C., et al., *STRING: known and predicted protein-protein associations, integrated and transferred across organisms*. *Nucleic Acids Res*, 2005. 33(Database issue): p. D433-7.
112. Laemmli, U.K., *Cleavage of structural proteins during the assembly of the head of bacteriophage T4*. *Nature*, 1970. 227(5259): p. 680-5.
113. Livak, K.J. and T.D. Schmittgen, *Analysis of relative gene expression data using real-time quantitative PCR and the 2(-Delta Delta C(T)) Method*. *Methods*, 2001. 25(4): p. 402-8.
114. Koch, H., K.-P. Wittern, and J. Bergemann, *In Human Keratinocytes the *Common Deletion* Reflects Donor Variabilities Rather Than Chronologic Aging and can be Induced by Ultraviolet A Irradiation*. *Journal of Investigative Dermatology*, 2001. 117(4): p. 892-897.
115. Miller, F.J., et al., *Precise determination of mitochondrial DNA copy number in human skeletal and cardiac muscle by a PCR-based assay: lack of change of copy number with age*. *Nucleic acids research*, 2003. 31(11): p. e61-e61.
116. Keyse, S.M., et al., *Oxidant stress leads to transcriptional activation of the human heme oxygenase gene in cultured skin fibroblasts*. *Mol Cell Biol*, 1990. 10(9): p. 4967-9.
117. Stocker, R., et al., *Bilirubin is an antioxidant of possible physiological importance*. *Science*, 1987. 235(4792): p. 1043-6.
118. Malik, A.N. and A. Czajka, *Is mitochondrial DNA content a potential biomarker of mitochondrial dysfunction?* *Mitochondrion*, 2013. 13(5): p. 481-92.
119. Imai, S., et al., *Transcriptional silencing and longevity protein Sir2 is an NAD-dependent histone deacetylase*. *Nature*, 2000. 403(6771): p. 795-800.

120. Landry, J., et al., *The silencing protein SIR2 and its homologs are NAD-dependent protein deacetylases*. Proc Natl Acad Sci U S A, 2000. 97(11): p. 5807-11.
121. Haigis, M.C., et al., *SIRT4 inhibits glutamate dehydrogenase and opposes the effects of calorie restriction in pancreatic beta cells*. Cell, 2006. 126(5): p. 941-54.
122. Liszt, G., et al., *Mouse Sir2 homolog SIRT6 is a nuclear ADP-ribosyltransferase*. J Biol Chem, 2005. 280(22): p. 21313-20.
123. Michishita, E., et al., *Evolutionarily conserved and nonconserved cellular localizations and functions of human SIRT proteins*. Mol Biol Cell, 2005. 16(10): p. 4623-35.
124. Vaquero, A., et al., *SIRT1 regulates the histone methyl-transferase SUV39H1 during heterochromatin formation*. Nature, 2007. 450(7168): p. 440-4.
125. Fan, W. and J. Luo, *SIRT1 regulates UV-induced DNA repair through deacetylating XPA*. Mol Cell, 2010. 39(2): p. 247-58.
126. Lin, Y.H., et al., *KAP1 Deacetylation by SIRT1 Promotes Non-Homologous End-Joining Repair*. PLoS One, 2015. 10(4): p. e0123935.
127. Brunet, A., et al., *Stress-dependent regulation of FOXO transcription factors by the SIRT1 deacetylase*. Science, 2004. 303(5666): p. 2011-5.
128. Rodgers, J.T., et al., *Nutrient control of glucose homeostasis through a complex of PGC-1alpha and SIRT1*. Nature, 2005. 434(7029): p. 113-8.
129. Luo, J., et al., *Negative control of p53 by Sir2alpha promotes cell survival under stress*. Cell, 2001. 107(2): p. 137-48.
130. Liu, T., P.Y. Liu, and G.M. Marshall, *The critical role of the class III histone deacetylase SIRT1 in cancer*. Cancer Res, 2009. 69(5): p. 1702-5.
131. Mouchiroud, L., et al., *The NAD(+)/Sirtuin Pathway Modulates Longevity through Activation of Mitochondrial UPR and FOXO Signaling*. Cell, 2013. 154(2): p. 430-41.
132. Salvatori, I., et al., *SIRT3 and mitochondrial metabolism in neurodegenerative diseases*. Neurochem Int, 2017. 109: p. 184-192.
133. Vaquero, A., R. Sternglanz, and D. Reinberg, *NAD+-dependent deacetylation of H4 lysine 16 by class III HDACs*. Oncogene, 2007. 26(37): p. 5505-20.
134. Ding, S., et al., *Chronic sun exposure is associated with distinct histone acetylation changes in human skin*. Br J Dermatol, 2018. 179(1): p. 110-117.
135. Vaquero, A., et al., *Human SirT1 interacts with histone H1 and promotes formation of facultative heterochromatin*. Mol Cell, 2004. 16(1): p. 93-105.
136. Yuan, J., et al., *Histone H3-K56 acetylation is important for genomic stability in mammals*. Cell cycle (Georgetown, Tex.), 2009. 8(11): p. 1747-1753.
137. Mouchiroud, L., et al., *The NAD(+)/Sirtuin Pathway Modulates Longevity through Activation of Mitochondrial UPR and FOXO Signaling*. Cell, 2013. 154(2): p. 430-41.
138. Gomes, A.P., et al., *Declining NAD(+) induces a pseudohypoxic state disrupting nuclear-mitochondrial communication during aging*. Cell, 2013. 155(7): p. 1624-38.
139. Yoshino, J., et al., *Nicotinamide mononucleotide, a key NAD(+) intermediate, treats the pathophysiology of diet- and age-induced diabetes in mice*. Cell Metab, 2011. 14(4): p. 528-36.
140. Frederick, D.W., et al., *Loss of NAD Homeostasis Leads to Progressive and Reversible Degeneration of Skeletal Muscle*. Cell Metab, 2016. 24(2): p. 269-82.
141. Massudi, H., et al., *Age-associated changes in oxidative stress and NAD+ metabolism in human tissue*. PLoS One, 2012. 7(7): p. e42357.
142. Braidy, N., et al., *Age related changes in NAD+ metabolism oxidative stress and Sirt1 activity in wistar rats*. PLoS One, 2011. 6(4): p. e19194.
143. Zhu, X.H., et al., *In vivo NAD assay reveals the intracellular NAD contents and redox state in healthy human brain and their age dependences*. Proc Natl Acad Sci U S A, 2015. 112(9): p. 2876-81.
144. Stein, L.R. and S. Imai, *Specific ablation of Nampt in adult neural stem cells recapitulates their functional defects during aging*. EMBO J, 2014. 33(12): p. 1321-40.
145. Hou, Y., et al., *NAD(+) supplementation normalizes key Alzheimer's features and DNA damage responses in a new AD mouse model with introduced DNA repair deficiency*. Proc Natl Acad Sci U S A, 2018. 115(8): p. E1876-E1885.

146. Choi, S.E., et al., *Elevated microRNA-34a in obesity reduces NAD⁺ levels and SIRT1 activity by directly targeting NAMPT*. *Aging Cell*, 2013. 12(6): p. 1062-72.
147. Gary, A.S. and P.J. Rochette, *Apoptosis, the only cell death pathway that can be measured in human diploid dermal fibroblasts following lethal UVB irradiation*. *Sci Rep*, 2020. 10(1): p. 18946.
148. Ame, J.C., C. Spenlehauer, and G. de Murcia, *The PARP superfamily*. *Bioessays*, 2004. 26(8): p. 882-93.
149. Jacobson, E.L., et al., *Poly(ADP-ribose) metabolism in ultraviolet irradiated human fibroblasts*. *J Biol Chem*, 1983. 258(1): p. 103-7.
150. Hegedus, C., et al., *PARP1 Inhibition Augments UVB-Mediated Mitochondrial Changes-Implications for UV-Induced DNA Repair and Photocarcinogenesis*. *Cancers (Basel)*, 2019. 12(1).
151. Kim, H., et al., *Combining PARP with ATR inhibition overcomes PARP inhibitor and platinum resistance in ovarian cancer models*. *Nat Commun*, 2020. 11(1): p. 3726.
152. Antolin, A.A., et al., *The kinase polypharmacology landscape of clinical PARP inhibitors*. *Sci Rep*, 2020. 10(1): p. 2585.
153. Kim, G., et al., *FDA Approval Summary: Olaparib Monotherapy in Patients with Deleterious Germline BRCA-Mutated Advanced Ovarian Cancer Treated with Three or More Lines of Chemotherapy*. *Clin Cancer Res*, 2015. 21(19): p. 4257-61.
154. Ge, Y., et al., *CD38 affects the biological behavior and energy metabolism of nasopharyngeal carcinoma cells*. *Int J Oncol*, 2019. 54(2): p. 585-599.
155. Hu, Y., et al., *Overexpression of CD38 decreases cellular NAD levels and alters the expression of proteins involved in energy metabolism and antioxidant defense*. *J Proteome Res*, 2014. 13(2): p. 786-95.
156. Lund, F.E., *Signaling properties of CD38 in the mouse immune system: enzyme-dependent and -independent roles in immunity*. *Mol Med*, 2006. 12(11-12): p. 328-33.
157. Glaria, E. and A.F. Valledor, *Roles of CD38 in the Immune Response to Infection*. *Cells*, 2020. 9(1).
158. Camacho-Pereira, J., et al., *CD38 Dictates Age-Related NAD Decline and Mitochondrial Dysfunction through an SIRT3-Dependent Mechanism*. *Cell Metab*, 2016. 23(6): p. 1127-1139.
159. Tarrago, M.G., et al., *A Potent and Specific CD38 Inhibitor Ameliorates Age-Related Metabolic Dysfunction by Reversing Tissue NAD(+) Decline*. *Cell Metab*, 2018. 27(5): p. 1081-1095 e10.
160. Verdin, E., *NAD(+) in aging, metabolism, and neurodegeneration*. *Science*, 2015. 350(6265): p. 1208-13.
161. Mouchiroud, L., et al., *The NAD⁺/Sirtuin Pathway Modulates Longevity through Activation of Mitochondrial UPR and FOXO Signaling*. *Cell*, 2013. 154(2): p. 430-441.
162. Mills, K.F., et al., *Long-Term Administration of Nicotinamide Mononucleotide Mitigates Age-Associated Physiological Decline in Mice*. *Cell Metab*, 2016. 24(6): p. 795-806.
163. Sakura, M., et al., *Differences in the Histopathology and Cytokine Expression Pattern between Chronological Aging and Photoaging of Hairless Mice Skin*. *Modern Research in Inflammation*, 2014. Vol.03No.03: p. 8.
164. Sander, C.S., et al., *Photoaging is associated with protein oxidation in human skin in vivo*. *J Invest Dermatol*, 2002. 118(4): p. 618-25.
165. Chung, J.H., et al., *Modulation of skin collagen metabolism in aged and photoaged human skin in vivo*. *J Invest Dermatol*, 2001. 117(5): p. 1218-24.
166. Fligel, S.E., et al., *Collagen degradation in aged/photodamaged skin in vivo and after exposure to matrix metalloproteinase-1 in vitro*. *J Invest Dermatol*, 2003. 120(5): p. 842-8.
167. Fisher, G.J., et al., *Molecular mechanisms of photoaging in human skin in vivo and their prevention by all-trans retinoic acid*. *Photochem Photobiol*, 1999. 69(2): p. 154-7.
168. Hwang, I.S., et al., *UV radiation-induced skin aging in hairless mice is effectively prevented by oral intake of sea buckthorn (*Hippophae rhamnoides* L.) fruit blend for 6 weeks through MMP suppression and increase of SOD activity*. *Int J Mol Med*, 2012. 30(2): p. 392-400.

169. Freund, A., C.K. Patil, and J. Campisi, *p38MAPK is a novel DNA damage response-independent regulator of the senescence-associated secretory phenotype*. The EMBO Journal, 2011. 30(8): p. 1536-1548.
170. Patil, P., et al., *Oxidative stress-induced senescence markedly increases disc cell bioenergetics*. Mechanisms of Ageing and Development, 2019. 180: p. 97-106.
171. Wajapeyee, N., et al., *Oncogenic BRAF Induces Senescence and Apoptosis through Pathways Mediated by the Secreted Protein IGFBP7*. Cell, 2008. 132(3): p. 363-374.
172. Harley, C.B., A.B. Futcher, and C.W. Greider, *Telomeres shorten during ageing of human fibroblasts*. Nature, 1990. 345(6274): p. 458-460.
173. De Cecco, M., et al., *Genomes of replicatively senescent cells undergo global epigenetic changes leading to gene silencing and activation of transposable elements*. Aging Cell, 2013. 12(2): p. 247-56.
174. Hutter, E., et al., *Senescence-associated changes in respiration and oxidative phosphorylation in primary human fibroblasts*. The Biochemical journal, 2004. 380(Pt 3): p. 919-928.
175. Bulteau, A.L., et al., *Proteasome and photoaging: the effects of UV irradiation*. Ann N Y Acad Sci, 2007. 1100: p. 280-90.
176. Coppé, J.P., et al., *Senescence-associated secretory phenotypes reveal cell-nonautonomous functions of oncogenic RAS and the p53 tumor suppressor*. PLoS Biol, 2008. 6(12): p. 2853-68.
177. Boraldi, F., et al., *Comparison of ex vivo and in vitro human fibroblast ageing models*. Mech Ageing Dev, 2010. 131(10): p. 625-35.
178. Zou, Z., et al., *A Single-Cell Transcriptomic Atlas of Human Skin Aging*. Dev Cell, 2020.
179. Waldera-Lupa, D.M., et al., *Proteome-wide analysis reveals an age-associated cellular phenotype of in situ aged human fibroblasts*. Aging (Albany NY), 2014. 6(10): p. 856-78.
180. Tanaka, T., et al., *Plasma proteomic biomarker signature of age predicts health and life span*. Elife, 2020. 9.
181. Lehallier, B., et al., *Undulating changes in human plasma proteome profiles across the lifespan*. Nat Med, 2019. 25(12): p. 1843-1850.
182. Short, K.R., et al., *Decline in skeletal muscle mitochondrial function with aging in humans*. Proc Natl Acad Sci U S A, 2005. 102(15): p. 5618-23.
183. Rooyackers, O.E., et al., *Effect of age on in vivo rates of mitochondrial protein synthesis in human skeletal muscle*. Proc Natl Acad Sci U S A, 1996. 93(26): p. 15364-9.
184. Trounce, I., E. Byrne, and S. Marzuki, *Decline in skeletal muscle mitochondrial respiratory chain function: possible factor in ageing*. Lancet, 1989. 1(8639): p. 637-9.
185. Petersen, K.F., et al., *Mitochondrial dysfunction in the elderly: possible role in insulin resistance*. Science, 2003. 300(5622): p. 1140-2.
186. Kim, Y., et al., *Mitochondrial Aging Defects Emerge in Directly Reprogrammed Human Neurons due to Their Metabolic Profile*. Cell reports, 2018. 23(9): p. 2550-2558.
187. Bowman, A. and M.A. Birch-Machin, *Age-Dependent Decrease of Mitochondrial Complex II Activity in Human Skin Fibroblasts*. J Invest Dermatol, 2016. 136(5): p. 912-919.
188. Harman, D., *The biologic clock: the mitochondria?* J Am Geriatr Soc, 1972. 20(4): p. 145-7.
189. Balaban, R.S., S. Nemoto, and T. Finkel, *Mitochondria, Oxidants, and Aging*. Cell, 2005. 120(4): p. 483-495.
190. Jastroch, M., et al., *Mitochondrial proton and electron leaks*. Essays in biochemistry, 2010. 47: p. 53-67.
191. Hosseini, M., et al., *Energy Metabolism Rewiring Precedes UVB-Induced Primary Skin Tumor Formation*. Cell Reports, 2018. 23(12): p. 3621-3634.
192. Zou, X., et al., *SIRT3-Mediated Dimerization of IDH2 Directs Cancer Cell Metabolism and Tumor Growth*. Cancer Res, 2017. 77(15): p. 3990-3999.
193. Rardin, M.J., et al., *Label-free quantitative proteomics of the lysine acetylome in mitochondria identifies substrates of SIRT3 in metabolic pathways*. Proceedings of the National Academy of Sciences, 2013. 110(16): p. 6601-6606.

194. Tyagi, A., et al., *SIRT3 deficiency-induced mitochondrial dysfunction and inflammasome formation in the brain*. Scientific Reports, 2018. 8(1): p. 17547.
195. Anderson, K.A. and M.D. Hirschey, *Mitochondrial protein acetylation regulates metabolism*. Essays Biochem, 2012. 52: p. 23-35.
196. Xu, H., et al., *Caffeine Targets SIRT3 to Enhance SOD2 Activity in Mitochondria*. Front Cell Dev Biol, 2020. 8: p. 822.
197. Bruls, W.A., et al., *Transmission of human epidermis and stratum corneum as a function of thickness in the ultraviolet and visible wavelengths*. Photochem Photobiol, 1984. 40(4): p. 485-94.
198. Meinhardt, M., et al., *Wavelength-dependent penetration depths of ultraviolet radiation in human skin*. J Biomed Opt, 2008. 13(4): p. 044030.
199. Sundaresan, N.R., et al., *Sirt3 blocks the cardiac hypertrophic response by augmenting Foxo3a-dependent antioxidant defense mechanisms in mice*. J Clin Invest, 2009. 119(9): p. 2758-71.
200. Gao, J., et al., *SIRT3/SOD2 maintains osteoblast differentiation and bone formation by regulating mitochondrial stress*. Cell Death Differ, 2018. 25(2): p. 229-240.
201. Qiu, X., et al., *Calorie restriction reduces oxidative stress by SIRT3-mediated SOD2 activation*. Cell Metab, 2010. 12(6): p. 662-7.
202. Singh, G., et al., *Mitochondrial DNA Damage and Diseases*. F1000Research, 2015. 4: p. 176-176.
203. Castellani, C.A., et al., *Thinking outside the nucleus: Mitochondrial DNA copy number in health and disease*. Mitochondrion, 2020. 53: p. 214-223.
204. Wredenberg, A., et al., *Increased mitochondrial mass in mitochondrial myopathy mice*. Proceedings of the National Academy of Sciences, 2002. 99(23): p. 15066-15071.
205. Bianco, A., et al., *Mitochondrial DNA copy number in affected and unaffected LHON mutation carriers*. BMC Research Notes, 2018. 11(1): p. 911.
206. Grady, J.P., et al., *mtDNA heteroplasmy level and copy number indicate disease burden in m.3243A>G mitochondrial disease*. EMBO Molecular Medicine, 2018. 10(6): p. e8262.
207. Haywood, R., et al., *Intensity-dependent Direct Solar Radiation- and UVA-induced Radical Damage to Human Skin and DNA, Lipids and Proteins*. Photochemistry and Photobiology, 2011. 87(1): p. 117-130.
208. Vile, G.F. and R.M. Tyrrell, *UVA radiation-induced oxidative damage to lipids and proteins in vitro and in human skin fibroblasts is dependent on iron and singlet oxygen*. Free Radic Biol Med, 1995. 18(4): p. 721-30.
209. Lu, A.L., et al., *Repair of oxidative DNA damage: mechanisms and functions*. Cell Biochem Biophys, 2001. 35(2): p. 141-70.
210. Ronson, G.E., et al., *PARP1 and PARP2 stabilise replication forks at base excision repair intermediates through Fbh1-dependent Rad51 regulation*. Nature Communications, 2018. 9(1): p. 746.
211. Menoni, H., et al., *ATP-dependent chromatin remodeling is required for base excision repair in conventional but not in variant H2A.Bbd nucleosomes*. Mol Cell Biol, 2007. 27(17): p. 5949-56.
212. Oei, S.L. and M. Ziegler, *ATP for the DNA ligation step in base excision repair is generated from poly(ADP-ribose)*. J Biol Chem, 2000. 275(30): p. 23234-9.
213. Dunlop, R.A., U.T. Brunk, and K.J. Rodgers, *Oxidized proteins: mechanisms of removal and consequences of accumulation*. IUBMB Life, 2009. 61(5): p. 522-7.
214. Singh, R. and A.M. Cuervo, *Autophagy in the cellular energetic balance*. Cell Metab, 2011. 13(5): p. 495-504.
215. Pickart, C.M. and R.E. Cohen, *Proteasomes and their kin: proteases in the machine age*. Nature Reviews Molecular Cell Biology, 2004. 5(3): p. 177-187.
216. Craven, L., et al., *Recent Advances in Mitochondrial Disease*. Annu Rev Genomics Hum Genet, 2017. 18: p. 257-275.
217. Rossignol, R., et al., *Mitochondrial threshold effects*. The Biochemical journal, 2003. 370(Pt 3): p. 751-762.

218. Nakada, K., et al., *Inter-mitochondrial complementation: Mitochondria-specific system preventing mice from expression of disease phenotypes by mutant mtDNA*. *Nature Medicine*, 2001. 7(8): p. 934-940.
219. Shoffner, J.M., et al., *Myoclonic epilepsy and ragged-red fiber disease (MERRF) is associated with a mitochondrial DNA tRNA^{Lys} mutation*. *Cell*, 1990. 61(6): p. 931-937.
220. White, S.L., et al., *Genetic Counseling and Prenatal Diagnosis for the Mitochondrial DNA Mutations at Nucleotide 8993*. *The American Journal of Human Genetics*, 1999. 65(2): p. 474-482.
221. Taylor, R.C. and A. Dillin, *Aging as an event of proteostasis collapse*. *Cold Spring Harb Perspect Biol*, 2011. 3(5).
222. Powers, E.T., et al., *Biological and chemical approaches to diseases of proteostasis deficiency*. *Annu Rev Biochem*, 2009. 78: p. 959-91.
223. Anisimova, A.S., et al., *Protein synthesis and quality control in aging*. *Aging*, 2018. 10(12): p. 4269-4288.
224. Walter, P. and D. Ron, *The unfolded protein response: from stress pathway to homeostatic regulation*. *Science*, 2011. 334(6059): p. 1081-6.
225. Wang, M. and R.J. Kaufman, *Protein misfolding in the endoplasmic reticulum as a conduit to human disease*. *Nature*, 2016. 529(7586): p. 326-35.
226. Reid, D.W., et al., *The unfolded protein response triggers selective mRNA release from the endoplasmic reticulum*. *Cell*, 2014. 158(6): p. 1362-1374.
227. Raghunathan, P.L. and C. Guthrie, *RNA unwinding in U4/U6 snRNPs requires ATP hydrolysis and the DEIH-box splicing factor Brr2*. *Current Biology*, 1998. 8(15): p. 847-855.
228. Newman, A., *RNA splicing*. *Current Biology*, 1998. 8(25): p. R903-R905.
229. Sawa, H., et al., *Requirement of ATP in the second step of the pre-mRNA splicing reaction*. *Nucleic acids research*, 1988. 16(8): p. 3157-3164.
230. Jewett, M.C., et al., *Continued Protein Synthesis at Low [ATP] and [GTP] Enables Cell Adaptation during Energy Limitation*. *Journal of Bacteriology*, 2009. 191(3): p. 1083-1091.
231. Stouthamer, A.H., *A theoretical study on the amount of ATP required for synthesis of microbial cell material*. *Antonie Van Leeuwenhoek*, 1973. 39(3): p. 545-65.
232. Yamada, H. and S. Koizumi, *Effect of ultraviolet irradiation on the protein synthesis of human skin cells: a study with a monochromatic ultraviolet irradiation apparatus*. *Ind Health*, 2003. 41(2): p. 88-93.
233. Iordanov, M.S., et al., *Ultraviolet Radiation Triggers the Ribotoxic Stress Response in Mammalian Cells **. *Journal of Biological Chemistry*, 1998. 273(25): p. 15794-15803.
234. Powley, I.R., et al., *Translational reprogramming following UVB irradiation is mediated by DNA-PKcs and allows selective recruitment to the polysomes of mRNAs encoding DNA repair enzymes*. *Genes & development*, 2009. 23(10): p. 1207-1220.
235. Kantor, G.J. and D.R. Hull, *An effect of ultraviolet light on RNA and protein synthesis in nondividing human diploid fibroblasts*. *Biophys J*, 1979. 27(3): p. 359-70.
236. Tornaletti, S., D. Reines, and P.C. Hanawalt, *Structural characterization of RNA polymerase II complexes arrested by a cyclobutane pyrimidine dimer in the transcribed strand of template DNA*. *J Biol Chem*, 1999. 274(34): p. 24124-30.
237. Andrade-Lima, L.C., et al., *DNA repair and recovery of RNA synthesis following exposure to ultraviolet light are delayed in long genes*. *Nucleic Acids Research*, 2015. 43(5): p. 2744-2756.
238. Rockx, D.A.P., et al., *UV-induced inhibition of transcription involves repression of transcription initiation and phosphorylation of RNA polymerase II*. *Proceedings of the National Academy of Sciences*, 2000. 97(19): p. 10503.
239. Mone, M.J., et al., *Local UV-induced DNA damage in cell nuclei results in local transcription inhibition*. *EMBO Rep*, 2001. 2(11): p. 1013-7.
240. Deng, J., et al., *Activation of GCN2 in UV-Irradiated Cells Inhibits Translation*. *Current Biology*, 2002. 12(15): p. 1279-1286.

241. Holcik, M. and N. Sonenberg, *Translational control in stress and apoptosis*. Nature Reviews Molecular Cell Biology, 2005. 6(4): p. 318-327.
242. Matveev, S.V., et al., *Effect of the ATP level on the overall protein biosynthesis rate in a wheat germ cell-free system*. Biochim Biophys Acta, 1996. 1293(2): p. 207-12.
243. Cao, C., et al., *SIRT1 confers protection against UVB- and H2O2-induced cell death via modulation of p53 and JNK in cultured skin keratinocytes*. Journal of cellular and molecular medicine, 2009. 13(9B): p. 3632-3643.
244. Haigis, M.C. and D.A. Sinclair, *Mammalian Sirtuins: Biological Insights and Disease Relevance*. Annual Review of Pathology: Mechanisms of Disease, 2010. 5(1): p. 253-295.
245. Feige, J.N., et al., *Specific SIRT1 activation mimics low energy levels and protects against diet-induced metabolic disorders by enhancing fat oxidation*. Cell Metab, 2008. 8(5): p. 347-58.
246. Milne, J.C., et al., *Small molecule activators of SIRT1 as therapeutics for the treatment of type 2 diabetes*. Nature, 2007. 450(7170): p. 712-716.
247. Sun, C., et al., *SIRT1 improves insulin sensitivity under insulin-resistant conditions by repressing PTP1B*. Cell Metab, 2007. 6(4): p. 307-19.
248. Zhang, X., et al., *Solar Simulated Ultraviolet Radiation Induces Global Histone Hypoacetylation in Human Keratinocytes*. PloS one, 2016. 11(2): p. e0150175-e0150175.
249. Guo, R., et al., *GCN5 and E2F1 stimulate nucleotide excision repair by promoting H3K9 acetylation at sites of damage*. Nucleic Acids Research, 2011. 39(4): p. 1390-1397.
250. Das, C., et al., *CBP/p300-mediated acetylation of histone H3 on lysine 56*. Nature, 2009. 459(7243): p. 113-117.
251. Allfrey, V.G., R. Faulkner, and A.E. Mirsky, *Acetylation and Methylation of Histones and Their Possible Role in the Regulation of Rna Synthesis*. Proc Natl Acad Sci U S A, 1964. 51: p. 786-94.
252. Piekna-Przybylska, D., R.A. Bambara, and L. Balakrishnan, *Acetylation regulates DNA repair mechanisms in human cells*. Cell cycle (Georgetown, Tex.), 2016. 15(11): p. 1506-1517.
253. Görisch, S.M., et al., *Histone acetylation increases chromatin accessibility*. Journal of Cell Science, 2005. 118(24): p. 5825-5834.
254. Ruan, K., et al., *Histone H4 acetylation required for chromatin decompaction during DNA replication*. Scientific Reports, 2015. 5(1): p. 12720.
255. Wang, J., M.Y. Chin, and G. Li, *The novel tumor suppressor p33ING2 enhances nucleotide excision repair via inducement of histone H4 acetylation and chromatin relaxation*. Cancer Res, 2006. 66(4): p. 1906-11.
256. Kuo, W.H., et al., *The ING1b tumor suppressor facilitates nucleotide excision repair by promoting chromatin accessibility to XPA*. Exp Cell Res, 2007. 313(8): p. 1628-38.
257. Han, C., et al., *Exogenous pyruvate facilitates ultraviolet B-induced DNA damage repair by promoting H3K9 acetylation in keratinocytes and melanocytes*. Biomedicine & Pharmacotherapy, 2020. 126: p. 110082.
258. Muñoz-Galván, S., et al., *Histone H3K56 acetylation, Rad52, and non-DNA repair factors control double-strand break repair choice with the sister chromatid*. PLoS Genet, 2013. 9(1): p. e1003237.
259. Chen, C.-C., et al., *Acetylated Lysine 56 on Histone H3 Drives Chromatin Assembly after Repair and Signals for the Completion of Repair*. Cell, 2008. 134(2): p. 231-243.
260. Vempati, R.K., et al., *p300-mediated Acetylation of Histone H3 Lysine 56 Functions in DNA Damage Response in Mammals* ^{*}. Journal of Biological Chemistry, 2010. 285(37): p. 28553-28564.
261. Li, X., et al., *MOF and H4 K16 acetylation play important roles in DNA damage repair by modulating recruitment of DNA damage repair protein Mdc1*. Molecular and cellular biology, 2010. 30(22): p. 5335-5347.
262. Sharma, G.G., et al., *MOF and Histone H4 Acetylation at Lysine 16 Are Critical for DNA Damage Response and Double-Strand Break Repair*. Molecular and Cellular Biology, 2010. 30(14): p. 3582.

263. Horikoshi, N., et al., *Pre-existing H4K16ac levels in euchromatin drive DNA repair by homologous recombination in S-phase*. *Communications Biology*, 2019. 2(1): p. 253.
264. Stucki, M., et al., *MDC1 Directly Binds Phosphorylated Histone H2AX to Regulate Cellular Responses to DNA Double-Strand Breaks*. *Cell*, 2005. 123(7): p. 1213-1226.
265. Rodriguez, Y., J.K. Horton, and S.H. Wilson, *Histone H3 Lysine 56 Acetylation Enhances AP Endonuclease I-Mediated Repair of AP Sites in Nucleosome Core Particles*. *Biochemistry*, 2019. 58(35): p. 3646-3655.
266. Etchegaray, J.-P. and R. Mostoslavsky, *Interplay between Metabolism and Epigenetics: A Nuclear Adaptation to Environmental Changes*. *Molecular Cell*, 2016. 62(5): p. 695-711.
267. Kaelin, William G., Jr. and Steven L. McKnight, *Influence of Metabolism on Epigenetics and Disease*. *Cell*, 2013. 153(1): p. 56-69.
268. Crispo, F., et al., *Metabolic Dysregulations and Epigenetics: A Bidirectional Interplay that Drives Tumor Progression*. *Cells*, 2019. 8(8): p. 798.
269. Kaochar, S. and B.P. Tu, *Gatekeepers of chromatin: Small metabolites elicit big changes in gene expression*. *Trends in biochemical sciences*, 2012. 37(11): p. 477-483.
270. Lee, K.K. and J.L. Workman, *Histone acetyltransferase complexes: one size doesn't fit all*. *Nat Rev Mol Cell Biol*, 2007. 8(4): p. 284-95.
271. Shahbazian, M.D. and M. Grunstein, *Functions of site-specific histone acetylation and deacetylation*. *Annu Rev Biochem*, 2007. 76: p. 75-100.
272. Wellen, K.E., et al., *ATP-citrate lyase links cellular metabolism to histone acetylation*. *Science*, 2009. 324(5930): p. 1076-80.
273. Cai, L., et al., *Acetyl-CoA induces cell growth and proliferation by promoting the acetylation of histones at growth genes*. *Mol Cell*, 2011. 42(4): p. 426-37.
274. Shen, F., et al., *Genome-scale network model of metabolism and histone acetylation reveals metabolic dependencies of histone deacetylase inhibitors*. *Genome Biology*, 2019. 20(1): p. 49.
275. Peleg, S., et al., *Life span extension by targeting a link between metabolism and histone acetylation in Drosophila*. *EMBO reports*, 2016. 17(3): p. 455-469.
276. Zhong, L., et al., *The histone deacetylase Sirt6 regulates glucose homeostasis via Hif1alpha*. *Cell*, 2010. 140(2): p. 280-293.
277. Durano, D., et al., *Histone acetylation landscape in S. cerevisiae nhp6ab mutants reflects altered glucose metabolism*. *Biochim Biophys Acta Gen Subj*, 2020. 1864(1): p. 129454.
278. King, B.S., et al., *Poly(ADP-ribose) contributes to an association between poly(ADP-ribose) polymerase-1 and xeroderma pigmentosum complementation group A in nucleotide excision repair*. *J Biol Chem*, 2012. 287(47): p. 39824-33.
279. Pines, A., et al., *PARP1 promotes nucleotide excision repair through DDB2 stabilization and recruitment of ALC1*. *Journal of Cell Biology*, 2012. 199(2): p. 235-249.
280. Purohit, N.K., et al., *Characterization of the interactions of PARP-1 with UV-damaged DNA in vivo and in vitro*. *Scientific Reports*, 2016. 6(1): p. 19020.
281. Ray Chaudhuri, A. and A. Nussenzweig, *The multifaceted roles of PARP1 in DNA repair and chromatin remodelling*. *Nat Rev Mol Cell Biol*, 2017. 18(10): p. 610-621.
282. Vodenicharov, M.D., et al., *Mechanism of early biphasic activation of poly(ADP-ribose) polymerase-1 in response to ultraviolet B radiation*. *J Cell Sci*, 2005. 118(Pt 3): p. 589-99.
283. O'Dea, E.L., J.D. Kearns, and A. Hoffmann, *UV as an Amplifier Rather Than Inducer of NF- κ B Activity*. *Molecular Cell*, 2008. 30(5): p. 632-641.
284. Devary, Y., et al., *NF-kappa B activation by ultraviolet light not dependent on a nuclear signal*. *Science*, 1993. 261(5127): p. 1442-5.
285. Alafiatayo, A.A., et al., *RNA-Seq analysis revealed genes associated with UV-induced cell necrosis through MAPK/TNF- α pathways in human dermal fibroblast cells as an inducer of premature photoaging*. *Genomics*, 2020. 112(1): p. 484-493.
286. Amici, S.A., et al., *CD38 Is Robustly Induced in Human Macrophages and Monocytes in Inflammatory Conditions*. *Frontiers in Immunology*, 2018. 9(1593).
287. Ben Baruch, B., et al., *CD38 in cancer-associated fibroblasts promotes pro-tumoral activity*. *Laboratory Investigation*, 2020. 100(12): p. 1517-1531.

288. Chini, C.C.S., et al., *Targeting of NAD metabolism in pancreatic cancer cells: potential novel therapy for pancreatic tumors*. *Clinical cancer research : an official journal of the American Association for Cancer Research*, 2014. 20(1): p. 120-130.
289. Hong, W., et al., *Nicotinamide Mononucleotide: A Promising Molecule for Therapy of Diverse Diseases by Targeting NAD⁺ Metabolism*. *Frontiers in cell and developmental biology*, 2020. 8: p. 246-246.
290. Song, J., et al., *Nicotinamide mononucleotide promotes osteogenesis and reduces adipogenesis by regulating mesenchymal stromal cells via the SIRT1 pathway in aged bone marrow*. *Cell Death & Disease*, 2019. 10(5): p. 336.
291. Huang, R.-X. and J. Tao, *Nicotinamide mononucleotide attenuates glucocorticoid-induced osteogenic inhibition by regulating the SIRT1/PGC-1 α signaling pathway*. *Molecular medicine reports*, 2020. 22(1): p. 145-154.
292. Kiss, T., et al., *Nicotinamide mononucleotide (NMN) supplementation promotes neurovascular rejuvenation in aged mice: transcriptional footprint of SIRT1 activation, mitochondrial protection, anti-inflammatory, and anti-apoptotic effects*. *GeroScience*, 2020. 42(2): p. 527-546.
293. Michishita, E., et al., *SIRT6 is a histone H3 lysine 9 deacetylase that modulates telomeric chromatin*. *Nature*, 2008. 452(7186): p. 492-496.
294. Večeřa, J., et al., *HDAC1 and HDAC3 underlie dynamic H3K9 acetylation during embryonic neurogenesis and in schizophrenia-like animals*. *J Cell Physiol*, 2018. 233(1): p. 530-548.
295. Chen, Y., et al., *Structural basis for the acetylation of histone H3K9 and H3K27 mediated by the histone chaperone Vps75 in *Pneumocystis carinii**. *Signal Transduction and Targeted Therapy*, 2019. 4(1): p. 14.
296. Kimball, A.B., et al., *Age-induced and photoinduced changes in gene expression profiles in facial skin of Caucasian females across 6 decades of age*. *J Am Acad Dermatol*, 2018. 78(1): p. 29-39.e7.

Appendix

Index of abbreviations

For time specifications, quantities, indication of size and other physical measures, base and derived units of the International System of Units (SI) were utilized. For established chemicals, molecular formula or correspondent names were chosen. Further acronyms or symbols that were used in this thesis are listed below:

Abbreviation	Meaning
$2^{-\Delta\Delta Ct}$	threshold cycle
8-oxoG	8-oxoguanine
γ -H2AX	phosphorylated histone H2AX
acetyl-CoA	acetyl coenzyme A
ADP	adenosine diphosphate
ANOVA	Analysis of Variance
AP-1	activator protein 1
APE-1	apurinic/apyrimidinic endonuclease 1
APS	ammonium persulfate
ATP	adenosine triphosphate
BER	base excision repair
bp	base pairs
BRCA	breast cancer gene
BSA	bovine serum albumin
CAT	catalase
CD38	cluster of differentiation 38
cDNA	complementary DNA
C_q	quantification cycle
CS	citrate synthase, mitochondrial
DAPI	4',6 diamidino 2 phenylindole
DAVID	Database for Annotation, Visualization and Integrated Discovery
DEPC	diethylpyrocarbonate
dH ₂ O	distilled water
DLST	dihydrolipoamide S-succinyltransferase
DMEM	Dulbecco's Modified Eagle Medium
DMSO	dimethyl sulfoxide

DNA	deoxyribonucleic acid
DNA-SCARS	DNA segments with chromatin alterations reinforcing senescence
DPBS	Dulbecco's Phosphate Buffered Saline
DSB	double-strand breaks
DTT	dithiothreitol
ECM	extracellular matrix
EDTA	ethylenediamine tetraacetic acid
EGTA	ethylene glycol-bis(β -aminoethyl ether)-N,N,N',N'-tetraacetic acid
eIF2 α	eukaryotic translation initiation factor 2 subunit 1
Em	emission
ER	endoplasmic reticulum
ERK	extracellular signal-regulated kinase
ETC	electron transport chain
Ex	excitation
FAD	flavin adenine dinucleotide
FC	fold change
FCS	fetal calf serum
FEA	functional enrichment analysis
FH	fumarate hydratase, mitochondrial
Fl	fluorescence
FOXO3a	Forkhead box O3
FW	forward
GO	gene ontology
GTP	guanosine-5'-triphosphate
H ₂ O ₂	hydrogen peroxide
H3	histone H3
H3K14ac	acetylated H3 at lysine 14
H3K56ac	acetylated H3 at lysine 56
H3K9ac	acetylated H3 at lysine 9
H3K9me3	tri-methylated H3 at lysine 9
H4	histone H4
H4K12ac	acetylated H4 at lysine 12
H4K16ac	acetylated H4 at lysine 16
H4K8ac	acetylated H4 at lysine 8
HAT	histone acetyltransferase
HDAC	histone deacetylase
HDM	histone demethylase

HMOX	heme oxygenase
HMT	histone methyltransferase
HRP	horseradish peroxidase
IDH2	isocitrate dehydrogenase [NADP], mitochondrial
IL	interleukin
IRA	infrared A radiation
IRB	infrared B radiation
IRC	infrared C radiation
IRE1	inositol requiring enzyme 1
IRR	infrared radiation
IS	internal standard
KCl	potassium chloride
KH ₂ PO ₄	potassium dihydrogenphosphate
kDa	kilodalton
LC-MS	liquid chromatography-mass spectrometry
LFQ	label-free quantification
M	middle-aged
MCL	Markov cluster
MCP	monocyte chemotactic protein
MDC1	mediator of DNA damage checkpoint protein 1
ME2	NAD-dependent malic enzyme, mitochondrial
M-MLV RT	Moloney Murine Leukemia Virus Reverse Transcriptase
MMP	matrix metalloproteinase
mRNA	messenger RNA
mtDNA	mitochondrial DNA
Na ₂ EDTA	disodium EDTA
Na ₂ HPO ₄	sodium hydrogen phosphate
Na ₃ VO ₄	sodium orthovanadate
NAD ⁺	nicotinamide adenine dinucleotide (oxidized form)
NADH	nicotinamide adenine dinucleotide (reduced form)
NADP	nicotinamide adenine dinucleotide phosphate
NAM	nicotinamide
NAMPT	nicotinamide phosphoribosyl transferase
nDNA	nuclear DNA
NER	nucleotide excision repair
NFκB	nuclear factor kappa-light-chain-enhancer of activated B cells
NHDF	normal human dermal fibroblasts

NHDF ^{FEXT}	NHDF isolated from extrinsically aged tissue
NHDF ^{FINT}	NHDF isolated from intrinsically aged tissue
NMN	β -nicotinamide mononucleotide
NMNAT	nicotinamide/nicotinic acid mononucleotide adenylyl transferase
NP-40	Nonidet P-40
NR	nicotinamide riboside
O	old
O ₂ ⁻	superoxide anion
OXPHOS	oxidative phosphorylation
PARP	poly(ADP-ribose) polymerase
PC	principal component
PCA	principal component analysis
PCR	polymerase chain reaction
PDHA1	pyruvate dehydrogenase E1 component subunit alpha, somatic form, mitochondrial
PFA	paraformaldehyde
PMSF	phenylmethylsulfonyl fluoride
PN	passage number
PPIN	protein-protein interaction networks
PVDF	polyvinylidene difluoride
r	Spearman's correlation coefficient
rcf	relative centrifugal force
RIPA	radio immunoprecipitation assay
RNA	ribonucleic acid
RNAP II	RNA polymerase II
ROS	reactive oxygen species
rpm	revolutions per minute
rRNA	ribosomal RNA
RT	room temperature
RTA	ready-to-assemble
RT-qPCR	Real-Time quantitative PCR
RV	reverse
SAASP	skin aging-associated secreted proteins
SALIA	study on the influence of air pollution on lung function, inflammation and aging
SASP	senescence-associated secretory phenotype
SDHA	succinate dehydrogenase [ubiquinone] flavoprotein subunit,

	mitochondrial
SDS	sodium dodecyl sulfate
SDS-PAGE	SDS-polyacrylamide gel electrophoresis
SEM	standard error of the mean
SIRT	sirtuin
SOD	superoxide dismutase
SOD2K68ac	acetylated SOD2 at lysine 68
SRP	signal recognition particle
SSB	single strand break
SSBR	single strand break repair
STRING	Search Tool for the Retrieval of Interacting Genes/Proteins
SUV39H1	suppressor of variegation 3 9 homologue
TBS-T	Tris-buffered saline with Tween-20
TCA	tricarboxylic acid
TC-NER	transcription coupled NER
TEMED	tetramethyl ethylenediamine
TG	Tris/Glycine
TGF- β	transforming growth factor- β
TGS	Tris/Glycine/SDS
TIMP	tissue inhibitor of metalloproteinases
Tris	tris(hydroxymethyl)aminomethane
tRNA	transfer RNA
u	units
UPS	ubiquitin-proteasome system
UVA	ultraviolet A radiation
UVB	ultraviolet B radiation
UVR	ultraviolet radiation
v	version
VL	visible light
XPA	xeroderma pigmentosum complementation group A
Y	young
yr.	years

List of figures

Figure 1: Structure of the human skin.....	1
Figure 2: Intrinsic and extrinsic factors driving skin aging.	4
Figure 3: Penetration depth of different radiation types of the solar spectrum into the human skin.....	6
Figure 4: Vicious cycle of mitochondrial dysfunction and ROS production.	8
Figure 5: Structured approach for the investigation of intrinsic and extrinsic skin aging and their interactions.....	11
Figure 6: Age-related increase of protein diversity of secretomes was observed in intrinsically (NHDF ^{INT}) but not in extrinsically aged normal human dermal fibroblasts (NHDF ^{EXT}).....	34
Figure 7: Age-related decline of protein diversity of proteomes was observed in NHDF ^{INT} and NHDF ^{EXT}	36
Figure 8: Age-associated changes of protein abundances in NHDF ^{EXT} unlike NHDF ^{INT} were characterized by a non-linear course.	38
Figure 9: <i>In situ</i> aging of NHDF was accompanied by an increase of proteins involved in extracellular matrix organization and wound healing.....	39
Figure 10: <i>In situ</i> aging of NHDF was characterized by a decline of proteins involved in tricarboxylic acid cycle and translation.	40
Figure 11: The intersection of shared proteins between NHDF ^{INT} and NHDF ^{EXT} decreased with age.....	41
Figure 12: Network analysis of 82 significantly regulated proteins in NHDF ^{EXT} vs NHDF ^{INT} of Y donors performed with the Search Tool for the Retrieval of Interacting Genes/Proteins (STRING).....	42
Figure 13: STRING network analysis of 61 significantly regulated proteins in NHDF ^{EXT} vs NHDF ^{INT} of M donors.	43
Figure 14: STRING network analysis of 54 significantly regulated proteins in NHDF ^{EXT} vs NHDF ^{INT} of O donors.	44
Figure 15: Metabolism-associated proteins were increased in NHDF ^{EXT} vs NHDF ^{INT} of Y and M donors.	46
Figure 16: NHDF ^{EXT} vs NHDF ^{INT} of M donors exhibited elevated tricarboxylic acid (TCA) cycle-related protein levels.....	47
Figure 17: Evidence for the presence of oxidative stress in NHDF ^{EXT} compared to NHDF ^{INT} of M donors.	50
Figure 18: NHDF ^{EXT} vs NHDF ^{INT} of M donors showed increased ADP/ATP ratio and NAD ⁺ depletion.	52
Figure 19: Abundance of sirtuins (SIRT) was dysregulated in NHDF ^{EXT} vs NHDF ^{INT} of M donors.	53

Figure 20: Deacetylation of histone 3 (H3) target sites of NAD⁺-dependent SIRT1 is impaired in NHDF^{EXT} vs NHDF^{INT} of M donors.54

Figure 21: Deacetylation of histone 4 (H4) target sites of NAD⁺-dependent SIRT1 is impaired in NHDF^{EXT} vs NHDF^{INT} of M donors.55

Figure 22: Treatment of NHDF^{EXT} of M donors with olaparib improved NAD⁺ level.....56

Figure 23: Treatment of NHDF^{EXT} of M donors with compound 78c tended to enhance NAD⁺ level.....57

Figure 24: Treatment of NHDF^{EXT} of M donors with β-nicotinamide mononucleotide (NMN) improved NAD⁺ level and ADP/ATP ratio.....58

Figure 25: Incubation of NHDF^{EXT} of M donors with NMN rescued SIRT1 protein level.59

Figure 26: NMN treatment led to a selective alleviation of hyperacetylation of specific H3 lysine residues in NHDF^{EXT} of M donors.....60

Figure 27: NMN treatment led to an alleviation of hyperacetylation of H4K16 in NHDF^{EXT} of M donors.61

Figure 28: Treatment of NHDF^{EXT} of M donors with NMN mitigated dysregulation of TCA cycle-related proteins.63

Figure 29: Treatment of NHDF^{EXT} of M donors with NMN did not attenuate oxidative stress levels.65

Figure 30: Overview of dysregulated processes and their potential interrelations in NHDF^{EXT} vs NHDF^{INT} of M probands.....71

Figure 31: Applied substances for intervention in NAD⁺ metabolism.77

Figure 32: Overview of the impact of NMN treatment on dysregulated processes in NHDF^{EXT} of M probands.....79

Figure 33: Interaction between intrinsic and extrinsic skin aging is more complex than a superimposition.83

List of tables

Table 1: Chemicals.	12
Table 2: Kits.	14
Table 3: Consumables.....	14
Table 4: Devices.	16
Table 5: Software.....	16
Table 6: Composition of cell culture medium for thawed cells.	18
Table 7: Composition of cell culture medium.	18
Table 8: Composition of DPBS.	19
Table 9: Composition of starvation medium.....	19
Table 10: Substances intervening in NAD ⁺ metabolism.....	19
Table 11: Composition of serum-free cell culture medium.	20
Table 12: Parameter settings in MaxQuant.....	21
Table 13: Composition of RIPA buffer.....	24
Table 14: Composition of SDS loading buffer.	25
Table 15: Composition of TGS buffer.	25
Table 16: Composition of transfer buffer.	25
Table 17: Composition of TBS-T buffer.....	26
Table 18: Primary antibodies.	26
Table 19: Secondary antibodies.	27
Table 20: Reaction mixture for primer annealing.	28
Table 21: Reaction mixture for preincubation for reverse transcription.	28
Table 22: Reaction mixture for reverse transcription.	28
Table 23: Primer sequences.	29
Table 24: Reaction mixture and protocol for RT-qPCR.	29
Table 25: Primer sequences for measurement of mtDNA content.....	31
Table 26: Reaction mixture and protocol for RT-qPCR for determination of mtDNA content.....	31
Table 27: Protein diversity in secretomes of NHDF ^{INT} and NHDF ^{EXT} of Y, M and O probands.	34
Table 28: Protein diversity in proteomes of NHDF ^{INT} and NHDF ^{EXT} of Y, M and O probands.	35
Table 29: Metabolism-associated proteins altered in NHDF ^{EXT} vs NHDF ^{INT} of M donors.	48

List of supplementary tables

Table S1: List of 297 age-dependently regulated proteins in both NHDF ^{INT} and NHDF ^{EXT}	106
Table S2: List of 304 age-dependently regulated proteins exclusively in NHDF ^{INT}	118
Table S3: List of 147 age-dependently regulated proteins exclusively in NHDF ^{EXT}	130
Table S4: List of 82 significantly regulated proteins in NHDF ^{EXT} vs NHDF ^{INT} of Y donors.....	136
Table S5: List of 61 significantly regulated proteins in NHDF ^{EXT} vs NHDF ^{INT} of M donors.	140
Table S6: List of 54 significantly regulated proteins in NHDF ^{EXT} vs NHDF ^{INT} of O donors.....	143

Supplementary tables

Table S1: List of 297 age-dependently regulated proteins in both NHDF^{INT} and NHDF^{EXT}. Label-free quantitative proteome analysis of NHDF^{INT} vs NHDF^{EXT} of Y vs M vs O donors. Spearman's correlation, $p < 0.05$; $FC > |1.5|$; $n = 5$.

Gene name	UniProt ID	Protein description	Regulation	FC NHDF ^{INT}	p-value NHDF ^{INT}	FC NHDF ^{EXT}	p-value NHDF ^{EXT}
AASS	Q9UDR5	Alpha-aminoadipic semialdehyde synthase, mitochondrial	↑	1.8	2.10E-02	1.9	9.98E-03
ABCC1	P33527	Multidrug resistance-associated protein 1	↑	2.1	3.39E-02	4.2	3.00E-04
ACAA2	P42765	3-ketoacyl-CoA thiolase, mitochondrial	↓	9.0	1.93E-04	26.4	2.04E-03
ACADVL	P49748	Very long-chain specific acyl-CoA dehydrogenase, mitochondrial	↓	6.8	3.65E-03	24.8	1.71E-02
ACAT1	P24752	Acetyl-CoA acetyltransferase, mitochondrial	↓	6.3	9.23E-04	26.3	9.32E-03
ACTA1	P68133	Actin, alpha skeletal muscle	↓	10.0	1.01E-04	18.4	1.09E-02
ACTC1	P68032	Actin, alpha cardiac muscle 1					
ACTG1	P63261	Actin, cytoplasmic 2	↓	5.7	7.12E-04	9.9	3.25E-02
ACTR2	P61160	Actin-related protein 2	↓	3.6	2.66E-03	6.1	1.04E-04
ACTR3	P61158	Actin-related protein 3	↓	7.4	2.38E-03	12.2	5.47E-03
ADD1	P35611	Alpha-adducin	↓	1.8	1.02E-03	1.8	2.45E-02
AGL	P35573	Glycogen debranching enzyme	↑	3.5	5.88E-04	3.5	1.24E-02
AHNAK	Q09666	Neuroblast differentiation-associated protein AHNAK	↑	2.2	2.54E-04	2.2	1.50E-03
AHNAK2	Q8IVF2	Protein AHNAK2	↑	1.8	3.07E-03	2.5	2.29E-02
AKAP12	Q02952	A-kinase anchor protein 12	↑	3.9	7.55E-03	3.9	8.24E-03
ALCAM	Q13740	CD166 antigen	↑	2.0	1.15E-04	2.2	7.33E-03
ALDH9A1	P49189	4-trimethylaminobutyraldehyde dehydrogenase	↓	2.8	2.34E-02	14.5	3.36E-03
ALDOA	P04075	Fructose-bisphosphate aldolase A	↓	6.1	2.68E-02	29.3	9.23E-03
ANKFY1	Q9P2R3	Rabankyrin-5	↑	2.8	3.35E-04	2.5	1.00E-02
ANO6	Q4KMQ2	Anoctamin-6	↑	1.8	4.43E-03	2.1	1.69E-03

ANPEP	P15144	Aminopeptidase N	↑	2.2	1.09E-02	2.9	4.92E-03
ANXA1	P04083	Annexin A1	↓	2.7	4.75E-02	6.8	1.97E-03
AP2M1	Q96CW1	AP-2 complex subunit mu	↓	3.0	1.82E-03	2.8	9.76E-04
AQR	O60306	RNA helicase aquarius	↑	1.8	2.96E-03	1.9	1.62E-03
ARPC3	O15145	Actin-related protein 2/3 complex subunit 3	↓	2.4	2.05E-02	2.6	3.16E-04
ARPC4	P59998	Actin-related protein 2/3 complex subunit 4	↓	20.1	1.52E-03	28.7	2.39E-03
ATAD3A	Q9NVI7	ATPase family AAA domain-containing protein 3A	↓	3.2	1.12E-03	3.5	1.69E-02
ATP11C	Q8NB49	Phospholipid-transporting ATPase IG	↑	2.0	3.83E-02	4.6	8.56E-04
ATP13A1	Q9HD20	Manganese-transporting ATPase 13A1	↑	1.9	9.79E-04	2.5	1.86E-02
ATP1A1	P05023	Sodium/potassium-transporting ATPase subunit alpha-1	↑	2.2	4.46E-03	2.8	3.35E-04
ATP1B3	P54709	Sodium/potassium-transporting ATPase subunit beta-3	↓	2.4	7.55E-03	2.6	3.29E-03
ATP2A2	P16615	Sarcoplasmic/endoplasmic reticulum calcium ATPase 2	↑	2.3	1.16E-03	2.7	1.83E-03
ATP2B1	P20020	Plasma membrane calcium-transporting ATPase 1	↑	2.4	8.97E-03	3.2	5.33E-04
ATP2B4	P23634	Plasma membrane calcium-transporting ATPase 4	↑	2.6	9.23E-03	2.8	4.14E-04
ATP5PO	P48047	ATP synthase subunit O, mitochondrial	↓	4.2	2.40E-04	5.0	1.15E-02
ATP6V0A1	Q93050	V-type proton ATPase 116 kDa subunit a1	↑	2.2	6.31E-03	2.6	3.18E-03
BASP1	P80723	Brain acid soluble protein 1	↑	3.2	1.27E-03	3.4	2.21E-03
CACNA2D1	P54289	Voltage-dependent calcium channel subunit alpha-2/delta-1	↑	3.2	2.57E-02	3.8	1.02E-03
CALR	P27797	Calreticulin	↓	3.7	1.27E-03	6.1	1.90E-02
CAP1	Q01518	Adenylyl cyclase-associated protein 1	↓	3.6	8.97E-03	15.3	7.81E-04
CAPZA1	P52907	F-actin-capping protein subunit alpha-1	↓	6.5	6.47E-04	6.6	3.96E-02
CAPZB	P47756	F-actin-capping protein subunit beta	↓	7.1	1.35E-03	18.9	3.68E-04
CAV1	Q03135	Caveolin-1	↑	2.0	5.24E-03	2.8	1.49E-02
CAV2	P51636	Caveolin-2	↑	2.3	8.24E-03	3.2	2.29E-02
CCT2	P78371	T-complex protein 1 subunit beta	↓	5.9	2.84E-04	13.7	4.61E-03
CCT3	P49368	T-complex protein 1 subunit gamma	↓	7.4	2.26E-04	14.4	3.17E-03
CCT4	P50991	T-complex protein 1 subunit delta	↓	7.8	2.54E-04	28.8	2.40E-04
CCT5	P48643	T-complex protein 1 subunit epsilon	↓	5.9	1.56E-03	16.4	1.31E-04

CCT6A	P40227	T-complex protein 1 subunit zeta	↓	6.5	2.25E-04	14.2	3.67E-02
CCT7	Q99832	T-complex protein 1 subunit eta	↓	5.8	1.90E-04	12.0	2.19E-02
CCT8	P50990	T-complex protein 1 subunit theta	↓	5.2	3.35E-04	10.6	1.09E-02
CD109	Q6YHK3	CD109 antigen	↑	2.4	1.28E-02	2.6	1.62E-03
CD276	Q5ZPR3	CD276 antigen	↑	3.2	9.36E-04	2.9	6.47E-04
CD44	P16070	CD44 antigen	↑	1.8	1.03E-02	1.6	4.84E-02
CDC42	P60953	Cell division control protein 42 homolog	↓	5.9	4.14E-04	10.4	1.09E-03
CDH2	P19022	Cadherin-2	↑	2.7	6.52E-03	3.2	6.13E-04
CFL1	P23528	Cofilin-1	↓	9.7	7.33E-03	51.9	3.16E-03
CLIC1	O00299	Chloride intracellular channel protein 1	↓	5.0	2.19E-02	15.8	1.60E-03
CLIC4	Q9Y696	Chloride intracellular channel protein 4	↓	3.9	1.31E-02	4.0	7.37E-03
CLIP1	P30622	CAP-Gly domain-containing linker protein 1	↑	2.5	1.13E-04	3.7	1.22E-03
CLTC	Q00610	Clathrin heavy chain 1	↑	2.2	9.36E-04	3.1	8.56E-04
CNOT1	A5YKK6	CCR4-NOT transcription complex subunit 1	↑	3.3	1.90E-04	3.1	1.38E-02
CNP	P09543	2',3'-cyclic-nucleotide 3'-phosphodiesterase	↓	2.8	1.75E-03	2.6	5.59E-03
CNTNAP1	P78357	Contactin-associated protein 1	↑	2.6	2.86E-03	3.3	2.38E-03
COLEC12	Q5KU26	Collectin-12	↑	3.6	4.09E-03	4.7	5.61E-03
COLGALT1	Q8NBJ5	Procollagen galactosyltransferase 1	↓	2.8	3.65E-03	3.7	1.56E-03
CORO1B	Q9BR76	Coronin-1B	↓	2.7	3.56E-02	2.5	3.25E-02
CORO1C	Q9ULV4	Coronin-1C	↓	4.3	7.81E-04	14.3	1.66E-02
CPT1A	P50416	Carnitine O-palmitoyltransferase 1, liver isoform	↑	2.6	1.32E-03	2.6	4.92E-03
CS	O75390	Citrate synthase, mitochondrial	↓	8.1	2.26E-04	11.7	2.86E-03
CSPG4	Q6UVK1	Chondroitin sulfate proteoglycan 4	↑	2.9	4.76E-03	2.8	9.49E-03
CTSA	P10619	Lysosomal protective protein	↓	3.2	1.03E-03	6.1	6.44E-03
CTSD	P07339	Cathepsin D	↓	7.8	1.58E-04	21.4	8.56E-04
CYC1	P08574	Cytochrome c1, heme protein, mitochondrial	↓	6.5	1.41E-04	6.8	4.63E-04
CYFIP1	Q7L576	Cytoplasmic FMR1-interacting protein 1	↑	2.4	2.84E-04	2.4	6.51E-03
DARS1	P14868	Aspartate--tRNA ligase, cytoplasmic	↓	3.9	6.28E-03	6.4	3.51E-02

DDB1	Q16531	DNA damage-binding protein 1	↑	2.5	3.78E-03	2.6	6.17E-04
DDX17	Q92841	Probable ATP-dependent RNA helicase DDX17	↓	6.3	1.01E-04	22.6	3.00E-04
DDX3X	O00571	ATP-dependent RNA helicase DDX3X	↓	2.6	2.86E-03	7.1	4.32E-03
DDX3Y	O15523	ATP-dependent RNA helicase DDX3Y					
DHX9	Q08211	ATP-dependent RNA helicase A	↑	1.9	8.72E-03	1.9	1.09E-02
DLD	P09622	Dihydrolipoyl dehydrogenase, mitochondrial	↓	4.3	4.20E-04	8.4	2.90E-03
DLST	P36957	Dihydrolipoyllysine-residue succinyltransferase component of 2-oxoglutarate dehydrogenase complex, mitochondrial	↓	2.5	1.86E-02	4.1	9.49E-03
DNAJC13	O75165	DnaJ homolog subfamily C member 13	↑	2.1	2.96E-03	2.4	1.09E-02
DOCK1	Q14185	Dedicator of cytokinesis protein 1	↑	2.3	6.53E-03	2.9	4.14E-04
DST	Q03001	Dystonin	↑	2.7	1.07E-03	5.1	3.35E-04
ECE1	P42892	Endothelin-converting enzyme 1	↑	2.3	8.24E-03	3.0	1.83E-03
EEF1G	P26641	Elongation factor 1-gamma	↓	5.2	5.41E-03	8.8	1.50E-03
EEF2	P13639	Elongation factor 2	↓	1.8	2.14E-02	6.9	1.44E-03
EFTUD2	Q15029	116 kDa U5 small nuclear ribonucleoprotein component	↑	1.8	5.41E-03	1.7	1.97E-03
EGFR	P00533	Epidermal growth factor receptor	↑	2.4	1.81E-02	3.3	1.07E-03
EHD2	Q9NZN4	EH domain-containing protein 2	↓	2.0	3.05E-02	4.6	4.61E-03
EIF3E	P60228	Eukaryotic translation initiation factor 3 subunit E	↓	2.2	5.19E-03	2.3	3.20E-02
EIF4A1	P60842	Eukaryotic initiation factor 4A-I	↓	9.1	4.61E-03	39.0	7.12E-04
EMC1	Q8N766	ER membrane protein complex subunit 1	↑	1.7	1.27E-03	1.9	1.07E-03
ENO1	P06733	Alpha-enolase	↓	5.1	8.00E-03	17.0	8.24E-03
ERAP2	Q6P179	Endoplasmic reticulum aminopeptidase 2	↑	5.0	1.17E-02	4.3	2.88E-02
ERO1A	Q96HE7	ERO1-like protein alpha	↓	3.3	1.65E-02	5.4	9.76E-03
ERP44	Q9BS26	Endoplasmic reticulum resident protein 44	↓	3.3	5.58E-03	2.7	7.12E-04
ESYT1	Q9BSJ8	Extended synaptotagmin-1	↑	2.0	5.08E-03	1.8	6.91E-03
ETFA	P13804	Electron transfer flavoprotein subunit alpha, mitochondrial	↓	6.4	5.42E-04	8.8	1.31E-03
FHL1	Q13642	Four and a half LIM domains protein 1	↓	7.2	1.12E-02	36.7	6.15E-03
FHL2	Q14192	Four and a half LIM domains protein 2	↓	3.9	3.08E-03	3.7	1.09E-02
FLNB	O75369	Filamin-B	↑	2.8	1.31E-04	3.6	1.50E-03

FNDC3B	Q53EP0	Fibronectin type III domain-containing protein 3B	↑	2.0	1.01E-04	2.2	2.21E-03
FSCN1	Q16658	Fascin	↓	5.4	4.93E-02	17.7	6.31E-03
GAPDH	P04406	Glyceraldehyde-3-phosphate dehydrogenase	↓	5.5	1.09E-02	19.4	5.58E-03
GCN1	Q92616	eIF-2-alpha kinase activator GCN1	↑	2.1	3.93E-04	1.7	3.46E-02
GLG1	Q92896	Golgi apparatus protein 1	↑	1.6	4.46E-03	2.6	8.00E-03
GLUD1	P00367	Glutamate dehydrogenase 1, mitochondrial	↓	5.6	9.36E-04	12.2	1.79E-04
GLUD2	P49448	Glutamate dehydrogenase 2, mitochondrial					
GNAI3	P08754	Guanine nucleotide-binding protein G(i) subunit alpha	↓	3.7	3.93E-03	5.3	2.17E-02
GNB1	P62873	Guanine nucleotide-binding protein G(I)/G(S)/G(T) subunit beta-1	↓	9.0	1.53E-04	24.5	3.10E-02
GOLGA2	Q08379	Golgin subfamily A member 2	↑	1.6	2.16E-02	1.9	3.07E-02
GOLGA3	Q08378	Golgin subfamily A member 3	↑	3.6	9.79E-04	6.3	7.33E-03
GOLGB1	Q14789	Golgin subfamily B member 1	↑	2.2	1.76E-03	4.9	4.18E-03
GPD2	P43304	Glycerol-3-phosphate dehydrogenase, mitochondrial	↓	3.7	3.65E-03	9.2	5.22E-04
GPX8	Q8TED1	Probable glutathione peroxidase 8	↓	2.7	1.58E-04	1.8	4.18E-03
GUSB	P08236	Beta-glucuronidase	↑	1.9	6.04E-03	2.1	1.12E-02
H2BC4/6/7/8/10	P62807	Histone H2B type 1-C/E/F/G/I	↓	3.0	6.17E-04	5.6	3.91E-03
H2BC5	P58876	Histone H2B type 1-D					
H2BC9	Q93079	Histone H2B type 1-H					
H2BC12	O60814	Histone H2B type 1-K					
H2BC13	Q99880	Histone H2B type 1-L					
H2BC14	Q99879	Histone H2B type 1-M					
H2BC15	Q99877	Histone H2B type 1-N					
H2BC18	Q5QNW6	Histone H2B type 2-F					
H2BS1	P57053	Histone H2B type F-S					
HACD3	Q9P035	Very-long-chain (3R)-3-hydroxyacyl-CoA dehydratase 3	↑	1.8	3.39E-02	2.3	1.42E-02
HADHA	P40939	Trifunctional enzyme subunit alpha, mitochondrial	↓	2.7	4.40E-02	8.0	1.02E-03
HLA-A	P04439	HLA class I histocompatibility antigen, A alpha chain	↓	3.3	1.41E-04	5.1	4.86E-03
HM13	Q8TCT9	Minor histocompatibility antigen H13	↑	1.9	4.61E-03	2.5	4.18E-03
HNRNPH1	P31943	Heterogeneous nuclear ribonucleoprotein H	↓	5.8	1.07E-03	6.2	2.21E-03
HNRNPK	P61978	Heterogeneous nuclear ribonucleoprotein K	↓	4.0	4.82E-04	5.4	4.36E-04

HNRNPL	P14866	Heterogeneous nuclear ribonucleoprotein L	↓	5.5	3.00E-04	4.9	3.30E-02
HNRNPM	P52272	Heterogeneous nuclear ribonucleoprotein M	↓	4.2	8.18E-04	4.1	4.82E-03
HNRNPU	Q00839	Heterogeneous nuclear ribonucleoprotein U	↓	5.1	5.08E-03	8.6	1.79E-04
HSPB1	P04792	Heat shock protein beta-1	↓	2.1	1.03E-02	5.4	2.80E-02
HSPD1	P10809	60 kDa heat shock protein, mitochondrial	↓	2.9	8.18E-04	3.8	8.00E-03
IARS1	P41252	Isoleucine--tRNA ligase, cytoplasmic	↑	2.4	1.21E-03	3.0	5.58E-03
IARS2	Q9NSE4	Isoleucine--tRNA ligase, mitochondrial	↑	1.7	8.24E-03	1.8	5.08E-03
IL6ST	P40189	Interleukin-6 receptor subunit beta	↑	1.9	3.20E-02	2.6	1.27E-02
ILF2	Q12905	Interleukin enhancer-binding factor 2	↓	4.2	2.60E-04	10.9	4.08E-03
ILF3	Q12906	Interleukin enhancer-binding factor 3	↓	2.3	5.41E-03	7.0	1.76E-03
IPO4	Q8TEX9	Importin-4	↑	3.0	3.35E-04	1.7	3.32E-02
ITGA2	P17301	Integrin alpha-2	↑	2.4	2.99E-02	7.6	1.44E-03
ITGA5	P08648	Integrin alpha-5	↑	3.2	9.79E-04	3.3	8.18E-04
ITGAV	P06756	Integrin alpha-V	↑	2.4	5.76E-03	3.7	2.38E-03
ITGB1	P05556	Integrin beta-1	↑	2.3	1.69E-03	2.8	2.30E-03
ITPR3	Q14573	Inositol 1,4,5-trisphosphate receptor type 3	↑	2.2	6.28E-03	2.6	3.14E-02
KHSRP	Q92945	Far upstream element-binding protein 2	↓	2.6	1.22E-02	3.5	1.17E-02
KTN1	Q86UP2	Kinectin	↑	2.2	3.78E-03	3.4	1.01E-04
LAMP1	P11279	Lysosome-associated membrane glycoprotein 1	↑	2.8	2.13E-03	4.0	1.77E-02
LAMP2	P13473	Lysosome-associated membrane glycoprotein 2	↑	2.6	1.49E-02	2.7	2.96E-03
LGALS1	P09382	Galectin-1	↓	11.7	2.69E-04	26.3	6.79E-04
LGALS3	P17931	Galectin-3	↓	3.8	1.21E-03	10.5	5.33E-04
LMAN2	Q12907	Vesicular integral-membrane protein VIP36	↓	3.3	2.13E-03	2.3	3.65E-03
LNPEP	Q9UIQ6	Leucyl-cystinyl aminopeptidase	↑	3.1	4.76E-03	3.0	4.92E-03
LRP1	Q07954	Prolow-density lipoprotein receptor-related protein 1	↑	2.0	8.24E-03	3.4	1.76E-03
LRRN4CL	Q8ND94	LRRN4 C-terminal-like protein	↓	2.4	1.53E-02	5.0	2.58E-03
MACF1	Q9UPN3	Microtubule-actin cross-linking factor 1, isoforms 1/2/3/5	↑	3.4	3.53E-04	5.9	3.93E-04
MAN2A1	Q16706	Alpha-mannosidase 2	↑	1.8	1.38E-03	2.2	2.40E-02

MARCKS	P29966	Myristoylated alanine-rich C-kinase substrate	↑	2.8	3.00E-04	2.4	4.57E-02
MASP1	P48740	Mannan-binding lectin serine protease 1	↑	2.2	2.45E-03	2.0	2.25E-03
MBOAT7	Q96N66	Lysophospholipid acyltransferase 7	↑	1.6	4.66E-02	2.3	2.96E-03
MMP14	P50281	Matrix metalloproteinase-14	↓	3.0	2.06E-02	2.2	2.26E-02
MRC2	Q9UBG0	C-type mannose receptor 2	↑	2.0	1.18E-02	3.5	3.18E-03
MYH10	P35580	Myosin-10	↑	2.0	8.56E-04	3.5	9.36E-04
MYH14	Q7Z406	Myosin-14	↑	2.7	8.00E-03	2.9	4.76E-03
MYH9	P35579	Myosin-9	↑	2.6	5.60E-04	2.7	1.12E-03
MYL6	P60660	Myosin light polypeptide 6	↓	4.1	1.69E-03	6.0	3.18E-03
MYO1B	O43795	Unconventional myosin-Ib	↑	1.7	1.99E-02	1.8	1.77E-02
MYOF	Q9NZM1	Myoferlin	↑	1.8	7.81E-04	2.2	9.79E-04
NCL	P19338	Nucleolin	↓	2.9	1.16E-03	4.9	1.09E-02
NCLN	Q969V3	Nicalin	↓	2.7	8.56E-04	2.4	1.58E-02
NCSTN	Q92542	Nicastrin	↑	2.4	5.94E-03	3.4	1.68E-04
NME1	P15531	Nucleoside diphosphate kinase A	↓	5.7	4.18E-03	21.4	2.40E-04
NME2	P22392	Nucleoside diphosphate kinase B					
NME2P1	O60361	Putative nucleoside diphosphate kinase					
NNT	Q13423	NAD(P) transhydrogenase, mitochondrial	↑	2.3	1.34E-02	3.1	1.32E-03
NOMO2	Q5JPE7	Nodal modulator 2	↑	1.8	1.21E-03	2.6	3.17E-04
NOMO3	P69849	Nodal modulator 3					
NOTCH2	Q04721	Neurogenic locus notch homolog protein 2	↑	2.2	1.42E-02	4.1	6.47E-04
NPR2	P20594	Atrial natriuretic peptide receptor 2	↑	2.9	1.99E-02	2.5	2.05E-03
NPTN	Q9Y639	Neuroplastin	↑	2.2	7.55E-03	1.8	4.61E-03
NRP1	O14786	Neuropilin-1	↑	2.2	8.72E-03	2.8	1.69E-03
NUMA1	Q14980	Nuclear mitotic apparatus protein 1	↑	2.0	1.69E-02	3.4	2.84E-04
NUP160	Q12769	Nuclear pore complex protein Nup160	↑	1.6	7.78E-03	2.6	6.47E-04
NUP188	Q5SRE5	Nucleoporin NUP188 homolog	↑	1.9	1.42E-02	2.6	4.36E-04
NUP205	Q92621	Nuclear pore complex protein Nup205	↑	1.9	1.65E-02	3.0	4.92E-03
P4HA1	P13674	Prolyl 4-hydroxylase subunit alpha-1	↓	3.9	1.90E-04	17.0	2.29E-02

P4HB	P07237	Protein disulfide-isomerase	↓	4.4	4.59E-04	5.8	3.32E-02
PABPC1	P11940	Polyadenylate-binding protein 1	↓	6.9	9.23E-03	17.5	3.06E-02
PARK7	Q99497	Parkinson disease protein 7	↓	6.0	2.54E-02	11.9	8.09E-03
PARP4	Q9UUKK3	Protein mono-ADP-ribosyltransferase PARP4	↑	2.5	5.60E-04	2.6	8.56E-04
PBXIP1	Q96AQ6	Pre-B-cell leukemia transcription factor-interacting protein 1	↑	2.4	1.81E-02	2.8	8.00E-03
PCBP1	Q15365	Poly(rC)-binding protein 1	↓	4.2	6.12E-03	7.3	2.58E-03
PCBP2	Q15366	Poly(rC)-binding protein 2	↓	4.0	1.12E-03	3.7	4.82E-03
PCYOX1	Q9UHG3	Prenylcysteine oxidase 1	↓	3.4	2.13E-03	5.9	1.68E-04
PDGFRA	P16234	Platelet-derived growth factor receptor alpha	↑	2.2	1.03E-02	3.3	1.08E-04
PDGFRB	P09619	Platelet-derived growth factor receptor beta	↑	2.1	8.72E-03	3.2	3.93E-04
PDHA1	P08559	Pyruvate dehydrogenase E1 component subunit alpha, somatic form, mitochondrial	↓	2.9	2.53E-03	6.6	1.46E-02
PDIA5	Q14554	Protein disulfide-isomerase A5	↓	4.1	5.19E-03	10.3	1.83E-02
PDIA6	Q15084	Protein disulfide-isomerase A6	↓	4.9	1.07E-03	6.4	2.19E-02
PFAS	O15067	Phosphoribosylformylglycinamide synthase	↑	2.4	2.80E-02	3.8	5.06E-03
PGK1	P00558	Phosphoglycerate kinase 1	↓	4.6	2.35E-02	16.6	1.49E-02
PHB2	Q99623	Prohibitin-2	↓	13.2	1.68E-04	23.2	6.05E-03
PHGDH	O43175	D-3-phosphoglycerate dehydrogenase	↓	4.1	2.14E-02	12.1	3.18E-03
PI4KA	P42356	Phosphatidylinositol 4-kinase alpha	↑	1.6	1.65E-02	1.8	1.99E-02
PLS3	P13797	Plastin-3	↓	4.6	2.19E-02	16.1	2.69E-04
PLXNA1	Q9UIW2	Plexin-A1	↑	1.9	1.18E-02	4.5	1.45E-02
PLXNB2	O15031	Plexin-B2	↑	2.0	6.51E-03	2.7	4.32E-03
PPP2R1A	P30153	Serine/threonine-protein phosphatase 2A 65 kDa regulatory subunit A alpha isoform	↓	3.7	2.77E-03	11.2	4.31E-04
PRDX1	Q06830	Peroxiredoxin-1	↓	8.5	1.12E-02	40.8	7.78E-04
PRDX2	P32119	Peroxiredoxin-2	↓	4.0	1.25E-02	7.1	2.53E-03
PRDX4	Q13162	Peroxiredoxin-4	↓	10.9	5.88E-04	26.8	1.31E-04
PRKDC	P78527	DNA-dependent protein kinase catalytic subunit	↑	2.1	1.18E-02	2.6	8.48E-03
PROCR	Q9UNN8	Endothelial protein C receptor	↓	2.6	1.73E-02	1.6	4.99E-02

PRPF40A	O75400	Pre-mRNA-processing factor 40 homolog A	↑	1.7	3.07E-03	2.1	2.40E-04
PSMD11	O00231	26S proteasome non-ATPase regulatory subunit 11	↓	7.4	1.36E-03	10.2	3.41E-02
PSMD6	Q15008	26S proteasome non-ATPase regulatory subunit 6	↓	1.7	9.79E-04	1.7	4.61E-03
PTBP1	P26599	Polypyrimidine tract-binding protein 1	↓	6.7	8.11E-03	14.2	7.55E-03
PTGFRN	Q9P2B2	Prostaglandin F2 receptor negative regulator	↑	3.4	1.00E-02	5.0	3.91E-03
PTPRS	Q13332	Receptor-type tyrosine-protein phosphatase S	↑	2.1	1.35E-03	3.1	1.01E-04
PXDN	Q92626	Peroxidasin homolog	↑	2.3	6.47E-04	3.2	2.54E-04
QARS1	P47897	Glutamine--tRNA ligase	↓	2.4	5.76E-03	5.4	2.64E-02
RAB11A	P62491	Ras-related protein Rab-11A	↓	6.7	5.07E-04	10.9	1.76E-03
RAB11B	Q15907	Ras-related protein Rab-11B					
RAB1A	P62820	Ras-related protein Rab-1A	↓	8.3	1.07E-03	13.8	2.17E-03
RAB3GAP2	Q9H2M9	Rab3 GTPase-activating protein non-catalytic subunit	↑	2.2	1.56E-04	2.8	8.95E-04
RAD50	Q92878	DNA repair protein RAD50	↑	1.8	1.42E-02	2.9	1.79E-04
RAN	P62826	GTP-binding nuclear protein Ran	↓	4.6	1.56E-02	13.5	1.68E-04
RARS1	P54136	Arginine--tRNA ligase, cytoplasmic	↓	3.1	1.38E-02	6.9	9.79E-04
RCN1	Q15293	Reticulocalbin-1	↓	2.1	4.46E-03	2.6	4.75E-02
RECK	O95980	Reversion-inducing cysteine-rich protein with Kazal motifs	↑	2.6	6.47E-04	3.0	1.38E-03
RHOG	P84095	Rho-related GTP-binding protein RhoG	↓	2.9	1.49E-04	2.9	6.37E-03
RNF213	Q63HN8	E3 ubiquitin-protein ligase RNF213	↑	3.3	4.04E-03	3.6	1.50E-03
RNH1	P13489	Ribonuclease inhibitor	↓	6.8	4.66E-02	10.1	2.82E-03
ROCK2	O75116	Rho-associated protein kinase 2	↑	2.9	6.21E-04	2.8	1.02E-03
RPL3	P39023	60S ribosomal protein L3	↓	2.9	4.73E-03	2.6	8.38E-04
RPL31	P62899	60S ribosomal protein L31	↓	1.7	6.31E-03	2.2	7.74E-03
RPL4	P36578	60S ribosomal protein L4	↓	4.1	6.71E-03	4.3	2.21E-03
RPL6	Q02878	60S ribosomal protein L6	↓	2.3	7.33E-03	2.8	6.12E-03
RPL7	P18124	60S ribosomal protein L7	↓	4.3	1.56E-02	9.0	3.65E-03
RPN1	P04843	Dolichyl-diphosphooligosaccharide--protein glycosyltransferase subunit 1	↑	1.6	6.91E-03	2.5	1.07E-03
RPS11	P62280	40S ribosomal protein S11	↓	4.5	3.65E-02	5.0	1.76E-03

RPS13	P62277	40S ribosomal protein S13	↓	6.1	5.94E-03	10.1	4.08E-03
RPS16	P62249	40S ribosomal protein S16	↓	7.2	5.41E-03	11.3	7.12E-04
RPS18	P62269	40S ribosomal protein S18	↓	3.1	8.97E-03	6.3	2.26E-02
RPS3	P23396	40S ribosomal protein S3	↓	5.7	7.12E-03	7.0	9.79E-04
RPS9	P46781	40S ribosomal protein S9	↓	7.9	1.16E-03	16.6	3.93E-04
RPSA	P08865	40S ribosomal protein SA	↓	2.3	1.77E-02	4.4	2.96E-03
RRBP1	Q9P2E9	Ribosome-binding protein 1	↑	1.8	8.00E-03	2.3	2.57E-02
RUVBL1	Q9Y265	RuvB-like 1	↓	3.5	3.70E-02	4.4	1.94E-02
SDHA	P31040	Succinate dehydrogenase [ubiquinone] flavoprotein subunit, mitochondrial	↓	3.0	2.66E-03	4.2	3.93E-02
SEPTIN11	Q9NVA2	Septin-11	↓	5.5	1.56E-03	18.8	8.95E-04
SEPTIN2	Q15019	Septin-2	↓	7.7	1.28E-02	32.8	7.12E-04
SEPTIN7	Q16181	Septin-7	↓	5.9	2.86E-03	12.4	1.71E-04
SEPTIN9	Q9UHD8	Septin-9	↓	3.6	2.04E-02	18.4	4.82E-04
SERINC1	Q9NRX5	Serine incorporator 1	↑	1.8	6.12E-03	2.3	4.69E-04
SERPINH1	P50454	Serpin H1	↓	7.3	4.61E-03	5.3	9.23E-03
SF3B3	Q15393	Splicing factor 3B subunit 3	↑	2.0	8.24E-03	2.8	9.79E-04
SFPQ	P23246	Splicing factor, proline- and glutamine-rich	↓	2.1	8.56E-04	3.1	1.73E-02
SFXN1	Q9H9B4	Sideroflexin-1	↓	3.6	6.91E-04	3.2	3.03E-03
SFXN3	Q9BWM7	Sideroflexin-3	↓	2.9	4.48E-04	3.7	8.24E-04
SLC1A5	Q15758	Neutral amino acid transporter B(0)	↑	1.9	1.27E-03	3.9	2.69E-04
SLC25A3	Q00325	Phosphate carrier protein, mitochondrial	↑	1.8	2.68E-02	3.2	1.53E-02
SLC39A14	Q15043	Metal cation symporter ZIP14	↑	1.8	1.38E-03	2.5	1.50E-03
SLC44A1	Q8WWI5	Choline transporter-like protein 1	↓	2.2	5.07E-04	2.2	4.04E-04
SLIT3	O75094	Slit homolog 3 protein	↑	2.2	1.56E-03	1.9	1.77E-02
SMC3	Q9UQE7	Structural maintenance of chromosomes protein 3	↑	2.9	1.53E-02	4.8	2.47E-03
SMCHD1	A6NHR9	Structural maintenance of chromosomes flexible hinge domain-containing protein 1	↑	2.6	1.24E-02	3.7	8.48E-03
SNRNP200	O75643	U5 small nuclear ribonucleoprotein 200 kDa helicase	↑	1.6	2.57E-02	2.4	1.95E-02

SNRPA	P09012	U1 small nuclear ribonucleoprotein A	↓	2.9	2.14E-04	5.3	1.02E-03
SPTAN1	Q13813	Spectrin alpha chain, non-erythrocytic 1	↑	2.4	2.19E-02	4.0	3.78E-03
SPTBN1	Q01082	Spectrin beta chain, non-erythrocytic 1	↑	2.2	1.73E-02	3.5	4.92E-03
SRPRB	Q9Y5M8	Signal recognition particle receptor subunit beta	↓	4.5	6.67E-04	2.8	2.87E-04
SSBP1	Q04837	Single-stranded DNA-binding protein, mitochondrial	↓	4.4	4.90E-04	3.3	1.62E-02
SSR4	P51571	Translocon-associated protein subunit delta	↓	6.9	1.56E-03	5.8	2.40E-04
STT3A	P46977	Dolichyl-diphosphooligosaccharide--protein glycosyltransferase subunit STT3A	↑	2.0	1.09E-02	2.5	7.78E-03
STT3B	Q8TCJ2	Dolichyl-diphosphooligosaccharide--protein glycosyltransferase subunit STT3B	↑	1.6	1.38E-02	2.1	2.80E-02
SYNE1	Q8NF91	Nesprin-1	↑	2.5	4.46E-03	4.5	4.92E-03
TAGLN2	P37802	Transgelin-2	↓	2.5	1.15E-02	3.7	3.85E-02
TCIRG1	Q13488	V-type proton ATPase 116 kDa subunit a3	↑	1.9	2.13E-03	3.0	2.84E-04
TCP1	P17987	T-complex protein 1 subunit alpha	↓	6.0	3.91E-03	7.1	7.78E-04
TLE1	Q04724	Transducin-like enhancer protein 1	↑	2.1	3.69E-04	1.7	1.68E-02
TLE2	Q04725	Transducin-like enhancer protein 2					
TLE4	Q04727	Transducin-like enhancer protein 4					
TMTC3	Q6ZXV5	Protein O-mannosyl-transferase TMTC3	↑	2.2	3.29E-03	3.5	8.56E-04
TNS1	Q9HBL0	Tensin-1	↓	2.7	7.12E-04	3.4	9.23E-03
TNXB	P22105	Tenascin-X	↑	1.9	1.69E-03	4.7	5.60E-04
TPBG	Q13641	Trophoblast glycoprotein	↑	2.7	1.77E-02	3.2	4.75E-02
TPI1	P60174	Triosephosphate isomerase	↓	6.3	1.12E-02	13.7	7.64E-03
TPP2	P29144	Tripeptidyl-peptidase 2	↑	2.2	5.58E-03	2.9	2.21E-03
TPR	P12270	Nucleoprotein TPR	↑	1.8	1.12E-02	3.0	1.38E-03
TRIM28	Q13263	Transcription intermediary factor 1-beta	↓	3.5	2.77E-03	7.2	6.44E-03
TUBA1B	P68363	Tubulin alpha-1B chain	↓	4.3	1.34E-02	11.0	9.36E-04
TUBB	P07437	Tubulin beta chain	↓	3.7	2.76E-03	8.2	1.07E-03
TUBB3	Q13509	Tubulin beta-3 chain	↓	4.1	9.89E-03	7.8	1.17E-03
TUBB4B	P68371	Tubulin beta-4B chain	↓	5.4	1.97E-03	15.1	5.88E-04
UBE4A	Q14139	Ubiquitin conjugation factor E4 A	↑	2.3	7.56E-03	2.6	1.06E-02

UBR4	Q5T4S7	E3 ubiquitin-protein ligase UBR4	↑	3.2	1.01E-04	2.6	1.57E-02
UGDH	O60701	UDP-glucose 6-dehydrogenase	↓	5.6	2.92E-02	15.6	1.60E-03
USO1	O60763	General vesicular transport factor p115	↑	2.8	3.00E-04	1.9	4.93E-02
UTRN	P46939	Utrophin	↑	1.8	5.58E-03	2.6	4.59E-04
VAPA	Q9P0L0	Vesicle-associated membrane protein-associated protein A	↓	2.3	1.56E-03	2.4	5.24E-03
VASN	Q6EMK4	Vasorin	↑	2.2	1.31E-02	3.1	7.12E-04
VAT1	Q99536	Synaptic vesicle membrane protein VAT-1 homolog	↓	3.0	2.86E-03	3.8	1.62E-03
VCAN	P13611	Versican core protein	↑	2.8	4.48E-02	3.7	2.62E-02
VCL	P18206	Vinculin	↑	3.4	1.31E-04	3.0	1.69E-03
VIM	P08670	Vimentin	↓	5.3	1.50E-03	6.4	1.16E-03
XRCC6	P12956	X-ray repair cross-complementing protein 6	↓	4.0	1.97E-03	14.3	3.53E-03
YWHAB	P31946	14-3-3 protein beta/alpha	↓	2.3	2.10E-02	3.6	7.78E-04
YWHAZ	P63104	14-3-3 protein zeta/delta	↓	3.4	3.91E-03	7.2	2.01E-04

Table S2: List of 304 age-dependently regulated proteins exclusively in NHDF^{INT}. Label-free quantitative proteome analysis of NHDF^{INT} vs NHDF^{EXT} of Y vs M vs O donors. Spearman's correlation, $p < 0.05$; $FC > |1.5|$; $n = 5$.

Gene name	UniProt ID	Protein description	Regulation	FC	p-value
ACAA1	P09110	3-ketoacyl-CoA thiolase, peroxisomal	↓	3.0	7.01E-03
ACAD9	Q9H845	Complex I assembly factor ACAD9, mitochondrial	↓	1.8	4.84E-03
ACO1	P21399	Cytoplasmic aconitate hydratase	↑	2.3	2.04E-02
ACOT9	Q9Y305	Acyl-coenzyme A thioesterase 9, mitochondrial	↓	1.8	3.97E-03
ACTN1	P12814	Alpha-actinin-1	↑	2.1	3.32E-02
ACTN4	O43707	Alpha-actinin-4	↑	2.1	1.65E-02
ADAM17	P78536	Disintegrin and metalloproteinase domain-containing protein 17	↑	2.3	1.04E-02
ADD3	Q9UEY8	Gamma-adducin	↓	3.2	3.93E-04
AHCY	P23526	Adenosylhomocysteinase	↓	2.0	4.23E-02
AK2	P54819	Adenylate kinase 2, mitochondrial	↓	6.4	5.10E-04
AK4	P27144	Adenylate kinase 4, mitochondrial	↓	2.3	1.14E-02
ALDH18A1	P54886	Delta-1-pyrroline-5-carboxylate synthase	↓	3.2	1.49E-02
ALDH1A3	P47895	Aldehyde dehydrogenase family 1 member A3	↓	3.7	3.30E-02
ALDH1B1	P30837	Aldehyde dehydrogenase X, mitochondrial	↓	3.7	3.23E-03
ALDH2	P05091	Aldehyde dehydrogenase, mitochondrial	↓	3.2	5.16E-03
ALDH7A1	P49419	Alpha-aminoadipic semialdehyde dehydrogenase	↓	5.0	3.66E-03
AP1B1	Q10567	AP-1 complex subunit beta-1	↑	1.7	1.03E-03
AP2S1	P53680	AP-2 complex subunit sigma	↓	2.2	1.71E-02
API5	Q9BZZ5	Apoptosis inhibitor 5	↓	1.7	4.11E-04
APMAP	Q9HDC9	Adipocyte plasma membrane-associated protein	↓	2.3	8.18E-04
ARF1	P84077	ADP-ribosylation factor 1	↓	4.9	1.46E-03
ARF4	P18085	ADP-ribosylation factor 4	↓	10.1	1.09E-02
ARPC2	O15144	Actin-related protein 2/3 complex subunit 2	↓	11.3	5.60E-04
ARSA	P15289	Arylsulfatase A	↓	2.1	7.01E-03
ASCC3	Q8N3C0	Activating signal cointegrator 1 complex subunit 3	↑	3.3	7.03E-03

ATP5B	P06576	ATP synthase subunit beta, mitochondrial	↓	2.2	5.41E-03
ATP5C1	P36542	ATP synthase subunit gamma, mitochondrial	↓	4.5	6.22E-03
ATP6V0D1	P61421	V-type proton ATPase subunit d 1	↓	4.2	3.75E-03
BAG2	O95816	BAG family molecular chaperone regulator 2	↓	5.6	1.66E-03
BSG	P35613	Basigin	↑	1.7	1.86E-02
BZW1	Q7L1Q6	Basic leucine zipper and W2 domain-containing protein 1	↓	2.0	2.70E-02
CAD	P27708	CAD protein	↑	3.3	5.33E-04
CAND1	Q86VP6	Ilin-associated NEDD8-dissociated protein 1	↑	2.7	5.88E-04
CASK	O14936	Peripheral plasma membrane protein CASK	↑	1.5	4.23E-02
CAVIN3	Q969G5	Caveolae-associated protein 3	↓	1.5	4.07E-02
CD248	Q9HCU0	Endosialin	↑	1.7	1.00E-02
CD47	Q08722	Leukocyte surface antigen CD47	↑	1.9	2.80E-02
CD55	P08174	Complement decay-accelerating factor	↑	2.4	5.41E-03
CDC42BPB	Q9Y5S2	Serine/threonine-protein kinase MRCK beta	↑	1.5	5.24E-03
CDH13	P55290	Cadherin-13	↑	2.6	7.37E-03
CKAP4	Q07065	Cytoskeleton-associated protein 4	↓	2.0	2.66E-03
COMT	P21964	Catechol O-methyltransferase	↓	9.0	7.12E-04
COPA	P53621	Coatomer subunit alpha	↑	2.1	7.81E-04
COPB2	P35606	Coatomer subunit beta'	↑	2.2	9.79E-04
COX5B	P10606	Cytochrome c oxidase subunit 5B, mitochondrial	↓	5.1	2.23E-03
CPD	O75976	Carboxypeptidase D	↑	1.9	9.49E-03
CPSF1	Q10570	Cleavage and polyadenylation specificity factor subunit 1	↑	1.8	4.50E-03
CRTAP	O75718	Cartilage-associated protein	↓	7.4	8.95E-04
CTNNA1	P35221	Catenin alpha-1	↑	1.9	5.08E-03
CTSC	P53634	Dipeptidyl peptidase 1	↓	6.4	1.84E-03
CTSZ	Q9UBR2	Cathepsin Z	↓	2.9	8.33E-03
DECR1	Q16698	2,4-dienoyl-CoA reductase, mitochondrial	↓	5.1	3.25E-04
DHX30	Q7L2E3	ATP-dependent RNA helicase DHX30	↑	1.7	3.91E-03

DIAPH1	O60610	Protein diaphanous homolog 1	↑	2.4	3.68E-04
DIS3	Q9Y2L1	Exosome complex exonuclease RRP44	↑	2.1	1.92E-03
DOCK6	Q96HP0	Dedicator of cytokinesis protein 6	↓	2.3	9.08E-03
DOCK7	Q96N67	Dedicator of cytokinesis protein 7	↑	1.5	2.92E-02
DPP3	Q9NY33	Dipeptidyl peptidase 3	↑	3.0	2.65E-02
DPP7	Q9UHL4	Dipeptidyl peptidase 2	↓	3.2	2.88E-02
DUT	P33316	Deoxyuridine 5'-triphosphate nucleotidohydrolase, mitochondrial	↓	2.1	2.68E-04
ECH1	Q13011	Delta(3,5)-Delta(2,4)-dienoyl-CoA isomerase, mitochondrial	↓	2.5	3.78E-02
ECHS1	P30084	Enoyl-CoA hydratase, mitochondrial	↓	5.1	3.96E-04
ECPAS	Q5VYK3	Proteasome adapter and scaffold protein ECM29	↑	1.6	3.53E-02
EEA1	Q15075	Early endosome antigen 1	↑	3.6	2.05E-03
EEF1A1	P68104	Elongation factor 1-alpha 1	↓	3.7	6.12E-03
EEF1A2	Q05639	Elongation factor 1-alpha 2			
EEF1A1P5	Q5VTE0	Putative elongation factor 1-alpha-like 3			
EFR3A	Q14156	Protein EFR3 homolog A	↑	1.5	1.69E-02
EHD1	Q9H4M9	EH domain-containing protein 1	↓	3.2	6.28E-03
EIF2B5	Q13144	Translation initiation factor eIF-2B subunit epsilon	↑	1.7	2.51E-02
EIF2S3	P41091	Eukaryotic translation initiation factor 2 subunit 3	↓	4.2	3.93E-02
EIF2S3L	Q2VIR3	Eukaryotic translation initiation factor 2 subunit 3B			
EIF3B	P55884	Eukaryotic translation initiation factor 3 subunit B	↑	2.4	4.59E-04
EIF4G1	Q04637	Eukaryotic translation initiation factor 4 gamma 1	↓	1.7	7.07E-03
EIF5A	P63241	Eukaryotic translation initiation factor 5A-1	↓	4.2	1.87E-02
EIF5AL1	Q6IS14	Eukaryotic translation initiation factor 5A-1-like			
EIF5B	O60841	Eukaryotic translation initiation factor 5B	↑	2.0	2.92E-02
ENG	P17813	Endoglin	↑	1.9	1.34E-02
EPHB3	P54753	Ephrin type-B receptor 3	↑	2.5	4.14E-02
ERC1	Q8IUD2	ELKS/Rab6-interacting/CAST family member 1	↑	2.5	1.17E-02
ERLIN2	O94905	Erlin-2	↓	1.9	2.57E-03
ERP29	P30040	Endoplasmic reticulum resident protein 29	↓	7.1	3.53E-04
ETFB	P38117	Electron transfer flavoprotein subunit beta	↓	7.0	1.30E-04

FAM120A	Q9NZB2	Constitutive coactivator of PPAR-gamma-like protein 1	↓	2.2	1.60E-03
FASN	P49327	Fatty acid synthase	↑	2.4	3.53E-03
FBL	P22087	rRNA 2'-O-methyltransferase fibrillar	↓	3.4	1.33E-03
FDXR	P22570	NADPH:adrenodoxin oxidoreductase, mitochondrial	↓	2.4	4.16E-02
FH	P07954	Fumarate hydratase, mitochondrial	↓	2.5	1.75E-03
FLOT1	O75955	Flotillin-1	↓	3.3	1.71E-04
FNDC3A	Q9Y2H6	Fibronectin type-III domain-containing protein 3A	↑	2.6	4.09E-02
FSTL1	Q12841	Follistatin-related protein 1	↓	2.5	2.39E-02
GANAB	Q14697	Neutral alpha-glucosidase AB	↑	2.0	4.31E-02
GET3	O43681	ATPase GET3	↓	1.9	2.24E-02
GFPT1	Q06210	Glutamine--fructose-6-phosphate aminotransferase [isomerizing] 1	↓	2.8	1.71E-02
GGH	Q92820	Gamma-glutamyl hydrolase	↓	2.5	2.40E-03
GLB1	P16278	Beta-galactosidase	↓	3.3	2.65E-03
GLS	O94925	Glutaminase kidney isoform, mitochondrial	↓	4.1	3.93E-03
H1-4	P10412	Histone H1.4	↓	2.0	1.76E-03
HERC4	Q5GLZ8	Probable E3 ubiquitin-protein ligase HERC4	↑	3.5	2.04E-02
HEXA	P06865	Beta-hexosaminidase subunit alpha	↓	1.9	3.46E-03
HIBADH	P31937	3-hydroxyisobutyrate dehydrogenase, mitochondrial	↓	2.8	8.59E-04
HIP1	O00291	Huntingtin-interacting protein 1	↑	1.9	1.47E-02
HK1	P19367	Hexokinase-1	↑	2.3	1.90E-02
HMGCL	P35914	Hydroxymethylglutaryl-CoA lyase, mitochondrial	↓	2.1	8.11E-04
HNRNPA3	P51991	Heterogeneous nuclear ribonucleoprotein A3	↓	3.6	4.61E-04
HNRNPAB	Q99729	Heterogeneous nuclear ribonucleoprotein A/B	↓	2.7	2.77E-04
HNRNPDL	O14979	Heterogeneous nuclear ribonucleoprotein D-like	↓	2.5	7.07E-03
HNRNPF	P52597	Heterogeneous nuclear ribonucleoprotein F	↓	3.9	4.64E-03
HNRNPH3	P31942	Heterogeneous nuclear ribonucleoprotein H3	↓	3.0	3.75E-03
HNRNPR	O43390	Heterogeneous nuclear ribonucleoprotein R	↓	2.3	6.28E-03
HNRNPUL1	Q9BUJ2	Heterogeneous nuclear ribonucleoprotein U-like protein 1	↓	3.0	2.05E-03

HP1BP3	Q5SSJ5	Heterochromatin protein 1-binding protein 3	↓	4.7	3.53E-03
HSD17B12	Q53GQ0	Very-long-chain 3-oxoacyl-CoA reductase	↓	1.6	1.94E-02
HSP90AB2P	Q58FF8	Putative heat shock protein HSP 90-beta 2	↑	1.6	3.25E-02
HSPE1	P61604	10 kDa heat shock protein, mitochondrial	↓	2.7	1.41E-02
IDE	P14735	Insulin-degrading enzyme	↑	2.8	4.99E-03
IDH3A	P50213	Isocitrate dehydrogenase [NAD] subunit alpha, mitochondrial	↓	2.1	1.48E-03
IGF2R	P11717	Cation-independent mannose-6-phosphate receptor	↑	3.1	2.47E-03
IKBIP	Q70UQ0	Inhibitor of nuclear factor kappa-B kinase-interacting protein	↓	1.7	1.49E-02
ILVBL	A1L0T0	2-hydroxyacyl-CoA lyase 2	↓	1.9	4.82E-04
INF2	Q27J81	Inverted formin-2	↓	1.7	1.18E-02
IPO8	O15397	Importin-8	↑	2.2	8.70E-03
IQGAP1	P46940	Ras GTPase-activating-like protein IQGAP1	↑	2.1	9.36E-04
ISLR	O14498	Immunoglobulin superfamily containing leucine-rich repeat protein	↓	2.5	1.99E-02
ITGA1	P56199	Integrin alpha-1	↑	1.9	1.21E-02
ITGA6	P23229	Integrin alpha-6	↑	3.6	7.59E-03
ITGB3	P05106	Integrin beta-3	↑	1.9	2.48E-02
ITGB5	P18084	Integrin beta-5	↑	1.8	3.41E-03
KANK2	Q63ZY3	KN motif and ankyrin repeat domain-containing protein 2	↓	1.6	2.70E-02
KPNA4	O00629	Importin subunit alpha-3	↓	1.5	2.14E-02
LAMB2	P55268	Laminin subunit beta-2	↑	1.9	7.12E-03
LAMC1	P11047	Laminin subunit gamma-1	↑	2.0	1.34E-02
LARS1	Q9P2J5	Leucine--tRNA ligase, cytoplasmic	↑	1.6	4.23E-02
LASP1	Q14847	LIM and SH3 domain protein 1	↓	2.6	3.85E-02
LDHA	P00338	L-lactate dehydrogenase A chain	↓	5.8	3.53E-03
LDHB	P07195	L-lactate dehydrogenase B chain	↓	3.7	2.22E-02
LGMN	Q99538	Legumain	↓	1.9	3.69E-02
LRPAP1	P30533	Alpha-2-macroglobulin receptor-associated protein	↓	2.0	2.53E-03
LRRC59	Q96AG4	Leucine-rich repeat-containing protein 59	↓	1.6	4.23E-02

MACROH2A1	O75367	Core histone macro-H2A.1	↓	5.0	5.91E-04
MAN2B1	O00754	Lysosomal alpha-mannosidase	↓	2.6	3.63E-04
MAP4	P27816	Microtubule-associated protein 4	↑	2.5	2.99E-02
MARS1	P56192	Methionine--tRNA ligase, cytoplasmic	↑	2.0	3.41E-03
ME2	P23368	NAD-dependent malic enzyme, mitochondrial	↓	1.7	2.34E-02
MIA3	Q5JRA6	Transport and Golgi organization protein 1 homolog	↑	2.1	3.07E-03
MMS19	Q96T76	MMS19 nucleotide excision repair protein homolog	↑	1.9	3.39E-02
MVP	Q14764	Major vault protein	↑	2.9	2.40E-04
MYDGF	Q969H8	Myeloid-derived growth factor	↓	10.7	1.28E-03
MYO1C	O00159	Unconventional myosin-Ic	↑	1.7	3.25E-02
NAGA	P17050	Alpha-N-acetylgalactosaminidase	↓	1.9	1.48E-02
NARS1	O43776	Asparagine--tRNA ligase, cytoplasmic	↓	3.1	1.92E-02
NBAS	A2RRP1	Neuroblastoma-amplified sequence	↑	1.9	2.01E-04
NCKAP1	Q9Y2A7	Nck-associated protein 1	↑	2.6	7.78E-04
NDUFA9	Q16795	NADH dehydrogenase [ubiquinone] 1 alpha subcomplex subunit 9, mitochondrial	↓	3.6	2.54E-04
NDUFB10	O96000	NADH dehydrogenase [ubiquinone] 1 beta subcomplex subunit 10	↓	1.5	4.55E-02
NDUFB4	O95168	NADH dehydrogenase [ubiquinone] 1 beta subcomplex subunit 4	↓	4.6	1.48E-04
NDUFS3	O75489	NADH dehydrogenase [ubiquinone] iron-sulfur protein 3, mitochondrial	↓	2.7	5.50E-03
NFASC	O94856	Neurofascin	↑	2.7	4.32E-04
NONO	Q15233	Non-POU domain-containing octamer-binding protein	↓	3.5	5.91E-04
NPC1	O15118	NPC intracellular cholesterol transporter 1	↑	2.0	6.04E-03
NPEPPS	P55786	Puromycin-sensitive aminopeptidase	↑	2.7	2.96E-03
NRD1	O43847	Nardilysin	↑	3.4	5.60E-04
NSF	P46459	Vesicle-fusing ATPase	↓	5.7	1.90E-04
OGDH	Q02218	2-oxoglutarate dehydrogenase, mitochondrial	↑	2.3	4.07E-02
OGT	O15294	UDP-N-acetylglucosamine--peptide N-acetylglucosaminyltransferase 110 kDa subunit	↑	2.0	4.31E-02
OTUB1	Q96FW1	Ubiquitin thioesterase OTUB1	↓	1.7	4.99E-02

OXCT1	P55809	Succinyl-CoA:3-ketoacid coenzyme A transferase 1, mitochondrial	↓	2.7	1.96E-04
P4HA2	O15460	Prolyl 4-hydroxylase subunit alpha-2	↓	7.9	3.41E-03
PABPC4	Q13310	Polyadenylate-binding protein 4	↓	2.3	4.05E-02
PCK2	Q16822	Phosphoenolpyruvate carboxykinase [GTP], mitochondrial	↓	5.8	1.57E-03
PDCD6IP	Q8WUM4	Programmed cell death 6-interacting protein	↑	1.8	4.40E-02
PDHB	P11177	Pyruvate dehydrogenase E1 component subunit beta, mitochondrial	↓	3.8	4.11E-04
PDIA3	P30101	Protein disulfide-isomerase A3	↓	3.9	1.56E-03
PDS5B	Q9NTI5	Sister chromatid cohesion protein PDS5 homolog B	↑	1.6	4.66E-02
PFN1	P07737	Profilin-1	↓	11.6	2.38E-03
PGAM1	P18669	Phosphoglycerate mutase 1	↓	3.8	4.85E-02
PGD	P52209	6-phosphogluconate dehydrogenase, decarboxylating	↓	2.2	4.33E-02
PGRMC2	O15173	Membrane-associated progesterone receptor component 2	↓	2.1	8.56E-04
PITRM1	Q5JRX3	Presequence protease, mitochondrial	↑	1.5	4.84E-02
PLBD2	Q8NHP8	Putative phospholipase B-like 2	↓	3.1	5.76E-03
PLCB3	Q01970	1-phosphatidylinositol 4,5-bisphosphate phosphodiesterase beta-3	↑	2.4	6.17E-04
PLD3	Q8IV08	5'-3' exonuclease PLD3	↓	2.2	9.49E-03
PLEC	Q15149	Plectin	↑	2.1	2.57E-03
PLPP1	O14494	Phospholipid phosphatase 1	↓	2.7	4.50E-03
PML	P29590	Protein PML	↓	1.8	4.48E-02
PMPCB	O75439	Mitochondrial-processing peptidase subunit beta	↓	3.6	3.97E-03
POFUT2	Q9Y2G5	GDP-fucose protein O-fucosyltransferase 2	↓	2.1	2.44E-02
POLR2B	P30876	DNA-directed RNA polymerase II subunit RPB2	↑	1.8	3.91E-03
PON2	Q15165	Serum paraoxonase/arylesterase 2	↓	1.7	1.50E-02
POR	P16435	NADPH--cytochrome P450 reductase	↓	2.3	1.72E-02
PPIA	P62937	Peptidyl-prolyl cis-trans isomerase A	↓	10.0	1.90E-03
PPIB	P23284	Peptidyl-prolyl cis-trans isomerase B	↓	12.3	8.95E-04
PPL	O60437	Periplakin	↑	2.0	2.86E-02
PPP1CB	P62140	Serine/threonine-protein phosphatase PP1-beta catalytic subunit	↓	11.1	2.26E-04

PPP1R12A	O14974	Protein phosphatase 1 regulatory subunit 12A	↓	2.0	1.21E-03
PRDX3	P30048	Thioredoxin-dependent peroxide reductase, mitochondrial	↓	5.3	1.95E-03
PRDX5	P30044	Peroxiredoxin-5, mitochondrial	↓	7.7	2.79E-04
PRDX6	P30041	Peroxiredoxin-6	↓	12.3	6.51E-03
PRPF19	Q9UMS4	Pre-mRNA-processing factor 19	↓	3.6	8.59E-04
PSMA1	P25786	Proteasome subunit alpha type-1	↓	5.1	3.17E-03
PSMA2	P25787	Proteasome subunit alpha type-2	↓	7.1	1.63E-02
PSMA4	P25789	Proteasome subunit alpha type-4	↓	4.3	4.25E-03
PSMA6	P60900	Proteasome subunit alpha type-6	↓	3.5	2.05E-02
PSMC2	P35998	26S proteasome regulatory subunit 7	↓	2.5	3.93E-02
PSMD1	Q99460	26S proteasome non-ATPase regulatory subunit 1	↑	1.7	4.82E-04
PSMD12	O00232	26S proteasome non-ATPase regulatory subunit 12	↓	1.6	3.79E-02
PSMD2	Q13200	26S proteasome non-ATPase regulatory subunit 2	↑	1.8	1.38E-02
PSME2	Q9UL46	Proteasome activator complex subunit 2	↓	1.6	2.44E-02
PSPC1	Q8WXF1	Paraspeckle component 1	↓	1.7	3.51E-02
PTK7	Q13308	Inactive tyrosine-protein kinase 7	↑	1.7	4.07E-02
RAB10	P61026	Ras-related protein Rab-10	↓	4.7	1.31E-04
RAB2A	P61019	Ras-related protein Rab-2A	↓	8.9	1.34E-02
RAB5C	P51148	Ras-related protein Rab-5C	↓	3.6	3.73E-03
RAB7A	P51149	Ras-related protein Rab-7a	↓	6.6	1.41E-04
RACK1	P63244	Receptor of activated protein C kinase 1	↓	8.8	2.16E-02
RASA1	P20936	Ras GTPase-activating protein 1	↑	2.3	2.34E-02
RECQL	P46063	ATP-dependent DNA helicase Q1	↓	1.6	4.23E-02
RHOA	P61586	Transforming protein RhoA	↓	7.7	3.17E-04
ROCK1	Q13464	Rho-associated protein kinase 1	↑	3.5	3.78E-03
RPL10A	P62906	60S ribosomal protein L10a	↓	1.6	3.61E-02
RPL12	P30050	60S ribosomal protein L12	↓	9.1	2.61E-02
RPL14	P50914	60S ribosomal protein L14	↓	7.0	8.75E-04

RPL15	P61313	60S ribosomal protein L15	↓	2.7	1.83E-03
RPL18	Q07020	60S ribosomal protein L18	↓	2.1	1.95E-02
RPL30	P62888	60S ribosomal protein L30	↓	7.0	9.32E-03
RPL5	P46777	60S ribosomal protein L5	↓	3.4	3.39E-02
RPL8	P62917	60S ribosomal protein L8	↓	4.4	3.07E-03
RPLP0	P05388	60S acidic ribosomal protein P0	↓	4.5	8.56E-04
RPLP0P6	Q8NHW5	60S acidic ribosomal protein P0-like			
RPLP1	P05386	60S acidic ribosomal protein P1	↓	3.1	1.80E-02
RPS10	P46783	40S ribosomal protein S10	↓	1.8	1.44E-02
RPS19	P39019	40S ribosomal protein S19	↓	3.1	2.28E-02
RPS2	P15880	40S ribosomal protein S2	↓	11.5	4.32E-03
RPS3A	P61247	40S ribosomal protein S3a	↓	5.8	2.68E-02
RPS5	P46782	40S ribosomal protein S5	↓	4.5	1.66E-02
RPS7	P62081	40S ribosomal protein S7	↓	7.9	4.50E-02
RRP12	Q5JTH9	RRP12-like protein	↑	1.6	1.81E-02
RSU1	Q15404	Ras suppressor protein 1	↓	1.6	4.42E-02
RTCB	Q9Y310	RNA-splicing ligase RtcB homolog	↓	2.6	4.11E-04
RUVBL2	Q9Y230	RuvB-like 2	↓	2.0	4.08E-02
SAMM50	Q9Y512	Sorting and assembly machinery component 50 homolog	↓	1.7	3.46E-03
SCFD1	Q8WVM8	Sec1 family domain-containing protein 1	↓	2.8	1.48E-02
SCP2	P22307	Non-specific lipid-transfer protein	↓	3.8	4.50E-03
SEC22B	O75396	Vesicle-trafficking protein SEC22b	↓	1.6	4.75E-02
SEC24C	P53992	Protein transport protein Sec24C	↑	2.1	1.86E-02
SEC63	Q9UGP8	Translocation protein SEC63 homolog	↑	1.7	1.06E-02
SEL1L	Q9UBV2	Protein sel-1 homolog 1	↑	1.7	4.15E-02
SERPINE2	P07093	Glia-derived nexin	↓	2.7	7.43E-03
SF3A3	Q12874	Splicing factor 3A subunit 3	↓	2.2	5.71E-04
SGCB	Q16585	Beta-sarcoglycan	↑	1.8	1.18E-02
SHMT2	P34897	Serine hydroxymethyltransferase, mitochondrial	↓	7.6	8.13E-04

SLC25A24	Q6NUK1	Calcium-binding mitochondrial carrier protein SCaMC-1	↓	3.4	2.94E-03
SLC27A1	Q6PCB7	Long-chain fatty acid transport protein 1	↑	1.7	3.53E-03
SND1	Q7KZF4	Staphylococcal nuclease domain-containing protein 1	↑	1.9	1.76E-03
SNRPB	P14678	Small nuclear ribonucleoprotein-associated proteins B and B'	↓	4.1	4.54E-03
SNRPN	P63162	Small nuclear ribonucleoprotein-associated protein N			
SNRPD1	P62314	Small nuclear ribonucleoprotein Sm D1	↓	4.0	1.48E-02
SNRPD3	P62318	Small nuclear ribonucleoprotein Sm D3	↓	4.1	3.23E-03
SNTB2	Q13425	Beta-2-syntrophin	↓	2.3	1.04E-03
SNX9	Q9Y5X1	Sorting nexin-9	↓	2.4	7.33E-03
SPCS3	P61009	Signal peptidase complex subunit 3	↓	2.5	1.36E-03
SPTLC1	O15269	Serine palmitoyltransferase 1	↓	1.9	6.47E-04
SQOR	Q9Y6N5	Sulfide:quinone oxidoreductase, mitochondrial	↓	3.6	2.56E-02
SRC	P12931	Proto-oncogene tyrosine-protein kinase Src	↓	2.2	2.79E-03
SRSF3	P84103	Serine/arginine-rich splicing factor 3	↓	3.9	4.55E-02
SRSF7	Q16629	Serine/arginine-rich splicing factor 7	↓	2.5	8.45E-03
SSR1	P43307	Translocon-associated protein subunit alpha	↓	1.5	2.24E-02
STOM	P27105	Erythrocyte band 7 integral membrane protein	↓	1.9	1.27E-03
STOML2	Q9UJZ1	Stomatin-like protein 2, mitochondrial	↓	3.2	7.79E-04
STX7	O15400	Syntaxin-7	↓	1.6	3.71E-03
SUCLG2	Q96199	Succinate--CoA ligase [GDP-forming] subunit beta, mitochondrial	↓	3.2	6.95E-03
TAF15	Q92804	TATA-binding protein-associated factor 2N	↓	2.3	3.39E-02
TBCD	Q9BTW9	Tubulin-specific chaperone D	↑	3.2	2.01E-04
THBS2	P35442	Thrombospondin-2	↑	2.9	5.68E-03
TLN2	Q9Y4G6	Talin-2	↑	2.4	6.91E-03
TMED9	Q9BVK6	Transmembrane emp24 domain-containing protein 9	↓	2.1	3.38E-02
TMOD3	Q9NYL9	Tropomodulin-3	↓	2.8	4.50E-02
TMX1	Q9H3N1	Thioredoxin-related transmembrane protein 1	↓	2.7	3.48E-03
TOMM70A	O94826	Mitochondrial import receptor subunit TOM70	↓	3.6	5.53E-04
TPP1	O14773	Tripeptidyl-peptidase 1	↓	2.2	9.76E-04

TRIM25	Q14258	E3 ubiquitin/ISG15 ligase TRIM25	↓	6.4	3.66E-03
TRIP12	Q14669	E3 ubiquitin-protein ligase TRIP12	↑	1.5	3.48E-02
TSPO	P30536	Translocator protein	↓	2.0	1.56E-03
TTC37	Q6PGP7	Tetratricopeptide repeat protein 37	↑	3.2	3.26E-04
TUBA1A	Q71U36	Tubulin alpha-1A chain	↓	5.4	1.06E-02
TUBA3C	P0DPH7	Tubulin alpha-3C chain			
TUBA3D	P0DPH8	Tubulin alpha-3D chain			
TUBA3E	Q6PEY2	Tubulin alpha-3E chain			
TWF1	Q12792	Twinfilin-1	↓	2.5	2.61E-02
TXNDC5	Q8NBS9	Thioredoxin domain-containing protein 5	↓	4.4	2.96E-03
UACA	Q9BZF9	Uveal autoantigen with coiled-coil domains and ankyrin repeats	↑	2.0	4.92E-03
UBA7	P41226	Ubiquitin-like modifier-activating enzyme 7	↑	4.7	2.63E-03
UFL1	O94874	E3 UFM1-protein ligase 1	↓	2.3	4.25E-03
UGGT1	Q9NYU2	UDP-glucose:glycoprotein glucosyltransferase 1	↑	1.8	1.16E-03
UPF1	Q92900	Regulator of nonsense transcripts 1	↑	2.4	3.00E-04
UQCRC2	P22695	Cytochrome b-c1 complex subunit 2, mitochondrial	↓	4.1	2.20E-03
USP5	P45974	Ubiquitin carboxyl-terminal hydrolase 5	↑	2.9	5.88E-04
USP7	Q93009	Ubiquitin carboxyl-terminal hydrolase 7	↑	2.1	1.07E-03
USP9X	Q93008	Probable ubiquitin carboxyl-terminal hydrolase FAF-X	↑	3.1	1.16E-03
VCP	P55072	Transitional endoplasmic reticulum ATPase	↑	1.8	1.06E-02
VDAC3	Q9Y277	Voltage-dependent anion-selective channel protein 3	↓	7.5	2.09E-04
VPS13C	Q709C8	Vacuolar protein sorting-associated protein 13C	↑	4.8	4.53E-02
VPS18	Q9P253	Vacuolar protein sorting-associated protein 18 homolog	↑	2.4	1.81E-02
VPS35L	Q7Z3J2	VPS35 endosomal protein sorting factor-like	↑	1.7	2.34E-02
WASHC4	Q2M389	WASH complex subunit 4	↑	2.7	3.04E-04
WASHC5	Q12768	WASH complex subunit 5	↑	2.4	4.04E-03
WDR1	O75083	WD repeat-containing protein 1	↓	4.7	1.61E-02
WFS1	O76024	Wolframin	↑	2.3	3.07E-03
XPO1	O14980	Exportin-1	↑	2.0	1.03E-02

XPO7	Q9UIA9	Exportin-7	↑	3.7	1.14E-02
XRCC5	P13010	X-ray repair cross-complementing protein 5	↓	5.6	5.60E-04
XRN2	Q9H0D6	5'-3' exoribonuclease 2	↓	1.8	1.71E-02
YWHAE	P62258	14-3-3 protein epsilon	↓	1.9	1.15E-02

Table S3: List of 147 age-dependently regulated proteins exclusively in NHDF^{EXT}. Label-free quantitative proteome analysis of NHDF^{INT} vs NHDF^{EXT} of Y vs M vs O donors. Spearman's correlation, $p < 0.05$; $FC > |1.5|$; $n = 5$.

Gene name	UniProt ID	Protein description	Regulation	FC	p-value
AARS2	Q5JTZ9	Alanine--tRNA ligase, mitochondrial	↑	2.2	1.21E-02
ABCA8	O94911	ATP-binding cassette sub-family A member 8	↑	15.5	1.66E-02
ADH1A	P07327	Alcohol dehydrogenase 1A	↓	7.2	2.56E-02
ADH1B	P00325	All-trans-retinol dehydrogenase [NAD(+)] ADH1B			
ADH5	P11766	Alcohol dehydrogenase class-3	↓	12.1	4.86E-04
AFG3L2	Q9Y4W6	AFG3-like protein 2	↑	1.5	2.40E-04
ANXA11	P50995	Annexin A11	↓	3.7	2.17E-02
ANXA4	P09525	Annexin A4	↓	5.6	3.45E-04
ANXA5	P08758	Annexin A5	↓	4.7	3.18E-03
ANXA6	P08133	Annexin A6	↓	4.1	1.03E-02
ANXA7	P20073	Annexin A7	↓	3.6	1.31E-03
AP2A2	O94973	AP-2 complex subunit alpha-2	↓	1.5	1.61E-02
AP3B1	O00203	AP-3 complex subunit beta-1	↓	2.8	7.81E-04
ARFGEF1	Q9Y6D6	Brefeldin A-inhibited guanine nucleotide-exchange protein 1	↑	1.6	1.49E-02
ASPH	Q12797	Aspartyl/asparaginyl beta-hydroxylase	↑	1.5	1.73E-02
ATP5F1A	P25705	ATP synthase subunit alpha, mitochondrial	↓	11.3	1.57E-02
ATP5MD	Q96IX5	ATP synthase membrane subunit DAPIT, mitochondrial	↑	2.7	4.98E-03
ATP5MF	P56134	ATP synthase subunit f, mitochondrial	↑	2.1	1.62E-03
ATP5MG	O75964	ATP synthase subunit g, mitochondrial	↓	3.7	1.71E-04
ATP5PB	P24539	ATP synthase F(0) complex subunit B1, mitochondrial	↓	2.9	6.51E-04
CAMK2B	Q13554	Calcium/calmodulin-dependent protein kinase type II subunit beta	↓	1.9	1.31E-02
CAMK2D	Q13557	Calcium/calmodulin-dependent protein kinase type II subunit delta			
CAPN1	P07384	Calpain-1 catalytic subunit	↓	3.8	2.86E-02
CD59	P13987	CD59 glycoprotein	↓	3.2	1.18E-02
CD63	P08962	CD63 antigen	↓	6.8	1.58E-02
CD81	P60033	CD81 antigen	↓	7.3	3.73E-04

COL12A1	Q99715	Collagen alpha-1(XII) chain	↑	3.5	8.56E-04
COL1A1	P02452	Collagen alpha-1(I) chain	↑	3.7	5.24E-03
COL1A2	P08123	Collagen alpha-2(I) chain	↑	3.7	2.47E-03
COL3A1	P02461	Collagen alpha-1(III) chain	↑	3.6	6.31E-03
COL5A1	P20908	Collagen alpha-1(V) chain	↑	2.8	1.90E-02
DAD1	P61803	Dolichyl-diphosphooligosaccharide--protein glycosyltransferase subunit DAD1	↑	1.9	3.60E-03
DCTN1	Q14203	Dynactin subunit 1	↑	2.1	2.38E-03
DDX39B	Q13838	Spliceosome RNA helicase DDX39B	↓	13.0	1.15E-04
DHX15	O43143	Pre-mRNA-splicing factor ATP-dependent RNA helicase DHX15	↓	2.0	1.98E-02
DPP4	P27487	Dipeptidyl peptidase 4	↑	3.8	1.61E-02
DPYSL2	Q16555	Dihydropyrimidinase-related protein 2	↓	6.0	2.54E-04
DPYSL3	Q14195	Dihydropyrimidinase-related protein 3	↓	4.4	2.82E-03
DYNC1H1	Q14204	Cytoplasmic dynein 1 heavy chain 1	↑	2.8	1.90E-02
EIF3C	Q99613	Eukaryotic translation initiation factor 3 subunit C	↓	2.9	9.49E-03
EIF3CL	B5ME19	Eukaryotic translation initiation factor 3 subunit C-like protein			
FLNA	P21333	Filamin-A	↑	2.8	6.47E-04
FLNC	Q14315	Filamin-C	↑	2.8	2.13E-03
FN1	P02751	Fibronectin	↑	2.1	4.48E-02
FTH1	P02794	Ferritin heavy chain	↑	7.4	1.57E-02
GAA	P10253	Lysosomal alpha-glucosidase	↓	2.3	7.78E-03
GARS1	P41250	Glycine--tRNA ligase	↓	9.6	1.84E-02
GART	P22102	Trifunctional purine biosynthetic protein adenosine-3	↓	2.4	7.64E-03
GDI2	P50395	Rab GDP dissociation inhibitor beta	↓	27.2	2.14E-04
GNAS	Q5JWF2 P63092	Guanine nucleotide-binding protein G(s) subunit alpha isoforms Xlas Guanine nucleotide-binding protein G(s) subunit alpha isoforms short	↓	3.7	3.73E-03
GNB2	P62879	Guanine nucleotide-binding protein G(I)/G(S)/G(T) subunit beta-2	↓	39.3	7.12E-04
GOLIM4	O00461	Golgi integral membrane protein 4	↑	2.7	4.48E-04
GOT2	P00505	Aspartate aminotransferase, mitochondrial	↓	10.1	4.59E-03
GPI	P06744	Glucose-6-phosphate isomerase	↓	3.4	1.45E-02

GSTO1	P78417	Glutathione S-transferase omega-1	↓	4.2	3.80E-03
H3C15	Q71DI3	Histone H3.2	↓	13.4	5.56E-04
H4C1	P62805	Histone H4	↓	7.9	1.49E-04
HADHB	P55084	Trifunctional enzyme subunit beta, mitochondrial	↓	12.9	9.36E-04
HARS1	P12081	Histidine--tRNA ligase, cytoplasmic	↓	3.5	3.65E-03
HDLBP	Q00341	Vigilin	↓	2.1	3.99E-02
HEATR1	Q9H583	HEAT repeat-containing protein 1	↑	2.4	1.14E-02
HNRNPA1	P09651	Heterogeneous nuclear ribonucleoprotein A1	↓	24.0	7.46E-04
HNRNPA1L2	Q32P51	Heterogeneous nuclear ribonucleoprotein A1-like 2			
HNRNPA2B1	P22626	Heterogeneous nuclear ribonucleoproteins A2/B1	↓	7.1	2.96E-03
HNRNPD	Q14103	Heterogeneous nuclear ribonucleoprotein D0	↓	5.4	3.07E-03
HSPA1A	P0DMV8	Heat shock 70 kDa protein 1A	↓	2.9	4.40E-02
HSPA1B	P0DMV9	Heat shock 70 kDa protein 1B			
HSPA8	P11142	Heat shock cognate 71 kDa protein	↓	3.0	1.09E-02
HSPG2	P98160	Basement membrane-specific heparan sulfate proteoglycan core protein	↑	2.2	1.24E-02
HSPH1	Q92598	Heat shock protein 105 kDa	↑	1.8	4.07E-02
HTRA1	Q92743	Serine protease HTRA1	↓	4.7	2.93E-02
HUWE1	Q7Z6Z7	E3 ubiquitin-protein ligase HUWE1	↑	2.8	7.33E-03
HYOU1	Q9Y4L1	Hypoxia up-regulated protein 1	↑	3.2	6.31E-03
IDH1	O75874	Isocitrate dehydrogenase [NADP] cytoplasmic	↓	17.7	7.52E-03
ITGA11	Q9UKX5	Integrin alpha-11	↑	4.4	1.61E-02
ITGA4	P13612	Integrin alpha-4	↑	3.0	1.18E-02
KIF5B	P33176	Kinesin-1 heavy chain	↑	2.2	5.58E-03
LBR	Q14739	Delta(14)-sterol reductase LBR	↑	2.1	2.96E-03
LMAN1	P49257	Protein ERGIC-53	↓	2.5	8.48E-03
LRPPRC	P42704	Leucine-rich PPR motif-containing protein, mitochondrial	↑	3.0	4.04E-03
LSS	P48449	Lanosterol synthase	↓	2.6	1.34E-02
MAGT1	Q9H0U3	Magnesium transporter protein 1	↑	1.8	2.01E-02
MAP1A	P78559	Microtubule-associated protein 1A	↓	2.1	2.50E-02

MAP1B	P46821	Microtubule-associated protein 1B	↓	2.9	2.21E-03
MFSD10	Q14728	Major facilitator superfamily domain-containing protein 10	↑	2.7	1.07E-03
MGAT2	Q10469	Alpha-1,6-mannosyl-glycoprotein 2-beta-N-acetylglucosaminyltransferase	↑	1.6	5.90E-03
MSN	P26038	Moesin	↓	13.7	1.42E-02
MTCH2	Q9Y6C9	Mitochondrial carrier homolog 2	↓	1.9	1.55E-03
MT-CO2	P00403	Cytochrome c oxidase subunit 2	↑	1.9	2.86E-02
MTHFD1	P11586	C-1-tetrahydrofolate synthase, cytoplasmic	↓	2.8	1.71E-02
MYL12A	P19105	Myosin regulatory light chain 12A	↓	4.6	4.08E-02
MYL12B	O14950	Myosin regulatory light chain 12B			
NLRX1	Q86UT6	NLR family member X1	↑	2.3	3.14E-03
NPM1	P06748	Nucleophosmin	↓	4.6	8.63E-04
OPLAH	O14841	5-oxoprolinase	↑	4.1	1.64E-02
PC	P11498	Pyruvate carboxylase, mitochondrial	↑	2.9	4.36E-04
PFKL	P17858	ATP-dependent 6-phosphofructokinase, liver type	↓	4.6	1.02E-03
PGM1	P36871	Phosphoglucomutase-1	↓	4.2	1.14E-02
PHB	P35232	Prohibitin	↓	19.3	2.01E-03
PKM	P14618	Pyruvate kinase PKM	↓	8.6	8.95E-04
PLIN3	O60664	Perilipin-3	↓	2.4	3.16E-02
PRPF8	Q6P2Q9	Pre-mRNA-processing-splicing factor 8	↑	1.8	4.31E-02
PRPS1	P60891	Ribose-phosphate pyrophosphokinase 1	↓	2.8	8.21E-03
PSAP	P07602	Prosaposin	↓	2.3	1.28E-02
PSMC4	P43686	26S proteasome regulatory subunit 6B	↓	6.4	4.85E-02
PSMD5	Q16401	26S proteasome non-ATPase regulatory subunit 5	↓	3.7	4.71E-02
PSME1	Q06323	Proteasome activator complex subunit 1	↓	3.9	4.59E-03
PTGIS	Q16647	Prostacyclin synthase	↑	2.4	1.21E-02
PTPRG	P23470	Receptor-type tyrosine-protein phosphatase gamma	↑	1.7	3.70E-02
PYGB	P11216	Glycogen phosphorylase, brain form	↓	2.4	4.48E-02
RABAC1	Q9UII4	Prenylated Rab acceptor protein 1	↑	1.6	2.41E-02

RAP1B	P61224	Ras-related protein Rap-1b	↓	20.9	1.49E-04
RDX	P35241	Radixin	↓	3.0	1.35E-02
RER1	O15258	Protein RER1	↑	1.5	3.17E-02
RPL27A	P46776	60S ribosomal protein L27a	↓	3.2	1.13E-02
RPS8	P62241	40S ribosomal protein S8	↓	17.9	5.07E-03
S100A10	P60903	Protein S100-A10	↓	11.9	1.08E-04
SACM1L	Q9NTJ5	Phosphatidylinositol-3-phosphatase SAC1	↑	1.5	5.58E-03
SARS1	P49591	Serine--tRNA ligase, cytoplasmic	↓	6.4	1.55E-03
SCARB2	Q14108	Lysosome membrane protein 2	↑	1.6	2.35E-02
SEC11A	P67812	Signal peptidase complex catalytic subunit SEC11A	↑	2.5	1.56E-02
SEC23A	Q15436	Protein transport protein Sec23A	↓	5.6	1.01E-04
SEC61A1	P61619	Protein transport protein Sec61 subunit alpha isoform 1	↑	2.3	1.03E-02
SELENBP1	Q13228	Methanethiol oxidase	↓	3.0	3.80E-03
SLC12A4	Q9UP95	Solute carrier family 12 member 4	↑	2.3	1.10E-02
SLC16A1	P53985	Monocarboxylate transporter 1	↑	2.0	1.76E-02
SLC3A2	SLC3A2	4F2 cell-surface antigen heavy chain	↑	2.1	3.53E-02
SOD2	P04179	Superoxide dismutase [Mn], mitochondrial	↓	19.0	2.90E-03
SPCS2	Q15005	Signal peptidase complex subunit 2	↑	2.4	6.91E-03
SRSF1	Q07955	Serine/arginine-rich splicing factor 1	↓	5.4	7.11E-03
ST13	P50502	Hsc70-interacting protein	↓	2.3	4.24E-02
ST13P4	Q8IZP2	Putative protein FAM10A4			
ST13P5	Q8NFI4	Putative protein FAM10A5			
STAT6	P42226	Signal transducer and activator of transcription 6	↓	2.2	7.40E-03
STIP1	P31948	Stress-induced-phosphoprotein 1	↓	2.5	1.18E-02
SYNCRIP	O60506	Heterogeneous nuclear ribonucleoprotein Q	↓	9.8	6.12E-03
TAGLN	Q01995	Transgelin	↓	4.0	2.82E-02
TGFBI	Q15582	Transforming growth factor-beta-induced protein ig-h3	↓	5.7	1.73E-02
THY1	P04216	Thy-1 membrane glycoprotein	↓	2.1	1.49E-02
TKT	P29401	Transketolase	↓	5.7	2.05E-02

TM9SF2	Q99805	Transmembrane 9 superfamily member 2	↑	1.6	2.19E-02
TM9SF3	Q9HD45	Transmembrane 9 superfamily member 3	↑	2.6	2.04E-02
TM9SF4	Q92544	Transmembrane 9 superfamily member 4	↑	1.7	2.99E-02
TMBIM1	Q969X1	Protein lifeguard 3	↓	1.6	3.11E-02
TMEM165	Q9HC07	Transmembrane protein 165	↑	1.9	2.41E-02
TNPO1	Q92973	Transportin-1	↓	3.0	3.65E-03
TUFM	P49411	Elongation factor Tu, mitochondrial	↓	14.8	1.44E-03
TXNRD1	Q16881	Thioredoxin reductase 1, cytoplasmic	↓	3.7	8.00E-03
UGP2	Q16851	UTP--glucose-1-phosphate uridylyltransferase	↓	6.5	2.00E-02
UQCRC1	P31930	Cytochrome b-c1 complex subunit 1, mitochondrial	↓	27.7	2.69E-04
VAMP2	P63027	Vesicle-associated membrane protein 2	↓	1.6	1.15E-02
VAMP3	Q15836	Vesicle-associated membrane protein 3			
VAR1	P26640	Valine--tRNA ligase	↑	2.6	6.91E-03
VDAC1	P21796	Voltage-dependent anion-selective channel protein 1	↓	22.5	7.81E-04
VDAC2	P45880	Voltage-dependent anion-selective channel protein 2	↓	10.0	2.54E-04
YWHAQ	P27348	14-3-3 protein theta	↓	5.2	6.18E-04

Table S4: List of 82 significantly regulated proteins in NHDF^{EXT} vs NHDF^{INT} of Y donors. Label-free quantitative proteome analysis of NHDF^{INT} vs NHDF^{EXT} of Y donors. Student's t-test, $p < 0.05$; $FC > |1.5|$; $n = 5$.

Gene name	UniProt ID	Protein description	Regulation	FC	p-value
ADK	P55263	Adenosine kinase	↑	1.5	2.05E-02
ADSL	P30566	Adenylosuccinate lyase	↑	1.6	1.12E-02
AGL	P35573	Glycogen debranching enzyme	↑	1.7	4.05E-02
AK3	Q9UIJ7	GTP:AMP phosphotransferase AK3, mitochondrial	↓	1.6	2.61E-02
AKR1A1	P14550	Aldo-keto reductase family 1 member A1	↑	1.6	2.85E-02
ALDH2	P05091	Aldehyde dehydrogenase, mitochondrial	↓	1.6	1.09E-02
ALDH3A2	P51648	Aldehyde dehydrogenase family 3 member A2	↑	1.5	4.74E-04
ANK2	Q01484	Ankyrin-2	↑	1.6	3.68E-02
ANXA4	P09525	Annexin A4	↑	1.9	1.77E-02
ANXA5	P08758	Annexin A5	↑	1.7	5.38E-03
ANXA6	P08133	Annexin A6	↑	1.8	2.33E-03
APEH	P13798	Acylamino-acid-releasing enzyme	↑	1.6	3.64E-02
CAMK2B	Q13554	Calcium/calmodulin-dependent protein kinase type II subunit beta	↑	1.9	2.18E-02
CAMK2D	Q13557	Calcium/calmodulin-dependent protein kinase type II subunit delta			
CAP1	Q01518	Adenylyl cyclase-associated protein 1	↑	1.5	4.30E-02
CAPG	P40121	Macrophage-capping protein	↑	1.5	3.74E-02
CDH13	P55290	Cadherin-13	↓	2.4	3.96E-02
CKAP4	Q07065	Cytoskeleton-associated protein 4	↓	1.6	4.56E-02
CLIC1	O00299	Chloride intracellular channel protein 1	↑	1.6	8.11E-03
CLU	P10909	Clusterin	↓	1.5	2.23E-02
CSNK1A1	P48729	Casein kinase I isoform alpha	↑	2.1	2.58E-02
CSNK1A1L	Q8N752	Casein kinase I isoform alpha-like			
CTSL	P07711	Cathepsin L1	↑	2.0	3.91E-02
DBN1	Q16643	Drebrin	↓	1.7	4.77E-02
DGKA	P23743	Diacylglycerol kinase alpha	↑	1.6	1.48E-02
ERP29	P30040	Endoplasmic reticulum resident protein 29	↓	1.8	4.03E-02

ESD	P10768	S-formylglutathione hydrolase	↑	1.6	2.25E-02
FHL1	Q13642	Four and a half LIM domains protein 1	↑	2.5	6.53E-03
FN1	P02751	Fibronectin	↓	1.5	4.47E-02
FXR1	P51114	Fragile X mental retardation syndrome-related protein 1	↓	1.8	3.89E-02
GBP1	P32455	Guanylate-binding protein 1	↑	1.8	4.64E-02
GDI1	P31150	Rab GDP dissociation inhibitor alpha	↑	1.6	1.98E-02
GDI2	P50395	Rab GDP dissociation inhibitor beta	↑	2.0	4.67E-02
GPI	P06744	Glucose-6-phosphate isomerase	↑	2.4	3.18E-02
GSN	P06396	Gelsolin	↑	1.7	4.74E-02
HINT2	Q9BX68	Histidine triad nucleotide-binding protein 2, mitochondrial	↓	1.9	3.42E-02
HNRNPDL	O14979	Heterogeneous nuclear ribonucleoprotein D-like	↓	1.7	4.47E-02
HNRNPH1	P31943	Heterogeneous nuclear ribonucleoprotein H	↓	1.7	1.70E-02
IFIT5	Q13325	Interferon-induced protein with tetratricopeptide repeats 5	↑	2.2	1.84E-02
IGF2BP2	Q9Y6M1	Insulin-like growth factor 2 mRNA-binding protein 2	↓	1.8	3.46E-02
ITGA7	Q13683	Integrin alpha-7	↑	2.6	4.11E-02
LASP1	Q14847	LIM and SH3 domain protein 1	↑	1.6	1.10E-02
LDHA	P00338	L-lactate dehydrogenase A chain	↑	1.9	1.86E-02
MAVS	Q7Z434	Mitochondrial antiviral-signaling protein	↓	1.9	2.76E-03
MIA3	Q5JRA6	Transport and Golgi organization protein 1 homolog	↓	1.5	4.10E-02
MSH2	P43246	DNA mismatch repair protein Msh2	↓	2.0	1.76E-02
MYBBP1A	Q9BQG0	Myb-binding protein 1A	↑	1.6	2.49E-02
NAGK	Q9UJ70	N-acetyl-D-glucosamine kinase	↑	1.6	8.10E-03
NRDC	O43847	Nardilysin	↑	2.0	4.86E-02
OXCT1	P55809	Succinyl-CoA:3-ketoacid coenzyme A transferase 1, mitochondrial	↓	1.5	2.60E-02
P3H4	Q92791	Endoplasmic reticulum protein SC65	↓	1.6	4.91E-02
PC	P11498	Pyruvate carboxylase, mitochondrial	↓	1.9	7.43E-03
PDIA6	Q15084	Protein disulfide-isomerase A6	↓	1.6	3.78E-02
PEBP1	P30086	Phosphatidylethanolamine-binding protein 1	↑	1.7	6.18E-03

PFKP	Q01813	ATP-dependent 6-phosphofructokinase, platelet type	↑	2.2	1.96E-02
PFN1	P07737	Profilin-1	↑	1.9	5.64E-03
PGK1	P00558	Phosphoglycerate kinase 1	↑	1.8	4.96E-02
PIGU	Q9H490	Phosphatidylinositol glycan anchor biosynthesis class U protein	↑	2.1	1.07E-02
PKM	P14618	Pyruvate kinase PKM	↑	1.5	4.74E-02
PLD3	Q8IV08	5'-3' exonuclease PLD3	↓	1.8	3.86E-02
PPA1	Q15181	Inorganic pyrophosphatase	↑	2.0	1.95E-02
PPIB	P23284	Peptidyl-prolyl cis-trans isomerase B	↓	1.5	4.34E-02
PROCR	Q9UNN8	Endothelial protein C receptor	↓	2.2	8.15E-03
PXK	Q7Z7A4	PX domain-containing protein kinase-like protein	↑	2.1	2.99E-02
PYCR1	P32322	Pyrroline-5-carboxylate reductase 1, mitochondrial	↓	2.3	3.81E-02
PYCR2	Q96C36	Pyrroline-5-carboxylate reductase 2	↓	1.6	4.61E-02
RAP2B	P61225	Ras-related protein Rap-2b	↓	1.7	3.52E-02
RBM39	Q14498	RNA-binding protein 39	↓	1.9	4.90E-02
RCN1	Q15293	Reticulocalbin-1	↓	1.7	6.45E-03
RRBP1	Q9P2E9	Ribosome-binding protein 1	↓	1.9	2.47E-02
SLC27A1	Q6PCB7	Long-chain fatty acid transport protein 1	↑	1.8	3.71E-02
SNU13	P55769	NHP2-like protein 1	↓	1.5	4.06E-02
SPTLC1	O15269	Serine palmitoyltransferase 1	↓	1.6	1.25E-02
SRSF10	O75494	Serine/arginine-rich splicing factor 10	↓	1.5	3.84E-02
SRSF3	P84103	Serine/arginine-rich splicing factor 3	↓	1.8	1.09E-02
SRSF9	Q13242	Serine/arginine-rich splicing factor 9	↓	1.6	3.03E-02
SVIL	O95425	Supervillin	↑	2.1	1.21E-02
TBCD	Q9BTW9	Tubulin-specific chaperone D	↑	1.7	1.69E-02
TGFB1I1	O43294	Transforming growth factor beta-1-induced transcript 1 protein	↑	1.5	2.76E-03
THOP1	P52888	Thimet oligopeptidase	↑	2.4	4.46E-03
TP53I3	Q53FA7	Quinone oxidoreductase PIG3	↑	1.8	1.27E-02
UACA	Q9BZF9	Uveal autoantigen with coiled-coil domains and ankyrin repeats	↓	1.6	1.32E-02

UGP2	Q16851	UTP--glucose-1-phosphate uridylyltransferase	↑	1.9	1.43E-02
UROD	P06132	Uroporphyrinogen decarboxylase	↑	2.1	1.05E-02

Table S5: List of 61 significantly regulated proteins in NHDF^{EXT} vs NHDF^{INT} of M donors. Label-free quantitative proteome analysis of NHDF^{INT} vs NHDF^{EXT} of M donors. Student's t-test, p<0.05; FC>|1.5|; n=5.

Gene name	UniProt ID	Protein description	Regulation	FC	p-value
ACAA2	P42765	3-ketoacyl-CoA thiolase, mitochondrial	↑	5.5	4.87E-02
ADH1A	P07327	Alcohol dehydrogenase 1A	↑	12.9	2.43E-02
ADH1B	P00325	All-trans-retinol dehydrogenase [NAD(+)] ADH1B			
AHNAK	Q09666	Neuroblast differentiation-associated protein AHNAK	↓	1.7	4.93E-02
AK3	Q9UIJ7	GTP:AMP phosphotransferase AK3, mitochondrial	↑	1.6	3.03E-02
ARL1	P40616	ADP-ribosylation factor-like protein 1	↓	1.8	4.90E-02
ARMCX3	Q9UH62	Armadillo repeat-containing X-linked protein 3	↑	1.7	2.85E-02
ARPC1B	O15143	Actin-related protein 2/3 complex subunit 1B	↓	1.9	3.21E-02
CKB	P12277	Creatine kinase B-type	↑	2.3	2.05E-02
CNPY2	Q9Y2B0	Protein canopy homolog 2	↓	3.2	1.03E-02
COL12A1	Q99715	Collagen alpha-1(XII) chain	↓	2.8	1.19E-04
CPQ	Q9Y646	Carboxypeptidase Q	↑	1.9	1.60E-02
CS	O75390	Citrate synthase, mitochondrial	↑	3.1	2.75E-02
DAZAP1	Q96EP5	DAZ-associated protein 1	↓	1.8	3.13E-02
DPM1	O60762	Dolichol-phosphate mannosyltransferase subunit 1	↓	1.7	2.02E-02
EIF1AX	P47813	Eukaryotic translation initiation factor 1A, X-chromosomal	↓	2.3	6.37E-03
EIF1AY	O14602	Eukaryotic translation initiation factor 1A, Y-chromosomal			
EPB41L2	O43491	Band 4.1-like protein 2	↓	1.6	1.56E-02
FH	P07954	Fumarate hydratase, mitochondrial	↑	1.8	2.50E-02
FKBP2	P26885	Peptidyl-prolyl cis-trans isomerase FKBP2	↓	1.6	1.89E-02
GLUD1	P00367	Glutamate dehydrogenase 1, mitochondrial	↑	3.1	3.71E-02
GLUD2	P49448	Glutamate dehydrogenase 2, mitochondrial			
GPD2	P43304	Glycerol-3-phosphate dehydrogenase, mitochondrial	↑	2.5	3.51E-02
H1-5	P16401	Histone H1.5	↑	1.8	3.96E-02
HEXA	P06865	Beta-hexosaminidase subunit alpha	↑	1.6	4.05E-02
HNRNPAB	Q99729	Heterogeneous nuclear ribonucleoprotein A/B	↑	1.7	4.20E-02

HSPA1A	P0DMV8	Heat shock 70 kDa protein 1A	↑	1.8	3.12E-02
HSPA1B	P0DMV9	Heat shock 70 kDa protein 1B			
IDH2	P48735	Isocitrate dehydrogenase [NADP], mitochondrial	↑	2.9	4.06E-02
LRRN4CL	Q8ND94	LRRN4 C-terminal-like protein	↑	2.5	5.10E-03
MATR3	P43243	Matrin-3	↓	2.3	1.97E-02
ME2	P23368	NAD-dependent malic enzyme, mitochondrial	↑	1.9	1.66E-03
MGST1	P10620	Microsomal glutathione S-transferase 1	↓	1.9	1.40E-02
MYLK	Q15746	Myosin light chain kinase, smooth muscle	↑	1.9	2.60E-02
NAGA	P17050	Alpha-N-acetylgalactosaminidase	↑	1.9	1.49E-03
NEK7	Q8TDX7	Serine/threonine-protein kinase Nek7	↓	2.6	1.28E-03
OXCT1	P55809	Succinyl-CoA:3-ketoacid coenzyme A transferase 1, mitochondrial	↑	1.6	4.05E-02
P3H4	Q92791	Endoplasmic reticulum protein SC65	↓	1.5	2.94E-02
PDHA1	P08559	Pyruvate dehydrogenase E1 component subunit alpha, somatic form, mitochondrial	↑	2.6	2.87E-02
PDLIM1	O00151	PDZ and LIM domain protein 1	↓	1.9	9.97E-04
PML	P29590	Protein PML	↑	2.1	3.28E-02
PMPCA	Q10713	Mitochondrial-processing peptidase subunit alpha	↑	1.6	2.10E-02
PRCP	P42785	Lysosomal Pro-X carboxypeptidase	↑	1.8	4.48E-02
RPL17	P18621	60S ribosomal protein L17	↓	3.1	1.77E-02
RPL23	P62829	60S ribosomal protein L23	↓	3.1	4.86E-03
RPL9	P32969	60S ribosomal protein L9	↓	2.5	2.60E-02
RPS17	P08708	40S ribosomal protein S17	↓	3.0	3.22E-02
RPS20	P60866	40S ribosomal protein S20	↓	2.4	1.47E-02
RPS6	P62753	40S ribosomal protein S6	↓	6.1	1.33E-03
RPS7	P62081	40S ribosomal protein S7	↓	3.9	1.87E-02
SAMHD1	Q9Y3Z3	Deoxynucleoside triphosphate triphosphohydrolase SAMHD1	↑	1.6	4.21E-02
SDHA	P31040	Succinate dehydrogenase [ubiquinone] flavoprotein subunit, mitochondrial	↑	1.9	4.42E-02
SF3A1	Q15459	Splicing factor 3A subunit 1	↓	1.6	4.36E-02
SFXN3	Q9BWM7	Sideroflexin-3	↑	2.0	4.40E-02

SGSH	P51688	N-sulphoglucosamine sulphohydrolase	↑	1.6	1.41E-02
SLC25A12	O75746	Calcium-binding mitochondrial carrier protein Aralar1	↑	1.6	1.52E-02
SNRPA1	P09661	U2 small nuclear ribonucleoprotein A	↓	1.6	6.52E-03
SQOR	Q9Y6N5	Sulfide:quinone oxidoreductase, mitochondrial	↑	4.6	2.47E-02
SRP68	Q9UHB9	Signal recognition particle subunit SRP68	↓	1.9	2.15E-02
TAF15	Q92804	TATA-binding protein-associated factor 2N	↓	1.9	1.83E-02
THOP1	P52888	Thimet oligopeptidase	↑	1.6	1.55E-02
TMX1	Q9H3N1	Thioredoxin-related transmembrane protein 1	↑	1.7	3.62E-02
TPP1	O14773	Tripeptidyl-peptidase 1	↑	1.5	2.49E-02
USP39	Q53GS9	U4/U6.U5 tri-snRNP-associated protein 2	↑	1.5	1.31E-02
ZYX	Q15942	Zyxin	↓	2.1	4.27E-02

Table S6: List of 54 significantly regulated proteins in NHDF^{EXT} vs NHDF^{INT} of O donors. Label-free quantitative proteome analysis of NHDF^{INT} vs NHDF^{EXT} of O donors. Student's t-test, p<0.05; FC>|1.5|; n=5.

Gene name	UniProt ID	Protein description	Regulation	FC	p-value
APP	P05067	Amyloid-beta precursor protein	↑	1.8	3.77E-02
ARFGEF1	Q9Y6D6	Brefeldin A-inhibited guanine nucleotide-exchange protein 1	↑	1.7	2.20E-02
ARL6IP1	Q15041	ADP-ribosylation factor-like protein 6-interacting protein 1	↑	1.6	5.61E-03
ATP5MD	Q96IX5	ATP synthase membrane subunit DAPIT, mitochondrial	↑	2.0	4.02E-02
CAVIN1	Q6NZI2	Caveolae-associated protein 1	↓	1.9	1.41E-02
CAVIN3	Q969G5	Caveolae-associated protein 3	↓	1.7	3.80E-02
CD248	Q9HCU0	Endosialin	↓	1.6	2.07E-02
CD97	P48960	CD97 antigen	↓	1.7	2.07E-02
CDH13	P55290	Cadherin-13	↓	2.7	1.14E-03
CPD	O75976	Carboxypeptidase D	↑	1.6	3.13E-02
CPT1A	P50416	Carnitine O-palmitoyltransferase 1, liver isoform	↑	1.5	1.44E-02
DNAJC13	O75165	DnaJ homolog subfamily C member 13	↑	1.6	2.76E-02
DNM1	Q05193	Dynamin-1	↓	1.6	9.07E-03
EEA1	Q15075	Early endosome antigen 1	↑	1.9	3.90E-02
EGFR	P00533	Epidermal growth factor receptor	↑	1.6	3.66E-02
EIF3A	Q14152	Eukaryotic translation initiation factor 3 subunit A	↓	2.0	2.64E-02
FBLN1	P23142	Fibulin-1	↓	3.0	2.74E-02
GLG1	Q92896	Golgi apparatus protein 1	↑	1.6	9.08E-03
HACD3	Q9P035	Very-long-chain (3R)-3-hydroxyacyl-CoA dehydratase 3	↑	1.8	4.74E-02
IARS	P41252	Isoleucine--tRNA ligase, cytoplasmic	↑	1.6	4.23E-02
ILF3	Q12906	Interleukin enhancer-binding factor 3	↓	3.6	2.77E-02
KHSRP	Q92945	Far upstream element-binding protein 2	↓	2.3	1.55E-02
LAMP1	P11279	Lysosome-associated membrane glycoprotein 1	↑	1.9	8.57E-03
LRP1	Q07954	Prolow-density lipoprotein receptor-related protein 1	↑	1.5	3.58E-02
LRPPRC	P42704	Leucine-rich PPR motif-containing protein, mitochondrial	↑	1.8	4.83E-02

MAGT1	Q9H0U3	Magnesium transporter protein 1	↑	1.8	6.19E-03
MCU	Q8NE86	Calcium uniporter protein, mitochondrial	↑	1.7	4.13E-03
MGST1	P10620	Microsomal glutathione S-transferase 1	↑	1.7	6.31E-03
MIA3	Q5JRA6	Transport and Golgi organization protein 1 homolog	↑	1.7	1.06E-02
MSN	P26038	Moesin	↓	6.2	3.94E-02
MYL6	P60660	Myosin light polypeptide 6	↓	1.7	4.84E-02
MYO1C	O00159	Unconventional myosin-Ic	↓	1.9	3.38E-02
NEK9	Q8TD19	Serine/threonine-protein kinase Nek9	↓	1.7	3.60E-02
NPC1	O15118	NPC intracellular cholesterol transporter 1	↑	1.7	3.39E-02
NUP205	Q92621	Nuclear pore complex protein Nup205	↑	1.6	3.75E-02
PFAS	O15067	Phosphoribosylformylglycinamide synthase	↑	1.9	4.04E-02
PRKDC	P78527	DNA-dependent protein kinase catalytic subunit	↑	1.6	2.43E-02
RCN1	Q15293	Reticulocalbin-1	↓	2.0	1.51E-02
SEC11A	P67812	Signal peptidase complex catalytic subunit SEC11A	↑	1.8	3.58E-02
SEC61A1	P61619	Protein transport protein Sec61 subunit alpha isoform 1	↑	2.6	3.16E-03
SLC25A3	Q00325	Phosphate carrier protein, mitochondrial	↑	1.9	1.49E-02
SLC7A5	Q01650	Large neutral amino acids transporter small subunit 1	↑	2.3	1.22E-02
SMARCC2	Q8TAQ2	SWI/SNF complex subunit SMARCC2	↓	1.8	1.75E-02
SRRT	Q9BXP5	Serrate RNA effector molecule homolog	↓	1.8	1.50E-04
STT3A	P46977	Dolichyl-diphosphooligosaccharide--protein glycosyltransferase subunit STT3A	↑	1.6	3.39E-02
STT3B	Q8TCJ2	Dolichyl-diphosphooligosaccharide--protein glycosyltransferase subunit STT3B	↑	1.6	2.57E-02
SVIL	O95425	Supervillin	↓	1.9	6.39E-03
TM9SF2	Q99805	Transmembrane 9 superfamily member 2	↑	1.8	3.03E-02
TM9SF3	Q9HD45	Transmembrane 9 superfamily member 3	↑	2.0	1.55E-02
TMTC3	Q6ZXV5	Protein O-mannosyl-transferase TMTC3	↑	1.7	7.80E-03
TSPO	P30536	Translocator protein	↑	1.6	9.55E-03
TTC17	Q96AE7	Tetratricopeptide repeat protein 17	↑	1.8	1.29E-02

VAPA	Q9P0L0	Vesicle-associated membrane protein-associated protein A	↓	1.6	1.52E-02
VKORC1	Q9BQB6	Vitamin K epoxide reductase complex subunit 1	↑	1.6	2.47E-02

Eidesstattliche Erklärung

Ich versichere an Eides Statt, dass die Dissertation von mir selbständig und ohne unzulässige fremde Hilfe unter Beachtung der „Grundsätze zur Sicherung guter wissenschaftlicher Praxis an der Heinrich-Heine-Universität Düsseldorf“ erstellt worden ist.

Ich versichere, dass ich diese Arbeit nur an der Mathematisch-Naturwissenschaftlichen Fakultät der Heinrich-Heine-Universität Düsseldorf vorgelegt habe. Ich habe bisher keine erfolglosen Promotionsversuche unternommen.

Düsseldorf, 13. September 2021

Sabine Schneider

Danksagung

An dieser Stelle möchte ich mich bei all den Menschen bedanken, die mich während meiner Promotionszeit begleitet und unterstützt haben und mir die Fertigstellung der Dissertation ermöglicht haben.

Zuerst gilt mein Dank Herrn Prof. Dr. Krutmann für die Bereitstellung des interessanten Forschungsthemas und die hervorragende wissenschaftliche Unterstützung. Ich möchte mich für die hilfreichen Anregungen und die Gespräche bedanken, die ich stets als sehr motivierend wahrgenommen habe.

Bei Herrn Prof. Dr. Martin möchte ich mich für die freundliche Übernahme des Zweitgutachtens bedanken.

Mein Dank gilt Herrn Prof Dr. Schwender für die Hilfsbereitschaft und Unterstützung bei mathematischen Fragen.

Beim BMFZ der HHU, insbesondere bei Dr. Anja Stefanski, möchte ich mich für die Durchführung der massenspektrometrischen Analysen bedanken.

Ein ganz großes Dankeschön geht an meine Arbeitskollegen für die angenehme Atmosphäre und den großartigen Zusammenhalt vor allem innerhalb der Arbeitsgruppe. Mein besonderer Dank gilt Dr. Marc Majora, Dr. Sonja Faßbender und Dr. Marius Pollet für eure hilfreiche, fachliche Unterstützung, eure Geduld und unermüdliche Gesprächsbereitschaft. Bedanken möchte ich mich außerdem bei Maren Knechten, Ingo Uthe, Jennifer Schindler, Katharina Rolfes und Selina Woeste sowie bei meinen ehemaligen Arbeitskollegen Dr. Kevin Sondenheimer und Judith Hüsemann. Danke euch allen und auch den nicht namentlich erwähnten Kollegen am IUF für eure tolle Unterstützung, die wunderbare Zusammenarbeit, die vielen interessanten und privaten Gespräche, euren fantastischen Humor und die aufmunternden Worte in der ein oder anderen Situation.

Von ganzem Herzen möchte ich mich bei meiner Familie und meinen Freunden bedanken. Danke für eure Motivation und den Rückhalt über die ganzen Jahre. Durch euch habe ich erfahren, wie wertvoll ein positives, liebevolles und unterstützendes Umfeld für das Leben selbst und das Erreichen von Zielen ist. Ein ganz besonderer Dank gilt meinem Freund, der mir immer Mut macht und mich bei allem unterstützt. Ganz besonders möchte ich auch meinen Brüdern danken, die immer bedingungslos hinter mir stehen und für mich da sind.